

U.S. Department of Transportation
Federal Highway Administration

Steel Bridge Design Handbook

Structural Behavior of Steel

Publication No. FHWA-HIF-16-002 - Vol. 4

December 2015



FOREWORD

This handbook covers a full range of topics and design examples intended to provide bridge engineers with the information needed to make knowledgeable decisions regarding the selection, design, fabrication, and construction of steel bridges. Upon completion of the latest update, the handbook is based on the Seventh Edition of the AASHTO LRFD Bridge Design Specifications. The hard and competent work of the National Steel Bridge Alliance (NSBA) and prime consultant, HDR, Inc., and their sub-consultants, in producing and maintaining this handbook is gratefully acknowledged.

The topics and design examples of the handbook are published separately for ease of use, and available for free download at the NSBA and FHWA websites: <http://www.steelbridges.org>, and <http://www.fhwa.dot.gov/bridge>, respectively.

The contributions and constructive review comments received during the preparation of the handbook from many bridge engineering professionals across the country are very much appreciated. In particular, I would like to recognize the contributions of Bryan Kulesza with ArcelorMittal, Jeff Carlson with NSBA, Shane Beabes with AECOM, Rob Connor with Purdue University, Ryan Wisch with DeLong's, Inc., Bob Cisneros with High Steel Structures, Inc., Mike Culmo with CME Associates, Inc., Mike Grubb with M.A. Grubb & Associates, LLC, Don White with Georgia Institute of Technology, Jamie Farris with Texas Department of Transportation, and Bill McEleney with NSBA.



Joseph L. Hartmann, PhD, P.E.
Director, Office of Bridges and Structures

Notice

This document is disseminated under the sponsorship of the U.S. Department of Transportation in the interest of information exchange. The U.S. Government assumes no liability for use of the information contained in this document. This report does not constitute a standard, specification, or regulation.

Quality Assurance Statement

The Federal Highway Administration provides high-quality information to serve Government, industry, and the public in a manner that promotes public understanding. Standards and policies are used to ensure and maximize the quality, objectivity, utility, and integrity of its information. FHWA periodically reviews quality issues and adjusts its programs and processes to ensure continuous quality improvement.

Technical Report Documentation Page

1. Report No. FHWA-HIF-16-002 – Vol. 4	2. Government Accession No.	3. Recipient's Catalog No.	
4. Title and Subtitle Steel Bridge Design Handbook: Structural Behavior of Steel		5. Report Date December 2015	
		6. Performing Organization Code	
7. Author(s) Don White, Ph.D. (Georgia Institute of Technology)		8. Performing Organization Report No.	
9. Performing Organization Name and Address HDR, Inc. 11 Stanwix Street Suite 800 Pittsburgh, PA 15222		10. Work Unit No.	
		11. Contract or Grant No. DTFH6114D00049	
12. Sponsoring Agency Name and Address Office of Bridges and Structures Federal Highway Administration 1200 New Jersey Avenue, SE Washington, D.C. 20590		13. Type of Report and Period Covered Technical Report Final Report December 2014 – November 2015	
		14. Sponsoring Agency Code	
15. Supplementary Notes The previous version of this Handbook was published as FHWA-IF-12-052 and was developed to be current with the AASHTO LRFD Bridge Design Specifications, 5th Edition with the 2010 Interims. FHWA-HIF-16-002 was updated in 2015 by HDR, Inc., to be current with the AASHTO LRFD Bridge Design Specifications, 7th Edition.			
16. Abstract The behavior of steel structures is an intricate and fascinating topic. This module is intended to serve as a guide to the AASHTO Load and Resistance Factor Design (LRFD) Specifications and their representation of the behavior of steel bridge systems and members. The module focuses on the structural form and function of bridge systems and members, with emphasis on strength limit states. Where relevant, recent advances in the AISC <i>Specification for Structural Steel Buildings</i> as well as findings from research developments are discussed in addition to the AASHTO LRFD Specifications. There are numerous areas where a broad understanding of the fundamental behavior of structures is key to the proper interpretation, application, and where necessary, extension of the AASHTO LRFD Specifications. This module aims to aid the Engineer in reviewing and understanding the essential principles of steel system and member strength behavior and design.			
17. Key Words Steel Bridge, Structural Behavior, Buckling, I-Section Members, Box-Section Members, Compression Members		18. Distribution Statement No restrictions. This document is available to the public through the National Technical Information Service, Springfield, VA 22161.	
19. Security Classif. (of this report) Unclassified	20. Security Classif. (of this page) Unclassified	21. No of Pages	22. Price

Steel Bridge Design Handbook: Structural Behavior of Steel

Table of Contents

1.0	INTRODUCTION	1
2.0	BEHAVIOR AND STRUCTURE TYPES.....	2
2.1	Rolled I-Section Stringer Systems	2
2.2	General I-Section Stringer Systems	3
2.2.1	Overview	3
2.2.2	Fundamental Behavior of I-Section Stringer Systems.....	7
2.2.3	Integral Piers and Abutments.....	14
2.2.4	Temperature Movements	16
2.3	Box-Section Stringer System.....	19
2.4	Truss Bridges	23
2.5	Arch Bridges	26
2.6	Cable-Supported Bridges.....	30
2.6.1	General.....	30
2.6.2	Suspension Bridges.....	32
2.6.3	Cable-Stayed Bridges.....	34
3.0	ELASTIC SYSTEM ANALYSIS, INELASTIC COMPONENT RESISTANCES.....	39
4.0	OVERALL SYSTEM BUCKLING VERSUS INDIVIDUAL MEMBER BUCKLING ...	44
4.1	Key Concepts	44
4.2	Lean-On Bracing Systems	47
4.3	General Consideration of System Stability Effects in Design.....	49
5.0	MEMBER BEHAVIOR AND DESIGN STRENGTH	51
5.1	Tension Members.....	51
5.1.1	Rolled or Built-Up Tension Members	51
5.1.2	Eyebars and Pin-Connected Plates.....	56
5.1.3	Strands.....	59

5.2	Compression Members	61
5.2.1	Base Column Strength Equations	61
5.2.2	Flexural Buckling and Column Effective Length.....	64
5.2.3	Column Torsional and Torsional-Flexural Buckling.....	66
5.2.3.1	Torsional buckling of doubly-symmetric cross-sections	66
5.2.3.2	Flexural or torsional-flexural buckling of singly-symmetric cross-sections	68
5.2.3.3	Torsional-flexural buckling of general unsymmetric cross-sections ..	69
5.2.3.4	Special handling of double-angles and tees with non-slender elements in AISC (2010).....	70
5.2.3.5	Special handling of single angle compression members in AASHTO (2014) and AISC (2010)	71
5.2.4	Columns with Slender Elements.....	75
5.2.4.1	Width-to-thickness limits to prevent local buckling under uniform axial compression.....	75
5.2.4.2	Compressive resistance of slender-element section members	81
5.2.4.3	Strength reduction Q_s for members composed entirely of unstiffened elements	82
5.2.4.4	Strength reduction $Q = Q_a Q_s$ for members with stiffened elements ...	82
5.2.4.5	Axial capacity of hybrid slender-web girders.....	87
5.2.4.6	Local buckling criteria for solid-web arch ribs.....	88
5.2.5	Built-up Columns Composed of Two or More Shapes.....	89
5.2.6	Columns with Tapered and/or Stepped Sections and/or Nonuniform Internal Axial Force	93
5.2.7	Composite Columns.....	96
5.2.7.1	AASHTO (2014) - AISC (1999) approach.....	96
5.2.7.2	AISC (2005) and (2010) approach.....	98
5.2.7.3	Axial compression resistance of composite bridge girders.....	101
5.3	I-Section Flexural Members	104
5.3.1	Introduction.....	104
5.3.2	Proportioning Limits.....	105

5.3.3	Compact Composite Sections in Positive Flexure	106
5.3.3.1	Section classification	106
5.3.3.2	Flexural resistance	108
5.3.3.3	Handling of creep and shrinkage effects.....	109
5.3.4	Noncompact Composite Sections in Positive Flexure	110
5.3.5	Composite Sections in Negative Flexure and Noncomposite Sections	112
5.3.5.1	Key concepts.....	112
5.3.5.2	Maximum potential flexural resistance, M_{max} or F_{max}	115
5.3.5.2.1	Compact- and noncompact-web sections.....	115
5.3.5.2.2	Slender-web sections	117
5.3.5.2.3	Hybrid-web strength reduction factor.....	118
5.3.5.2.4	Other considerations	120
5.3.5.3	Tension flange yielding (TFY) resistance.....	120
5.3.5.4	Compact bracing limit, L_p	121
5.3.5.5	Compact flange slenderness limit, λ_{pf}	125
5.3.5.6	Compression flange stress at the nominal onset of inelastic buckling, F_{yr}	125
5.3.5.7	Elastic LTB stress, $F_{e.LTB}$	126
5.3.5.8	Noncompact bracing limit, L_r	128
5.3.5.9	Elastic FLB stress, $F_{e\ell}$	128
5.3.5.10	Noncompact flange slenderness limit, λ_{rf}	129
5.3.5.11	Moment gradient modifier, C_b	129
5.3.5.12	Other considerations specific to composite I-section members in negative bending	138
5.3.5.13	LTB effective lengths	140
5.3.5.14	Inelastic redistribution of interior pier moments in continuous-span bridges	143
5.3.6	Stepped, Variable Web Depth and Other Nonprismatic I-Section Members	146
5.3.7	Combined Major-Axis Bending, Minor-Axis Bending and Torsion	153
5.3.7.1	General.....	153
5.3.7.2	Calculation of flange lateral bending stresses.....	156
5.3.7.3	One-third rule concept	157

5.3.8	Shear Strength.....	159
5.3.8.1	General.....	159
5.3.8.2	Longitudinally-stiffened members.....	163
5.3.8.3	Variable web depth members.....	163
5.3.8.4	Web transverse stiffeners.....	164
5.3.9	Shear Connectors.....	167
5.3.10	Secondary Limit States.....	173
5.3.10.1	Net section fracture.....	173
5.3.10.2	Web bend buckling.....	174
5.3.10.3	Longitudinal stiffeners.....	176
5.3.10.4	Bearing stiffeners.....	181
5.3.10.5	Web yielding and web crippling.....	181
5.4	Box-Section Flexural Members.....	182
5.4.1	Introduction.....	182
5.4.2	Categorization of Box-Girder Bridges in AASHTO (2014).....	184
5.4.2.1	Straight multiple-box-girder bridges satisfying the restrictions in Article 6.11.2.3 and having fully effective flanges.....	184
5.4.2.2	Box-girder bridges not satisfying one or more of the above requirements.....	186
5.4.3	Other General Requirements Applicable to All Types of Box-Girder Bridges..	188
5.4.3.1	Diaphragm requirements at supports (Article 6.7.4.3).....	188
5.4.3.2	Bearing requirements (Article 6.11.1.2).....	189
5.4.3.3	Top lateral bracing requirements in tub girders (Article 6.7.5.3).....	189
5.4.4	Additional Requirements for Specific Box-Girder Bridge Types.....	190
5.4.4.1	Horizontally curved boxes (multiple or single).....	191
5.4.4.2	Single boxes.....	191
5.4.4.3	Closed boxes.....	191
5.4.5	Proportioning Limits.....	192
5.4.6	Compact Composite Sections in Positive Flexure.....	192
5.4.7	Noncompact Composite Sections in Positive Flexure.....	193
5.4.8	Noncomposite Sections.....	195

5.4.9	Composite Sections in Negative Flexure	196
5.4.10	Bottom Box Flange at Interior Pier Sections	200
5.4.11	Concrete Slab	201
5.4.12	Stepped, Variable Web Depth and Other Nonprismatic Box-Section Members	201
5.4.13	Web Shear Strength	202
5.4.14	Shear Connectors	203
5.4.15	Comparison to the Wolchuk and Mayrbaurl (1980) Proposed Specifications for Long-Span Steel Box-Girder Bridges	204
5.4.15.1	Box flange effective widths	204
5.4.15.2	Resistance of unstiffened box flanges in compression	207
5.4.15.3	Resistance of stiffened box flanges in compression	208
5.4.15.4	Shear resistance.....	209
5.5	Miscellaneous Flexural Members	210
5.5.1	Introduction.....	210
5.5.2	I-Section Members in Weak-Axis Bending.....	210
5.5.3	Noncomposite Box-Section Members	211
5.5.4	Circular Tubes.....	214
5.5.5	Tees and Double Angles in Strong-Axis Bending.....	215
5.5.6	Channels in Strong- and Weak-Axis Bending	217
5.5.7	Rectangular Bars and Rounds.....	218
5.5.8	Single Angles	219
5.5.9	Concrete-Encased and Filled Members	219
5.5.9.1	AASHTO (2014) - AISC (1999) approach.....	219
5.5.9.2	AISC (2010) Approach.....	221
5.6	Combined Flexure and Axial Load.....	222
5.6.1	Introduction.....	222
5.6.2	AASHTO (2014) and Primary AISC (2010) Beam-Column Interaction Equations 222	
5.6.3	Noncomposite Members	224
5.6.3.1	In-plane resistance of doubly-symmetric I-section members subjected to axial load and major- or minor-axis bending.....	224

5.6.3.1.1	Enhanced strength interaction curves for singly-symmetric members loaded in their plane of symmetry.....	233
5.6.3.1.2	Usage of the AASHTO (2014) and primary AISC (2010) bilinear interaction equations with relaxed flange and/or web compactness limits...	235
5.6.3.2	Out-of-plane strength of doubly-symmetric rolled nonslender-element I-section members with $KL_z < KL_y$ subjected to axial load and major-axis bending	236
5.6.3.3	Other types of beam-columns, general loading conditions.....	240
5.6.4	Composite Members	241
5.6.4.1	I- and box-section members with a composite concrete deck	241
5.6.4.2	Concrete-encased sections and concrete-filled boxes and tubes.....	242
5.6.5	Summary Assessment of Beam-Column Strength Calculations.....	246
6.0	CONCLUDING REMARKS.....	247
7.0	REFERENCES	248

List of Figures

Figure 1 Typical composite rolled I-beam or welded I-girder bridge cross-section.....	3
Figure 2 Effect of Shear lag.	4
Figure 3 Typical composite I-girder substringer system.	5
Figure 4 Two-girder system with floor beams and stringers.	5
Figure 5 Two-girder system with cross-girders.	5
Figure 6 Example complex plan geometry (courtesy of HDR Engineering, Inc.)	7
Figure 7 Plan view illustrating the required resultants for the reactions due to dead load at the ends of a simply-supported horizontally-curved bridge with radial supports.....	7
Figure 8 Transfer of vertical shear forces due to torsion (V-loads) by the cross-frames and the slab in a curved bridge	8
Figure 9 Illustration of twisting and warping deformation of an I-section member.....	9
Figure 10 Simplified calculation of flange lateral bending stresses on a curved I-girder subjected to uniform bending moment.....	10
Figure 11 Use of lateral bracing within a few unbraced lengths adjacent to supports to reduce I-girder lateral bending stresses due to wind.	11
Figure 12 Plan view of deflections at the bottom and top of skewed diaphragms or cross-frames at a bearing line, forcing a coupling between major-axis bending and torsional rotation of the girders.	12
Figure 13 Cross-frame, bridge cross-section, and girder torsional rotations due to differential girder displacements in skewed bridges (Coletti and Yadlosky 2005).....	13
Figure 14 Use of staggered cross-frames to reduce the forces attracted to the cross-frame members near the supports in skewed I-girder bridges.	13
Figure 15 Typical post-tensioned concrete integral bent cap with a single column pier (Wasserman 1997) (courtesy of Tennessee DOT and NSBA).	15
Figure 16 Straddle bents with integral steel pier caps (Abu-Hawash et al. 2005) (courtesy of Iowa DOT, HDR Engineering, and NSBA).....	15
Figure 17 Typical integral abutment detail (courtesy of Tennessee DOT).	17
Figure 18 Typical semi-integral abutment detail (courtesy of Tennessee DOT).....	18
Figure 19 Bearing orientation to accommodate thermal movement on a horizontally curved alignment (NSBA 2004).	18

Figure 20 Stresses in a single box girder subjected to an eccentric load.	19
Figure 21 Representative tub-girder bridge cross-section.	21
Figure 22 Shear center location and predominant torsional deformations for a tub girder section that does not have a top-flange bracing system.	21
Figure 23 Costa-e-Silva Bridge in Rio de Janeiro, Brazil, second-longest box-girder span, 980 ft (courtesy of www.structurae.de).....	22
Figure 24 Costa-e-Silva Bridge side elevation and cross-section (adapted from Ito et al. (1992) and Wolchuk (1997))	23
Figure 25 Sfalassà Bridge in Calabria, Italy, longest box-girder span, 1230 ft (courtesy of www.structurae.de)	23
Figure 26 Ikitsuki Ohashi Bridge, Nagasaki, Japan, longest-span continuous truss bridge, 1300 ft main span (www.sight-seeing.japan.com)	25
Figure 27 Quebec Bridge in Quebec, Canada, longest span cantilever truss bridge, 1800 ft main span (courtesy of www.structurae.de).	25
Figure 28 La Roize Bridge in France, triangular cross-section geometry using a single member bottom chord and post-tensioning strand (courtesy of HNTB).	26
Figure 29 Slant-legged rigid-frame bridge (courtesy of HDR Engineering, Inc.).....	28
Figure 30 LuPu Bridge in Shanghai, China, longest span steel arch, 1800 ft (courtesy of www.structurae.de).	29
Figure 31 LuPu Bridge deck system (courtesy of www.structurae.de).	29
Figure 32 New River Gorge Bridge in West Virginia, longest span steel arch in the United States, 1700 ft (courtesy of HDR Engineering, Inc.).....	29
Figure 33 Cable suspended bridge systems, (a) suspension and (b) cable-stayed (reprinted with permission from Podolny and Scalzi).	30
Figure 34 Akashi Kaikyo Bridge, longest suspension span (6530 ft) (courtesy of www.structurae.de).	31
Figure 35 Cooper River Bridge, longest cable-stayed span in the USA (1550 ft) (courtesy South Carolina DOT).	32
Figure 36 Sutong Bridge, longest cable-stayed span in the world (3570 ft) (courtesy of New Jersey DOT).	33
Figure 37 Representative two-span cable-stayed bridge system.	35

Figure 38 Methods to avoid large tower bending moments in cable-stayed bridge systems with more than three spans (Tang 2000).....	35
Figure 39 Duisberg-Neuenkamp Bridge, Duisberg, Germany, 3-span cable-stayed bridge utilizing a single plane of stay cables (1150 ft main span) (courtesy of www.structurae.de).	36
Figure 40 Alternative stay layouts, (a) harp pattern and (b) semi-harp pattern.....	36
Figure 41 Dual-girder subassembly composed of two equal-size doubly-symmetric I-girders ..	45
Figure 42 Example determination of whether system buckling or buckling of the girders between the cross-frames governs for two equal-size doubly-symmetric I-girders.	47
Figure 43 A single cross-frame bridge cross-section showing multiple I-girders braced by a single cross-frame	48
Figure 44 Plan view of a proof-of-concept skewed I-girder bridge utilizing lean-on bracing to alleviate large cross-frame forces and to reduce the number of required cross-frames (Herman et al. 2005) (reprinted with permission from Texas DOT). The x marks indicate the location of cross-frames.	49
Figure 45 Dimensional requirements for eyebars specified to ensure good member performance and development of the full yield capacity of an eyebar.	57
Figure 46 Requirements in addition to the checks of tension yielding, tension fracture and plate bearing, for a specific pin connected plate with two equal size pin plates (w , a and e of pin plates = w , a and e of main plate) bolted on each side of the main plate.....	59
Figure 47 AASHTO (2014) and AISC (2010) column strength curve in terms of both KL/r and $(P_o/P_e)^{0.5}$ versus the SSRC multiple column curves 1P, 2P and 3P (Galambos 1998) and the theoretical elastic buckling strength, steel columns with $F_y = 50$ ksi	63
Figure 48 Torsional buckling of an I-section member.....	67
Figure 49 Single-angle cross-section and definition of geometric axes utilized by the AISC (2010) and AASHTO (2014) equivalent KL/r expressions.	72
Figure 50 Test end conditions associated with the recommended equivalent KL/r equations for single angle struts.....	72
Figure 51 General form of AISC (2010)-AASHTO (2014) nominal strength curve for plate local buckling.....	76
Figure 52 Theoretical k_c values for elastic plate buckling (adapted from Salmon and Johnson (1996)).....	80

Figure 53 Representative physical average (through thickness) stress distribution across the width of a postbuckled stiffened plate (i.e., both edges supported transversely) versus idealized equivalent stress distribution acting on the plate effective width b_e	83
Figure 54 AISC (2005) column resistances versus the resistance obtained using the AISI (2001) unified effective width approach, using the larger AISC-AASHTO $k_c = 4.8$ rather than the AISI $k_c = 4.0$, uniform-thickness square box section with $b/t = 150$ and $F_y = 50$ ksi.....	86
Figure 55 Variation of Q ($= Q_a = b_e/b$) as a function of the column slenderness for the uniform-thickness square box section with $b/t = 150$ and $F_y = 50$ ksi.	86
Figure 56 Types of built-up columns, (a) columns with closely-spaced components and (b) columns with widely-spaced components.	91
Figure 57 Conceptual mapping of a tapered-web I-section member subjected to constant axial compression to an equivalent prismatic member.....	95
Figure 58 Cross-section displacements and relevant cross-section dimensions for torsional buckling about an enforced axis at the depth of the shear connectors.....	103
Figure 59 Illustrative plastic cross-section models for composite I-sections in positive bending. Cases for plastic neutral axis (PNA) in concrete deck below P_{rb} , concrete deck at P_{rb} , concrete deck at P_{rt} and concrete deck above P_{rt} are not shown.....	107
Figure 60 Basic form of flange local buckling (FLB) and lateral-torsional buckling (LTB) strength curves for all composite I-section members in negative bending and noncomposite I-section members (reprinted with permission from AASHTO (2004)).	113
Figure 61 Variation of M_{max} for FLB and LTB versus the web slenderness $\lambda_w = 2D_c/t_w$	116
Figure 62 Variation of the tension flange yielding (TFY) resistance $M_{n(TFY)}$ versus the web slenderness $\lambda_w = 2D_c/t_w$	121
Figure 63 Comparison of rolled beam I-section uniform bending test results from Dux and Kitipornchai (1983) and Wong-Chung and Kitipornchai (1987) to the AASHTO (2014) and AISC (2010) flexural resistances ($F_{yc} = 41.3$ and 42.5 ksi, LTB effective length factors $K = 0.66$ and 0.91).	124
Figure 64 Comparison of compact-flange noncompact-web welded member test results for uniform bending, from Richter (1998), to the AASHTO (2014) and AISC (2010) flexural resistances ($b_{fc}/2t_{fc} = 8.0$ to 8.1 , $D/t_w = 110$, $D/b_{fc} = 3.6$, $F_{yc} = 48.4$ ksi.	125

Figure 65 Sample cases for calculation of the AASHTO (2014) moment gradient modifier, adapted from AASHTO (2014) Article C6.4.10.....	132
Figure 66 Calculation of C_b by AISC (2010) and AASHTO (2014) for several representative design examples.....	134
Figure 67 Cross-sections used in the example C_b calculations.....	135
Figure 68 Simple-span I-girder and critical moment envelope for example calculation of LTB effective length factor K	142
Figure 69 Conceptual mapping of a tapered-web I-section member subjected to bending moment to an equivalent prismatic member.....	148
Figure 70 Ratio of elastic LTB stress at the section with the largest moment M_2 to the LTB stress determined assuming that the member is prismatic with the larger cross-section throughout the unbraced length (adapted from Carskaddan and Schilling (1974) and Dalal (1969)).	152
Figure 71 Comparison of the AASHTO (2014) one-third rule equation to the theoretical fully-plastic cross-section resistance for several doubly-symmetric noncomposite compact-flange, compact-web I-sections (adapted from White and Grubb (2005)).	158
Figure 72 Sketch of a fully plastic stress distribution, including flange lateral bending.	159
Figure 73 Assumed tension field used in determining the angle θ implicit in Basler's (1961) shear postbuckling strength (Eq. (8)), and used in determining the "true Basler" shear resistance (Eq. (9)).....	162
Figure 74 Normalized transverse stiffener bending rigidity I_t / Dt_w^3 necessary to develop the AASHTO (2014) web shear buckling resistance V_{cr}	166
Figure 75 Idealized free-body diagrams of the slab and the steel I-section for a single I-girder taken from approximately one-half of the span of a hypothetical simple-span composite I-girder bridge.	167
Figure 76 Plan view of the slab in the idealized free-body diagram of Figure 75.....	169
Figure 77 Plan view simplification of the free-body diagram of the slab in Figure 76.	169
Figure 78 Plan view free-body diagram of the slab between the maximum positive moment and maximum negative moment positions.	173
Figure 79 Flange local buckling resistance for box flanges in compression.	197
Figure 80 Flange effective widths, reproduced with permission from AASHTO (2014) and Wolchuk (1997).	206

Figure 81 Resistance curves for unstiffened box flanges.	207
Figure 82 Representative first-yield and fully-plastic axial force-moment strength envelopes for short compact doubly-symmetric I-section members subjected to major-axis bending.....	225
Figure 83 Representative first-yield and fully-plastic axial force-moment strength envelopes for short compact doubly-symmetric I-section members subjected to minor-axis bending.....	226
Figure 84 Representative maximum in-plane strength envelopes for strong- and weak-axis bending and axial compression on finite length column-type wide-flange members, from Maleck (2001).....	227
Figure 85 Strength interaction curves in terms of different calculated moments, $M_1 = HL/4$, $M_u = M_{2,elastic} = M_1 + P\delta_{2,elastic}$ and $M_{2,inelastic} = M_1 + P\delta_{2,inelastic}$ for the Figure 84 example beam-columns subjected to minor axis bending.....	228
Figure 86 Representative first-yield and fully-plastic axial force-moment strength envelopes for a short compact singly-symmetric I-section member.	230
Figure 87 Comparison of a representative strength envelope for a hypothetical simply-supported finite-length beam-column with noncompact and/or slender cross-section elements, the AISC (2010) strength interaction curves (Eqs. (5.6.2-1)), and the cross-section yield and fully-plastic strength.....	231
Figure 88 Representative simply-supported Tee-section member considered by Galambos (2001a) (WT18x67.5, $F_y = 50$ ksi, $L = 20$ ft).....	232
Figure 89 Effect of relaxing the plate slenderness limits by use of $f_a + f_b$ rather than F_y in Eqs. (5.2.4-4), (5.2.4-19) and (5.2.4-20) (the use of f_a in Eq. (5.2.4-17) and $f_a + f_b/3$ in Eq. (5.2.4-19) has a similar effect).....	235
Figure 90 Theoretical elastic out-of-plane strength envelope for simply-supported doubly-symmetric I-section beam-columns versus the base AISC (2010) beam-column strength interaction curve.....	238
Figure 91 Beam-column resistances under tensile and compressive axial force (tension is shown as negative) and uniform primary bending (W16x57, $F_y = 50$ ksi, $L_b = 18.3$ ft, $C_b = 1.0$).....	239
Figure 92 Stress distributions corresponding to key points on the beam-column strength envelope.....	243
Figure 93 Strength envelope for encased or filled composite beam-column.....	244

List of Tables

Table 1 Recommended AASHTO (2014) values and equations for the shear lag factor U	55
Table 2 Effective minimum elastic moduli of prestretched structural strand and structural rope (ASTM 2004; ASTM 1998).	60
Table 3 Recommended SSRC column curves for various types of steel cross-sections, adapted from (Ziemian 2010).	64
Table 4 Approximate values of effective length factor K for cases where the rotational and/or translational end restraints are either nominally fixed or nonexistent (reprinted with permission from AISC (2010)).	65
Table 5 AASHTO (2014) values for the plate local buckling coefficient, k_c , plates supported along one edge (defined as “unstiffened” elements).	78
Table 6 AASHTO (2014) values for the plate local buckling coefficient, k_c , plates supported along two edges (defined as “stiffened” elements).	78

1.0 INTRODUCTION

The behavior of steel structures is an intricate and fascinating topic. This module is intended to serve as a guide to the AASHTO (2014) Load and Resistance Factor Design (LRFD) Bridge Design Specifications, 7th Edition, and their representation of the behavior of steel bridge systems and members. The module focuses on the structural form and function of bridge systems and members, with emphasis on strength limit states. Where relevant, recent advances in the AISC (2010) *Specification for Structural Steel Buildings* as well as findings from research developments are discussed in addition to the AASHTO provisions.

Selection of the most cost effective bridge structural systems and members is of course dependent on many factors, far beyond the fundamental behavior, which affect the overall material, fabrication, shipping, construction and maintenance costs for a given bridge. The companion Steel Bridge Design Handbook modules address these considerations. Also, steel bridge behavior is tied inextricably to the physical loadings or actions that the structure must resist, the corresponding load models implemented by the AASHTO Specifications to represent these actions, and the analysis of the structural systems to predict the overall responses and the individual component requirements. The Steel Bridge Design Handbook modules titled Loads and Load Combinations addresses the AASHTO (2014) load models and the module titled Systructural Analysis discusses methods of analysis. Service and fatigue limit states, redundancy and fracture control, and constructability are addressed in separate modules. In addition, the design of cross-frames and diaphragms and their connections, girder splices, bearings, decks and substructure units are addressed separately.

Many of the words of J.A.L. Wadell (1916), a famous engineer and teacher of the early 20th century, are still very relevant to the design of bridge structures today. Principle V in Wadell's Chapter XV on "First Principles of Designing," which he refers to as "the most important (chapter) in the book," reads:

"There are No Bridge Specifications Yet Written, and there Probably Never Will be Any, which will Enable an Engineer to Make a Complete Design for an Important Bridge without Using His Judgment to Settle Many Points which the Specifications Do Not thoroughly Cover... the science of bridge-designing is such a profound and intricate one that it is absolutely impossible in any specification to cover the entire field and to make rules governing the scientific proportioning of all parts of all structures.

The author, however, has done his best in Chapter LXXVIII of this treatise to render the last statement incorrect."

Certainly, the AASHTO LRFD Bridge Design Specifications (2014) have also done their best in this regard. Nevertheless, there are numerous areas where a broad understanding of the fundamental behavior of structures is key to the proper interpretation, application, and where necessary, extension of the AASHTO provisions. This module aims to aid the Engineer in reviewing and understanding the essential principles of steel system and member strength behavior and design.

2.0 BEHAVIOR AND STRUCTURE TYPES

There are many ways to classify steel highway bridges. Classification of bridge systems in terms of maximum achievable span lengths is possibly the most relevant pertaining to fundamentals of the structural behavior. Steel highway bridges range from minor structures spanning only a few feet over creeks or streams to major technical achievements with spans larger than 4000 feet that define the geographic regions in which they are located. For bridges with spans ranging up to about 400 feet, stringer systems are very common. These types of structures are very important since they constitute the majority of the highway bridges within the nation's transportation system. These types of bridges are discussed first, followed by other systems that are viable at longer span lengths. (Note that here and throughout this module, the section number of the module is not included in the citation of any equations, when the citation is located in the same section as the reference.)

2.1 Rolled I-Section Stringer Systems

Steel bridge spans smaller than about 100 feet are often achieved most economically using rolled I-section members. For the shortest spans, the efficiency of the structural system tends to play a minor role in the overall cost and competitiveness relative to other attributes pertaining to simplicity, standardization, and speed of design, fabrication, delivery and construction. AISI (2000) has developed short-span bridge plans and software that address these considerations. For the shortest spans, the primary structural members in these types of bridges are typically simple-span rolled I-beams. Both composite and noncomposite deck systems are common in these types of bridges.

Spans longer than 100 feet start to push the technical limits of rolled I-beam stringer systems. Flexibility of the structure, vibration and motion perception tend to become more significant considerations in simple-span I-beam systems as the ratio of the span length, L , to the total structural section depth, D_{total} , exceeds roughly $L/D_{total} = 25$. These limits may be extended by establishing continuity between structural elements (i.e., making the I-beams composite with a concrete deck), use of continuous spans or simple-spans for dead load that are subsequently made continuous for live load (Talbot 2005), making the I-beams integral with the substructure at piers (Wasserman 1997), or use of rigid-frame bridges in which major structural elements of the superstructure and a portion of the substructure are steel I-sections (Heins and Firmage 1979). In addition, other modifications to the structural system are possible such as the use of cover plates within negative moment regions and/or longitudinal post-tensioning (Troitsky 1990, Xanthakos 1994). However, these modifications have only a minor influence on the structure stiffness and dynamic characteristics, and their cost may often outweigh their benefits. Generally, one can achieve the largest overall stiffness for a minimum constant depth by using composite continuous spans with integral piers, and by applying AASHTO (2014) Appendix B6 to allow for minor inelastic redistribution of the interior pier moments. Nevertheless, L/D_{total} values larger than about 35 are exceedingly difficult to achieve in stringer-type systems by any of the above measures. Also, as discussed in Stringer Bridge module, where the depths are not limited due to clearance restrictions, etc., often the greatest economy can be achieved by using sections that are deeper than suggested by the above maximum L/D_{total} limits.

2.2 General I-Section Stringer Systems

2.2.1 Overview

Welded plate I-girders become an attractive option at span lengths within the upper range applicable for rolled I-beams. Furthermore, depending on the costs of welded I-section fabrication versus the production costs of rolled I-shapes, welded I-section members can be cost-effective at smaller span lengths. Figure 1 shows a typical composite rolled I-beam or welded I-girder bridge cross-section. In this system, the I-sections are spaced such that the deck spans between them. The I-section members are referred to generally as girders in the following discussions.

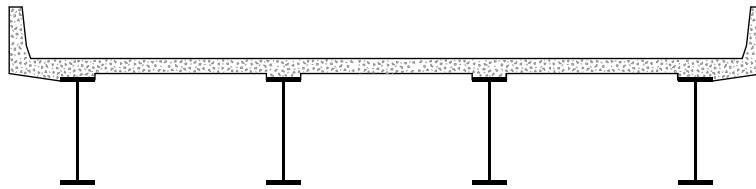


Figure 1 Typical composite rolled I-beam or welded I-girder bridge cross-section.

Cast-in-place composite concrete slabs may be designed in straight bridges of these types, without skew or with small skew, using the AASHTO (2014) Article 9.7.2 Empirical Design rules. AASHTO (2014) does not explicitly restrict the use of empirical design to straight bridges with small skew; however, it does require additional reinforcing in the end zones if the skew exceeds 25 degrees. Additional considerations may be prudent in some cases with horizontally curved bridges. The slab empirical design rules account for beneficial arching action in transferring loads to the girders, and are allowed for cast-in-place slabs up to approximately 13.5 feet spacing between the girders, S , or a maximum ratio of the girder spacing to the slab thickness of $S/t_s = 18$, among other requirements.

Precast decks and a number of other deck systems also are capable of spanning a large S with relatively small t_s . Wider girder spacing potentially eliminates one or more extra girder lines and the corresponding cross-frames and bearings, and also tends to give a more efficient structural system. This is because the live loads are positioned to produce the maximum response in each girder, but they do not generally produce the maximum effects in all the girders at a given bridge cross-section simultaneously. With wider girder spacing, the sum of the girder resistances in a given bridge cross-section will tend to be closer to the total required live load capacity for the various positions of the live load. Trade-offs associated with wider girder spacing include increases in deck thickness, and reinforcing and forming costs (which are typically offset by reduced labor costs). Also, future staged redecking considerations may influence how many girders may be removed from the cross-section. Cross-frame forces tend to be larger with wider girder spacing, due to larger differential live loads and live load deflections of the girders, as well as larger stiffness of the cross-frames relative to the slab. Interestingly, the design efficiency associated with wider spacing in ordinary stringer bridges is no longer impacted by the approximation of slab shear lag effects by effective width rules. This consideration is discussed below.

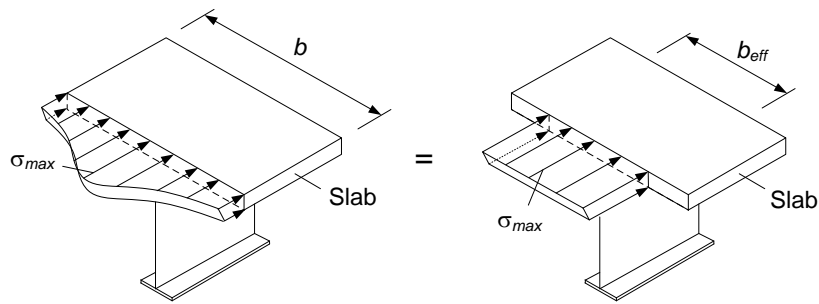


Figure 2 Effect of Shear lag.

Prior AASHTO Specification provisions, such as AASHTO (2004) Article 4.6.2.6.1, restricted the effective width of the slab, b_{eff} , to a maximum of $12t_s + b_f/2$ or $1/4$ of the effective span length for interior girders, along with a comparable limit for exterior girders, to account for the effect of shear lag in the slab (illustrated in Figure 2). Basically, slab flexural stresses arising from major-axis bending of the girders are developed by shear stresses in the plane of the slab. This can be seen by making a longitudinal cut to isolate a portion of the slab from the rest of a given girder and drawing a free-body diagram. Shear deformations associated with these shear stresses tend to reduce the magnitude of the flexural stresses at the slab locations farther from the girder webs. The prior slab effective width rules limited the slab contribution to the composite section in some situations with wider girder spacing.

The 2008 interims of Article 4.6.2.6.1, which have been retained in subsequent editions of the AASHTO LRFD Bridge Design Specifications, replaced the above traditional rules simply with the use of the full tributary width perpendicular to the axis of the member. The new provisions are applicable to all concrete deck slabs in composite or monolithic construction, except that separate slab effective width requirements are retained for segmental concrete box and single-cell cast-in-place box beams, orthotropic steel decks, and for transverse floor beams and integral bent caps. In negative moment regions, the new simplified rule is based on the use of the idealized fully-cracked section for cross-section level resistance calculations under both service and strength loading conditions. However, for the structural analysis, AASHTO (2014) Article 6.10.1.5 states that the concrete deck is to be assumed fully effective (uncracked) over the entire bridge length for structural analysis, using specified concrete modular ratios for short- and long-term loadings applied to the composite bridge. These changes in Article 4.6.2.6.1 are based on extensive studies by Chen et al. (2005) and others. Chen's studies indicate that the use of a slab effective width b_e equal to the full tributary width has a negligible influence on the design calculations relative to the physical bridge response in the above permitted situations. The research by Chen et al. (2005) demonstrated that there is no significant relationship between the slab effective width and the slab thickness within the practical ranges of the deck proportions in ordinary stringer bridge systems, as implied by previous Specifications.

Similar to rolled I-beam bridges, the structural efficiency of welded I-girder bridges can be improved substantially by establishing continuity between the various components or sub-systems. Also, welded I-girder cross-section proportions are typically changed at field splice locations or at the limits of available plate lengths. The use of cross-section transitions at other

locations may or may not be cost effective depending on the specifics of the bridge and the economics of welding and inspecting a splice compared to the cost of extending a thicker plate. The Steel Bridge Design Handbook module titled Stringer Bridges discusses these considerations in detail. Variable web depth members with haunches over the interior supports may be used in continuous spans, thus following the shape of the elastic moment envelopes more closely. Hall (1992) indicates that haunched composite girders are usually advantageous for spans in excess of 250 feet, when the depth is limited in a portion of the span, or when a decrease in the positive moments reduces critical fatigue stresses. Current rules of thumb place this limit at 350 to 400 feet (Pfeifer 2006). Up to these span lengths, AASHTO (2014) Appendix B6 can be used to design the lightest straight I-girder bridges with limited skews using prismatic sections between the field splice locations.

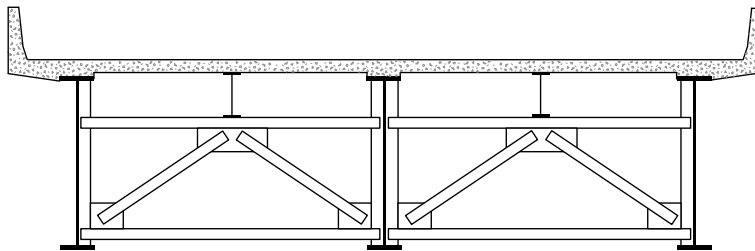


Figure 3 Typical composite I-girder substringer system.

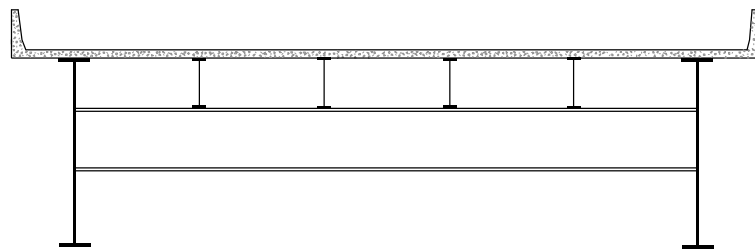


Figure 4 Two-girder system with floor beams and stringers.

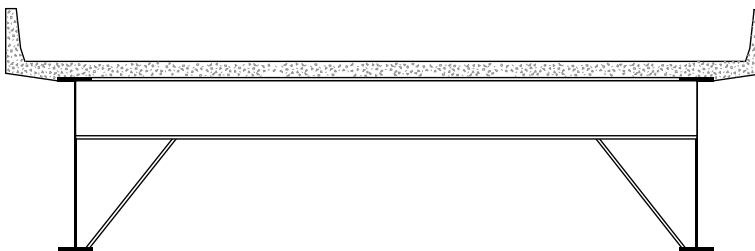


Figure 5 Two-girder system with cross-girders.

At spans exceeding about 250 feet, the I-girders in a bridge cross-section such as the one shown in Figure 1 need to be spaced relatively close together compared to their depths for the deck to span efficiently between the girders while keeping its thickness low to minimize the dead weight. In these cases, it may be attractive to use a girder-substringer system such as in Figure 3. In this type of system, shallower rolled I-section substrings are framed over the top of the cross-

frames to support the deck. Both the main girders and the substringers may be designed compositely. In addition, it is advantageous for the substringers to be continuous over two or more of their supports.

For larger spans, the Engineer may consider using multiple substringers between each of the main girders. This eventually leads to the consideration of two-girder systems with floor beams and stringers, as shown in Figure 4. A two-girder system with cross-girders (Figure 5) is another option (Brown 1992). In this system, the bridge deck spans longitudinally between the cross-girders. As such, the deck must be designed for the combined loading due to the local bending between the cross-girders plus the stresses due to overall composite action with the primary girders. Conversely, for the systems shown in Figure 1 through Figure 4, the local bending of the deck is predominantly in the transverse direction; hence, it may be considered separately from the composite action with the main girders. Furthermore, in the system shown in Figure 5, the shear connectors near the intersection of the main- and cross-girders are subjected to significant combined longitudinal and transverse loads. Because of the above complexities, the system in Figure 5 requires greater design effort. However, it may be a viable option in some longer-span applications such as cable-stayed bridges. For these types of structures, design of the deck to span in two-way action between the main girders and the cross-girders also may be an option worth considering. Another significant factor in designs such as those shown in Figure 4 and Figure 5 is that two-girder systems are often identified as being nonredundant, and thus fracture critical. Nevertheless, fractures have occurred in the primary members of a number of two-girder bridges in the past without precipitating the collapse of the structure (Fisher et al. 1988, Fisher et al. 1977). Redundancy considerations and fracture control are discussed in detail in the Steel Bridge Design Handbook module titled Redundancy.

I-girder bridges typically become less practical at spans above about 400 feet. Economical main I-girders at these span lengths tend to have relatively narrow flanges compared to their web depths. As such, the girders are less efficient with respect to lateral-torsional buckling. Also, the flange thicknesses start to become inordinately large, particularly for the bottom flanges in composite I-girders, and the contribution of a composite slab becomes a smaller fraction of the overall stiffness and resistance of the primary members. In addition, field splices must be located in high moment regions rather than at points of contraflexure in these longer spans. Nevertheless, the use of High Performance Steel (HPS) has allowed maximum economical span lengths to increase over past rules of thumb.

For spans somewhat beyond those of the shortest rolled I-beam systems and typically somewhat less than the largest practical spans for welded I-girders, significant site and highway geometry restrictions often lead to demands for complex bridge geometries. These include horizontally curved alignments, bifurcated structures, splayed girder arrangements, stacked roadways, unequal spans and/or significant support skew. Figure 6 shows one example of a complex framing plan for a highway exit ramp.

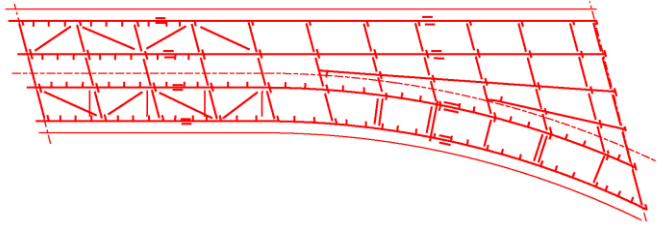


Figure 6 Example complex plan geometry (courtesy of HDR Engineering, Inc.)

2.2.2 Fundamental Behavior of I-Section Stringer Systems

An obvious behavioral characteristic of I-section members, but one that is essential to note, is their efficiency in major-axis bending. For welded I-girders, a single relatively thin web provides for efficient transfer of shear forces while the flanges, located at the top and bottom of the cross-section, provide an efficient transfer of bending moments for a given cross-section depth. Straight composite I-girder bridges without skew behave largely as a set of parallel singly-symmetric I-girders with a large top flange when the bridge is subjected predominantly to overall major-axis bending. However, individual I-section members are relatively inefficient in weak-axis bending and in torsion. As such, they need to be braced laterally by diaphragms or cross-frames, or alternatively in the final constructed configuration, the top flange needs to be embedded in or compositely connected to the slab in positive bending regions, to achieve adequate strength with respect to lateral-torsional buckling.

In horizontally curved and/or skewed bridges, the structure is commonly subjected to significant torsion. Figure 7 shows the resultant of the total dead load, W , and the resultant of the corresponding total vertical end reactions, R , for a simply-supported horizontally curved bridge with radial supports. If the resultant reactions R are assumed to act at the middle of the bridge cross-section at the end supports, one can observe that additional end torques, T , are necessary for equilibrium. These torques increase the vertical reactions on the outside girders (the ones farther away from the center of curvature) and decrease the vertical reactions on the inside girders.

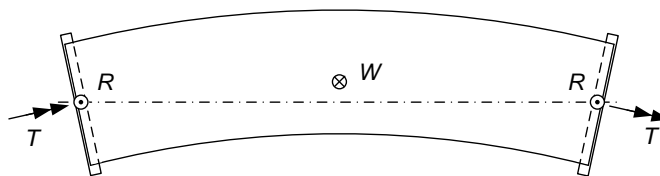


Figure 7 Plan view illustrating the required resultants for the reactions due to dead load at the ends of a simply-supported horizontally-curved bridge with radial supports.

The internal torsional resistance of horizontally curved I-girder bridges is developed predominantly via the transfer of vertical shear forces between the girders by the cross-frames and the slab as shown in Figure 8. These vertical shears, referred to traditionally as V-loads (NSBA 1996), increase the downward forces on the outside I-girders and offset the applied vertical loads on the inside I-girders. This increases the major-axis bending moments and end

reactions on the outside girders and decreases them on the inside girders. The overall internal torque on the structure at any bridge cross-section is developed predominantly by the differences in the girder shears across the width of the structure. The couples generated by the V-loads on each of the individual girder free-body diagrams of Figure 8 also resist the tendency of the I-girders to twist about their individual axes relative to the overall torsional rotation of the bridge cross-section.

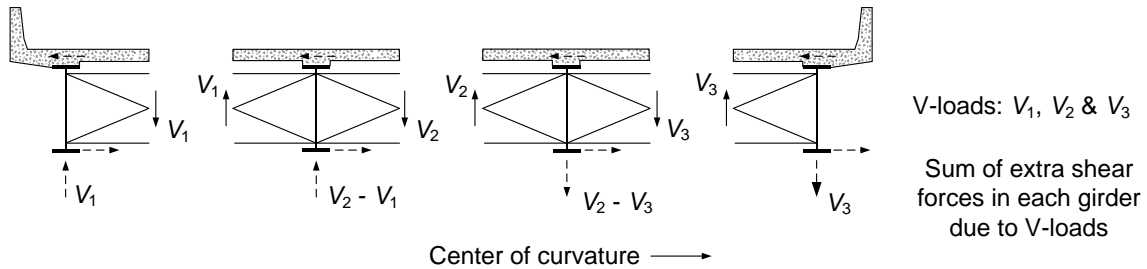


Figure 8 Transfer of vertical shear forces due to torsion (V-loads) by the cross-frames and the slab in a curved bridge

In continuous-span curved I-girder bridges, the portion of the major-axis bending moments in the outside girders due to the downward V-loads can be negative in shorter adjacent spans, due to the transfer of the associated hogging moments at the interior supports into the adjacent spans. Conversely, upward V-loads on the inside girders can induce additional positive moments in the inside girders of shorter adjacent spans due to the rotational continuity across the interior supports.

Since individual I-girders are relatively flexible and weak in torsion, curved I-girders must be supported by cross-frames or diaphragms at relatively close intervals along their lengths to avoid having large torsional stresses and rotations between these brace points. Therefore, the cross-frames are essential (primary) components in horizontally curved I-girder bridges. They are essential not only to transfer a large share of the V-loads between the I-girders but also they provide torsional support to the individual I-girders.

For cross-frame spacings necessary to ensure adequate stiffness and bending resistance in completed I-girder bridges, the girder torsional responses are dominated generally by nonuniform or warping torsion. Warping torsion is tied to the lateral bending of the I-section flanges in opposite directions due to the twisting of the member. Figure 9 illustrates the idealized case of a cantilever I-beam subjected to end torque. The warping torque is developed by the shear forces associated with the flange lateral bending moments developed at the fixed end, where warping is restrained. These forces are labeled as H_f in the figure. Figure 10 shows a simplified model for calculation of the flange lateral bending stresses on a curved I-girder subjected to uniform major-axis bending moment. Twisting of the member is assumed restrained at the cross-frame locations in this analysis; the focus is on the localized twisting of the member between the cross-frame locations. The horizontal curvature induces a radial loading effect on each of the flanges as shown in the figure. This radial loading effect in turn gives a maximum first-order elastic lateral bending stress of approximately

$$f_\ell = 0.5 \frac{L_b}{b_f} \frac{L_b}{R} f_b \quad (2.2.2-1)$$

in the flanges (White et al. 2001) where L_b is the unsupported length between the cross-frames, b_f is the width of the flange under consideration, R is the horizontal radius of curvature of the I-girder, L_b/R is the subtended angle between the cross-frame locations, and f_b is the flange stress due to major-axis bending. In traditional practice, the coefficient 0.5 often is increased to 0.6 in Eq. (1) to compensate for the simplifying assumptions utilized in the derivation. AASHTO (2014) Article C4.6.1.2.4b gives the expression for M_ℓ corresponding to Eq. (1).

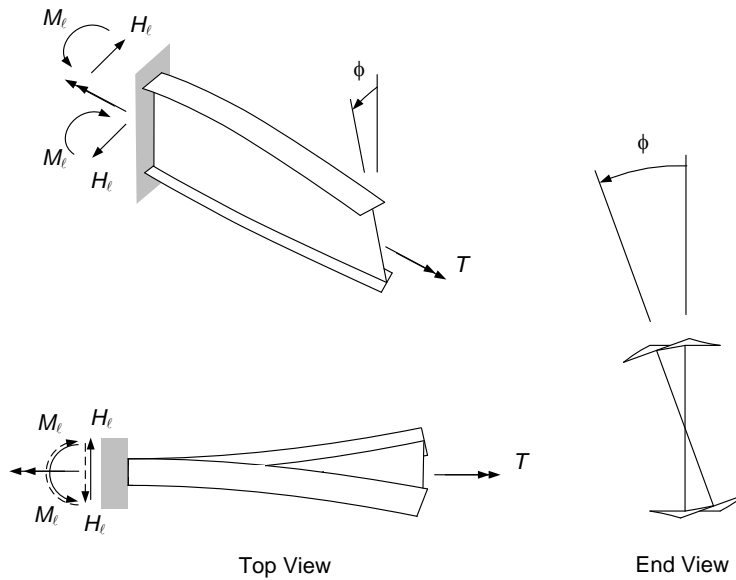
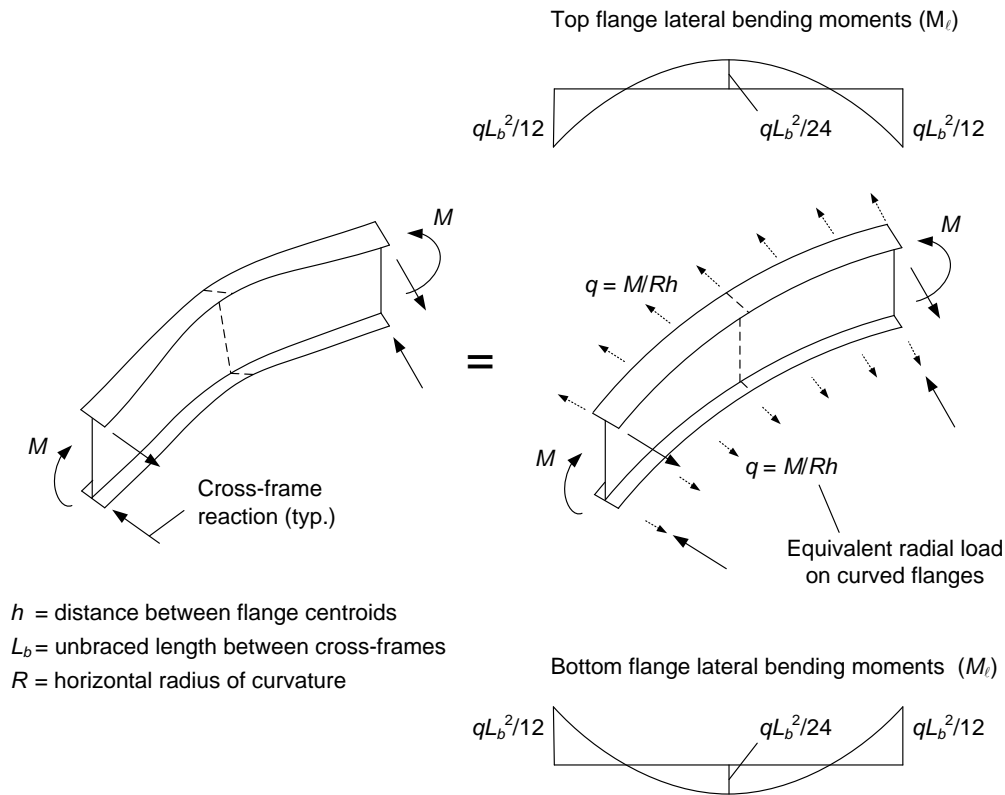


Figure 9 Illustration of twisting and warping deformation of an I-section member.

If one considers a spacing of the cross-frames such that the subtended angle between them is equal to the maximum value of $L_b/R = 0.1$ permitted by AASHTO (2014) Article 6.7.4.2 for curved I-girder bridges in the final constructed condition, then one can see that L_b/b_f must be limited to 6.0 in order to restrict f_ℓ to $0.3f_b$. At $L_b/R = 0.05$, the corresponding value of L_b/b_f increases to 12. The value $f_\ell = 0.3f_b$ is suggested as a target for preliminary design in the Commentary to this article.



Maximum flange lateral bending stress:

$$f_t = \frac{M_t}{S_{yt}} = \frac{qL_b^2/12}{A_f b_f / 6} = \frac{[M/Rh]L_b^2/12}{A_f b_f / 6} = \frac{[(f_b A_f h)/Rh]L_b^2/12}{A_f b_f / 6} = 0.5 \frac{L_b}{R} \frac{L_b}{b_f} f_b$$

Figure 10 Simplified calculation of flange lateral bending stresses on a curved I-girder subjected to uniform bending moment.

Torsional loading on fascia girders, due to eccentric concrete deck overhang loads acting on cantilever forming brackets, can be important to consider during construction in straight as well as curved bridges. Also, the use of discontinuous cross-frames in straight or curved bridges with significant support skew, while alleviating excessive cross-frame forces in certain situations, can lead to significant torsional loading and flange lateral bending on the I-girders. Furthermore, significant flange lateral bending can be induced due to wind loads acting laterally on the bridge, particularly prior to placement of the slab. In this latter case, it is sometimes beneficial to provide lateral bracing in one or a few unbraced lengths adjacent to the piers and abutments, as shown in Figure 11, to reduce the span of the I-girders in weak-axis lateral bending. AASHTO (2014) Article C6.7.5.2 recommends this practice, and suggests that this type of bracing should be considered in general to help prevent relative horizontal movement of the girders in spans larger than 200 feet. Heins et al. (1982) have shown that there is rarely a need for bottom flange wind bracing on I-girder bridges in the final constructed condition when full-depth cross-frames are used. Shorter span bridges can be designed efficiently and economically without the use of flange lateral bracing.

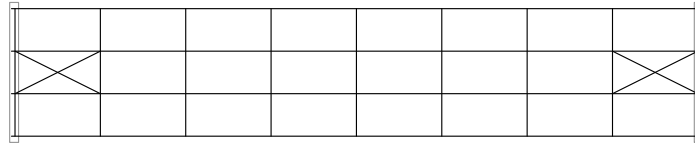


Figure 11 Use of lateral bracing within a few unbraced lengths adjacent to supports to reduce I-girder lateral bending stresses due to wind.

Article C6.7.5.2 recommends that when flange lateral bracing is employed, it should be placed near the top flange of the I-girders. Otherwise, the bracing acts with the deck in the final constructed configuration to form a pseudo box section, and thus it must be designed in general for significant live-load effects. The structural response of the completed bridge system is more efficient when the bracing is placed near the bottom flange, but the lateral bracing and its connections to the I-girders must be designed appropriately for the resulting forces.

Skewed cross-frames or diaphragms deform negligibly in their own plane when the girders experience major-axis bending rotations. Rather, at the bearing lines, these components tend to rotate about their own skewed axis and/or warp out of their plane due to the girder rotations, as illustrated by the sketch in Figure 12. This forces a coupled torsional rotation of the girders (Beckman and Medlock 2005; Coletti and Yadlosky 2005). When subjected to major-axis bending rotations at the bearing lines, the girders have to twist to maintain compatibility with the bearing-line cross frames or diaphragms. Furthermore, right (non-skewed) intermediate cross-frames in skewed bridges connect to the girders at different points along their spans. As a result, these intermediate cross-frames are subject to differential displacements as shown in Figure 13 (Coletti and Yadlosky 2005). Due to the large in-plane stiffness of the cross-frames relative to the resistance of the girders to vertical displacement at the cross-frame connections, the intermediate cross-frames (i.e., the cross-frames within the span) tend to rotate about an axis parallel to the longitudinal axis of the girders. These cross-frame rotations cause the girders and the overall bridge cross-section to twist.

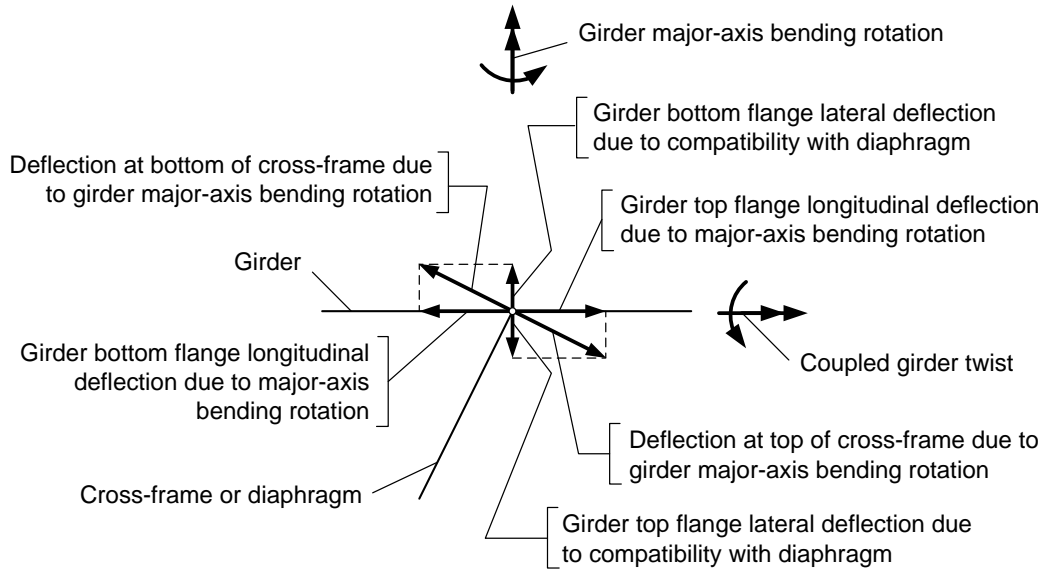


Figure 12 Plan view of deflections at the bottom and top of skewed diaphragms or cross-frames at a bearing line, forcing a coupling between major-axis bending and torsional rotation of the girders.

When one end of a cross-frame line is close to the vertical supports while the other end frames into the girders at a significantly larger distance into the span (see Figure 14a), relatively large forces are attracted to the cross-frame members. When the skew angle is larger than 20° , in which case AASHTO (2014) requires that the intermediate cross-frames must be perpendicular to the girders, the cross-frame member forces may be reduced, at the expense of larger flange lateral bending in the I-girders, by removing the cross-frames that frame into the girders closest to the supports or by using staggered cross-frames as illustrated in Figure 14b. Another way of reducing the cross-frame member forces near the supports, as well as to eliminate a large number of cross-frames, is to use lean-on bracing concepts. The use of lean-on bracing is discussed subsequently in Section 4.2 of this module.

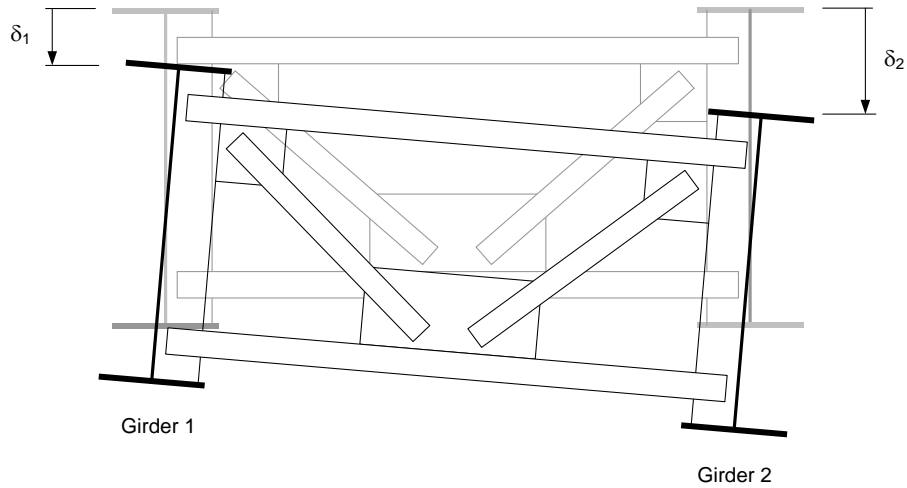


Figure 13 Cross-frame, bridge cross-section, and girder torsional rotations due to differential girder displacements in skewed bridges (Coletti and Yadlosky 2005).

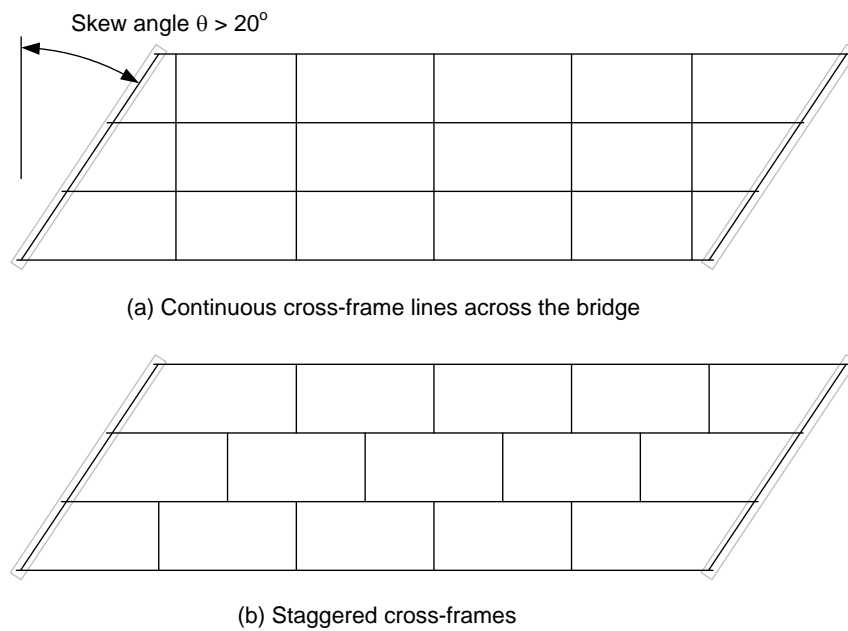


Figure 14 Use of staggered cross-frames to reduce the forces attracted to the cross-frame members near the supports in skewed I-girder bridges.

2.2.3 Integral Piers and Abutments

The use of integral piers allows the Engineer to remove skewed interior support conditions by moving the pier cap up into the superstructure and using a single column pier as shown in Figure 15 or a straddle bent as shown in Figure 16. Continuity of the cap with the pier as shown in Figure 15 maximizes the pier column efficiency by approximately halving the longitudinal moments compared to conventional cantilever columns. Furthermore, integral pier caps help satisfy vertical clearance requirements and improve the design aesthetics. Abu-Hawash et al. (2005) suggest that redundancy requirements at integral steel pier caps can be satisfied by using twin HPS I-girders.

In addition, jointless bridge decks and integral abutments are used commonly in many U.S. states for steel stringer-type bridges having maximum total lengths from 250 up to 400 feet (Wasserman 1987; Wasserman and Walker 1996). In these bridges, the girders are encased in the abutments at the ends of the structure, thus eliminating joints that potentially leak and damage the girder ends, and are costly to maintain. Thermal movements are accommodated within the foundation, and are assumed unrestrained in the design of the superstructure. Figure 17 shows a typical integral abutment detail for a steel I-girder bridge. Various devices are utilized by different organizations to accommodate the thermal movements without causing damage to the substructure or superstructure. These include: (a) limiting the bridge length, skew and/or horizontal curvature, (b) use of select backfill materials and/or uncompacted backfill, (c) spanning the area disturbed by the foundation movements immediately behind the abutments with the approach slab, thus avoiding settlement of the slab and the associated surcharge loads, (d) limiting the foundations to a single row of vertical piles, (e) specifying the pile type and requiring a minimum pile length, (f) orienting vertical H-piles such that they are subjected to weak-axis bending due to the longitudinal movements, (g) providing a hinge detail within the abutment to limit the moment developed at the tops of the piles, (h) anchoring the approach slab to the superstructure with a detail that allows rotation of the approach slab at the abutment, to accommodate settlement of the approach fill and (i) provision of an expansion joint at the roadway end of the approach pavement (FHWA 1980; Wasserman 1987; Wasserman and Walker 1996; Weakley 2005; Yannotti et al. 2005).



Figure 15 Typical post-tensioned concrete integral bent cap with a single column pier (Wasserman 1997) (courtesy of Tennessee DOT and NSBA).

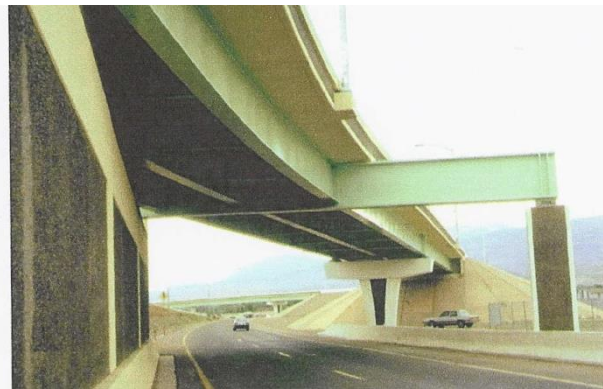


Figure 16 Straddle bents with integral steel pier caps (Abu-Hawash et al. 2005) (courtesy of Iowa DOT, HDR Engineering, and NSBA).

In cases involving longer bridges, larger skew angles, abutments resting on rock, massive cantilever abutments, etc., where the foundation is less likely to accommodate the required movements, semi-integral abutments are a second option to eliminate deck joints. In this case, the girders typically are integral with the backwall, but the required movements are accommodated by separating the backwall from the abutment stem, as shown in Figure 18. In semi-integral abutments, the girders are seated on expansion bearings.

2.2.4 Temperature Movements

In bridges where expansion joints are required, orientation of the bearings toward a fixed point allows the bridge to expand freely in both the longitudinal and transverse directions. In curved bridges, this is accomplished by orienting the bearings to permit expansion along a chord that runs from the fixed point to the bearing element under consideration, as shown in Figure 19 (NSBA 2004). This bearing arrangement does not eliminate thermal stresses due to a temperature differential through the depth of the superstructure. AASHTO (2014) Article 3.12.3 provides requirements for consideration of these thermal effects, but the commentary to this section indicates that these effects may be neglected at the discretion of the bridge owner for cases such as multi-beam bridges, where experience has indicated successful performance without their consideration.

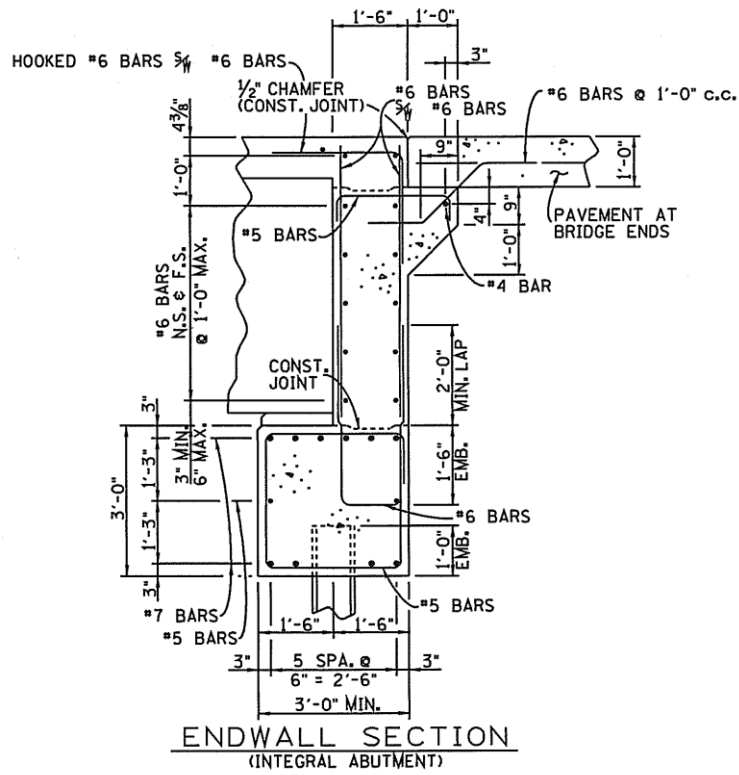


Figure 17 Typical integral abutment detail (courtesy of Tennessee DOT).

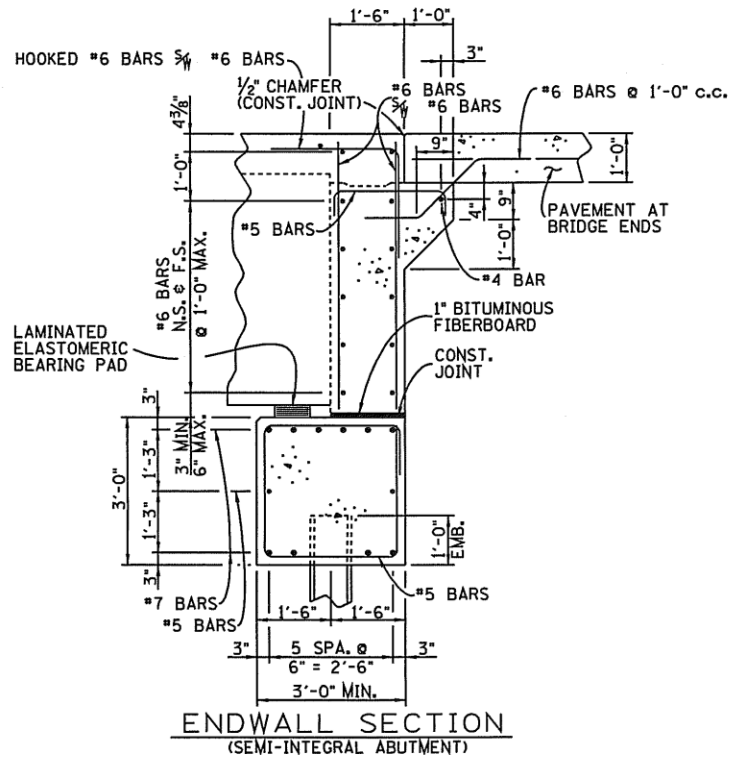


Figure 18 Typical semi-integral abutment detail (courtesy of Tennessee DOT).

Poellot (1997) describes one variation of the above approach used by the Pennsylvania DOT. In this approach, an interior support in a continuous-span unit is fixed in the tangential direction but is freed to move radially. The end bearings are fixed in the radial direction and are freed to move tangentially. Other interior bearings are designed as “floating,” or free to move in all directions. Both the above chord method and the Pennsylvania method are essentially statically determinate and therefore do not develop any forces due to uniform temperature change. The Pennsylvania method eliminates potential misalignments of the roadway at the abutments by allowing radial movements at the interior supports rather than at the end bearings.

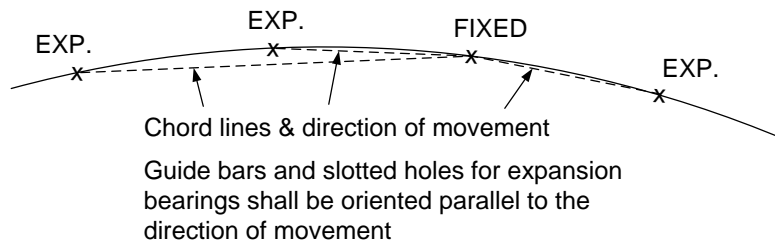


Figure 19 Bearing orientation to accommodate thermal movement on a horizontally curved alignment (NSBA 2004).

2.3 Box-Section Stringer System

For bridges subjected to significant torsion, box-girders provide a more efficient usage of material. Because of their significant torsional stiffness, box girders are also better suited for cantilevering during construction and generally exhibit smaller deflections during erection handling. Curved I-girders typically must be connected with cross-frames to ensure their stability, but they are more easily deformed to fit up with the other deflected portions of the partially completed structure during erection.

Box girders resist torsion predominantly by uniform or St. Venant torsional shear stresses that act circumferentially around their closed *cross-section periphery* as shown in Figure 20. For practical bridge box cross-sections, the warping constant is essentially zero and therefore the warping stresses associated with the thin-walled beam theory response are small. Nevertheless, distortion of the cross-sectional shape in box girders leads to important plate bending and normal (warping) stresses (see Figure 20). The magnitude of these stresses must be limited by providing intermediate internal cross-frames to maintain the cross-sectional geometry of the box.

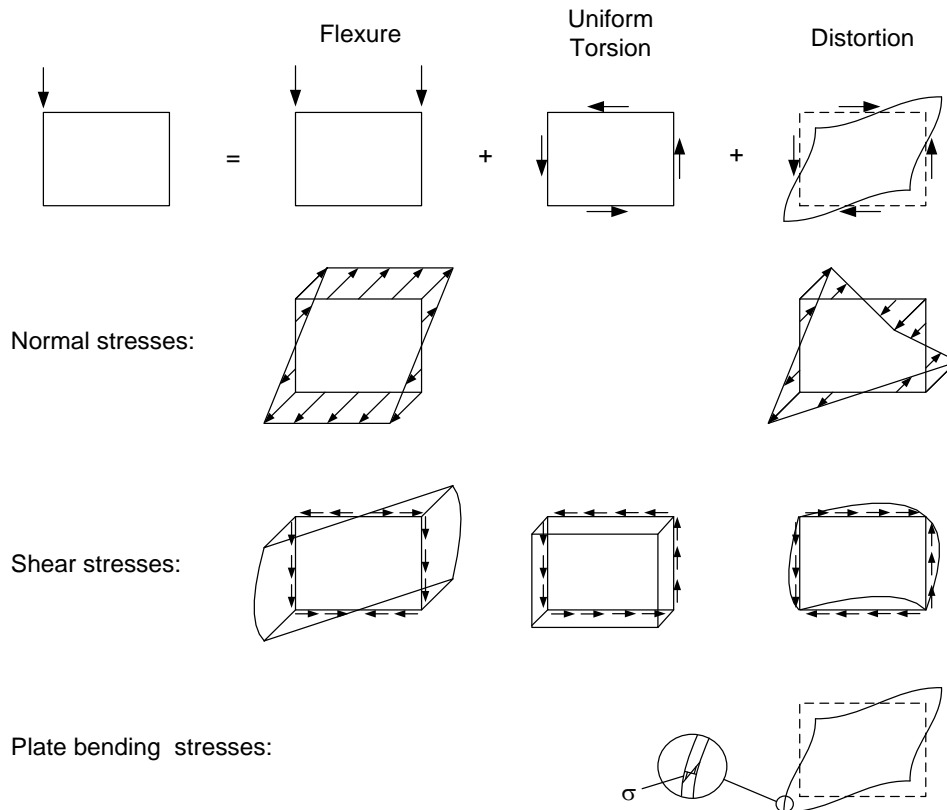


Figure 20 Stresses in a single box girder subjected to an eccentric load.

Box girders are also an efficient option in bridges requiring shallow section depths. Their flanges can be made much wider than in I-girders of comparable depth, thus avoiding the need for inordinately thick flanges with shallow-depth I-girders. Although AASHTO (2014) Article 2.5.2.6.3 does not suggest optional L/D limits for steel box-girder bridges, it does suggest a

maximum limit of $L/D = 40$ for continuous-span adjacent box beams in prestressed concrete. This limit also appears to be a reasonable maximum for continuous-span steel boxes. However, box girder web depths usually should not be less than 5 feet to facilitate fabrication and inspection (Hall 1997; Kase 1997). Also, Article 2.5.2.6.3 suggests that girder depths generally should be larger in curved bridges to help control relative girder deflections. Due to these requirements, steel box girders are used mostly for spans larger than 125 to 150 feet.

Box girders are somewhat less efficient than I-girders in shorter spans having relatively small torsion and/or liberal depth requirements, essentially because they have two webs. Furthermore, support skew in box girder bridges results in high localized stresses that are difficult to analyze and are difficult to design for. Due to this complication, Poellot (1997) states, “I-girders often provide the best solution for skewed bridges.” Article C6.11.1 of AASHTO (2014) states, “Transverse bending stresses [i.e., the plate bending stresses illustrated in Figure 20] are of particular concern in boxes that may be subjected to large torques, e.g., boxes on skewed supports.”

The torsional equilibrium of box-girder bridges is less dependent on the interaction between the girders, i.e., the transfer of the V-loads shown in Figure 10. The significantly higher torsional stiffness of individual box girders allows them to develop substantial St. Venant torques that resist the overall torsion on the structure. This reduces the differences in the major-axis bending moments across the bridge width caused by the overall torsion and the transfer of the V-loads in I-girder bridges. In fact, bridges supporting a roadway with single or dual traffic lanes often can be supported by a single box, assuming that redundancy (fracture critical) member considerations are addressed. Box girders are very efficient in resisting the torsion in curved bridges without the need for interaction between girders through a system of external diaphragms and cross-frames. As a result, intermediate external cross-frames often can and should be avoided. However, the Engineer should check for differential displacements between girders during construction. For example, in some cases, external cross-frames may be beneficial in limiting the differential displacements during partial width slab pours. If a pair of bearings is provided to develop a torsional reaction under each box at the supports, external diaphragms also may be eliminated at these locations unless they are needed to support an expansion joint at end supports. AASHTO (2014) requires external cross-frames or diaphragms at end supports to accommodate expansion joints and presumably to ensure robust girder end conditions. It is important to note that girder torsional rotations at the bearing lines produce rotations within the spans that add with torsional rotations due to the girder deformations.

Tub-girders (Figure 21) are the most common type of steel box cross-section in US bridge construction. The use of closed-box sections, i.e., sections with a wide steel plate for both the bottom and top flanges, is rare due to costs associated with safety requirements for working inside of these types of sections. AASHTO (2014) requires that tub girders must be constructed with a full-length top lateral bracing system with one exception – straight tub girders in which the stability of the top flanges between the diaphragms and the overall global stability of the bridge are investigated using the Engineer’s assumed construction sequence. Prior to the composite concrete deck becoming effective, girder lengths that do not have a top lateral bracing system are open sections with a shear center located below the bottom flange (see Figure 22). As

such, they exhibit significant torsional warping stresses and deformations, and their overall lateral torsional buckling resistance is substantially reduced.

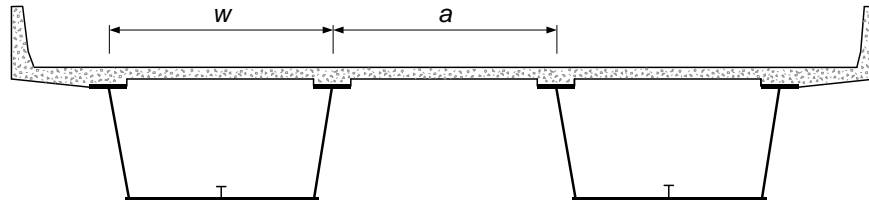


Figure 21 Representative tub-girder bridge cross-section.

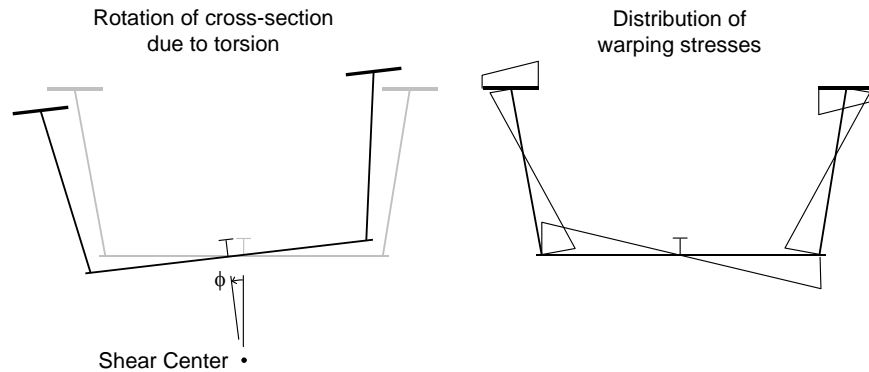


Figure 22 Shear center location and predominant torsional deformations for a tub girder section that does not have a top-flange bracing system.

The top lateral bracing system in tub-girder bridges participates with the girder top flanges in resisting major-axis flexure. Fan and Helwig (1999) provide equations for estimating the corresponding bracing member forces due to overall girder flexure. The forces in the lateral bracing system tend to be sensitive to the deck casting sequence. As such, if these members are optimized based on an assumed casting sequence, it is imperative that the casting sequence be shown on the contract plans. AASHTO (2014) Article C6.7.5.3 indicates that field tests have shown that the additional forces attracted to the top lateral system are negligible after composite action of the deck is achieved.

The participation of the top lateral bracing system in resisting the overall flexure also can induce significant lateral bending stresses in tub-girder top flanges during construction. Alternating Warren type single-diagonal lateral bracing systems tend to produce the largest flange lateral bending stresses. In curved bridges, the bracing member forces and top flange lateral bending stresses can be mitigated by the use of a Pratt type configuration for the top lateral bracing (see AASHTO (2014) Article C6.7.5.3). The bracing members are oriented based on the sign of the torque, such that the forces induced in these members due to torsion offset their compressive or tensile forces caused by overall flexure.

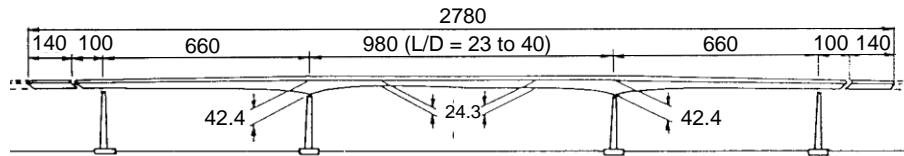
Prior to the deck being made composite, lateral bending also occurs in discretely-braced top flanges of tub sections with inclined webs, due to distributed lateral loads transmitted from the

webs. These loads come from changes in the web flexural and St. Venant torsional shears per unit length along the members. In terms of elementary beam theory, this is similar to $p = dV/dx$, where p is the transverse distributed load per unit length, V is the internal shear force and x is the position along the member length. Other sources of significant top flange lateral bending are the same as for I-section members. During construction, prior to the slab being made composite, flange lateral bending stresses due to horizontal curvature as well as due to eccentric concrete deck overhang loads acting on cantilever forming brackets are of particular importance.

Steel box girders with a normal density concrete deck are efficient up to about 500 to 700 feet span lengths. Beyond these lengths, the dead weight of the structure becomes more and more significant, and the use of an orthotropic steel deck is common. Also, other structural systems discussed below are competitive at these longer span lengths. The two longest steel box girder spans in the world are 980 and 1230 feet respectively in the Costa-e-Silva Bridge in Rio de Janeiro, Brazil (Figure 23 and Figure 24) and the Sfalassà Bridge in Calabria, Italy (Figure 25). The Costa-e-Silva Bridge has three continuous spans of 660 – 980 – 660 feet. Both of the end spans are cantilevered an additional 100 feet into the adjacent spans. The Sfalassà Bridge achieves its record span by the use of slanted leg supports, reducing the girder bending moments by arch action.

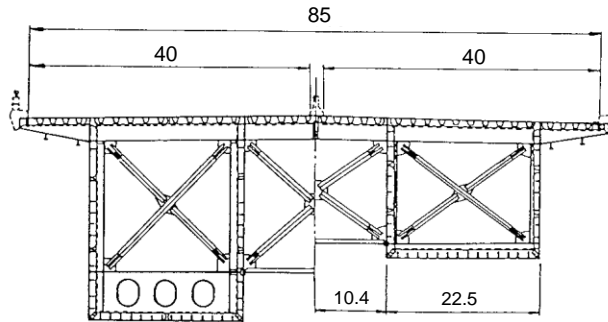


Figure 23 Costa-e-Silva Bridge in Rio de Janeiro, Brazil, second-longest box-girder span, 980 ft (courtesy of www.structurae.de)



(a) Side elevation

units: ft



(b) Cross-section

Figure 24 Costa-e-Silva Bridge side elevation and cross-section (adapted from Ito et al. (1992) and Wolchuk (1997))



Figure 25 Sfalassà Bridge in Calabria, Italy, longest box-girder span, 1230 ft (courtesy of www.structurae.de)

2.4 Truss Bridges

In all of the above bridge types, the structure tends to conform to the roadway and supports it from underneath. Through-girder bridges have been constructed in the past, but these systems are relatively inefficient since the deck cannot be used compositely. Also, all of the above structures

generally support their loads primarily by stringer bending actions. In addition, the stringers have solid webs that frame between their flange elements.

As the largest spans discussed in the above sections are approached, the Engineer must consider alternative arrangements that involve “open” webs, greater overall depth, and components that are primarily loaded in tension or compression. The use of high-strength elements becomes particularly beneficial for these systems, due to their larger depth, longer spans, higher dead-to-live load ratios and smaller live-to-dead load stresses. Furthermore, the roadway may be located above, within and or below the structural system, and the roadway geometry tends to be relatively simple compared to complex plans such as that shown previously in Figure 6. Truss and arch bridges are viable for intermediate spans beyond the above limits, while cable-stayed and suspension bridges are necessary for the longest spans. Any of these systems may be used of course for smaller span lengths, where stringer systems are viable, for various aesthetic and/or functional reasons (e.g., maximizing clearance below the roadway). Also, it is common that various combinations of the different structural systems may be used in moderate to longer-span structural systems, e.g., use of bottom flange bracing on an I-girder bridge to accomplish pseudo-box action, use of trussed arches, or use of I-girders, box-girders or trusses as deck systems and stiffening elements in cable-stayed and suspension bridges. Truss bridges are addressed briefly in this section, followed by arch and cable-supported systems in the next two sections.

Truss bridges achieve their efficiency for spanning longer distances via their light weight due to triangulation and the primary action of their members in axial tension and compression. Modern highway truss bridges are predominantly either continuous or cantilever structures. Cantilever (or Gerber) bridges have intermediate hinges between the supports in their main span and a central portion of the main span that is suspended between these points. Typical configurations of truss bridges include deck trusses, half-through trusses and through trusses, based on the location of the roadway with respect to the depth of the structure. The Ikitsuki Ohashi Bridge in Nagasaki, Japan (Figure 26) holds the record span length for a continuous truss bridge (1300 feet) while the Quebec Bridge in Quebec, Canada (Figure 27) has the longest cantilever span at 1800 feet.

Truss bridges behave essentially as closed box structures when there are four planes capable of resisting shear and the end portals participate significantly in transferring lateral loads to the bearings. Their chord and web members are typically H, channel, or box-sections. AASHTO (2014) Article 6.14.2.2 requires the members to be symmetrical about the plane of the truss. The top chord in a half-through truss is typically unsupported in the lateral direction at the panel points, and therefore must be considered as a column with elastic lateral supports at these locations. In deck trusses, the slab provides the dual function of supporting the live loads as well as bracing the top chords of the truss. A concrete deck can be made to act compositely with a deck truss, thus achieving additional structural efficiency. Also, closed-section compression chords can be filled with concrete to increase their efficiency.



Figure 26 Ikitsuki Ohashi Bridge, Nagasaki, Japan, longest-span continuous truss bridge, 1300 ft main span (www.sight-seeing.japan.com)



Figure 27 Quebec Bridge in Quebec, Canada, longest span cantilever truss bridge, 1800 ft main span (courtesy of www.structurae.de).

Trusses are an ideal system to take advantage of recent advances in high-performance steels (HPS): high strength, high toughness, and improved weldability. For example, a triangular bridge cross-section geometry with a single member along the bottom chord is possible by addressing issues of redundancy via improved HPS toughness and/or post-tensioning (see Figure 28).

The reader is referred to Kulicki et al. (2006) and to Kulicki (2000) for detailed discussions of various attributes of the design of truss bridges.



Figure 28 La Roize Bridge in France, triangular cross-section geometry using a single member bottom chord and post-tensioning strand (courtesy of HNTB).

2.5 Arch Bridges

Arches are one of the most beautiful and expressive structural forms. The arch form reduces the bending moments in the superstructure and resists loads largely by axial compression in the arch ribs, which are the distinctive primary elements of the structure. This compression must be balanced either by large horizontal thrusts at the foundation spring lines or by a tension tie between the ends of the arch. Arches that rely on their foundations to provide these horizontal thrusts are typically referred to as true arches, whereas arches in which the thrusts are developed through tie members are referred to as tied arches. In addition, arch bridges may be classified as deck, through or half-through. True arches are typically deck type, whereas tied arches are often through type. However, both true and tied arches may be constructed with the deck at an intermediate elevation between the spring line and the crown, resulting in a half-through arch. This would occur for example if the foundation needs to be located above the high-water elevation, or if variable foundation conditions require location of the abutments at a specific elevation relative to the height of the deck.

The arch rib itself may be either a truss or a girder. Accordingly, arch bridges are referred to as truss-ribbed or solid-ribbed. Another classification pertains to the articulation of the arch: fixed, two-hinged, or three-hinged. A fixed arch is designed based on complete rotational fixity at its supports. If the span is continuous but free to rotate at its ends, the structure is a two-hinged arch. Tied arches are practically always two-hinged. In some cases, e.g., during construction, a hinge is located at the crown in addition to the end supports. For instance, the top chord in a trussed arch rib may be closed at the crown to complete the erection of the structure. If the axis of the bottom chord follows the load-thrust line for the three-hinged condition, there is zero stress in the top chord and web system. The top chord and the web are stressed only under loads applied after the closure. Therefore, they can be made relatively light and the bottom chord of the rib becomes the main load-carrying member (Wright and Bunner 2006). Solid rib arches are often designed using boxes, to improve their lateral stability. These members may be fabricated with a constant

or a variable depth. Concrete-filled high-strength steel box sections can be particularly advantageous as arch ribs. The light high-strength steel box section greatly facilitates the construction of the rib, and serves to reduce the overall rib weight, while the concrete in-fill significantly enhances its compressive strength as well as the completed system stiffness.

In a tied arch, the tension tie is typically a plate or box girder. If the tie is relatively stiff in bending compared to the arch rib, it will carry a substantial portion of the live loads. Conversely, if the arch rib is stiff in bending relative to the tie, it will support a larger share of the live loads. Since the contribution of each of these elements to the live load resistance depends on their relative stiffness, it is possible to optimize their sizes based on aesthetics and/or cost. A shallow flexible tie girder requires a deep stiff arch rib, whereas a shallow flexible arch rib requires a deep stiff tie girder.

Tie girders often are considered as fracture critical members. Their redundancy can be improved by bolting their plate components together such that a fracture in one plate will be less likely to precipitate the fracture of the entire member. The tie girder can also be prestressed with post-tensioning tendons, and/or the deck can be designed to participate with the tie girder to ensure redundancy. The longitudinal tension can be minimized in a composite deck by making the connection to the girders using a closure pour after the majority of the deck has been placed (Cassity et al. 2003). The above modifications also increase the structural efficiency of the tie girders in resisting the live load. Tied arches typically experience significant variations in length of the tie under different load conditions. As such, it is common to provide deck joints at intermediate positions along the bridge length. Petzold (2005) discusses a design in which the deck joints are eliminated while the deck is structurally separated from the arch itself. The design by Cassity et al. (2003) utilizes a jointless composite concrete deck with the tie girders to resist residually applied dead loads and live loads.

Most through or half-through arch bridges are constructed with two arch ribs that are each located within a vertical plane. However, the arch ribs are sometimes inclined inwards toward each other to improve their lateral stability. This can also lead to some economy in the design of the bracing system between the arches. A few bridges have been constructed with only one rib and with roadways cantilevered on each side of the rib. In this case, both the arch rib and the deck system must have considerable torsional and lateral rigidity.

Wire rope, bridge strand or rolled sections are used typically for the hangers in tied arch bridges. Bending in the tie girders and the arch rib is reduced generally by shorter spacing of the hangers. Diagonal hangers have been used in some tied arch bridges. These types of hangers participate in transferring vertical shear forces and tend to reduce the bending moments in the arch ribs and tie girders.

Both the in-plane and out-of-plane stability of arch ribs are essential considerations. AASHTO (2014) provides limited guidance with respect to the stability design of these components. Article 4.5.3.2.2c of AASHTO (2014) gives in-plane effective length factors for use in beam-column moment amplification equations for three-hinge, two-hinged and fixed arches. It is inferred that these effective length factors also may be utilized with the AASHTO column strength equations in determining the axial resistance of prismatic solid-rib arches. AASHTO also requires that

refined methods of analysis for arches, if used, shall include second-order effects. (AASHTO (2014) defines refined methods of analysis as methods that consider the entire superstructure as an integral unit and provide directly the system and component deflections and actions.) The above approximate AASHTO equations do not account for any vertical restraint from the deck. Where such restraint exists, refined analysis methods will give larger buckling loads and smaller moment amplification.

For checking stability in the lateral direction, the effective length may be taken as the distance between the rib bracing points when a lateral bracing system of adequate stiffness is provided. Special consideration of arch-end portal areas is generally necessary. Refined analysis tools provide one way of assessing the adequacy of the lateral bracing system and the end portals.

Slant-legged rigid-frame bridges such as the one shown in Figure 29 are essentially a deck-type arch form. In this type of bridge, the primary I-girders in the center span function both to support the floor system, which spans between the rigid frames, as well as to resist the overall loads by arch action and axial compression. The slanted legs in these bridge types typically have variable depth webs. The Sfalassà Bridge shown in Figure 25 is a slant-legged rigid-frame design.

The LuPu Bridge in Shanghai, China (Figure 30 and Figure 31) holds the record span for a steel arch bridge (1800 feet). This structure is a two-hinged half-through arch with a steel box girder rib and an orthotropic deck on floor beams and longitudinal box girders.

The New River Gorge Bridge in West Virginia (Figure 32) is the longest span steel arch bridge in the United States (1700 feet). This structure is a two-hinged deck-type arch with a trussed rib. The reader is referred to Wright and Bunner (2006), Petzold (2005) and Xanthakos (1994) for detailed discussions of various attributes of the design of arch bridges. Heins and Firmage (1979) discuss the design of slant-legged rigid-frame highway bridges.



Figure 29 Slant-legged rigid-frame bridge (courtesy of HDR Engineering, Inc.)



Figure 30 LuPu Bridge in Shanghai, China, longest span steel arch, 1800 ft (courtesy of www.structurae.de).



Figure 31 LuPu Bridge deck system (courtesy of www.structurae.de).



Figure 32 New River Gorge Bridge in West Virginia, longest span steel arch in the United States, 1700 ft (courtesy of HDR Engineering, Inc.)

2.6 Cable-Supported Bridges

2.6.1 General

The lightness and overall structural efficiency of cable-supported structures are readily apparent even to non-engineers. The two major classes of cable-supported bridges are suspension and cable-stayed. The fundamental difference between these bridge types is the manner in which the deck system is supported by the cables. In suspension bridges, the deck system is supported at relatively short intervals by vertical suspenders, which in turn, are supported by the main cables (see Figure 33a). Furthermore, the main cables are relatively flexible since they are form-active; that is, their geometry is influenced significantly by the magnitude and distribution of the loadings. Conversely, in cable-stayed bridges, the deck system is supported directly from the towers by relatively straight cables (Figure 33b). This results in a stiff elastic support of the deck by the cable system compared to typical suspension bridges. The suspension bridge tends to be more efficient in supporting dead load, via the load transfer to the towers in pure tension by the funicular action of the main cables. As such, this system type is required for the longest bridge spans, where the dead load stresses become more and more dominant. Conversely, cable-stayed systems are generally more efficient in supporting live loads, which are less uniform.

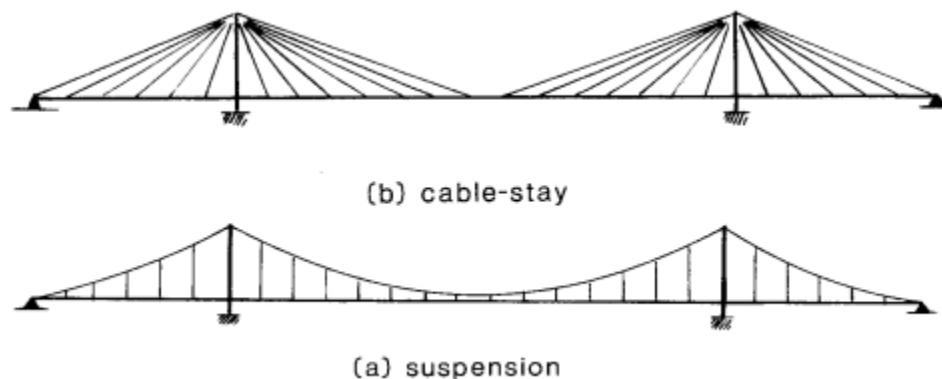


Figure 33 Cable suspended bridge systems, (a) suspension and (b) cable-stayed (reprinted with permission from Podolny and Scalzi).



Figure 34 Akashi Kaikyo Bridge, longest suspension span (6530 ft) (courtesy of www.structurae.de).

The Akashi Kaikyo Bridge on the Kobe-Naruto Route in Japan currently has the longest suspension span at 6530 feet (Figure 34), whereas, until recently, the world's longest cable-stayed span was 2920 feet in the Tataro Bridge on the Onomichi-Imabari Route in Japan. The Cooper River Bridge between Mount Pleasant and Charleston, South Carolina, has the longest cable-stayed span in the United States at 1550 feet (Figure 35). This three-span bridge has steel I-girder edge beams composite with a precast deck system.

The Sutong Bridge (Figure 36) between the towns of Suzhou and Nantong in Jiangsu province, China, has recently set a new record for a cable-stayed span-length (3570 feet). This is a three-span continuous bridge with a steel deck system. The deck system consists of an orthotropic steel box girder, 108 feet wide and 15 feet deep, accommodating six traffic lanes.



(a) Aerial view



(b) Elevation view of pylons and cable stays



(c) Installation of edge girder showing cable anchorage and studs for development of composite concrete deck



(d) Placement of a precast concrete deck panel

Figure 35 Cooper River Bridge, longest cable-stayed span in the USA (1550 ft) (courtesy South Carolina DOT).

Longer spans have been contemplated for both of the above system types; however, for larger span lengths, an increasing fraction of the allowable cable stresses is taken up by dead load. Also, the efficiency of the stays in cable-stayed bridges is reduced more and more by the sag under their self weight as the length of the stays is increased. The Akashi Kaikyo Bridge utilizes cables with a tensile strength of 260 ksi. Higher strength and/or lighter cables will be needed to achieve significantly longer spans in the future.

2.6.2 Suspension Bridges

Most suspension bridges utilize stiffening box girders or trusses at the deck level to ensure aerodynamic stability of the structure as well as to limit the local live load deformations in the deck system and to distribute these loads among the vertical suspenders. The bridge towers transfer a large vertical compression from the main cables to the foundation, and act as lateral

supports for the cables and the deck system. The main cables are tied externally to massive anchorages at the ends of the structure in most suspension bridges. However, for moderate spans, the ends of the main cables can be attached to the stiffening system, in which case the structure is self-anchored. If net uplift occurs at the end supports, a tie-down system is necessary.



Figure 36 Sutong Bridge, longest cable-stayed span in the world (3570 ft) (courtesy of New Jersey DOT).

Suspension bridges usually have three spans. When the side spans are relatively short or are not required, a single suspended span may be used. In this case, the portions of the main cables from the towers to the anchorages are essentially straight and are referred to as straight backstays. Two- or four-span suspension bridges are rare because generally it is difficult to resist the longitudinal forces at the tops of the towers resulting from live loads; due to the bending of the towers, these types of structures are highly flexible.

The center and side spans of suspension bridges are usually simply supported. The stiffening girder or truss is sometimes made continuous to reduce the difference in slopes occurring between the adjacent spans. However, this results in relatively large bending stresses at the towers. I-girders are not typically used as stiffening elements, except for short spans, because of the better aerodynamic characteristics of boxes and trusses. Typical span-to-depth ratios for stiffening girders or trusses range from about 1/60 to 1/70 of the main span (Podolny and Goodyear 2006).

Most suspension bridges utilize vertical suspender cables. However, inclined suspender cables have been used in some cases. Inclined cables are capable of transferring vertical loads by truss action between the main cables and the stiffening truss or girder.

Typical suspension bridge towers are portal frames. The towers must have a minimum width in the direction of the spans sufficient to provide stability, but the width also must be sufficient at their top to support the cable saddles. Most suspension bridges have their cables fixed at the top of the towers. The towers in longer span bridges generally have fixed bases, but rockers can be used at the base for short spans. Because of the tower relative slenderness, the bending stresses in the towers due to longitudinal deflections at the tower tops are relatively small.

The main cables in modern long-span suspension bridges usually consist of high-strength parallel wire strands. However, helical-strand type cables are used in many small to moderate-length suspension bridges. The strength and modulus of elasticity of these types of cables are reduced by a factor of about one-eighth due to the helical placement of the strands.

Suspension bridges generally require the use of deflection theory, or geometric nonlinear analysis, for the calculation of load effects. Use of linear elastic theory results in an overestimation of the system stresses and deflections.

2.6.3 Cable-Stayed Bridges

The deck system in cable-stayed bridges acts as a continuous girder over the interior piers, but with additional intermediate elastic, but relatively stiff, supports at the anchoring points of the stay cables. Typical depths of the deck system range from $1/60$ to $1/80$ of the span (Podolny and Goodyear 2006). The cables induce compressive forces within the deck system. Generally, the deck is designed to participate with the girders in supporting these forces. The overall structure is usually a closed or self-anchored system.

The designer has a wide range of attributes at his or her disposal that influence the behavior of cable-stayed bridge structural systems. These include the number and arrangement of the spans, the number and orientation of the cable-stay planes, the layout and number of stays, the type of cable, the type of deck system and the construction of the towers.

Although three-span arrangements such as those shown in Figure 33b, Figure 35a and Figure 36 are the most efficient, two-span layouts such as in Figure 37 are also feasible for cable-stayed bridges. It is usually desirable to anchor the stays within the side spans of the bridge. However, if the side-span is relatively short, some or all of the stay cables may be tied to an independent anchorage in the ground. Three-span bridges with a center span length of about 55 % of the total length and two equal side anchor spans are common (see Figure 33b). The cables tied to the end supports or to ground anchorages within the anchor spans attract larger forces than the cables attached to the deck system in these spans.

Cable-stayed bridges with more than three spans tend to induce large bending in the towers under live load. The efficiency of these structures can be improved by tying the tower tops together with horizontal cables (Figure 38a), tying the tower tops to the girder and tower intersection points at the adjacent towers (Figure 38b), adding additional tie-down piers at the span centers (Figure 38c) or adding crossing cables at the midspans (Figure 38d) (Tang 2000).

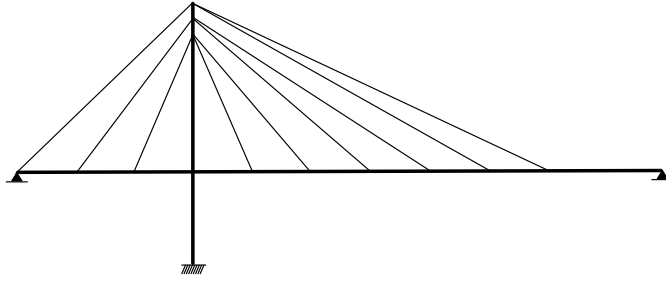


Figure 37 Representative two-span cable-stayed bridge system.

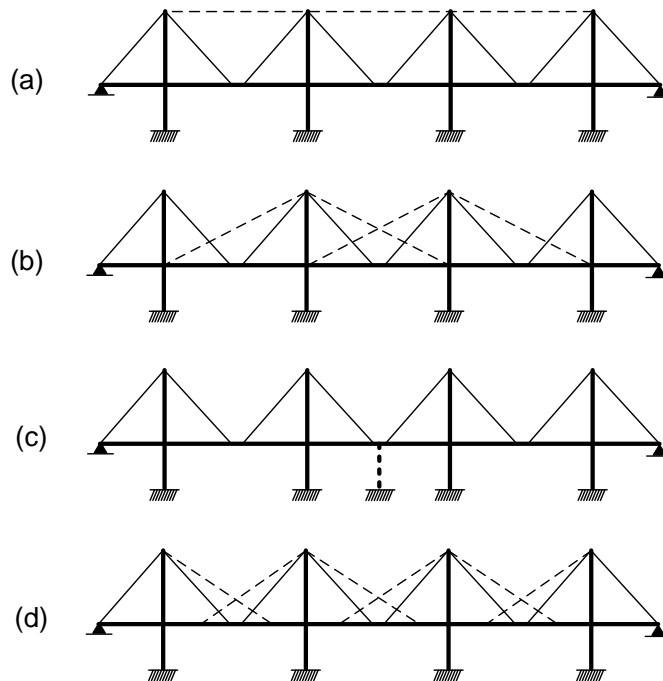


Figure 38 Methods to avoid large tower bending moments in cable-stayed bridge systems with more than three spans (Tang 2000).

The use of one plane of cable stays (Figure 39) is aesthetically pleasing and halves the number of required shafts in the towers. However, this requires the use of a torsionally stiff deck system. Conversely, the use of two planes of stays at the edges of the superstructure permits the use of torsionally flexible I-girders (see Figure 35), although the use of box girders can be advantageous with two-plane systems in certain bridges. The two-plane system can be oriented vertically or twin inclined planes can be connected from the edge of the deck to either an A or inverted Y tower. Inclined stays increase the torsional stiffness of the overall structural system.

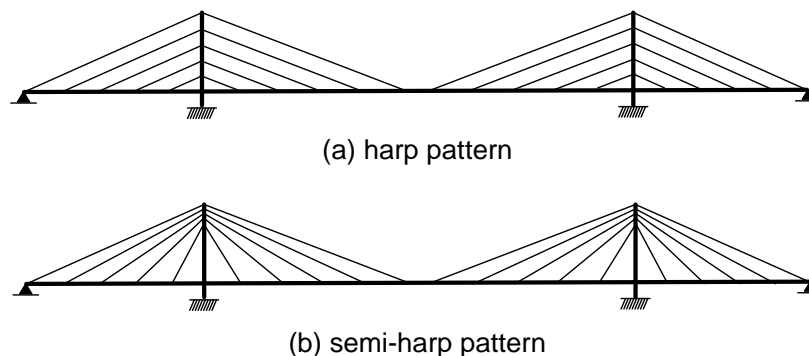


(a) Overall view

(b) Deck svstem

Figure 39 Duisberg-Neuenkamp Bridge, Duisberg, Germany, 3-span cable-stayed bridge utilizing a single plane of stay cables (1150 ft main span) (courtesy of www.structurae.de).

The two extreme layouts of cable stays are the radial pattern, in which every stay passes over the top of the tower(s) (Figure 33b) and the harp pattern, in which all the stays are parallel and are spaced roughly equally over the height of the towers (Figure 40a). Structurally, the radial pattern is the most efficient, since it avoids placing primary bending moments on the towers and gives the largest angle between the stays and the deck. Also, this pattern allows one heavy backstay cable to support the full unbalanced component of force from the other cables. However, this arrangement complicates the detailing at the top of the tower. The harp pattern induces significant bending in the tower unless every backstay cable is anchored to the ground or above a pier. It is less efficient structurally, but it is easier to detail. The semi-harp pattern is often a satisfactory compromise between these two extremes, allowing fixing of individual cables at the towers while reducing the amount of tower bending relative to that caused by the use of the harp pattern. AASHTO (2014) requires that cable-stayed bridges must be designed such that the stay cables are individually replaceable under reduced traffic loading. This requirement tends to steer the designer away from systems with only a few stay cables. Also, in most contemporary designs, all the stays are fixed to the towers.



(a) harp pattern

(b) semi-harp pattern

Figure 40 Alternative stay layouts, (a) harp pattern and (b) semi-harp pattern

Either spiral or parallel wire strand may be used for the stays in cable-stayed bridges. Spiral strand is easier to handle during construction, but has a reduced elastic modulus that depends on the lay length of the spiral. Stays composed of prestressing steels are the most prevalent in recent

cable-stayed bridge construction. The pitch of the twisted wires in common seven-wire prestressing strand is relatively long, and therefore the stiffness of the strand is close to that of straight-wire strand and the breaking strength is somewhat larger. The number of strands assembled into the stay cables varies depending on the design force. One of the key considerations in the development of the end sockets or anchorages for cable stays is the fatigue resistance. A number of systems are available that accommodate parallel prestressing strands.

Cable-stayed bridges are highly redundant structures. One important concept of cable-stayed bridge design is the freedom to assign a desired value of force to every unknown in the indeterminate structure. Therefore, the bending moments and forces under the dead load condition can be determined solely based on static equilibrium. There are an infinite number of combinations of dead load conditions for a given cable-stayed bridge. The Engineer can select the one that gives the most advantageous distribution of stresses throughout the structure when the other loads are combined with the dead load.

The construction process must reproduce the selected dead load condition. In a noncomposite bridge, the construction stage analysis, which checks the stresses and deflections in the structure at every stage of the construction, starts from the selected final condition and works backwards to determine the no-load geometry of all the structural components. However, in composite structures, creep and shrinkage effects also must be accounted for in a forward calculation starting from the beginning of the construction.

For moderate-span cable-stayed bridges, composite concrete decks are common. Orthotropic steel decks are used typically in longer spans, where the dead weight is at a more serious premium. The underlying girders are usually I-sections or box-sections; box sections are essential when torsional stiffness is required. The compression stress in the deck system tends to increase proportionally with the span length. For longer spans, the cross-section of the deck system may be increased in size near the towers, where the compression is largest, to offset the axial compression effects.

High-performance steel is ideal for design of the longitudinal girders in cable-stayed bridges. The global moments attracted to the longitudinal girders can be reduced by making the girders smaller and more flexible via the use of higher yield strengths, while influencing the overall stiffness of the structure little.

The towers in cable-stayed bridges may be steel or concrete. For moderate span lengths, steel towers may be advantageous since they can be erected more easily in a limited number of pieces. The behavior of the bridge differs depending on whether the towers are fixed or pinned at their base. Base fixity increases the moments in the towers significantly, but increases the overall rigidity of the structure. Steel towers generally must be designed for overall and local stability. The tower members typically have a variable cross-section depth, width and plate thickness over their height and are subjected to combined axial compression and biaxial bending moment. In addition, they are supported elastically by the cables and in some cases by the deck system. Therefore, it is most appropriate to design these members using a refined stability analysis.

Tang (1976) considers the elastic buckling of the flexible deck system in cable-stayed bridges. He shows that the buckling load is influenced more by the axial stiffness of the cables than the flexural stiffness of the deck system. Even if the stiffness of the deck system is neglected, the buckling load is typically much larger than the actual loads on the bridge. Model tests (Walther et al. 1999) on cable-stayed bridges with slender concrete decks and closely spaced cables have confirmed that the deck system usually is not critical with respect to buckling. However, the ultimate load capacity of the Tataru Bridge (2920 feet main span) is governed by buckling of its steel box girders. A loading test was conducted on a 1/50 scale model to verify the accuracy of the analysis and to confirm the structural capacity on this bridge (HSBA 2005).

In contrast to suspension bridge structural systems, the second-order effects on the internal forces and system deflections tend to be significant only in longer-span cable-stayed bridges. Nevertheless, similar to the behavior of arches, the internal stresses in cable-stayed bridges are generally increased due to the second-order effects. This is opposite from the behavior of suspension bridges. The geometric nonlinearity of cable-stayed bridges is small enough such that a first-order analysis is sufficient in many cases. When second-order effects are expected to be more significant, they may be accounted for by first conducting a linear analysis using the nominal geometry to determine the deflections, using these deflections to revise the geometry, and finally conducting a second linear analysis using the revised geometry. The cable stiffnesses are a nonlinear function of the cable tension, due to the sagging of the cables under their self-weight. AASHTO (2014) gives the following equation for the effective instantaneous elastic modulus of stay cables

$$E_{MOD} = E / \left\{ 1 + EAW^2 \cos^5 \alpha / 12H^3 \right\} \quad (2.6.3-1)$$

(AASHTO 4.6.3.7-1)

Where

E = modulus of elasticity of the cable

A = cross-sectional area of the cable

W = cable total weight

α = angle between the chord of the cable and the horizontal

H = horizontal component of the cable force

Note that in the above equation, and throughout this module, the AASHTO number is denoted “AASHTO” and provided for any equations defined explicitly in the AASHTO (2014) Specifications. For example, Eq. (1) above is AASHTO Eq. 4.6.3.7-1. (Note that here and throughout this module, the section number of the module is not included in the citation of any equations, when the citation is located in the same section as the reference.)

The reader is referred to Podolny and Goodyear (2006), Walther et al. (1999), ASCE (1992), Troitsky (1988) and Podolny and Scalzi (1986) for detailed discussions pertaining to the behavior and design of cable-supported bridges.

3.0 ELASTIC SYSTEM ANALYSIS, INELASTIC COMPONENT RESISTANCES

The load and resistance factor design approach implemented in AASHTO (2014) uses the general form

$$\sum \eta_i \gamma_i Q_i \leq \phi R_n \quad (3-1)$$

(AASHTO 3.4.1-1)

for assessment of the adequacy of the structure. The left-hand side of this equation represents a given design load effect, typically calculated by analysis. The right-hand side represents the design resistance corresponding to a given limit state. When used to define strength limit states, the left- and right-hand sides of Eq. (1) can be referred to as the required and the available design strengths respectively. A selected component is adequate for a given limit state if the required strength determined by structural analysis is less than or equal to its available design strength. The design load effect or required strength is determined as the largest value from various sums (or combinations) of appropriate nominal load effects, Q_i , multiplied by the load factors η_i and γ_i . The terms γ_i are scale factors that account for the variability and uncertainty associated with each of the nominal loads for a given load combination. The various load combinations account generally for a maximum lifetime event for a certain loading taken with appropriate arbitrary point in time values of other loadings. On the right-hand side of Eq. (1), the ϕ terms are resistance factors, which account for the variability, uncertainty and consequences of failure associated with different limit states. The parameters η_i increase or decrease the nominal loads based on broad considerations of the ductility, redundancy and operational importance of the structure.

With the exception of inelastic redistribution of pier section moments in specific types of continuous-span stringer bridges, and inelastic analysis for extreme event limit states (i.e., earthquake, ice loads, collision by vessels or vehicles and certain hydraulic events), AASHTO (2014) specifies the use of elastic structural analysis for calculation of the design load effects. Conversely, the nominal resistances, R_n , in Eq. (1) are based in general on inelastic behavior of the structural components. For composite stringers, the concrete section is assumed fully effective in positive and negative bending for calculation of the internal forces and moments (in the structural analysis), but it is assumed to be fully cracked for calculation of the resistances at strength limit states. These apparent inconsistencies are explicitly addressed in several locations within the AASHTO (2014) Commentary, i.e., see Articles C1.3.1, C4.1, C4.5.2.2, and C6.10.6.2.1. Simply put, the Engineer is allowed to neglect the influence of all material nonlinearity on the distribution of forces and moments within the structure up to the limit of resistance of the most critical component. Neglected effects include residual stresses in the steel, concrete cracking, and various stress contributions that are considered incidental. Numerous physical tests indicate that this approximation is acceptable. It is assumed that the resistance of the complete structure is reached when the left and right-hand sides of Eq. (1) are equal for the most critically loaded component. As explained in Article 1.3.2.4 of AASHTO (2014), multi-stringer bridges usually have substantial additional reserve capacity beyond this resistance level. This is because the live load cannot be positioned to maximize the force effects on all parts of the bridge cross-section simultaneously. However, this reserve capacity is not necessary to justify the above elastic analysis assumptions.

There are three situations in steel design where AASHTO (2014) implements specific restrictions to ensure the validity of the above elastic analysis-design approach:

1. For continuous-span girders that are composite in positive bending, AASHTO Article 6.10.7.1 limits the moment capacity to

$$M_n = 1.3R_h M_y \tag{3-2}$$

(AASHTO 6.10.7.1.2-3)

unless specific Appendix B6 requirements are satisfied that ensure ductility of the adjacent pier sections. Equation (2) is intended to limit the yielding in positive moment regions of continuous-span girders, where the shape factor M_p/M_y can be larger than 1.5, when the inelastic rotation capability of the pier sections is somewhat limited or undefined. In many cases, compact-flange pier sections in straight I-girder bridges satisfy the Appendix B6 requirements without any special modification. However, the support skew must be less than 10 degrees and the ratio of the lateral unbraced length to the compression flange width, L_b/b_{fc} , at the pier sections must be approximately 10 or less in addition to other requirements for the use of Appendix B. All continuous-span box girders are required to satisfy Eq. (2) or more restrictive limits. Equation (2) guards against significant partial yielding of the cross-section over a relatively large length within the positive moment region, where the moment diagrams and envelopes are relatively flat. This helps restrict inelastic redistribution of positive moments to pier sections that may have limited ability to sustain these additional uncalculated moments. Also, the Engineer should note that the analysis assumption that the slab concrete is fully effective in tension and compression tends to give a slightly conservative estimate of the true pier section moments, assuming that the cross-sections remain fully elastic in the positive moment regions.

2. For curved I-girder bridges, all the composite sections in positive bending are required to be considered as noncompact sections. Furthermore, the use of AASHTO (2014) Appendix A6 is not permitted for curved I-girder sections in negative bending with compact or noncompact webs. Both of these restrictions limit the calculated girder flexural resistance to a maximum potential value of

$$M_n = R_b R_h M_{yc} \tag{3-3}$$

in the absence of any flange lateral bending, where R_b is the web load shedding strength reduction factor, equal to 1.0 for noncompact and compact webs, R_h is the hybrid factor, and M_{yc} is the nominal yield moment capacity with respect to the compression flange. These restrictions are due to the limited data on the influence of partial cross-section yielding on the distribution of forces and moments within curved I-girder bridges.

Beshah and Wright (2010) and Jung and White (2010) provide extensive results from a full-scale curved composite I-girder bridge test as well as parametric extensions of these test results using refined inelastic finite element analysis. All cases considered indicate that the influence of partial yielding on the internal forces and moments is small in

curved I-girder bridges up to the limit of resistance of the most critical bridge component based on the plastic moment M_p with a reduction for flange lateral bending effects. However, the majority of these studies focus solely on simple-span bridges. Further studies are needed to address the influence of partial cross-section yielding on continuous-span curved I-girder bridges. The benefits of designing positive moment sections using the plastic moment resistance M_p or Eq. (2) can be significant, although AASHTO Article 6.10.7.1.2 specifies a reduction relative to M_p based on ductility considerations (see Section 5.3.3 of this module). No studies have been conducted to date (2010) that address the potential use of a Eq. (2) or other plastic moment-based resistance formulas for curved composite box girders in positive bending.

The Engineer should note that the resistance equations for curved I- and box-girders are based generally on some partial cross-section yielding at the calculated limit of the resistance. However, Eq. (2) and other M_p -based resistance equations rely on the development of a larger extent of yielding.

3. The maximum compression stress in the concrete deck is limited to $0.6f'_c$ under all strength loading conditions for noncompact composite I-sections and box-sections in positive bending (see Sections 5.3.3.1 and 5.3.4 of this module for the definition of a noncompact composite I-section). This limit is required to ensure linear behavior of the concrete. Furthermore, Article C6.10.1.1 of AASHTO (2014) recommends against the use of shored composite construction, which is one of the situations where this limit can potentially be exceeded. Unshored construction is considered generally more economical. Furthermore, as indicated in AASHTO (2014) Article C6.10.1.1.1a, there is limited data on the influence of concrete creep on the response of shored composite I-girders subjected to large dead load.

In addition to the above restrictions, the structural analysis is required generally to consider the separate noncomposite stresses generated in the structure due to self weight and other loadings before composite action is achieved, as well as the short and long-term stresses generated in the composite structure. Moments from these three different loading conditions may not be added for the purpose of calculating stresses, and superposition (based on small-deflection theory) cannot be applied for the analysis of construction processes that include changes in the stiffness of the structure. Long-term loading effects are considered by use of a modular ratio of $3n$, where $n = E_s/E_c$ is the modular ratio of the composite section for short term loading. Finally, Article 6.10.1.7 of AASHTO (2014) implements specific slab reinforcing steel requirements for regions subjected to negative flexure. These requirements are intended to control concrete cracking, i.e., to ensure distributed cracking with small crack widths. This helps ensure the validity of the assumption of taking the concrete as fully effective in tension for calculation of the elastic internal forces and moments.

AASHTO (2014) Article C4.5.3.1 states that small-deflection theory, or a geometrically linear or first-order analysis, is usually adequate for stringer-type bridges. The terms first-order analysis, geometrically linear analysis or small-deflection theory all indicate that equilibrium of the structure is considered on the undeflected geometry. Article C4.5.3.1 also indicates that bridges that resist loads by a couple whose tensile and compressive forces remain essentially in fixed

positions relative to each other while the bridge deflects, such as trusses and tied arches, tend to be insensitive to deformations. However, the internal forces and bending moments can be influenced significantly by second-order effects in structures with members or components subjected to significant axial compression relative to their elastic buckling resistance. Also, the internal forces in form-active structures, such as suspension bridges, are influenced significantly by these effects.

In some stringer-type bridges, construction deflections and stresses (prior to the completion of the full structure) may be influenced significantly by second-order effects. For example, the torsional deformations during construction of some curved and/or skewed I-girder bridges are sensitive to these effects (Jung and White 2010; Chang and White 2010). The influence of second-order effects on the flange lateral bending stresses can be significant in straight or curved fascia I-girders subjected to eccentric concrete deck overhang loads acting on cantilever forming brackets. In these cases, an approximate second-order analysis consisting of applying amplification factors to the internal stresses obtained from first-order methods is essential at a minimum (Section 5.3.7.2 outlines AASHTO (2014) recommendations for such an analysis). As the second-order effects become larger, the use of a refined second-order analysis is prudent.

The term second-order analysis indicates that equilibrium is evaluated on the deflected geometry of the structure. The second-order effects are the changes in the deflections, internal forces and internal moments, relative to those estimated from first-order analysis, due to considering equilibrium on the deflected geometry. First-order analysis is sufficient generally for calculation of live load effects on all stringer-type bridges in their final constructed configuration.

The component resistance equations in AASHTO (2014), and the strength limit states checks represented by Eq. (1), are based on the assumption that the second-order elastic internal stresses on the initially perfect structure (no consideration of geometric imperfections), are calculated with sufficient accuracy in cases where these effects are important. That is, initial geometric imperfections within fabrication and erection tolerances do not need to be considered in the analysis. These effects are considered in addition to the effects of initial residual stresses within the component resistance equations. Various other incidental contributions to the internal stresses are neglected generally at the discretion of the engineer. These include flange lateral bending stresses in straight non-skewed I-girder bridges, stresses due to restraint of thermal expansion, longitudinal warping stresses in boxes under strength loading conditions, and St. Venant torsional shear stresses in I-section members.

Article C6.7.2 of AASHTO (2014) states that the Engineer may need to consider the potential for problematic locked-in stresses in curved I-girder flanges or the cross-frames or diaphragms of curved I-girder bridges when the cross-frames are detailed such that they fit up with the I-girders in an idealized web-plumb position under the steel or total dead load. This article states further, “The decision as to when these stresses should be evaluated is currently a matter of engineering judgment. It is anticipated that these stresses will be of little consequence in the vast majority of cases ...” Chang and White (2010) have developed and applied prototype tools that permit the precise calculation of erection stresses and deflections in curved I-girder bridges. Their results support the above statement, although one of their examples illustrates a curved I-girder bridge where consideration of lack-of-fit and second-order effects is important.

Many of the provisions in AASHTO (2014) Chapter 4 address the appropriate assumptions and limits for the use of approximate analysis methods. The approximate analysis of stringer-type bridges using line-girder models receives substantial attention in this chapter. AASHTO Article 4.1 states:

“The primary objective in the use of more sophisticated methods of analysis is to obtain a better understanding of the structural behavior. Such improved understanding may often, but not always, lead to the potential for saving material. . . . With rapidly improving computing technology, the more refined and complex methods of analysis are expected to become commonplace. Hence, this section addresses the assumptions and limitations of such methods. It is important that the user understand the method employed and its associated limitations.”

One of the limitations of general second-order elastic analysis methods is that superposition of the effects from separate loading types is not valid. With these methods, the structure strictly must be analyzed for each load combination and load placement. However, various simplifications and approximations allow for limited superposition of certain results. For example, for a curved I-girder bridge that is sensitive to second-order effects in its noncomposite condition but insensitive to these effects after the structure is made composite, second-order analysis can be employed to determine the dead load and construction stresses. The results from a first-order geometrically linear analysis can be subsequently added to these stresses for evaluation of the composite structure (Jung and White 2010; Chang and White 2010). For suspension bridges, Podolny and Goodyear (2006) discuss commonly employed approximate linearized solutions that allow the development and use of influence lines.

4.0 OVERALL SYSTEM BUCKLING VERSUS INDIVIDUAL MEMBER BUCKLING

4.1 Key Concepts

One question that has been raised by numerous organizations in the recent past is what type of analysis and/or AASHTO provision checks are sufficient to assess the overall stability of a bridge structural system during construction. For instance, what constitutes a sufficient check of the overall stability of a straight tub girder that does not have a full-length top lateral bracing system? At issue is the fact that in most cases, the overall stability of stringer-type bridges is ensured by checking member buckling resistances for the unbraced lengths between the cross-frame or diaphragm locations. However, checking of the top flanges of a single tub girder in this fashion does not generally represent an adequate assessment of the overall stability of the structure. For this type of system, a direct global assessment of the buckling load of the full structure is necessary. Yura and Widiyanto (2005) discuss a number of approximate and refined solutions for assessment of the overall buckling of tub girders that do not have a full-length top-flange bracing system. In addition, an expanded set of related recommendations have been published recently for I-girders by Yura et al. (2008). Yura and Widiyanto demonstrate that the overall elastic buckling of individual tub-girders with no top-flange bracing is represented accurately, for the case of uniform bending ($C_b = 1$), by the analytical solution for a singly-symmetric open-section member. This solution may be written concisely as

$$M_{cr} = \frac{\pi^2 EI_y}{L^2} \left\{ \frac{\beta_x}{2} + \sqrt{\left(\frac{\beta_x}{2} \right)^2 + \frac{C_w}{I_y} \left[1 + 0.039 \frac{J}{C_w} L^2 \right]} \right\} \quad (4-1)$$

(White and Jung 2003b), where β_x and C_w are respectively the coefficient of monosymmetry and the warping constant for the cross-section. These constants are determined from thin-walled open-section beam theory, e.g., see Galambos (1968) and Heins (1975). The properties I_y and J are the moment of inertia of the tub section about the axis orthogonal to the axis of bending and the St. Venant torsional constant, and L is the overall span length. Yura and Widiyanto (2005) also illustrate that modified forms of Eq. (1), which account for the influence of pre-buckling displacements on M_{cr} , have little practical significance because of necessary stress and deflection limits. In addition, they point out that the alternate modified forms are not appropriate for cambered girders. The Engineer should note that Eq. (1) applies only to tub girders that do not have top-flange bracing. Tub girders designed with a full-length top lateral bracing system satisfying the AASHTO (2014) requirements do not need to be checked for overall lateral-torsional buckling. In addition, it should be noted that this equation applies to both straight and curved tub-girders. Similar to the fact that the in-plane *elastic* flexural buckling of a beam-column is relatively insensitive to the applied bending moments (McGuire 1968), the overall elastic buckling load of structural members generally is insensitive to horizontal curvature.

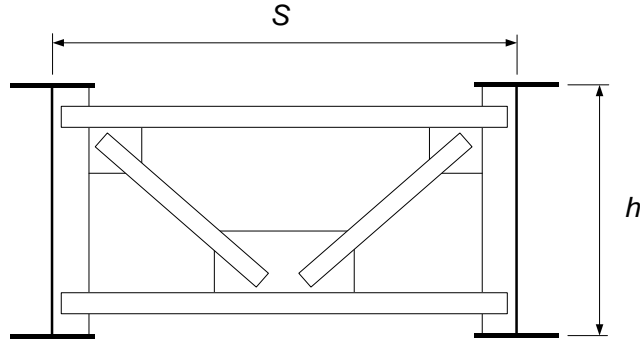


Figure 41 Dual-girder subassembly composed of two equal-size doubly-symmetric I-girders

Yura and Widiyanto (2005) and Yura et al. (2008) also show that twin-I-girder systems also can be susceptible to overall lateral-torsional buckling in some cases where the spacing between the girders is small relative to the span length. That is, their equations show that in some cases, the stability of two I-girder assemblies connected together by cross-frames may be governed by overall buckling rather than by buckling of the individual I-girders between the cross-frame locations. The elastic critical moment of the simply-supported doubly-symmetric two-girder system shown in Figure 41 is obtained for the case of uniform bending simply by substituting $I_y = 2I_{yo}$, $J = 2J_o$ and $C_w = 2I_{yo} (h/2)^2 + 2I_{xo} (S/2)^2$ into the classical elastic LTB equation from Timoshenko and Gere (1961),

$$M_{cr} = \frac{\pi}{L} \sqrt{EI_y GJ + \left(\frac{\pi E}{L}\right)^2 I_y C_w} \quad (4-2)$$

Where

J_o = St. Venant torsional constant

I_{yo} = weak-axis moment of inertia

The above expression for C_w is obtained from thin-walled open-section beam theory for the equal-size doubly-symmetric two-I-girder cross-section which gives

$$M_{cr} = \frac{2\pi}{L} \sqrt{EI_{yo} GJ_o + \left(\frac{\pi E}{2L}\right)^2 I_{yo} (I_{yo} h^2 + I_{xo} S^2)} \quad (4-3)$$

By retaining only the I_{xo} term from Eq. (3), Yura and Widiyanto (2005) and Yura et al. (2008) obtain the following simplified expression, which is typically only a few percent conservative:

$$M_{cr} = \frac{\pi^2 SE}{L^2} \sqrt{I_{yo} I_{xo}} \quad (4-4)$$

In some two-girder cases, M_{cr} from Eq. (4) will be smaller than the elastic buckling capacity of the girder unbraced lengths between the cross-frames. That is, the lateral-torsional buckling strength of two I-girders, connected together by cross-frames for handling as a single unit during erection, is governed by overall buckling of the assembly, not by the buckling of the members between the brace points. This can be demonstrated by considering the conditions that make M_{cr} from Eq. (4) smaller than the following simplified form of the elastic critical moment for lateral-torsional buckling of the doubly-symmetric I-section members between the cross-frames:

$$M_{cr} = \frac{\pi^2 EI_{yo} h}{L_b^2} \quad (4-5)$$

After algebraic manipulation, one can observe that the buckling of the two girders as a system is more critical when

$$\left(\frac{L_b}{L}\right)^2 < \frac{h}{S} \sqrt{\frac{I_{yo}}{I_{xo}}} \quad (4-6)$$

Furthermore, if one substitutes the approximations $I_{yo} = b_f^3 t_f / 6$ and $I_{xo} = b_f t_f h^2 / 2$ into Eq. (6), this equation simplifies to

$$\frac{L_b}{L} < 0.6 \sqrt{\frac{b_f}{S}} \quad \text{or} \quad \frac{L_b}{L} < 0.6 \sqrt{\frac{b_f h}{h S}} \quad (4-7)$$

The Engineer may note that Eq. (7) is based on the assumption of uniform bending throughout the span length L . If one considers the influence of moment gradient, the critical moment for overall buckling of the system (Eq. (4)) tends to be increased more than that for the buckling between the critical cross-frame locations (Eq. (5)). However, continuity of the critical unbraced segments with adjacent unbraced lengths, which is neglected in Eq. (5), tends to offset this moment gradient effect. Therefore, Eq. (7) gives a reasonable estimate of the ratio L_b/L below which the twin-girder system buckling moment is smaller than the moment at the buckling of the individual unbraced lengths between the cross-frames.

Figure 42 illustrates the determination of whether system buckling or buckling of the girders between the cross-frames governs for two example cases based on Eq. (7). The plot on the left shows the L_b/L limit versus the girder depth-to-flange width ratio h/b_f for two equal-size doubly-symmetric girders with a spacing-to-depth ratio S/h of 2. The plot on the right shows the L_b/L limit versus S/h for two equal-size doubly-symmetric girders with $h/b_f = 3$. Suppose that the girders have five equally spaced unbraced lengths, or four internal cross-frames, such that $L_b/L = 0.2$. The plot on the left shows that the buckling of the twin-girder system with $S/h = 2$ is more critical than that of the individual girders when h/b_f is smaller than about 4.5. The plot on the right shows that the buckling of the twin-girder system with $h/b_f = 3$ is more critical than that of the individual girders when S/h is less than about 3.0.

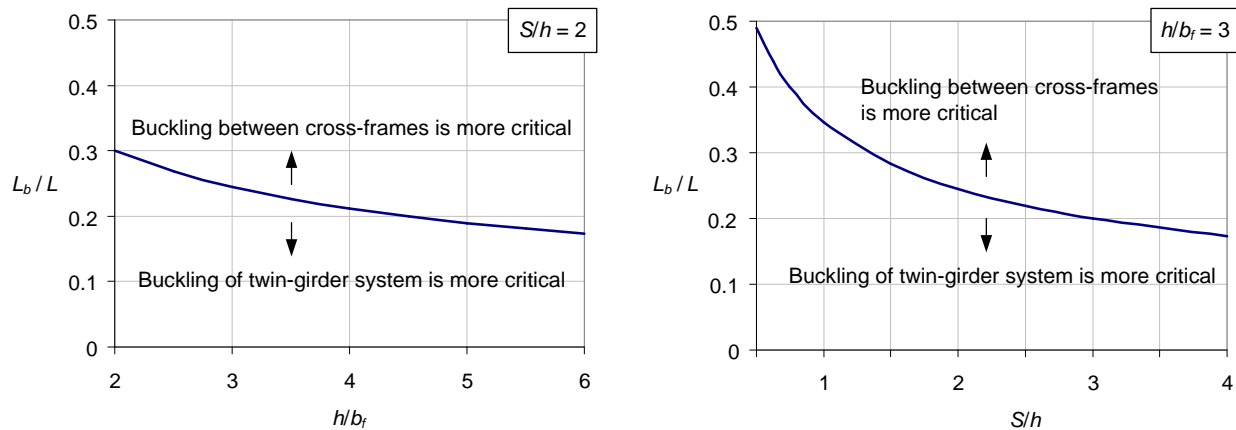


Figure 42 Example determination of whether system buckling or buckling of the girders between the cross-frames governs for two equal-size doubly-symmetric I-girders.

Expressions similar to Eq. (7) can be derived for assemblies of three or more girders. Such expressions show that in some cases, system buckling of these assemblies can be more critical than the buckling of the individual I-girder unbraced lengths. In addition, the overall elastic buckling capacity of two equal-size singly-symmetric I-girders can be estimated in a manner similar to the development of Eqs. (3) and (4), by using an effective lateral bending moment of inertia, and moment gradient effects can be approximated by including a C_b factor (Yura et al. 2008).

Bridge I-section members are commonly non-prismatic (e.g., they have cross-section transitions), they are subjected to non-constant bending moment along their lengths, and I-girder pairs are not necessarily composed of equal-size I-section members. Nevertheless, the above are useful base equations that are helpful for gaging when overall system buckling may govern relative to the common design assumption of buckling of the girders between the brace points. For realistic practical cases involving deep, closely-spaced, narrow-flange I-section members, the Engineer should consider running a refined buckling analysis to check the lateral-torsional buckling capacity of girder assemblies during construction. If the governing elastic buckling load is sufficiently large relative to the applied loads, then neither local nor global stability is an issue. Section 4.3 of this module outlines the specifics of this type of global stability check.

4.2 Lean-On Bracing Systems

It is possible to achieve substantial economy in the design of cross-frames in straight I-girder bridges by utilizing lean-on bracing concepts (Helwig et al. 2005; Herman et al. 2005). Using these concepts, multiple I-girders can be braced by a single cross-frame, given that they are tied to the cross-frame by top and bottom struts as shown in Figure 43. This approach can be particularly useful to eliminate cross-frames that may otherwise attract large forces, and to reduce the I-girder flange lateral bending stresses, in skewed I-girder bridges. Such a case is illustrated in Figure 44, which illustrates the cross-frame placement in a two-span TxDOT proof-of-concept bridge as presented by Helwig et al. (2005) and Herman et al. (2005). In this design, the individual I-girders tend to respond in a fashion closer to that of a non-skewed bridge. The top and bottom struts across the width of the bridge work with the bays containing cross-frame

diagonals provide the lateral stability to all of the girders. However, the bays containing only top and bottom struts and no diagonals rack due to differential girder vertical displacements (i.e., the top and bottom struts rotate relative to the girder cross-sections in the plane of the cross frames), thus reducing the twisting of the girders and avoiding the development of large cross-frame forces.

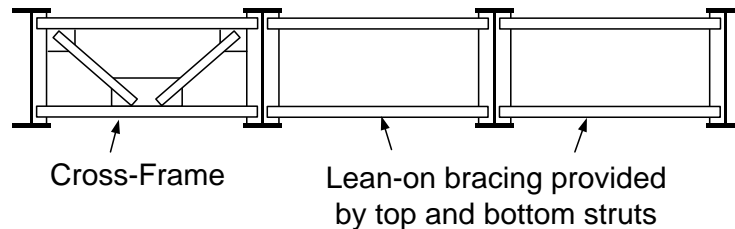


Figure 43 A single cross-frame bridge cross-section showing multiple I-girders braced by a single cross-frame

Equations (4-4) and (4-7), or related equations for singly-symmetric I-girders, are not valid for bridges that utilize lean-on bracing concepts. The cross-frame sizes and their locations must be designed to provide overall lateral and lateral-torsional stability of the structural system at all stages of the erection process. Helwig et al. (2005) and Herman et al. (2005) provide equations for estimating the bracing stiffness and force requirements due to stability effects. Refined analysis tools can be valuable for checking the overall stability of this type of bridge during various stages of construction.

In the design shown in Figure 44, cross-frames are placed across the entire width of the bridge at the supports. Also, a pair of cross-frames is provided at the mid-width of the bridge near the middle of each span. Furthermore, at least one in-span cross-frame is located between each of the girders, several additional cross-frames are located near the field splice locations, and a few additional cross-frames are provided to limit the differential deflection between adjacent girders during the slab casting. The reader is referred to Helwig et al. (2005) or Herman et al. (2005) for discussion of the detailed considerations. The total number of intermediate cross-frames is reduced from 128 to 35 after accounting for all of these factors. The authors suggest that a larger number of cross-frames should be used in broader implementation of the lean-on bracing concepts, with an important goal being flexibility for the erector to select various sequences of erection. For instance, they suggest that cross-frames should be located between each of the girders near field splice locations.

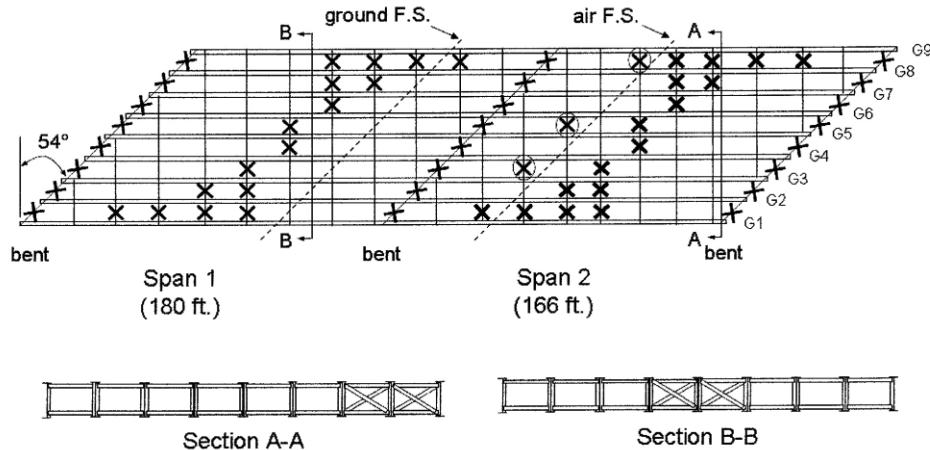


Figure 44 Plan view of a proof-of-concept skewed I-girder bridge utilizing lean-on bracing to alleviate large cross-frame forces and to reduce the number of required cross-frames (Herman et al. 2005) (reprinted with permission from Texas DOT). The x marks indicate the location of cross-frames.

4.3 General Consideration of System Stability Effects in Design

In all of the above cases, when the *system* elastic buckling resistance is smaller than the elastic lateral-torsional buckling resistance of the I-girders between the cross-frame brace points, the Engineer generally should evaluate whether the maximum compression flange elastic buckling stress is larger than the nominal stress magnitude, F_{yr} , at which yielding occurs due to residual stress effects. When the elastic critical stress $F_e = M_e/S_{xc}$ is larger than F_{yr} , an inelastic system buckling should be considered using the generalized equations discussed subsequently in Section 5.3.6 of this module. These situations will rarely occur in practical stringer bridge. The structure in its final constructed configuration will typically be such that its member strengths are not governed by an overall global buckling mode, and for the structure at critical intermediate stages during construction, the stresses should generally be small enough such that the structure is not close to the onset of any nominal yielding.

In cases where the girder flanges are subjected to significant lateral bending in addition to the major-axis bending stresses, f_b , the Engineer should consider the second-order elastic amplification of the flange lateral bending stresses due to the overall system stability effects when f_b/F_e is larger than about 0.1 to 0.2. For most bridges where this consideration may be important, it is expected that it will be important only during construction.

For large arch and cable-supported bridges, detailed three-dimensional finite element analyses of the overall structure including geometric and material nonlinearity, residual stresses and geometric imperfections may be desirable for assessment of the overall response at strength load levels. This type of analysis may be conducted with a number of the most sophisticated commercially available software packages. Detailed elastic finite element analysis of these types of structures is commonly employed for evaluation of component stresses at a minimum (Ito et al. 1992). However, it must always be recognized that good design of bridges is not achieved simply by running computer programs. Computer software should be considered as only one of

many essential design tools. Also, the Engineer should always keep in mind the famous words of Professor Hardy Cross (1952),

“...strength is essential and otherwise unimportant.

Various sources aid the engineer in determining strength. No one of them is more important than another. Analyses, tests, experience and such intuitive common sense as may be personally developed about structural stability; these are all helpful, but they can also be dangerously misleading. Evidence from the four sources rarely agrees completely. Great engineers are those who can weigh this evidence and arrive at a reasonable answer through judgment as to its dependability....

The important point here is that some types of planning, designing and experimenting can be put on an assembly line and some types can be put on an assembly line of skilled brains only, but much of the most important work cannot be done by using fixed rules, standardized formulas or rigid methods.

In general the objectives are flexibility of design and simplicity of construction....

...Men must learn to think more clearly in space and be less restricted to two-dimensional design. They must pay more attention to movements and vibrations. They need much more information on the properties of materials. Probably they need to reappraise seriously the importance of durability...”

5.0 MEMBER BEHAVIOR AND DESIGN STRENGTH

5.1 Tension Members

5.1.1 Rolled or Built-Up Tension Members

The strength of rolled section tension members, or tension members built up from rolled sections and/or steel plates, is governed by the most critical of the following limit states:

- Overall tension yielding of the member along its length,
- Tension fracture of the member across a net section (referred to by AISC (2010) as tension rupture),
- Block shear rupture along a shear failure path or paths combined with a perpendicular tension failure path at the end connections,
- Failure of the connecting bolts or welds in one of a number of modes, or
- Failure of the connecting elements such as gusset plates or splice plates.

The last three are considered as connection limit states by AASHTO (2014) and hence are not within the scope of this module. They are addressed in Article 6.13 of the AASHTO Specification. However, the first two limit states are considered as member limit states and are addressed in Article 6.8. The tension yielding resistance is given by the equation

$$\phi_y P_{ny} = 0.95 F_y A_g \quad (5.1.1-1)$$

(AASHTO 6.8.2.1-1)

Where

F_y = specified minimum yield strength and
 A_g = gross cross-sectional area of the member,

while the tension fracture resistance is expressed as

$$\phi_u P_{nu} = 0.80 F_u A_n R_p U \quad (5.1.1-2)$$

(AASHTO 6.8.2.1-2)

Where

F_u = ultimate tensile strength
 A_n = member net area

R_p = reduction factor for holes, taken equal to 0.90 for bolt holes punched full size and 1.0 for bolt holes drilled full size or subpunched and reamed to size

U = shear lag factor

Although ductile steel members loaded in axial tension can generally resist a force greater than the product of their gross area and the specified minimum yield stress, substantial elongation due to yielding throughout the gross area along the member length can precipitate the failure of the structural system of which the member is a part. Therefore, overall yielding of the gross area is considered as a strength limit state.

On the other hand, depending on the mechanical properties of the steel (the most important of which is the tensile-to-yield ratio F_u/F_y), the ratio of the net area to the gross area A_n/A_g and the end connection geometry (captured by the parameter U), a member can fail by tension fracture at one of its end connections before full yielding of its gross area. However, the larger tensile strains at the end connections are highly localized. Therefore, yielding at the end connections does not constitute a limit state of practical significance.

If fastener holes are located at some position along the member length, the net section at these holes also must be checked in general for tension fracture on the net section through the holes. However, AASHTO (2014) indicates appropriately that holes larger than typical fastener holes shall be deducted from the gross area rather than from the net area. This includes access holes and perforations in built-up members. In other words, these locations are designed for general yielding over their net area.

The net area for the tension fracture check can be expressed generally as:

$$A_n = A_g - \text{area lost due to holes} \quad (5.1.1-3)$$

Therefore, for fully welded connections without any plug or slot welds, $A_n = A_g$. In cases with plug or slot welds, the width of the original hole for the weld is handled in the same fashion as a fastener hole. For hole arrangements without any stagger, Eq. (3) becomes:

$$A_n = A_g - \sum d_e t \quad (5.1.1-4)$$

Where

d_e = effective width deducted for a given hole, equal to the nominal diameter or width of the hole perpendicular to the tension direction.

T = thickness of the plate at the hole.

Although AISC (2010) adds an additional 1/16 in to the nominal diameter in its calculation of d_e , to account in general for potential damage due to the fabrication of the hole, AASHTO (2014) does not. In the AASHTO provisions, the influence of damage around the hole is included, for

bolt holes punched full size, by the using $R_p = 0.9$. No net area reduction is taken for bolt holes drilled full size or subpunched and reamed to size.

The summation in Eq. (4) is over all of the holes located across a potential transverse fracture path through all of the components of the member cross-section. For staggered hole arrangements, the net area is given by:

$$A_n = A_g - \Sigma d_e t + \Sigma (s^2/4g) t \quad (5.1.1-5)$$

where:

s = longitudinal center-to-center spacing (pitch) between two consecutive holes

g = transverse center-to-center spacing (gage) between the hole gage lines

t = plate thickness along a given diagonal.

The second summation is over each diagonal in a potential zigzag fracture path through a chain of holes across all the member components

For angles, channels, boxes, etc. where the diagonal in the fracture path goes around a corner from one to another plate, the gage g is the transverse distance between the adjacent holes along the mid-thickness of the plates. That is, the gage can be determined by imagining that the plates are unfolded into a single flat plate at the mid-thickness of the plates. The critical chain of holes is taken as the one that gives the smallest net area. The corresponding fracture path can be either a straight or a zigzag transverse line.

The above approach is based on the assumption that the full tensile force acts at every potential straight or zigzag transverse fracture path through a set of holes. AASHTO (2014) indicates that a slightly less conservative calculation is obtained by subtracting the force removed by each bolt ahead of the fracture path being considered, i.e., closer to the mid-length of the member, from the full tensile force. The full force is assumed to be transferred equally by each bolt in the connection in making this calculation. In this case, a pseudo net area that can be used to determine the full member tension fracture resistance may be calculated as

$$A_n = \left[A_g - \Sigma d_e t + \Sigma (s^2 / 4g) \right] \frac{n_{total}}{n_r} \quad (5.1.1-6)$$

where:

n_{total} = total number of bolts in the connection

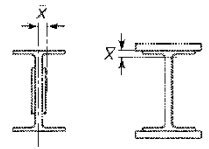
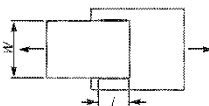
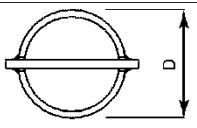
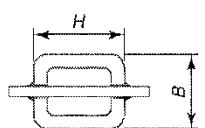
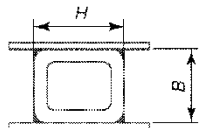
n_r = remaining number of bolts after deducting the number ahead of the fracture path

McGuire (1968) provides extensive discussion of the “ $s^2/4g$ ” rule for estimating the effect of zigzag paths on the tension fracture resistance. Although other approaches exist that have a

stronger theoretical basis, the corresponding equations are more complex without any significant improvement in accuracy.

As noted in the definitions just after Eq. (2), U accounts for the shear lag effects associated with the end connection geometry. If a line of fastener holes is placed across the cross-section of a member at some location within the member length, but no bolts or welds that transmit tension force to the member are located in these holes, $U = 1$. Also, if the tension force is transmitted directly to every component plate of a member cross-section by bolts or welds, $U = 1$. However, if some of the components are unconnected at the member ends, the critical net section may not be fully effective. Table 1 gives the recommended values and equations for U in AASHTO (2014). AASTHO (2014) Article 6.8.2.2 also states that for members composed of more than one plate element, the calculated value of U should not be taken less than the ratio of the gross area of the connected element(s) to the member gross area.

Table 1 Recommended AASHTO (2014) values and equations for the shear lag factor U .

Case	Description of Element		Shear Lag Factor, U	Example
1	All tension members where the tension load is transmitted directly to each of cross-sectional elements by fasteners or welds. (except as in Cases 3, 4, 5 and 6)		$U = 1.0$	—
2	All tension members, except plates and HSS, where the tension load is transmitted to some but not all of the cross-sectional elements by fasteners or longitudinal welds (Alternatively, for W, M, S and HP, Case 7 may be used.)		$U = 1 - \bar{x}/l$	
3	All tension members where the tension load is transmitted by transverse welds to some but not all of the cross-sectional elements.		$U = 1.0$ and A_n = area of the directly connected elements	—
4	Plates where the tension load is transmitted by longitudinal welds only.		$l \geq 2w \dots U = 1.0$ $2w > l \geq 1.5w \dots U = 0.87$ $1.5w > l \geq w \dots U = 0.75$	
5	Round HSS with a single concentric gusset plate		$l \geq 1.3D \dots U = 1.0$ $D \leq l < 1.3D \dots U = 1 - \bar{x}/l$ $\bar{x} = D/\pi$	
6	Rectangular HSS	with a single concentric gusset plate	$l \geq H \dots U = 1 - \bar{x}/l$ $\bar{x} = \frac{B^2 + 2BH}{4(B + H)}$	
		with two side gusset plates	$l \geq H \dots U = 1 - \bar{x}/l$ $\bar{x} = \frac{B^2}{4(B + H)}$	
7	W, M, S or HP Shapes or Tees cut from these shapes. (If U is calculated per Case 2, the larger value is permitted to be used)	with flange connected with 3 or more fasteners per line in direction of loading	$b_f \geq 2/3d \dots U = 0.90$ $b_f < 2/3d \dots U = 0.85$	—
		with web connected with 4 or more fasteners in the direction of loading	$U = 0.70$	—
8	Single angles (If U is calculated per Case 2, the larger value is permitted to be used)	with 4 or more fasteners per line in direction of loading	$U = 0.80$	—
		with 2 or 3 fasteners per line in the direction of loading	$U = 0.60$	—

l = length of connection, in. (mm); w = plate width, in. (mm); \bar{x} = connection eccentricity, in. (mm); B = overall width of rectangular HSS member, measured 90 degrees to the plane of the connection, in. (mm); H = overall height of rectangular HSS member, measured in the plane of the connection, in. (mm)

These AASHTO provisions are adapted from similar provisions in AISC (2005) and are based on the research by Munse and Chesson (1963), Easterling and Gonzales (1993) and Cheng and Kulak (2000).

The AISC (2010) provisions for the shear lag reduction factor U include the above rule for the limit on the minimum U value, and they address a few additional refinements not included in the AISC (2005) and AASHTO (2014) provisions: (1) both single and double angles are included in Case 8 in Table 1, (2) for the case of single angles with fewer than three fasteners per line in the direction of the loading, Case 2 of Table 1 is recommended, and (3) the provisions state explicitly that the above limit on the minimum U value does not apply to closed sections, such as HSS, nor to plates.

AASHTO (2014) specifies limits on the slenderness ratio L/r for rolled and built-up I-section members to ensure adequate performance, where L is the member unsupported length and r is the minimum radius of gyration of the cross-section. For main members subject to stress reversals, L/r is limited to 140, for main members not subject to stress reversals, L/r is limited to 200, and for bracing members, L/r is limited to 240. For tension members with perforated plates or tie plates with or without lacing, a number of other requirements (dimensional, etc.) are specified in AASHTO (2014) Article 6.8.5 or are provided in the commentary to this section by reference to AISC (2005) and AASHTO (2002).

5.1.2 Eyebars and Pin-Connected Plates

AASHTO (2014) Article 6.8.6 specifies that the factored resistance of eyebars is given by Eq. (5.1.1-1) based on the area of the body, $w t$, and provides dimensional requirements to ensure that tension fracture will not occur. Figure 45 shows these and several additional dimensional requirements. Two requirements are listed from AISC (2010) that are believed to be intended, given the origins of the rules (McGuire 1968). The requirements in Figure 45 are based largely on judgment and traditional rules of practice that have evolved over many years. McGuire (1968) points out that the behavior of eyebars and pin-connected plates differs somewhat from that of bolted or riveted tension members and provides an extensive review of the traditional requirements and their relationship to theory and experimental studies. The in-plane bending deformations and localized strains tend to be larger around the large pin hole compared to typical local deformations in bolted or riveted connections.

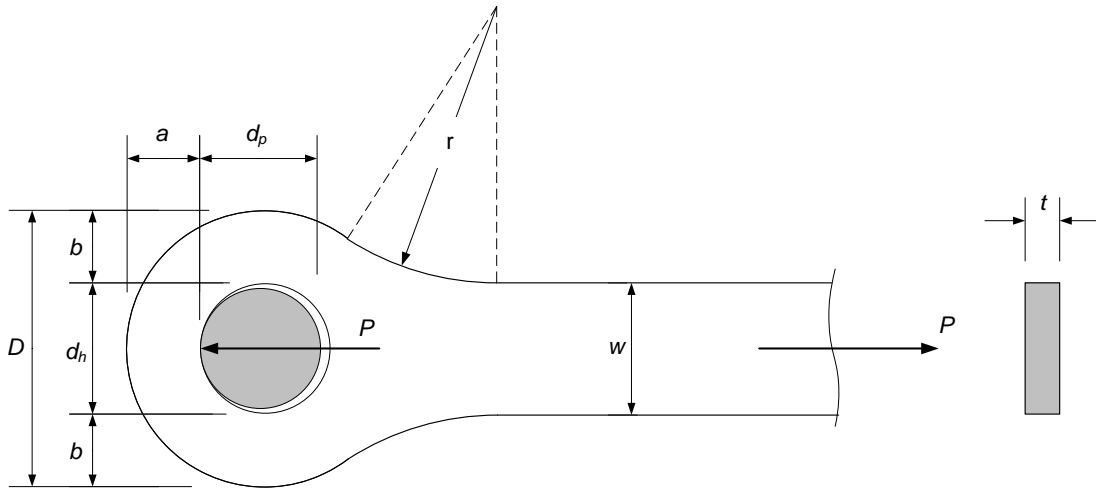
AASHTO (2014) Article 6.8.7 requires that pin-connected plates shall be designed using Eqs. (5.1.1-1) and (5.1.1-2) with $U = 1.0$. Pin-connected plates are defined as members in which “pin-plates” may be attached to a main plate by bolts or welds to increase the thickness near the pin. AASHTO requires that the pin plates, if used, should be arranged to minimize the load eccentricity, and that they must be attached to the main plate by sufficient welds or bolts to transmit the pin bearing forces from the pin-plates to the main plate. The combination of the main and pin plates must be checked for net section fracture at the pin hole. Also, the main plate and pin plates must be checked for fracture across their individual net sections at the attachments of the pin plates to the main plate, considering the force transfer between the plates. In addition, AASHTO specifies a bearing resistance on the projected area of the pin, $A_b = t_m d_p$ or $t_p d_p$, of

$$\phi_b P_n = 1.0 A_b F_y \quad (5.1.2-1)$$

(AASHTO 6.8.7.2-1)

for each of the plates, where F_y is the specified minimum yield strength of the plate. Figure 46 summarizes additional requirements for a specific pin-connected plate with two equal size pin plates bolted on each side of the main plate, a width of the pin plates equal to the width of the main plate, w , and an end distance from the pin to the end of the pin plates equal to that of the main member, a . These requirements, combined with the above tension yielding, tension fracture and plate bearing checks, are intended to ensure acceptable behavior of the assembly.

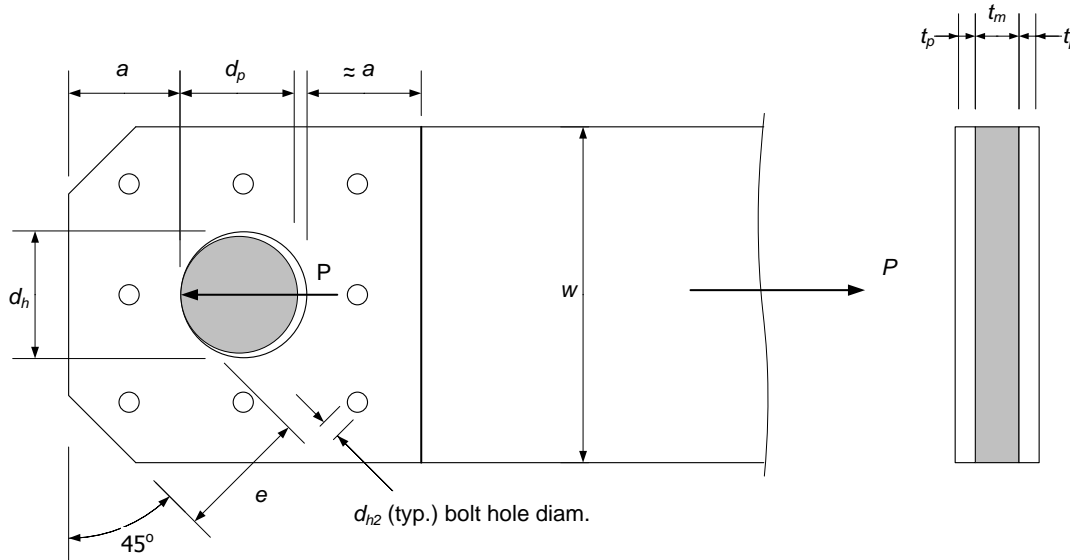
One additional requirement is shown in Figure 46 that is not specified explicitly in AASHTO (2014) or AISC (2010). It would appear that the dimension from the edge of the pin-hole to the edge of the pin-plates parallel to the direction of the load should be essentially the same on each side of the pin to ensure good performance (hence the dimension labeled “ $\approx a$ ”). Also, the connection of the pin plates to the main plates should be distributed over the pin plates such that the localized effects of the pin are diminished at the critical net section for the tension fracture check of the main plate.



- | | |
|--|--|
| <p>(1) Thickness (t) shall be uniform, with no hole reinforcement</p> <p>(2) $0.5 \text{ in} \leq t \leq 2 \text{ in}$</p> <p>(3) $r \geq D$</p> <p>(4) $D \geq 1.35 w$</p> <p>(5) $a \geq 0.75 w$</p> <p>(6) $w \leq 8 t$</p> <p>(7) $d_h - d_p \leq 1/32 \text{ in}$</p> <p>(8) $d_h \leq 5t$ for steels with $F_y > 70 \text{ ksi}$</p> <p>(9) $a = b$ (AISC 2010)</p> <p>(10) $d_p \geq 0.875 w$ (AISC 2010)</p> | <p>(11) Eyebars of a set shall be sym. about central plane of member & as parallel as practical</p> <p>(12) Eyebars shall be restrained against lateral movement on the pins and lateral distortion</p> <p>(13) Adjacent bars in the same panel shall be separated by at least 0.5 in; Ring shaped spacers shall be provided to fill gaps between adjacent eyebars on a pin</p> <p>(14) Intersecting diagonal bars that are not sufficiently spaced to clear each other at all times shall be clamped together at the intersection</p> |
|--|--|

Figure 45 Dimensional requirements for eyebars specified to ensure good member performance and development of the full yield capacity of an eyebar.

AASHTO (2014) states that pin-connected plates should be avoided wherever possible. AISC (2010) indicates that pin-connected plates are not recommended when there is sufficient variation in live loading to cause wearing of the pins in the holes. McGuire (1968) points out that pin-connected plates and eyebars were common in the nineteenth century, when they were more economical and faster to erect than hand-riveted construction, and when Engineers were often concerned with minimizing secondary stresses. Also, he indicates that given current knowledge about secondary stresses, and when they are or are not important, there is less concern in modern design about their minimization in all structures. Consequently, trusses having all or most joints pinned have largely disappeared.



- (1) Thickness (t) need not be uniform, i.e., the main plate may be reinforced by pin plates in the vicinity of the pin hole
- (2) The pin plates, if used, shall be arranged to minimize the load eccentricity
- (3) The pin plates, if used, shall be attached to the main plate by sufficient welds or bolts to transmit the bearing forces from the pin plates to the main plate
- (4) Transverse net area requirement, to ensure against tensile fracture at a transverse section through the centerline of the pin hole:

$$\left\{ \left[w - \left(d_h + \frac{1}{16} \right) - 2 \left(d_{h2} + \frac{1}{16} \right) \right] (t_m + 2 t_p) \right\} \geq 1.4 \left(\frac{P_u}{0.8 F_{u,main}} \right)$$

- (5) Longitudinal net area requirement, to ensure against tearing of the pin out of the end of the pin connected member:

$$\left\{ \left[a - \left(d_{h2} + \frac{1}{16} \right) \right] (t_m + 2 t_p) \right\} \geq \frac{P_u}{0.8 F_{u,main}}$$

- (6) The pin hole shall be centered on the longitudinal axis of the main plate
- (7) $d_h - d_p < 1/32$ in
- (8) $d_h \leq 5 (2 t_p + t_m)$ for steels with $F_y > 70$ ksi
- (9) $2 t_p + t_m \geq 0.12 [w/2 - (d_h + 1/16)/2 - (d_{h2} + 1/16)]$
- (10) $w \leq 8 t_m$
- (11) Pin-connected plates shall be restrained against lateral movement on the pins and lateral distortion
- (12) Corners may be cut at 45° if $e \geq a$ (assuming one bolt hole along e , and one bolt hole along a in this example)
(AISC 2010)

Figure 46 Requirements in addition to the checks of tension yielding, tension fracture and plate bearing, for a specific pin connected plate with two equal size pin plates (w , a and e of pin plates = w , a and e of main plate) bolted on each side of the main plate.

5.1.3 Strands

AASHTO (2014) references three types of strand commonly used in bridge construction:

- Uncoated seven-wire stress-relieved strand for prestressed concrete (also used for stay cables and for prestressing of steel members), ASTM A416,

- Zinc-coated parallel and helical wire structural strand, ASTM A586, and
- Zinc-coated steel structural wire rope, ASTM A603.

The latter two strand types are referred to generally as bridge strand. Bridge strand is not used for major cable-stayed bridges or for prestressing steel, generally due to its lower stiffness. However, structural strand and structural wire rope are used for hangers in arch and suspension bridges.

In helical steel wire structural strand, the wires are laid helically about a center wire to produce a symmetrical section. Structural wire rope involves a group of strands placed helically around a core composed of either a strand or another rope. Both of these bridge strand types are usually prestretched by the manufacturer to remove the permanent “constructional stretch” caused by lengthening of the strand lay due to adjustment of the wires into a denser cross-section under load. The prestretching is achieved by subjecting the strand to a load up to 55 % of the breaking strength for a sufficient length of time to permit the adjustment of the wires to that load. As a result, under working loads, the elongation of the strand is effectively elastic and can be calculated using the elastic moduli given in Table 2. These moduli are reduced relative to that of the base material due to the helical geometry of the wires and the zinc coating. The wires tend to straighten when subjected to tension. Also, the strength is reduced due to the helical geometry. The breaking strengths of Grade 1 structural strand and wire rope with Class A zinc coating are approximately 190 to 200 ksi based on the gross metallic area. The breaking strength of Grade 2 structural strand with Class A zinc coating is approximately $F_u = 220$ to 230 ksi based on the gross metallic area of the strand.

Table 2 Effective minimum elastic moduli of prestretched structural strand and structural rope (ASTM 2004; ASTM 1998).

Type	Nominal Diameter (in)	Minimum Modulus (ksi) Class A Coating*
Strand	$\frac{1}{2}$ to $2\frac{9}{16}$	24,000
	$2\frac{5}{8}$ and larger	23,000
Rope	$\frac{3}{8}$ to 4	20,000

* For Class B or Class C weight of zinc-coated outer wires, reduce minimum modulus by 1000 ksi

Seven-wire prestressing strand has a straight core wire surrounded by a single layer of six helically-placed outer wires with a uniform pitch of not less than 12 and not more than 16 times the nominal diameter of the strand. This pitch is longer than that of bridge strand such that the elastic stiffness is essentially the same as that of the base material. AASHTO (2014) specifies $E = 28,500$ ksi for seven-wire strand. ASTM 416 covers two types of seven-wire strand: low-relaxation and stress-relieved (normal relaxation). AASHTO (2014) and ASTM 416 both state that low-relaxation strand shall be regarded as the standard type, and that stress-relieved (normal-relaxation) strand will not be furnished unless specifically ordered, or by arrangement between the purchaser and supplier. Low-relaxation strand is produced by a combined process of low-temperature heat treatment and high tension. Seven-wire strand is produced with nominal

breaking or ultimate strengths F_u of both 250 ksi and 270 ksi on the nominal area of the strand (smaller than the area based on the nominal diameter). The minimum yield strength F_y of low relaxation strand is 90 % of F_u , measured at 1% extension under load. Both seven-wire and bridge strand exhibit a gradual (non-sharp) yield response.

AASHTO (2014) does not specify a procedure for design of bridge strands or cables composed of seven-wire strand. In past practice, bridge strands were checked against working loads using a factor of safety of 3 to 4 with respect to their breaking strength (Podolny and Scalzi 1986, Wright and Bunner 2006). Cables composed of seven-wire strand were commonly checked against working loads using a factor of safety of 2 with respect to their minimum yield strength (Podolny and Scalzi 1986). Chapter 5 of AASHTO (2014) addresses the use of prestressing in concrete structures, but does not specifically address the use of prestressing steel for composite or noncomposite steel construction. The design calculations for prestressed steel structures may be based largely on the same fundamental principles of equilibrium and strain compatibility utilized within the AASHTO concrete provisions, combined with the steel design provisions of Chapter 6 for consideration of the stability of the structural steel elements. However, prestress losses due to elastic shortening and long-term shrinkage and creep of the concrete are in general different in structural steel applications. The reader is referred to Troitsky (1990) for detailed discussion of the design of prestressed steel bridges.

5.2 Compression Members

5.2.1 Base Column Strength Equations

AASHTO (2014) and AISC (2010) both effectively use the following single column-curve equations to characterize the nominal axial resistance of all types of steel and composite steel-concrete members to concentrically-applied axial compression:

$$P_n = \left[0.658^{\left(\frac{P_e}{P_o}\right)} \right] P_o \quad \text{for } \frac{P_e}{P_o} \geq 0.44 \quad (5.2.1-1)$$

(AASHTO 6.9.4.1-1 & 6.9.5.1-1, AISC E3-1 & E3-2, E7-1 & E7-2 & I2-2)

(the number for equations specified by AISC (2005) is preceded by the word “AISC” followed by the equation number). $P_n = 0.877 P_e$ for $P_e/P_o < 0.44$, where P_e is the elastic or effective elastic member buckling load, which can be calculated by the famous expression:

$$P_e = \frac{\pi^2 EI}{(KL)^2} \quad \text{or} \quad \frac{\pi^2 E}{(KL/r)^2} A_g = F_e A_g \quad (5.2.1-2)$$

(AASHTO 6.9.4.1.2-1, AISC E3-4)

for flexural buckling about either the major or minor principal axis of the cross-section, and P_o is the effective cross-section or stub-column yield strength. That is, P_o is the strength in the limit of zero length ($KL = 0$). For a homogeneous prismatic steel member in which none of the cross-section plates are classified as slender, P_o is the full yield capacity given by:

$$P_o = P_y = F_y A_g \quad (5.2.1-3)$$

Equations (1, 2, and 3) are expressed in various specific forms in the AASHTO and AISC Specifications. The format shown here allows for a unified discussion of all the different column strength calculations. For flexural buckling of a homogeneous prismatic member, the square root of P_o/P_e is the member normalized slenderness parameter

$$\sqrt{\frac{P_o}{P_e}} = \left(\frac{KL}{r}\right) \frac{1}{\pi} \sqrt{\frac{F_y}{E}} \quad (5.2.1-4)$$

(AASHTO 6.9.5.1-3)

The other terms in Equations (1) through (4) are defined as follows:

A_g = gross area of the cross-section,

E = steel elastic modulus, taken equal to 29,000 ksi,

F_y = column minimum specified yield strength,

I = moment of inertia of the cross-section about the principal axis normal to the plane of buckling,

r = radius of gyration about the principal axis normal to the plane of buckling = $(I/A_g)^{0.5}$,

K = effective length factor in the plane of buckling.

Equations (1) and (2) represent the nominal inelastic and elastic column buckling resistances respectively, as illustrated in Figure 47 in terms of both KL/r and $(P_o/P_e)^{0.5}$. Although these equations are often considered solely in terms of the column effective slenderness ratio KL/r , the above general form of these equations is utilized in AASHTO (2014) and in AISC (2010) to define the resistance of all types of steel and composite steel concrete columns, including cases where P_e corresponds to limit states other than flexural buckling. Furthermore, this form is applied in Kaehler et al. (2011) to quantify the resistance of columns having general tapered and/or stepped cross-sections subjected to uniform or nonuniform axial compression. Equations (1 and 2) account in a broad fashion for the influence of residual stresses and geometric imperfections (out-of-straightness and out-of-plumbness) on the column resistance. They provide a close fit to SSRC column curve 2P, which is based on a mean initial out-of-straightness of 1/1470 of the equivalent simply-supported column length KL (Ziemian 2010) (see Figure 47).

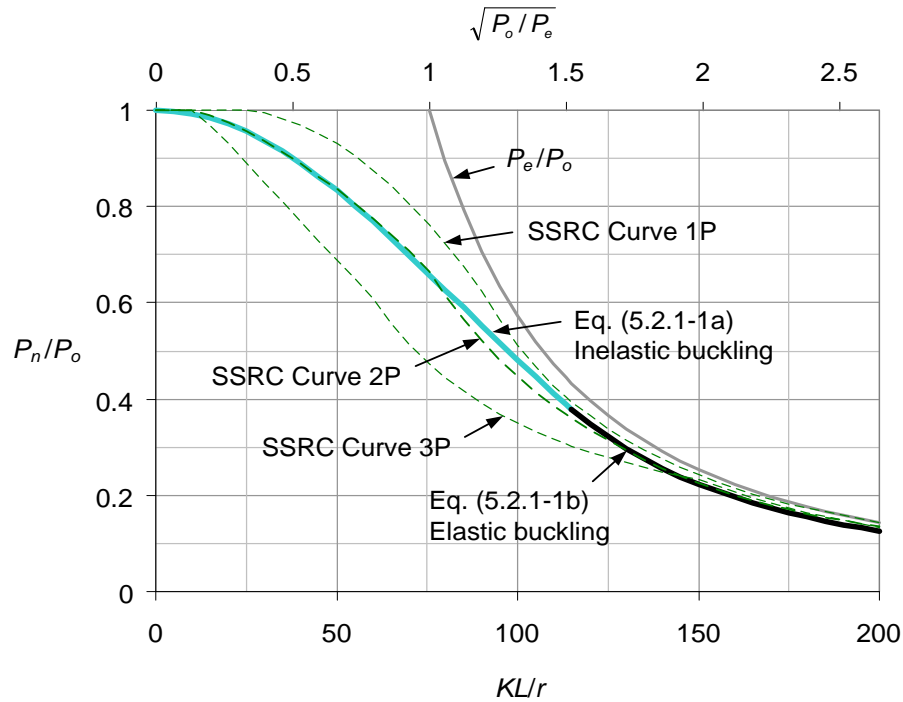


Figure 47 AASHTO (2014) and AISC (2010) column strength curve in terms of both KL/r and $(P_o/P_e)^{0.5}$ versus the SSRC multiple column curves 1P, 2P and 3P (Galambos 1998) and the theoretical elastic buckling strength, steel columns with $F_y = 50$ ksi

Generally, there are significant differences in the mean column resistances for various column types. This is evidenced by the differences between SSRC curves 1P, 2P and 3P in Figure 47. Table 3 summarizes the recommended usage of these multiple column curves for a range of steel column cross-sections. One can observe that the normalized column resistances are larger on average for lightweight sections, larger yield strengths and buckling about the major-axis of bending for I-shapes. They tend to be smaller for heavy sections, low yield strengths, and buckling about the minor-axis of bending for I-shapes. Column curve 3P applies only to heavy W-shapes with $F_y < 50$ ksi and welded H-shapes built-up from universal mill plate with $F_y < 50$ ksi for major-axis buckling and $F_y < 60$ ksi for minor-axis buckling. Welded built-up shapes are no longer manufactured from universal mill plates; furthermore, the minimum yield strength is usually 50 ksi or larger in new construction. Therefore, the resistances of all practical columns in new construction are best fit by column curves 1P and 2P, with 2P being the appropriate curve for most of the column types. AASHTO (2014) applies a resistance factor of $\phi_c = 0.9$ to Eqs. (5.2.1-1) for all types of steel and composite steel-concrete columns, versus $\phi = 0.75$ for concrete columns. This is consistent with the use of the single column curve Eqs. (5.2.1-1) and the use of the same resistance factor for steel and composite steel-concrete columns in AISC (1999). AISC (2005) and (2010) use a substantially smaller ϕ_c factor in their provisions for composite steel-concrete columns along with a more accurate but more liberal calculation of the nominal resistance P_n . AISC (2005) and (2010) also have increased their ϕ_c factor slightly for steel columns in recognition of the fact that column curve 3P is no longer applicable for new steel construction.

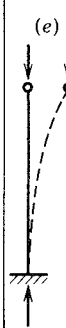
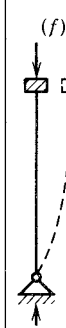
Table 3 Recommended SSRC column curves for various types of steel cross-sections, adapted from (Ziemian 2010).

Cross-section type		Axis of Bending	Specified Minimum Yield Strength F_y (ksi)				
			≤ 36	37 to 49	50 to 59	60 to 89	≥ 90
Hot-rolled W-shapes	Light and medium Weight sections	Major	2	2	1	1	1
		Minor	2	2	2	1	1
	Heavy sections (flange thickness > 2 in)	Major	3	2	2	2	2
		Minor	3	3	2	2	2
Welded Built-up H-shapes	Flame-cut plates	Major	2	2	2	1	1
		Minor	2	2	2	2	1
	Universal mill plates	Major	3	3	2	2	2
		Minor	3	3	3	2	2
Welded Box Shapes	Flame-cut and Universal mill plates	Major	2	2	2	1	1
		Minor	2	2	2	1	1
Square and Rect. Tubes	Cold-formed	Major	N/A	2	2	2	2
		Minor	N/A	2	2	2	2
	Hot-formed and cold-formed heat-treated	Major	1	1	1	1	1
		Minor	1	1	1	1	1
Circular Tubes	Cold-formed	N/A	2	2	2	2	2
	Hot-formed	N/A	1	1	1	1	1

5.2.2 Flexural Buckling and Column Effective Length

The effective length factor K accounts for the influence of the column end conditions on the flexural buckling resistance, including interactions with other members in the structure. Table 4, from AISC (2010), AASHTO (2014) and Ziemian (2010), summarizes the theoretical K values for cases in which the rotational and/or translational restraints at the ends of a column are either full (i.e., effectively rigid compared to the column stiffness) or nonexistent. Recommended design values are also provided. These values are simple modifications of the ideal values, taking into account the fact that the physical end translations and rotations can never be perfectly fixed or perfectly unrestrained.

Table 4 Approximate values of effective length factor K for cases where the rotational and/or translational end restraints are either nominally fixed or nonexistent (reprinted with permission from AISC (2010)).

Buckled shape of column is shown by dashed line						
Theoretical K value	0.5	0.7	1.0	1.0	2.0	2.0
Recommended K value when ideal conditions are approximated	0.65	0.80	1.2	1.0	2.10	2.0
End condition code	   	Rotation fixed, Translation fixed Rotation free, Translation fixed Rotation fixed, Translation free Rotation free, Translation free				

In numerous other cases, K values are often specified based on established practice. For instance, Ziemian (2010) recommends the use of $K = 0.85$ for in-plane buckling of web members in bridge trusses. This is because the position of live load that produces the maximum force a given web member typically causes less than the maximum force in the adjacent members. Therefore, the adjacent members are able to provide some rotational restraint. In lieu of analysis, AASHTO (2014) allows a more liberal value of $K = 0.75$ for any truss or frame member that has bolted or welded end connections and is braced against lateral translation at its ends, with the exception of single angle members where $K = 1.0$ is suggested. One can observe from Table 4 that $K = 0.75$ implies no translation and nearly rigid end rotational restraints. Thus, it would appear that this assumption is appropriate only for relatively light web members compared to the truss chords. Ziemian (2010) suggests $K = 0.9$ for in-plane buckling of an interior panel of the compression chord of a constant depth truss, when the chord has the same cross-section along its entire length. In the out-of-plane direction, Ziemian (2010) suggests $K = 0.7$ and 0.8 for the web compression members of a through truss when a substantial knee brace is provided in the cross-frames at both chords and at only one chord respectively. When the cross-frames depend only on their flexural stiffness and frame action to resist sidesway, K is greater than one for the web compression members in the out-of-plane direction. Also, in these cases, the compression chord has a K greater than one. The K factor is greater than one in general for the compression chord of pony trusses and half-through trusses. The reader is referred to Ziemian (2010) and Johnston (1976) for further discussion of appropriate K calculations in these cases.

In many situations where rotational restraint exists at the ends of a single bridge column or at the ends of the columns in a bridge frame, e.g. pier columns integral with bridge girders, the

traditional sidesway inhibited or sidesway uninhibited alignment charts (AASHTO 2010; AISC 2010; Kavanagh 1962) provide acceptable solutions for K . However, it is essential to recognize that the alignment charts are based on idealized assumptions that in certain cases make their application invalid. The commentary to Appendix 7 of AISC (2010) discusses these assumptions in detail and provides a number of modifications to the alignment chart procedures that extend their range of applicability. AASHTO (2014) Article C4.6.2.5 gives closed form equations that provide a close fit to the base sidesway inhibited and sidesway uninhibited alignment charts. The AISC (2010) modifications also must be applied in general in the use of these equations.

As noted previously in Section 2.5 of this module, AASHTO (2014) Article 4.5.3.2.2c provides suggested effective length factors for in-plane buckling of arches. These values range from 0.70 for a fixed arch with a small rise-to-span ratio to 1.16 for two- or three-hinged arches with a large rise-to-span ratio. These values are applied to *one-half* of the total arc length of the arch rib. For checking stability in the out-of-plane direction, the effective length KL may be taken as the distance between the rib bracing points when a lateral bracing system of adequate stiffness is provided. However, special consideration of arch-end portals is generally necessary. Refined eigenvalue buckling analysis is the simplest way to check the out-of-plane stability in these cases. The reader is referred to the discussion in Section 5.2.6 of this module for the handling of nonuniform compression and/or nonuniform cross-section properties along the length of an arch.

In trusses, frames and arches where a refined analysis is employed to assess the stability, it is simpler and more convenient to work directly with the member elastic buckling load, P_e , than back-calculate an equivalent pinned-ended length KL . In this case, P_e in Eqs. (5.2.1-1) is simply the axial load in a given member at incipient elastic buckling of the structure or subassembly considered in the buckling analysis. The use of P_e in Eqs. (5.2.1-1) is also essential for the application of these equations in determining the torsional and torsional-flexural buckling resistances of certain types of members (see Section 5.2.3 of this module). Also, all of the above K factor considerations pertain solely to flexural buckling. In several of the following sections, KL is taken as an “equivalent length” accounting for attributes other than just the flexural response.

5.2.3 Column Torsional and Torsional-Flexural Buckling

AASHTO (2014) Article C6.9.4.1.3 and AISC (2010) Section E4 give the applicable resistance equations for members that are susceptible to torsional or torsional-flexural buckling. These include some singly-symmetric members such as double angles and tees, and built-up members such as columns with cruciform cross-sections and/or with relatively thin cross-section plate elements. As noted in the previous section, all the AISC (2010) and AASHTO (2014) column resistance calculations use Eqs. (5.2.1-1); however, the calculation of P_e is different than in the previous section.

5.2.3.1 Torsional buckling of doubly-symmetric cross-sections

Doubly-symmetric cross-section members that are relatively weak in torsion, e.g., cruciform columns or columns that are braced but are not sufficiently restrained against twisting at a number of their brace points, can fail by a buckling mode involving a pure twisting about the

axis of the member (see Figure 48). In these cases, the elastic torsional buckling load may be expressed as

$$P_e = P_{ez} = \left[\frac{\pi^2 EC_w}{(KL_z)^2} + GJ \right] \frac{A_g}{I_x + I_y} \quad (5.2.3-1)$$

(AASHTO 6.9.4.1.3-1, AISC E4-4)

where

C_w = warping constant for the cross-section, equal to zero for a cruciform section,

KL_z = effective length for torsional buckling,

G = steel shear modulus, taken as 11,200 ksi,

J = St. Venant torsional constant for the cross-section, and

I_x and I_y = moments of inertia about the major and minor principal axes of bending respectively.

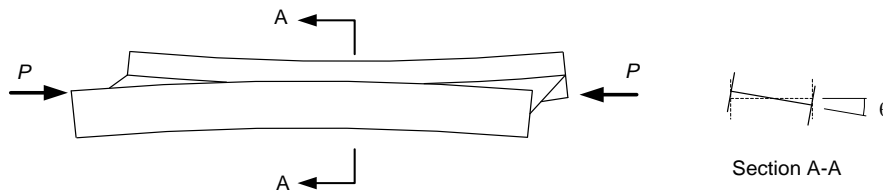


Figure 48 Torsional buckling of an I-section member.

The effective length for torsional buckling, KL_z , is usually taken as the distance between locations where the member is restrained against twisting. For the case of a cantilever column fully restrained against twisting and warping at one end and with the other end free, $KL_z = 2L$. For a member where twisting and warping are fully restrained at each of its ends, $KL_z = 0.5L$. (Note that the notation “ KL_z ” is a unification of the different symbols used for these terms in AISC (2010) and AASHTO (2014); in this module, the subscripts x , y , or z are placed at the end of the general effective length symbol, KL , to indicate the effective lengths for flexural buckling about the major (x) or minor (y) principal axes of the section, or torsional buckling about the longitudinal z axis of the member.)

Doubly-symmetric compression members can fail either by flexural buckling about one of the cross-section principal axes, or by torsional buckling. However, torsional buckling rarely governs except for members such as cruciforms. Torsional buckling never needs to be considered for doubly-symmetric I-section members that satisfy the AASHTO Article 6.10.2 proportion limits, unless KL_z is significantly larger than the weak-axis flexural buckling effective length, KL_y . Generally, P_{nz}/P_{ny} (the ratio of the nominal column strengths using Eq. (1) with KL_y rather than Eq. (3) for calculation of P_e) is smaller for smaller D/b_f , larger b_f/t_f , larger D/t_w and larger

P_o/A_g . Based on $D/b_f = 1$, $b_f/t_f = 24$, $D/t_w = 192$ (corresponding to $t_f/t_w = 8$) and $P_o/A_g = 100$ ksi as the worst-case combined cross-section parameters, the smallest value of P_{nz}/P_{ny} is still only 0.974 at $KL_y/r_y = 37$, assuming $KL_z = KL_y$. That is, torsional buckling leads to a maximum reduction of only 2.6 percent for all practical doubly-symmetric I-shapes. The consideration of end-restraint effects (if they are accounted for at all) in the calculation of the column buckling loads is not anywhere near this precise. Also, P_{nz}/P_{ny} increases rapidly with increases in D/b_f .

5.2.3.2 Flexural or torsional-flexural buckling of singly-symmetric cross-sections

Compression members with singly-symmetric cross-sections, where the y -axis is taken as the axis of symmetry, either can fail by flexural buckling about the x -axis or by torsion combined with flexure about the y -axis. The elastic torsional-flexural buckling load for these types of members is given by the expression

$$P_e = P_{eTF} = \left(\frac{P_{ey} + P_{ez}}{2H} \right) \left[1 - \sqrt{1 - \frac{4P_{ey}P_{ez}H}{(P_{ey} + P_{ez})^2}} \right] \quad (5.2.3-2)$$

(AASHTO 6.9.4.1.3-2, AISC E4-5)

where

$$P_{ey} = \frac{\pi^2 EI_y}{(KL_y)^2} = \frac{\pi^2 E}{(KL_y/r_y)^2} A_g \quad (5.2.3-3)$$

(AASHTO 6.9.4.1.3-4, AISC E4-8)

$$P_{ez} = \left[\frac{\pi^2 EC_w}{(KL_z)^2} + GJ \right] \frac{1}{\left(y_o^2 + \frac{I_x + I_y}{A_g} \right)} = \left[\frac{\pi^2 EC_w}{(KL_z)^2} + GJ \right] \frac{1}{\bar{r}_o^2} \quad (5.2.3-4)$$

(AASHTO 6.9.4.1.3-5, AISC E4-9)

$$H = 1 - \frac{y_o^2}{\bar{r}_o^2} \quad (5.2.3-5)$$

(AASHTO 6.9.4.1.3-3, AISC E4-10)

KL_y = effective length for flexural buckling about the y -axis (the axis of symmetry of the cross-section),

C_w = cross-section warping constant, equal to zero for cross-sections where the component plates are all joined at a single common point, e.g., tee sections,

y_o = distance along the y -axis between the shear center and the cross-section centroid,

\bar{r}_o = polar radius of gyration about the shear center

$$\bar{r}_o^2 = y_o^2 + \frac{I_x + I_y}{A_g} \quad (5.2.3-6)$$

(AASHTO 6.9.4.1.3-6, AISC E4-11)

The governing column strength, P_n , is obtained by substituting the smaller value of P_{eTF} (which is always smaller than P_{ey}) or P_{ex} (flexural buckling about the x -axis) into Eqs. (5.2.1-1).

As noted above, P_{eTF} is generally smaller than P_{ey} . However, the flanges of singly-symmetric I-sections often have equal widths (only the flange thicknesses differ). Therefore, for these types of member, y_o tends to be relatively small and the influence of the smaller P_{eTF} on P_n is always less than 4 % as long as

$$KL_z \leq KL_y \text{ and } 0.67 \leq t_{f1}/t_{f2} \leq 1.5$$

where t_{f1} and t_{f2} are the flange thicknesses. For I-section members with equal-width flanges, the largest reduction in P_n due to the smaller P_{eTF} occurs for $b_f/t_f = 24$, $D/b_f = 6$, $D/t_w = 150$, $P_o/A_g = 100$ ksi, $KL_y/r_y = 114$ and $KL_z = KL_y$ (smaller D/t_w gives a larger reduction for this case, but causes $t_f/t_w \leq 1$). Therefore, if the above limit is satisfied, torsional-flexural buckling never needs to be considered for practical I-section members with equal-width flanges and $KL_z \leq KL_y$.

Interestingly, the reductions in the torsional-flexural buckling resistance for I-section members with unequal width flanges are significant in many practical cases even when there are rather small differences in the flange widths. This is because the lateral moment of inertia of the flanges varies with b_f^3 , and hence only minor changes in the relative flange widths result in a significant shift in the cross-section shear center relative to the centroid. The shift in the cross-section shear center is similar to the shift in the centroid due to changes in the flange thickness; however, the shift in the shear center is significantly different than the shift in the centroid due to changes in the flange width. Therefore, there does not appear to be any simple way to exclude the need to consider torsional-flexural buckling for any I-section members with unequal flange widths.

5.2.3.3 Torsional-flexural buckling of general unsymmetric cross-sections

Lastly, for members with no cross-section axis of symmetry, the failure mode under axial compression always involves torsion combined with flexure about both the x and y axes. In this case, P_e is the smallest root of the following cubic equation

$$(P_e - P_{ex})(P_e - P_{ey})(P_e - P_{ez}) - P_e^2 (P_e - P_{ey}) \left(\frac{x_o}{\bar{r}_o} \right)^2 - P_e^2 (P_e - P_{ex}) \left(\frac{y_o}{\bar{r}_o} \right)^2 = 0 \quad (5.2.3-9)$$

(AASHTO 6.9.4.1.3-7, AISC E4-6)

where

$$P_{ex} = \frac{\pi^2 EI_x}{(KL_x)^2} = \frac{\pi^2 E}{(KL_x/r_x)^2} A_g \quad (5.2.3-10)$$

(AASHTO 6.9.4.1.3-8, AISC E4-7)

P_{ey} is as defined in Eq. (3),

$$P_{ez} = \left[\frac{\pi^2 EC_w}{(K_z L)^2} + GJ \right] \frac{1}{\bar{r}_o^2} \quad (5.2.3-11)$$

(AASHTO 6.9.4.1.3-5, AISC E4-9)

$$\bar{r}_o^2 = x_o^2 + y_o^2 + \frac{I_x + I_y}{A_g} \quad (5.2.3-12)$$

(AASHTO 6.9.4.1.3-9, AISC E4-11)

And

$x_o, y_o = x$ and y coordinates of the shear center with respect to the cross-section centroid.

As noted previously, once the elastic buckling load, P_e , is calculated, it is substituted into Eqs. (5.2.1-1) to determine the nominal elastic or inelastic column buckling resistance.

5.2.3.4 Special handling of double-angles and tees with non-slender elements in AISC (2010)

For double-angle and tee-section compression members in which none of the cross-section elements are classified as slender, AISC (2010) specifies a modified approach that, in some cases, gives a slightly more liberal estimate of the capacity. For these member types, P_{ez} is calculated as

$$P_{ez} = \frac{GJ}{\bar{r}_o^2} \quad (5.2.3-13)$$

(AISC E4-3)

which is simply Eq. (4) with $C_w = 0$. Secondly, P_{ny} is calculated using Eqs. (5.2.1-1) based on the flexural buckling mode about the y -axis. Finally, the nominal column strength for torsional-flexural buckling is determined by substituting P_{ny} directly into Eq. (2) in place of P_{ey} . This gives:

$$P_{nTF} = \left(\frac{P_{ny} + P_{ez}}{2H} \right) \left[1 - \sqrt{1 - \frac{4P_{ny}P_{ez}H}{(P_{ny} + P_{ez})^2}} \right] \quad (5.2.3-14)$$

(AISC E4-2)

The governing column strength is then taken as the smaller value of P_{nx} (flexural buckling about the x -axis) and P_{nTF} (buckling by twisting and combined bending about the y -axis). AISC (2010) references Galambos (1991) for justification of the above calculation of the torsional-flexural buckling resistance.

The reader should note that all of the previous equations are based on a “mapping” of the theoretical elastic buckling resistance, P_e , to the nominal column buckling resistance, P_n , using Eqs. (5.2.1-1). Equation (14) deviates from this pattern by assuming that the torsional buckling contribution to the resistance, P_{nz} , is always elastic for these member types (i.e., $P_{nz} = P_{ez}$ in Eq. (14)). Interestingly, Eq. (14) does not necessarily give a larger calculated resistance P_{nTF} than the above direct “mapping” of P_{eTF} to P_n using Eqs. (5.2.1-1). This is due to subtle aspects of the algebra associated with the different equations and the conversion of the elastic buckling load to the inelastic column resistance.

AASHTO (2014) does not specify Eqs. (13) and (14) for the above member types. Rather, it uses the general mapping of the elastic buckling resistance to the nominal buckling resistance given by Eqs. (5.2.1-1) for all types of steel and composite steel concrete members. Given the limited test data on which Eqs. (13) and (14) are based, it was felt that the use of this separate set of equations was not justified.

The commentary to Chapter E of AISC (2005) (Table C-E4.2) indicates that torsional-flexural buckling can be neglected in tee-section members having non-slender cross-section elements when $b_f/d \geq 0.5$ and $t_f/t_w \geq 1.10$ for rolled tees and 1.25 for built-up tees. Interestingly, these limits remove the need to consider torsional-flexural buckling for *all* ASTM A6 WT, ST and MT sections as long as the stem is not slender under uniform axial compression. However, a simple plotting of the above equations indicates that this recommendation is not well founded. The ratio of P_{nTF}/P_{ny} for tees with nonslender cross-section elements and $KL_z = KL_y$, calculated using Eq. (14), can be as small as 0.75 for short tee-section members. This ratio is smaller than 0.90 for many tee section members at intermediate to long unbraced lengths. The AISC (2010) commentary no longer includes this table in view of the fact that P_{nTF} generally should be calculated for tee-section members. This is consistent with the findings for unequal-width flange I-section members discussed previously in Section 5.2.3.2 of this module.

5.2.3.5 Special handling of single angle compression members in AASHTO (2014) and AISC (2010)

Single angle compression members are used extensively as cross-frame and lateral-bracing members in steel bridge construction. AISC (2010) and AASHTO (2014) provide highly simplified provisions for design of specific types of single angle web members subjected to axial compression. These provisions define an equivalent slenderness (KL/r) for use with Eqs. (5.2.1-1) and (5.2.1-2) applicable when:

1. The end connections are to a single leg,
2. The member is loaded through the same leg at each of its ends,
3. The end connections are welded or use a minimum of two bolts,
4. The member is not subjected to any transverse loads, and
5. If used as web members in trusses, all adjacent web members are attached to the same side of the gusset plate or chord.

For these types of single-angle members, the equivalent KL/r accounts for the effects of end eccentricities, and the member may be proportioned using Eqs. (5.2.1-1) and (5.2.1-2) as if it were a concentrically compressed strut subjected solely to flexural buckling. The equivalent KL/r expressions also presume significant end rotational restraint about the Y -axis shown in Figure 49, where the Y -axis is perpendicular to the connected leg and to the gusset or the plate component of another member to which the angle is connected. This leads to the angle member tending to buckle primarily about the X -axis. As such, r is taken as the r_x for the angle for bending *about an*

axis parallel to the connected leg. It is *not* taken as the minimum $r = r_z$ about the angle minor principal axis. In addition, it should be noted that a capital X is used here because, for an unequal leg angle, the X axis can be either the x or y axis of the angle shown in property tables, depending on which of the legs is the connected one.

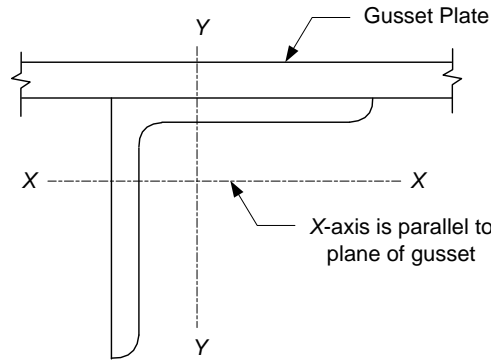


Figure 49 Single-angle cross-section and definition of geometric axes utilized by the AISC (2010) and AASHTO (2014) equivalent KL/r expressions.

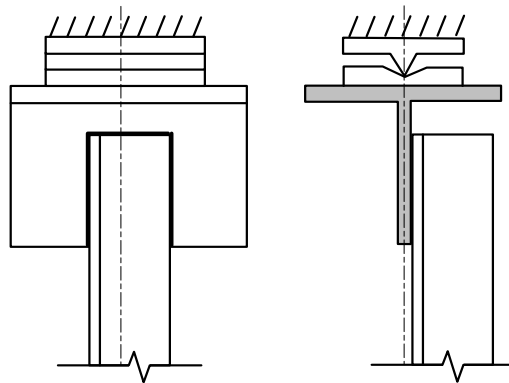


Figure 50 Test end conditions associated with the recommended equivalent KL/r equations for single angle struts.

AISC (2010) provides two sets of equations for the equivalent KL/r , one based on the assumption of significant rotational restraint about the X and Y axes in Figure 49 and the other based on tests having close to the knife-edge end conditions shown in Figure 50 (but with less than rigid Y -axis restraint and considering some minor X -axis restraint). The more optimistic equations, which assume substantial X - and Y -axis end restraint, are essentially equivalent to the ASCE 10-97 (ASCE 2000) equations for equal-leg angles in latticed transmission towers. These equations are classified by AISC (2010) as being applicable for “web members of box or space trusses.” The less optimistic equations are classified by AISC (2010) as being applicable for “web members of planar trusses.” Based on the data presented by Lutz (2006), these equations are considered applicable for all types of single angles commonly employed in bridge cross-frames and lateral bracing systems. These equations are as follows.

For equal-leg angles, and unequal-leg angles connected through the longer leg,

$$\frac{KL}{r} = 72 + 0.75 \frac{L}{r_x} \quad \text{when } 0 \leq \frac{L}{r_x} \leq 80 \quad (5.2.3-15a)$$

(AASHTO 6.9.4.4-1, AISC E5-1)

and

$$\frac{KL}{r} = 32 + 1.25 \frac{L}{r_x} \quad \text{when } \frac{L}{r_x} > 80 \quad (5.2.3-15b)$$

(AASHTO 6.9.4.4-2, AISC E5-2)

where L is the length of the member between the end-connection work points. It is intended that the design should not be used in any case where the maximum value of KL/r in Eq. (15b) is greater than 200.

For unequal-leg angles with the ratio of the leg widths less than 1.7, connected through the shorter leg,

$$\frac{KL}{r} = 72 + 0.75 \frac{L}{r_x} + 4 \left[\left(\frac{b_\ell}{b_s} \right)^2 - 1 \right] \quad \text{when } 0 \leq \frac{L}{r_x} \leq 80 \quad 5.2.3-16a$$

(AASHTO 6.9.4.4-3, AISC E5-1)

and

$$\frac{KL}{r} = 32 + 1.25 \frac{L}{r_x} + 4 \left[\left(\frac{b_\ell}{b_s} \right)^2 - 1 \right] \geq 0.95 \frac{L}{r_z} \quad \text{when } \frac{L}{r_x} > 80 \quad 5.2.3-16b$$

(AASHTO 6.9.4.4-4, AISC E5-2)

where b_ℓ and b_s are the widths of the longer and shorter legs respectively, and as in Eq. (15b), it is intended that the design should not be used if the equivalent KL/r is greater than 200 in Eq. (16b).

It is important to emphasize in the above that r_x is the radius of gyration about the angle geometric axis parallel to the connected leg. For an unequal-leg angle connected through the longer leg, r_x is actually the smaller r value about the angle's geometric axes, typically listed as r_y in section property tables. Equations (16) account for the fact that the strength is enhanced by using the longer leg as the outstanding leg, but also recognize that this tends to force the actual buckling axis to be closer to the z -axis of the angle (Lutz 2006). The limit of $b/b_s \leq 1.7$ is based on the limits of the available experimental tests.

Lutz (2006) obtains a mean professional bias factor for the above equations of $P_n/P_{max} = 0.998$ with a coefficient of variation of 0.109 relative to single-angle tests approximating the knife-edge end conditions shown in Figure 50. In addition, Lutz (2006) shows a representative equal-leg angle example in which the above equations give results close to those obtained using the more generally applicable approach of treating the single-angle as a beam-column under specific conditions. The more general procedure requires the use of Eq. (9), the calculation of moments

based on assumed end eccentricities, the calculation of single-angle moment capacities, and beam-column interaction checks. The two approaches are roughly equivalent when:

1. The end eccentricity e_x (normal to the X -axis) is taken as $\bar{Y} + t/2$,
2. The end eccentricity e_y is taken as the value necessary to theoretically achieve uniform stress along the connected leg,
3. The effective length for buckling about the X -axis (parallel to the connected leg) is taken with $K_x = 1.0$, and
4. The effective length for buckling about the Y -axis is calculated as $K_y = 0.65$ (Lutz (1992) gives a procedure for calculating this effective length factor).

Lutz (2006) also compares the AISC (2010) equations to other equivalent KL/r procedures in Eurocode 3 (CEN 1993) and in the British Standard BS5950 (1990). The Eurocode 3 procedure gives results that are very close to the AISC space truss equations for $L/r_x > 60$, but is more optimistic than the AISC space-truss provisions for smaller L/r_x values. The BS5950 equations predict larger capacities than the AISC space-truss provisions for $L/r_x < 120$ in Lutz's equal-leg angle example, and predict essentially the same capacities for larger L/r_x . The above Eqs. (15) fall below the European and British predictions for all ranges of L/r_x . Eq. (15a) gives a result that is 21 and 44 percent below these predictions at $L/r_x = 40$.

One of Lutz's (2006) examples is a single angle strut that requires the use of an equivalent yield strength QF_y , where Q is the AISC (2010) form factor accounting for local buckling effects (see Section 5.2.4 of this module). The AISC Q factor equations are believed to provide adequate estimates of the capacity of angles with slender leg elements. ASCE 10-97 (ASCE 2000) applies a similar reduction for these types of angles.

The fifth restriction on the equivalent KL/r equations, listed at the beginning of this section, is based largely on the test results presented by Woolcock and Kitipornchai (1986). These investigators found that single angle web members in trusses have less theoretical capacity when they are connected alternately on opposite sides as opposed to connecting the members all on the same side of T-section truss chords. This is apparently due to the shear transfer within a Warren-type truss system with the diagonals in alternating tension and compression, and the additive eccentricity effects of compression in one web diagonal with tension in the other adjacent web diagonal.

With the exception of "X" bracing in cross-frames or lateral bracing systems, single-angle members typically are all connected on the same side at their end connections (NSBA 2006). Nevertheless, it is common in some bridge applications to have both diagonals in compression at a joint in a Warren truss. This can occur for example when a Warren truss is used for the top lateral bracing system in a box girder. In this case, the compression in the two adjacent diagonals would cause an additive detrimental eccentric loading effect if both members are connected on the same side. That is, depending on the specific loads being transferred at the bracing connections, connecting the angles on the same side could be detrimental or beneficial.

Upon looking at the fifth restriction more broadly, considering the potential restraints from typical single-angle connection details in steel bridge cross-frames and lateral-bracing systems, it is suggested that the approximate knife-edge boundary conditions about the X -axis, upon which Eqs. (15) and (16) are based, are an acceptable approximation for calculation of the single-angle capacities for any configuration of cross-frames or flange level lateral bracing in steel bridge applications. The approximate knife-edge boundary conditions are judged typically to be more detrimental to the angle member strengths than the physical end conditions for these members.

The special case of “X” bracing systems merits some further discussion. In cases where one diagonal is in tension, and if this member has a force of not less than 20 % of the force in the compression member, ASCE 10-97 (ASCE 2000) indicates that the cross-over point may be considered as a braced point for out-of-plane buckling. It would appear that a similar approach might be applied with Eqs. (15) and (16). However, this approach needs validation. If only a single bolt is used to connect the angles at the cross-over point, the restraint about the Y -axis assumed in Eqs. (15) and (16) may not be present at this point. It is suggested here that Eqs. (15) and (16) may be applied conservatively in X-bracing systems by using the full length of the diagonal between the end connection work points for L .

El-Tayem and Goel (1986) have studied the X-bracing problem where the compression and tension member are equally loaded and the connections are welded. Their research has involved both theoretical and experimental investigations. They indicate that the compression diagonal of cross-bracing systems made of equal-leg single-angle members may be checked neglecting the effect of end eccentricity, using a KL in Eq. (5.2.1-2) equal to 85 % of the half-length of the compression diagonal and using the radius of gyration $r = r_z$ taken about the minor principal axis of the angle cross-section.

5.2.4 Columns with Slender Elements

5.2.4.1 Width-to-thickness limits to prevent local buckling under uniform axial compression

Slender cross-section elements are plates that are unable to develop their full nominal yield strength in uniform axial compression because of local buckling. The solid curve in Figure 51 illustrates the general form of the AISC (2010) local buckling strength. For an average applied axial stress $P/A_g \leq 2F_y/3$, the nominal local buckling resistance is quantified by the classical elastic critical stress formula:

$$F_{nl} = F_{el} = \frac{\pi^2 E k_c}{12(1-\nu^2)(b/t)^2} = \frac{0.90 E k_c}{(b/t)^2} \quad (5.2.4-1)$$

(AASHTO 6.9.4.2.2-8, 6.9.4.2.2-6, 6.9.4.2.2-4 & 6.9.4.2.2-2, AISC E7-9, E7-15, E7-12 & E7-6)

Where

k_c = plate local buckling coefficient

ν = Poisson’s ratio for steel (0.3)

b/t = relevant width-to-thickness ratio.

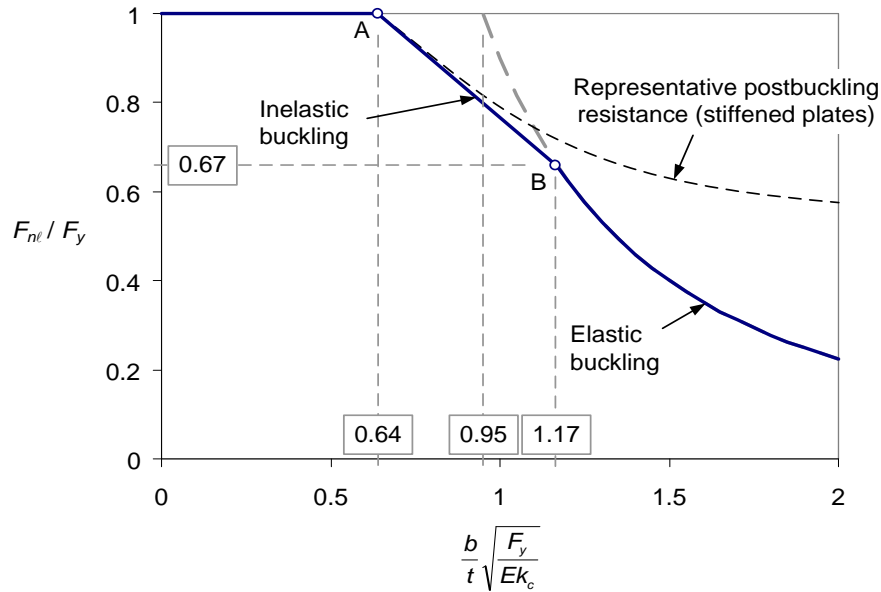


Figure 51 General form of AISC (2010)-AASHTO (2014) nominal strength curve for plate local buckling.

AASHTO (2014) and AISC (2010) list the k_c values explicitly only for a few plate edge conditions. Rather, a k_c value is implicit the most of the AASHTO and AISC equations. All the explicit and implicit k_c values are discussed below, since this allows for a better understanding of the underlying assumed behavior.

For plates that are stocky enough to develop applied stress levels larger than $2F_y/3$, the local buckling resistance is defined by a straight-line inelastic buckling curve between the two anchor points A and B. The width-to-thickness ratio corresponding to anchor point B is obtained by setting Eq. (1) equal to $2F_y/3$ and solving for b/t . This gives

$$b/t = 1.17 \sqrt{\frac{Ek_c}{F_y}} \quad (5.2.4-2)$$

For a perfectly flat plate with zero residual stress, $F_{e\ell} \geq F_y$ for a width-to-thickness ratio of

$$b/t \leq 0.95 \sqrt{\frac{Ek_c}{F_y}} \quad (5.2.4-3)$$

However, due to residual stresses and geometric imperfections, a smaller value of b/t is required nominally to develop an average applied stress of $P/A_g = F_{n\ell} = F_y$. The AISC (2010) and AASHTO (2014) provisions assume that a plate can develop its nominal full yield strength in uniform axial compression when

$$b/t \leq \left[\lambda_r = 0.64 \sqrt{\frac{Ek_c}{F_y}} \right] \quad (5.2.4-4)$$

(AASHTO 6.9.4.2.1-1 & 6.9.4.2.1-2, AISC Table B4.1)

which corresponds to $F_{e\ell} \geq 2.20 F_y$. That is, the abscissa of anchor point A is given by Eq. (4) and the ordinate is $F_{n\ell} = F_y$. Equation (4) is the same form as Eq. (6.9.4.2-2) in the AASHTO Specification, which applies to flanges of built-up I-sections. AASHTO uses this general form for these element types, but defines another parameter $k = 0.64 \sqrt{k_c}$ in its Eq. (6.9.4.2-1) to address all other cross-section elements. Equation (4) also is identical to the formula for the maximum b/t at which the AISI (2001) *Specification for Design of Cold-Formed Steel Structural Members* assumes that a cross-section plate element can develop its full yield strength, $F_y b t$ (see AISI (2001) Eqs. (B2.1-1) & (B2.1-4)).

The AASHTO (2014) k_c values corresponding to Anchor Point A are summarized in Table 5 and Table 6 along with the definitions of b . These values and definitions are based on AASHTO (2014) Article 6.9.4.2. AASHTO (2014) has adopted the AISC terminology of referring to plates supported along one longitudinal edge as “unstiffened” and plates supported along two longitudinal edges as “stiffened.” The same values and definitions are utilized in AISC (2010) with the exception that AISC (2010) uses:

(1) $k_c = 5.4$ for rectangular box sections with unequal thickness plates (Case 8 in Table B4.1a of AISC (2010)) and $k_c = 4.8$ for boxes of uniform thickness (Case 6 in Table B4.1a), compared to $k_c = 4.8$ for box section flanges (Case 5 of Table 6) and $k_c = 5.4$ for webs (Case 6 of Table 6).

(2) $k_c = 5.4$ for flange cover plates (Case 7 of AISC Table B4.1a and $k_c = 4.8$ for other cover plates (Case 8 of Table B4.1a) compared to $k_c = 4.8$ for non-perforated cover plates (Case 5 of Table 6) and 8.4 for perforated cover plates (Case 8 of Table 6).

(3) $k_c = 4.8$ for the walls of rectangular tube sections (Case 6 of AISC Table B4.1a), but with b defined as the clear distance between the adjacent plates or the distance between the edge support minus the inside corner radius on each side, compared to $k_c = 7.1$ (Case 8 of Table 6) but with b defined as the full width of the face).

Table 5 AASHTO (2014) values for the plate local buckling coefficient, k_c , plates supported along one edge (defined as “unstiffened” elements).

Case	Plate Description	k_c	b
1	Flanges of built-up I-sections	$4/\sqrt{D/t_w} \leq 0.76$ ≥ 0.35	• Half flange width
2	Flanges of rolled I-, tee and channel sections; Plates projecting from rolled I-sections; Outstanding legs of pairs of angles in continuous contact	0.76	• Half-flange width of rolled I-sections and tees • Full flange width of channels • Distance between free edge and first line of bolts or welds in plates • Full width of an outstanding leg for pairs of angles in continuous contact
3	Stems of rolled tee sections	1.38	• Full depth of tee
4	All other projecting elements	0.50	• Full width of outstanding leg for single angles or double angles with separators • Full projecting width for other cases

Table 6 AASHTO (2014) values for the plate local buckling coefficient, k_c , plates supported along two edges (defined as “stiffened” elements).

Case	Plate Description	k_c	b
5	Box section flanges; Non-perforated cover plates	4.8	• For box section flanges, clear distance between the webs • For cover plates, distance between lines of welds or fasteners
6	Webs and other plate elements	5.4	• Clear distance between flanges minus fillet radius for webs of rolled I-sections • Clear distance between edge supports for all other case
7	Perforated cover plates	8.4	• Clear distance between edge supports
8	Walls of rectangular tubes	7.1	• Width of face

The use of $k_c = 5.4$ for box sections with unequal thickness plates in AISC (2010) appears to be an oversight. This value is considered acceptable for checking typical thinner web plates in closed steel box sections. However, a smaller k_c value is appropriate for checking the thicker flange plates. The flange plates provide rotational restraint to the edges of the web plates, but conversely, the web plates cannot possibly also restrain the edges of the flange plates. The smaller AISC values of $k_c = 5.4$ or 4.8 for perforated cover plates is a conservative approximation. The larger value of 8.4 for perforated cover plates in AASHTO (2014) is consistent with AISC (1999) and is based on the use of the smallest net area at the holes rather than the gross area A_g in calculating the column resistance. The smaller value of $k_c = 4.8$ for the walls of rectangular tube sections is consistent with the AASHTO (2014) Case 5 provisions in

Table 6 for box section flanges. The larger value of $k_c = 7.1$ for tubes in Case 8 is an approximation tied to the simpler definition of b as the full width of the face of the tube.

It is informative to compare the nominal k_c values in Table 5 against the theoretical minimum k_c values for elastic plate buckling shown in Figure 52. One can observe from the first case in Table 5 that the nominal k_c is 0.35 for flanges of built-up I-sections with a web width-to-thickness $D/t_w \geq 131$. This value is smaller than the theoretical k_c of 0.425 for s.s. (simply-supported) - free longitudinal edge conditions (case E of Figure 52), indicating that the flanges are assumed to be destabilized by the local buckling of the web for these geometries. For $D/t_w \leq 28$, a k_c value of 0.76 is assumed for the flanges, which is intermediate between the theoretical s.s.-free and fixed-free values of 0.425 and 1.28. These limits and the transition equation $k_c = 4/\sqrt{D/t_w}$ are based on the studies by Johnson (1985). The specific AASHTO-AISC equation for k_c is a simplification of Johnson's recommendations first introduced in AISC (1989). The value of $k_c = 0.76$ for the flanges of rolled I-, tee- and channel-section members is based on traditional AISC practice.

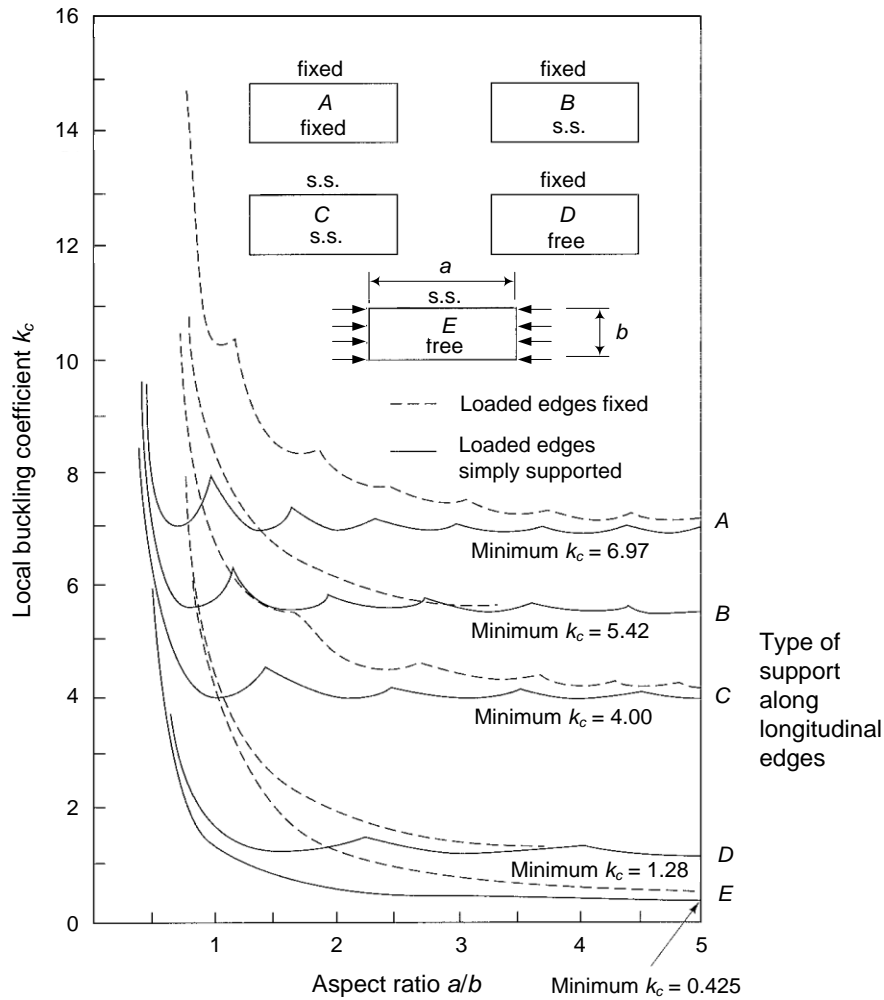


Figure 52 Theoretical k_c values for elastic plate buckling (adapted from Salmon and Johnson (1996)).

AISC (2010) refers to plates supported along only one edge as unstiffened plates. For plates supported along two longitudinal edges, defined as stiffened plates in AISC (2010), AASHTO (2014) assumes a nominal k_c value of 4.8 for box-section flanges and nonperforated cover plates, and 5.4 for all other non-perforated plates. These values lie between the theoretical k_c of 4.0 for s.s.-s.s. and 6.97 for fixed-fixed edges.

One other important slenderness limit addressed in AASHTO (2014) Article 6.9.4.2 and AISC (2010) Table B4.1 is the limit for the axial strength of circular tubes not to be influenced by local buckling. This limit is

$$\frac{D}{t} \leq 0.11 \frac{E}{F_y} \quad (5.2.4-5)$$

(AASHTO 6.9.4.2.1-5, AISC Table 4.1a)

where D is the outside diameter of the tube and t is the tube thickness. This limit was first used in the 1978 AISC Allowable Stress Design Specification. Analytical buckling solutions significantly overestimate the physical local buckling resistance of longitudinally compressed cylinders due to imperfections in the shape and eccentricities of the load. Therefore, Eq. (5) is based on test evidence from Sherman (1976) that local buckling will not occur for applied axial stress up to F_y .

5.2.4.2 Compressive resistance of slender-element section members

AASHTO (2014) Article C6.9.4.2.2 addresses the resistance of compression members with slender cross-section elements. This article is based predominantly on the corresponding AISC (2010) Section E7 provisions. Many beam-type ASTM A6 rolled wide-flange sections (i.e., sections with $d/b_f \geq 1.7$) have slender webs under uniform axial compression. Also, the stems of a large number of WT sections and one or both legs of many of the rolled angles are slender by the above definitions, i.e., $b/t > \lambda_r$ from Eq. (4). Welded I- and box-girders practically always have webs that are slender under uniform axial compression. The Engineer should note, with the exception of the provisions for filled composite-section members in AISC (2010), cross-section components are classified either as slender or non-slender under uniform axial compression in AASHTO (2014) and AISC (2010). There are no compactness requirements for uniform axial compression. Compactness requirements apply only to member flexural resistances, where the flange and web elements need to withstand larger inelastic strains for local buckling not to influence the nominal strength. AISC (2010) has recently clarified this consideration by splitting its Table B4.1 into two separate Table 5 and Table 6. The different approach to classification of filled composite-section members in AISC (2010) is addressed subsequently in Section 5.2.7 of this module.

When a steel cross-section contains slender elements, the AASHTO and AISC column resistances are calculated in the context of Eqs. (5.2.1-1) by using a reduced equivalent yield capacity $P_o = QP_y$, where $Q \leq 1$ is referred to as the cross-section form factor. The AISC Specifications have utilized this approach to determine the strength of columns with slender cross-section elements since AISC (1969), which emulated the 1968 AISI Specification (AISI 1968). Prior to 1969, AISC used the more conservative practice of disregarding any portion of the plate width that exceeded the corresponding λ_r limit.

In calculating the reduction factor Q , the AASHTO and AISC Specifications handle unstiffened and stiffened cross-section elements differently. Unstiffened elements are assumed to attain their limit of resistance when they reach their nominal local buckling strength defined by the solid curve in Figure 51. Conversely, the resistance of stiffened elements is based on their inherent postbuckling strength illustrated by the dashed curve in this figure. The postbuckling strength is quantified using a plate effective width concept. The 1986 AISI Specification (AISI 1986) adopted an effective width approach for both stiffened and unstiffened cross-section elements. However, subsequent editions of the AISC Specifications have not adopted the updated AISI approach. This is partly because the advantages of postbuckling strength are insignificant for all but highly slender elements. Such dimensions are common in cold-formed columns, but are rarely encountered in unstiffened elements of fabricated steel structures. Furthermore, the AISI

effective width approach generally uses smaller k_c values than those listed in Table 5 and Table 6. This results in more conservative predictions in a number of cases for elements with b/t values near the AISC λ_r limits. This is particularly true for the local buckling resistance of tee stems, where the AISC provisions count on substantial restraint from the flange in determining $F_{n\ell}$ (see Case 3 of Table 5) and the elastic torsional buckling associated with Eq.(5.2.3-13) is essentially the same as the elastic local buckling associated with Eq. (1) (McGuire 1968). Tee sections do not appear to have been addressed specifically in the development of the AISI provisions. Also, the internal residual stresses are different in cold-formed versus hot-rolled and fabricated steel members.

5.2.4.3 Strength reduction Q_s for members composed entirely of unstiffened elements

For columns composed entirely of unstiffened elements, AASHTO (2014) and AISC (2010) calculate the column equivalent yield capacity $P_o = QP_y$ by determining Q as

$$Q = Q_s = (F_{n\ell})_{min}/F_y \quad (5.2.4-6)$$

(AASHTO 6.9.4.2.2-1 to 6.9.4.2.2-8, AISC E7-4 to E7-15)

where $(F_{n\ell})_{min}$ is the smallest local buckling stress from all of the elements of the cross-section. That is, the stub-column or cross-section equivalent yield strength is taken as the average applied axial stress at which the most critical unstiffened element reaches its local buckling capacity illustrated in Figure 51 (elastic or inelastic, depending on b/t , k_c and F_y). Interestingly, the implicit k_c values for single angles and for stems of tees are different for anchor point B compared to the values used for anchor point A in Figure 51. The values for anchor point A are shown in Table 5 whereas the values for anchor point B and the elastic local buckling resistance curve shown in Figure 51 are $k_c = 0.59$ and 0.76 for single angle legs and for tee stems respectively. The fact that these values are larger than the theoretical $k_c = 0.425$ for *s.s.* - free edge conditions is due to the close coupling between (i.e., the similarity of the buckling modes for) local plate buckling and overall member torsional-flexural buckling (governed by Eqs. (5.2.3-2) through (5.2.3-12)) for these member types.

5.2.4.4 Strength reduction $Q = Q_a Q_s$ for members with stiffened elements

The use of an effective width concept for postbuckled stiffened plates was first proposed by von Kármán et al. (1932). Winter (1947) subsequently modified von Kármán's equation to provide a transition between the strength of very slender elements and stockier elements shown to be fully effective in tests. Additional testing (Winter 1970) led to further modification to the following general form utilized in the AISI (1968) Specification, written in a strength format:

$$b_e = 1.90t \sqrt{\frac{E}{f}} \left[1 - \frac{0.415}{b/t} \sqrt{\frac{E}{f}} \right] \leq b \quad \text{for } \frac{b}{t} > 1.29 \sqrt{\frac{E}{f}} \quad (5.2.4-7)$$

However, for the specific case of flanges of square and rectangular sections of uniform thickness, AISI (1968) used the equation

$$b_e = 1.90t \sqrt{\frac{E}{f}} \left[1 - \frac{0.378}{b/t} \sqrt{\frac{E}{f}} \right] \leq b \quad \text{for } \frac{b}{t} > 1.38 \sqrt{\frac{E}{f}} \quad (5.2.4-8)$$

(implicitly, in an allowable stress format), which gives a slightly more liberal estimate of the postbuckling strength. These equations give the effective width of the rectangular stress blocks b_e over which the maximum edge stress f can be assumed to act uniformly to produce the same total force as the actual stresses acting over the full width of the plate (see Figure 53). The average physical stresses in the middle of the plate (averaged through the thickness) are smaller due to the postbuckling deformations. Generally, b_e is larger for smaller values of the edge stress f . That is, the buckles are less developed and a larger portion of the plate is effective for smaller f . As the axial load is increased and f increases, the plate postbuckling deformations become larger, the average stresses within the middle of the plate become smaller relative to the edge stress, and b_e becomes smaller. The largest potential plate postbuckling resistance is obtained nominally when the edge stress f reaches F_y .

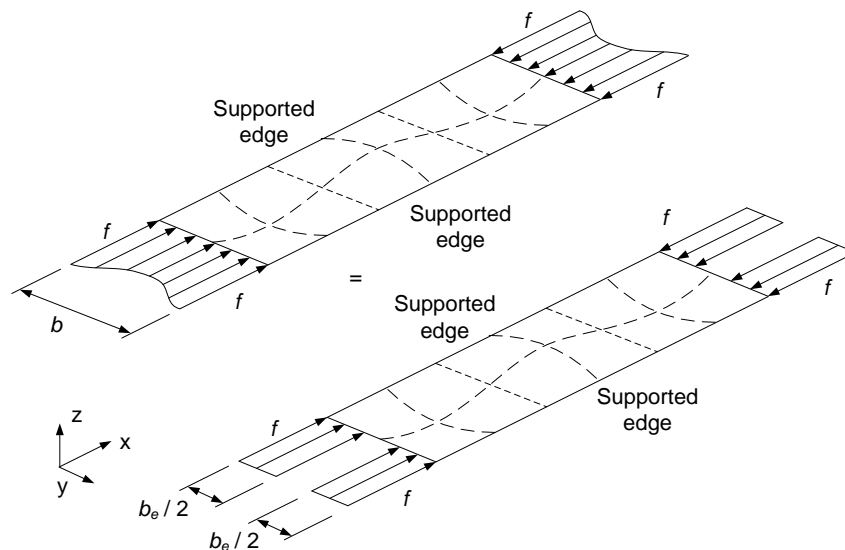


Figure 53 Representative physical average (through thickness) stress distribution across the width of a postbuckled stiffened plate (i.e., both edges supported transversely) versus idealized equivalent stress distribution acting on the plate effective width b_e .

AISC (1969) adopted Eq. (8) (in an allowable stress format) for flanges of square and rectangular sections of uniform thickness. Furthermore, it specified

$$b_e = 1.90t \sqrt{\frac{E}{f}} \left[1 - \frac{0.332}{b/t} \sqrt{\frac{E}{f}} \right] \leq b \quad \text{for } \frac{b}{t} > 1.48 \sqrt{\frac{E}{f}} \quad (5.2.4-9)$$

for other stiffened elements, which is a further liberalization of Eqs. (7) and (8). This was an enhancement intended to obtain a better fit to test results for cases “where appreciable torsional restraint is provided, as for example the web of an I-shaped column” (AISC 1969). These equations are based implicitly on corresponding k_c values similar to those listed in Table 5 and Table 6, and $E = 29,500$ ksi.

The AASHTO (2014) Specification uses the following modified forms of Eqs. (8) and (9):

$$b_e = 1.92t \sqrt{\frac{E}{f}} \left[1 - \frac{0.38}{b/t} \sqrt{\frac{E}{f}} \right] \leq b \quad \text{for } \frac{b}{t} \geq 1.40 \sqrt{\frac{E}{f}} \quad (5.2.4-10)$$

(AASHTO 6.9.4.2.2-10, AISC E7-18)

for flanges of square and rectangular box sections or uniform thickness, all the plate components of square and rectangular hollow structural sections (HSS), and nonperforated cover plates, and

$$b_e = 1.92t \sqrt{\frac{E}{f}} \left[1 - \frac{0.34}{b/t} \sqrt{\frac{E}{f}} \right] \leq b \quad \text{for } \frac{b}{t} \geq 1.49 \sqrt{\frac{E}{f}} \quad (5.2.4-11)$$

(AASHTO 6.9.4.2.2-11, AISC E7-17)

for all other uniformly compressed slender stiffened elements. The modifications in these equations reflect the fact that E is taken as 29,500 ksi in Eqs. (7) through (9), consistent with design practice for cold-formed steel, whereas $E = 29,000$ ksi is used with Eqs. (10) and (11). AISC (2010) applies Eq. (10) to the first two categories mentioned above, but implicitly applies Eq. (11) to any cover plates.

For calculation of the column strength, the stiffened element edge stress f in the above equations is determined fundamentally as

$$f = P_n / A_{eff} \quad (5.2.4-12)$$

where

$$\begin{aligned} A_{eff} &= \text{effective area of the stiffened elements plus the gross area of unstiffened elements} \\ &= Q_a A_g = A_g - \Sigma (b - b_e)t \end{aligned} \quad (5.2.4-13)$$

$$\begin{aligned} P_n &= \text{nominal axial capacity of the column, obtained from Eqs. (5.2.1-1) using} \\ P_o &= Q_s F_y Q_a A_g = Q_s Q_a F_y A_g = Q F_y A_g \end{aligned} \quad (5.2.4-14)$$

For a stub-column ($KL \cong 0$), $f = P_n / A_{eff} = P_o / A_{eff} = Q_s F_y Q_a A_g / Q_a A_g = Q_s F_y = (F_{n\ell})_{min}$, the local buckling strength of the most critical unstiffened cross-section element. If none of the unstiffened cross-section elements are slender, or if the cross-section does not contain any unstiffened elements, $f = F_y$ for this case. However, for a finite length column, P_n is generally smaller than P_o and thus f is generally smaller than $(F_{n\ell})_{min}$. In this case, a rigorous application of the above equations requires iteration since f is a function of P_n via Eq. (12), the stiffened element effective width b_e given by Eq. (10) or (11) is a nonlinear function of f , Q_a depends on b_e , P_o depends on Q_a via Eq. (14), and P_n depends on P_o via Eqs. (5.2.1-1). After substituting the applicable equations into Eq. (12) and simplifying, one obtains

$$f = Q_s F_y \left(0.658 \frac{P_o}{P_e} \right) \quad \text{for } P_e \geq 0.44 P_o \quad (5.2.4-15)$$

As noted above, the effective width b_e is generally smaller for larger values of f . For stiffened slender elements other than the plate components of square and rectangular sections of uniform thickness, AISC (2010) sets Q_s and Q_a equal to 1.0 in Eq. (15) to make the calculations non-iterative. This gives simply

$$f = F_{n(Q=1)} = P_{n(Q=1)} / A_g \quad (5.2.4-16)$$

where $P_{n(Q=1)}$ is the value of P_n determined from Eqs. (5.2.1-1) assuming $Q = Q_s Q_a = 1$. For members that do not have any slender unstiffened elements, $Q_s = 1$ and the value of f obtained from Eq. (16) is generally smaller than that obtained from a rigorous application of Eq. (15). This results in a larger (more liberal) estimated value of b_e than determined iteratively using Eq. (15) for f , and thus a larger (more liberal) estimate of the column resistance P_n .

For slender flanges of square and rectangular sections of uniform thickness, AISC (2010) specifies the direct use of Eq. (12), which requires an iterative solution. However, AISC suggests that f may be taken conservatively as F_y in a user note. The use of Eq. (16) for slender-element box sections gives an anomalous prediction in some cases – the calculated P_n increases with increasing KL/r (White et al. 2006). Figure 54 shows the result from the AISC (2010) calculations for a uniform thickness square box section with $b/t = 150$ and $F_y = 50$ ksi, where $Q_s = 1$ (since there are no unstiffened elements). The factor $Q = Q_a$ is taken equal to b_e/b to simplify the generation of the curves in this figure, neglecting the difference between b and the out-to-out widths of the box. Also, the AISC (2010) results are compared to the AISI (2001) unified effective width equations in the figure, but using $k_c = 4.8$ rather than the AISI (2001) k_c value of 4.0. For $KL/r < 49$ and 64 respectively, the iterative and non-iterative AISC calculations give a smaller column resistance P_n than the AISI-based solution. However, for larger slenderness values, the AISI-based solution gives smaller column strengths. The AISC solution using $f = F_y$ matches more closely with the AISI-based solution.

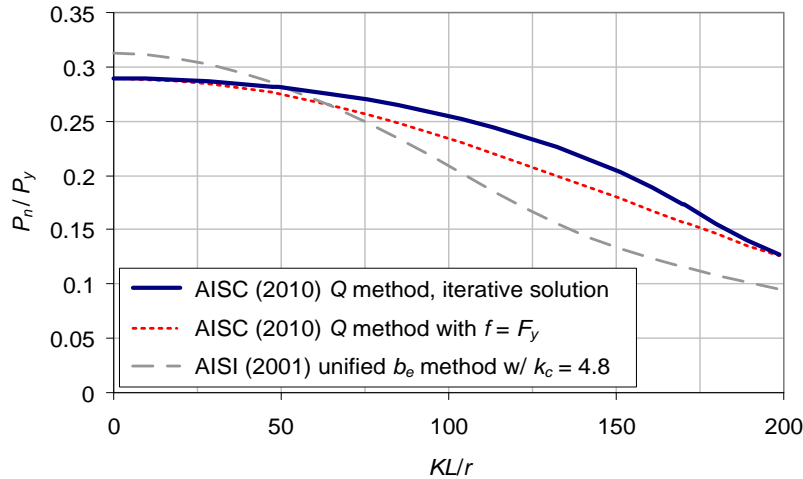


Figure 54 AISC (2005) column resistances versus the resistance obtained using the AISI (2001) unified effective width approach, using the larger AISC-AASHTO $k_c = 4.8$ rather than the AISI $k_c = 4.0$, uniform-thickness square box section with $b/t = 150$ and $F_y = 50$ ksi.

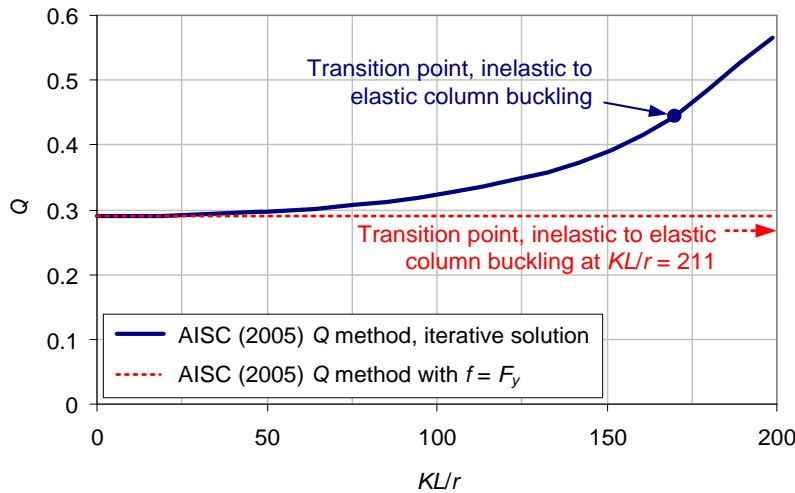


Figure 55 Variation of Q ($= Q_a = b_e/b$) as a function of the column slenderness for the uniform-thickness square box section with $b/t = 150$ and $F_y = 50$ ksi.

The reason for the smaller AISI-based resistances for larger KL/r can be explained with the help of Figure 55. The AISC Q factor approach uses $P_o = Q_s F_y Q_a A_g$ ($= F_y Q_a A_g$ for a box section) as an equivalent cross-section yield capacity, and then assumes that the value of P_n/P_o is given by Eqs. (5.2.1-1) for all values of the column slenderness $(P_o/P_e)^{0.5}$, or KL/r given by Eq. (5.2.1-4). For $P_e < 0.44 P_o$, the elastic buckling equation (Eq. (5.2.1-1b)) governs, and thus the column resistance is independent of P_o . However, Figure 55 shows that Q from both the iterative and the non-iterative AISC procedures is still significantly less than one for the example box column at the idealized transition from inelastic to elastic column buckling. That is, local buckling should still be having a significant effect on the column resistance at the inelastic-to-elastic buckling

transition point in the example, but the Q factor method does not recognize this fact. The AISI-based solution resolves this anomaly by calculating the column resistance as

$$P_n = F_n A_{eff} \quad (5.2.4-17) \quad (\text{AISI C4-1})$$

where F_n is the average compressive axial stress P_n/A_g obtained from Eqs. (5.2.1-1), without accounting for local buckling effects, and A_{eff} is the total effective area of the stiffened *and unstiffened* cross-section elements. (AISI (2001) equation numbers are preceded by the word “AISI” followed by the equation number.) The AISI-based A_{eff} is significantly less than A_g at the larger KL/r values in Figure 54 and Figure 55.

The differences between the AISC (2010) and the AISI-based solutions are not as large as illustrated by Figure 54 for typical I-sections with slender webs and for box-sections with stocker plate elements. White et al. (2006) recommend that the AISC (2010) Q factor approach should be limited to $b/t \leq 100$ for square and rectangular box sections that do not have any longitudinal stiffeners. They indicate that the AISC (2010) approach is sufficient for other stiffened plates (i.e., plates supported along their two longitudinal edges) without intermediate longitudinal stiffeners up to $b/t = 150$. Also, White et al. (2006) indicate that the simpler use of $f = Q_s F_y$ in Eqs. (10) and (11) provides a more representative calculation of the true resistance in all cases. The “bulge” in the column curve obtained by using smaller values of f for longer columns, illustrated by the iterative AISC (2010) solution versus the non-iterative $f = F_y$ solution in Figure 54, does not appear to be justified.

The above discussions apply only to the calculation of the effective widths, b_e , for stiffened elements and the corresponding cross-section form factor, Q_a . The calculation of the form factor Q_s by Eq. (6) for slender unstiffened plate elements is generally adequate to conservative (White et al. 2006). Based on the above considerations, it is recommended that $f = Q_s F_y$ be used in all cases for calculation of the effective widths in Eqs. (10) and (11). AASHTO (2014) adopts these recommendations.

One should note that there is no reduction in the theoretical elastic buckling resistance, P_e , due to plate local buckling in either the AISC (2010) Q factor or the AISI (2001) unified effective width calculations. Peköz (1987) found that Eq. (17) gives a sufficient approximation of experimental column strengths compared to an iterative procedure where P_e is calculated using an effective moment of inertia, I_{eff} , based on the AISI unified plate effective widths, b_e . Therefore, complexities such as shifts in the cross-section effective centroid and shear center with changes in b_e are neglected in both the AISC (2010) and AISI (2001) methods.

5.2.4.5 Axial capacity of hybrid slender-web girders

For girders subjected predominantly to flexural loading, the most economical use of high-performance steels often involves one or two high-performance steel (HPS) flanges combined with a lower strength web. As noted at the beginning of Section 5.2.4 of this module, the webs of girders designed predominantly for flexure are practically always classified as slender elements under uniform axial compression according to Eq. (4). Although the use of homogeneous

sections is most appropriate for members that resist substantial axial compression, hybrid slender-web girders are still acceptable when the axial loads are small. In these cases, the axial capacity $\phi_c P_n$ may be calculated by using the largest effective flange yield strength $Q_s F_{yf}$ for f in Eq. (11) to determine the web effective width b_e , but using the actual web yield strength, F_{yw} , with b_e in determining P_o . This accounts approximately for the level of strain in the web at the strength limit under uniform axial compression. In the unusual case that the web has a larger yield strength than the flanges, F_{yw} should be taken equal to F_{yf} in calculating $\phi_c P_n$. If the flanges have different yield strengths, the smaller F_{yf} value should be used for both flanges in determining $\phi_c P_n$. These are conservative approximations of the complex behavior associated with the post-buckled state of the web plate as well as shifts in the effective centroid and shear center of the cross-section as the true strength limit is approached.

5.2.4.6 Local buckling criteria for solid-web arch ribs

AASHTO (2014) Article 6.14.4.2 limits the web slenderness of solid web arch ribs with no longitudinal stiffeners to

$$\frac{D}{t_w} = 1.25 \sqrt{\frac{E}{f_a}} \quad (5.2.4-18)$$

(AASHTO 6.14.4.2-1)

where f_a is the maximum axial stress along the length of the box section under the factored loads. One can observe that this equation is based on Eq. (4) with F_y replaced by f_a and with $k_c \cong 4.0$, the theoretical minimum plate buckling coefficient for *s.s.* - *s.s.* edge conditions. Web longitudinal stiffeners and flange overhangs in solid web arch ribs are limited to

$$\frac{b}{t} = 0.41 \sqrt{\frac{E}{f_a + f_b/3}} \leq 12 \quad (5.2.4-19)$$

(AASHTO 6.14.4.2-2)

and

$$\frac{b}{t} = 0.41 \sqrt{\frac{E}{f_a + f_b}} \leq 12 \quad (5.2.4-20)$$

(AASHTO 6.14.4.3-2)

respectively where $f_a + f_b$ is the maximum combined stress due to axial load plus flexure along the length of the box section under the factored loads, including second-order amplification. These equations are based on Eq. (4) with F_y replaced by $f_a + f_b/3$ or $f_a + f_b$ (with both stress quantities taken as positive values), and with $k_c = 0.42$, which is essentially the coefficient for plate buckling under uniform axial compression with *s.s.* - free edge conditions. The value $f_b/3$ is the flexural stress at the depth of the stiffeners for the case of two uniformly-spaced longitudinal stiffeners, which is the largest number of web longitudinal stiffeners considered in Article 6.14.4.2. The width-to-thickness ratio of the rib flanges is limited to

$$\frac{b}{t} = 1.06 \sqrt{\frac{E}{f_a + f_b}} \quad (5.2.4-21)$$

(AASHTO 6.14.4.3-1)

for the width between webs. For $f_a + f_b = F_y$, this equation is approximately equal to the AISC (2010) *compact* flange limit for rectangular box sections, which is somewhat more restrictive than Eq. (4) with $k_c \cong 4.0$. Flange compactness limits are discussed in Sections 5.3.5 and 5.4.9 of this module.

For arch ribs with one or two web longitudinal stiffeners, AASHTO (2014) Article 6.14.4 increases the coefficient in Eq. (18) from 1.25 to 1.88 and 2.51 respectively, and specifies minimum requirements for the moment of inertia of the stiffeners, I_s , where I_s is taken about an axis parallel to the face of the web at the base of the stiffeners. With f_a taken equal to P_n/A_g , these provisions ensure conservatively that the axial resistance P_n is not affected by local buckling. This statement is based on a detailed analysis of worst-case box section members that satisfy the AASHTO requirements, using the procedures in AISI (2001).

All of the above limits preclude local buckling in solid web arch ribs at the factored load levels, i.e., under the applied stresses f_a and f_b . Equations (20) and (21) typically, but do not necessarily, preclude local buckling of the flanges at the axial and flexural capacity limits $\phi_c P_n$ and $\phi_b M_n$ used in the AASHTO (2014) axial force-moment interaction equations (see Section 5.6 of this module). The web equations do not preclude local buckling of the web under an axial load equal to $\phi_c P_n$, since $f_a = P_u/A_g$ in Eq. (18) can be substantially smaller than $\phi_c P_n/A_g$. Also, they do not preclude web local buckling under a moment equal to the $\phi_b M_n$ of a box rib (see Section 5.5.3). As such, if P_n and M_n are calculated for an arch rib neglecting local buckling effects, which is the intended practice demonstrated by Wright and Bunner (2006), it is suggested that a linear axial-force moment interaction equation should be used rather than the AASHTO (2014) bilinear interaction equation. The AASHTO (2014) - AISC (2010) bilinear interaction curve is based on the calculation of P_n using the hypothetical state of uniform axial compression with $P_u = P_n$. The last paragraph of AASHTO Article 6.9.4.2.1 requires that the appropriate linear beam-column interaction equation must be used if the local buckling limits are relaxed in the calculation of $\phi_c P_n$ or $\phi_b M_n$. The strength behavior under combined flexure and axial load is discussed further in Section 5.6.

5.2.5 Built-up Columns Composed of Two or More Shapes

AASHTO (2014) Article 6.9.4.3 addresses the design of built-up columns composed of two or more shapes. These member types include closely-spaced back-to-back angles attached by intermittent bolted or welded filler plates or boxed channels (Figure 56a) as well as large compression members with flange components that are spaced widely apart. In the latter case, the flange components may be connected together by perforated cover plates, lacing with flat bars, angles, channels or other shapes, or batten plates as shown in Figure 56b.

The strength behavior of the above types of members differs from the previously discussed cases due to the influence of shear deformations or displacements between the connected shapes. The

shear deformations reduce the member buckling capacity and induce stresses in the elements that connect the shapes together.

Box columns with perforated cover plates designed to Specification rules do not require any strength reduction or other special considerations for shear effects. In new bridge construction, perforated cover plates are likely to be used rather than laced or battened columns. Conversely, the member buckling resistance can be reduced significantly for laced or battened members, with the largest reductions occurring for battened columns.

AASHTO Article 6.9.4.3.2 gives an equation for the shear force due to column stability effects, which perforated cover plates must be designed for in addition to the shear force from factored loads. Article 6.8.5.2 provides additional dimensional requirements for perforated plates that ensure adequate member performance.

In built-up members other than box columns with perforated cover plates, the shear deformations or displacements between the connected shapes has a significant influence on the built-up member axial capacity. In all cases, the end connections must be sufficient to essentially prevent the relative longitudinal slip displacement between the connected shapes at the member ends, if the built-up member is to be effective as a structural member. This connection is the dominant contributor to making the connected shapes act together. However, the compressive strength is also affected to some extent by the shear restraint provided by the intermediate connectors.

AASHTO (2014) and AISC (2010) both provide equations for a modified slenderness ratio that accounts for the effect of shear deformations in the connectors between closely-spaced shapes. Article 6.9.4.3.1 of AASHTO (2014) gives the following equation for members with intermediate connectors that are welded or fully-tensioned bolted:

$$\left(\frac{KL}{r}\right)_m = \sqrt{\left(\frac{KL}{r}\right)_o^2 + 0.82\left(\frac{\alpha^2}{1+\alpha^2}\right)\left(\frac{a}{r_{ib}}\right)^2} \quad (5.2.5-1)$$

(AASHTO 6.9.4.3.1-1)

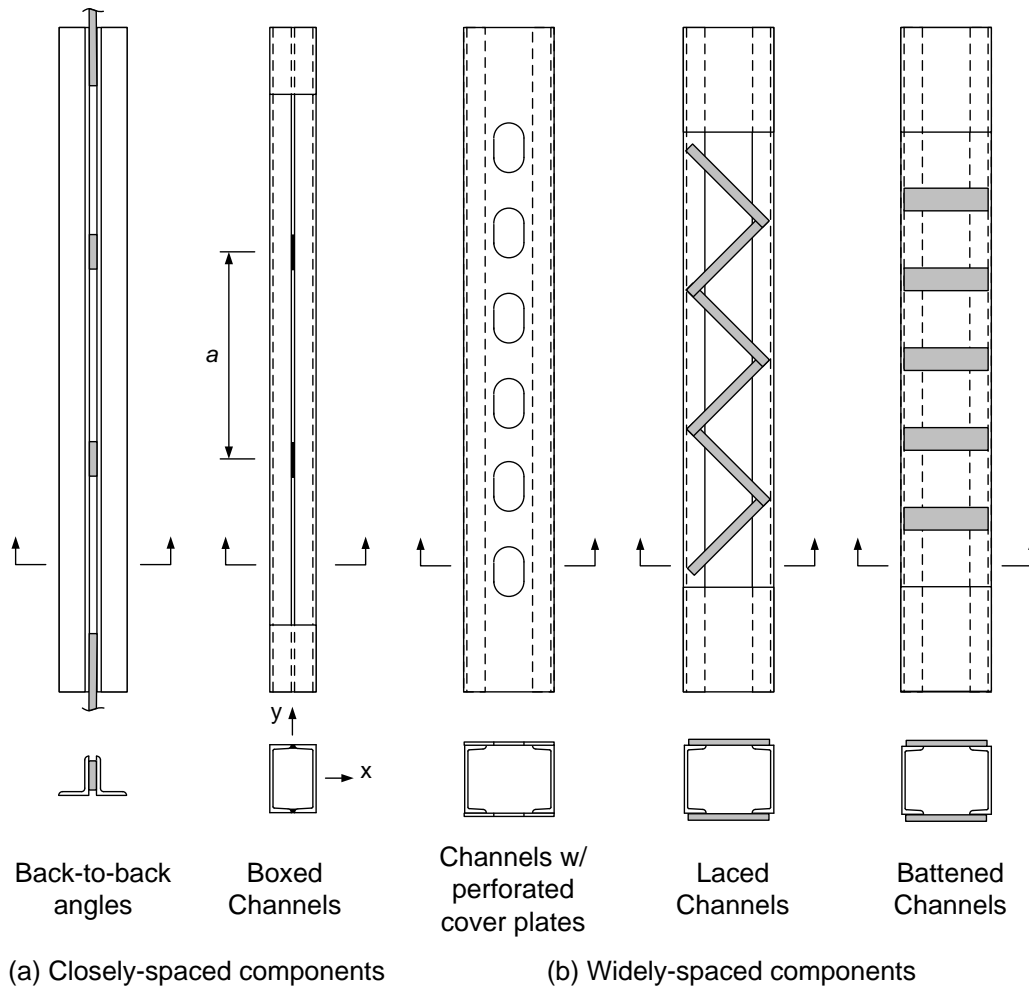


Figure 56 Types of built-up columns, (a) columns with closely-spaced components and (b) columns with widely-spaced components.

Where

$\left(\frac{KL}{r}\right)_o$ = slenderness ratio of the built-up member acting as a unit (with shear deformation neglected) in the buckling direction being considered,

$\left(\frac{KL}{r}\right)_m$ = modified slenderness ratio accounting for shear deformation effects,

a = distance between connectors,

r_{ib} = radius of gyration of an individual component relative to its centroidal axis parallel to the axis of buckling,

α = separation ratio = $h/2r_{ib}$, and

H = distance between the centroids of the individual components perpendicular to the axis of buckling.

This equation is that same as Eq. (E6-2) in the previous AISC (2005) Specification. Given the above modified slenderness ratio $(KL/r)_m$, the ratio P_o/P_e is determined from Eq. (5.2.1-4) and then substituted into Eqs. (5.2.1-1) to determine the nominal column capacity. The buckling capacity about the y -axis of the two channel sections shown in Figure 56a, attached either toe-to-toe or back-to-back at the spacing a , is determined in this fashion. The strength of this type of column is governed either by flexural buckling about the y -axis, including the reduction in strength due to the shear displacement between the shapes via Eq. (1), or by flexural buckling about the x -axis, which is calculated in the manner described in the previous sections and does not include any reduction for shearing deformation effects. In the case of back-to-back double angles such as in Figure 56a, $(KL/r)_m$ is used in place of $(KL/r)_y$ in determining P_{ey} . This modified P_{ey} is then utilized in the torsional-flexural buckling equations as discussed in Section 5.2.3 and 5.2.4 of this module as applicable. The column strength is governed by the smaller value of the resistance due to flexural buckling about the x -axis or torsional-flexural buckling involving twisting combined with bending about the y -axis.

AISC (2010) has adopted a simpler alternative to Eq. (1) that also gives somewhat better predictions relative to test results for fully-tensioned bolted built-up members with closely-spaced individual components, i.e., members such as double-angles or double-channels. The new AISC equation is based on the research by Sato and Uang (2007).

AASHTO (2014) Article C6.9.4.3.1 gives a separate equation that it considers applicable for riveted connectors on existing bridges. This equation is adopted from an AISC (2005 and 2010) equation for snug-tight bolted members, and was developed empirically based on the test results from Zandonini (1985). The ends of the member must be connected rigidly, such as attained by welding, fully-tensioned bolting or the use of end tie plates, for this equation to be valid.

In both of the above cases, the connectors must be adequate to resist the shear forces that develop in the buckled member. AISC (2010) and AASHTO (2014) do not provide guidelines for this check. The AASHTO (2014) Article 6.9.4.3.2 equation for the additional required member transverse shear force in perforated cover plates may be applied for these cases. In addition, AISC (2010) indicates in a user note that it is acceptable to design a bolted end connection of a built-up compression member for the full compressive load with the bolts acting in shear and the bolt resistances based on bearing values. The implication is that connections designed in this way are sufficient to prevent slip between the components at the member ends. It is emphasized that the prevention of slip is necessary for the structural efficiency of the built-up member and for the validity of the corresponding AASHTO (2014) and AISC (2010) resistance equations.

Lastly, an essential requirement for built-up members composed of two or more shapes is that the minimum a/r_i of each component shape between the connectors, lacing or batten plates must be less than or equal to $3/4$ the governing L/r of the built-up member as a whole, where r_i is the least radius of gyration of a component part. Duan et al. (2002) studied the effect of larger a values theoretically, and concluded that a wider spacing makes the built-up member susceptible to further reductions in the axial capacity due to interaction between the buckling of the

component members within the length a between the intermediate elements and the buckling of the entire member over its full length L .

Neither AASHTO (2014) nor AISC (2010) address the influence of the strain energy developed in lacing or batten plates on the column capacity. Equation (1) is a refinement and generalization of an equation that Bleich (1952) derived for battened columns neglecting the energy due to local bending of the battened plates, but assuming zero shearing deformation of the end tie plates. Aslani and Goel (1991) summarize the theoretical development of this equation and show that it gives accurate to slightly conservative predictions of experimental results for double-angle braces. However, their derivation is general, and they suggest that it is also applicable to built-up columns with widely-spaced components.

Ziemian (2010) outlines other solutions for determining the elastic buckling load, P_e , in laced or battened columns, which include the contribution from the lacing or battens to the strain energy. It references Johnston (1976) for further details and illustrative example designs. Once the load P_e is determined, it may be substituted into Eqs. (5.2.1-1) to determine the nominal design compressive strength P_n . There is little benefit to be gained by using formulations other than Eq. (1) for battened members. However, the alternate formulations from Ziemian (2010) tend to give larger capacities than Eq. (1) for laced columns.

5.2.6 Columns with Tapered and/or Stepped Sections and/or Nonuniform Internal Axial Force

Kaehler et al. (2011) detail a procedure for calculation of the compressive resistance of general prismatic or nonprismatic steel members subjected to constant or nonconstant internal axial force along their length. For these types of members, it is convenient to work directly with the following concise form for the axial capacity ratio $P_u/\phi P_n$ associated with Eqs. (5.2.1-1):

$$\frac{P_u}{\phi P_n} = \frac{1}{\phi} \rho_o \left(0.658^{\frac{-1}{\rho_o \gamma_e}} \right) \quad \text{for } \rho_o \gamma_o \geq 0.44 \quad (5.2.6-1a)$$

$$\frac{P_u}{\phi P_n} = \frac{1}{\phi} \frac{1}{0.877 \gamma_e} \quad \text{for } \rho_o \gamma_o < 0.44 \quad (5.2.6-1b)$$

where P_u is the axial load at a given cross-section due to the factored loadings, ϕP_n is the corresponding design resistance,

$$\rho_o = \frac{P_u}{P_o} = \frac{f_a}{QF_y} \quad (5.2.6-2)$$

is the ratio of the factored axial load P_u to the stub-column strength P_o , and

$$\gamma_e = \frac{P_e}{P_u} = \frac{F_e}{f_a} \quad (5.2.6-3)$$

is the ratio of the member elastic buckling resistance, P_e , to the factored (i.e., the required) axial load, P_u . As noted previously, the stub-column strength, P_o , is equal to $F_y A_g$ for cross-sections that do not have slender elements, and it is equal to $Q_s Q_a F_y A_g = Q_s F_y Q_a A_g$ for slender element cross-sections. The term ρ_o also may be considered as the ratio of the average required cross-section axial stress $f_a = P_u/A_g$ to the cross-section effective yield stress, QF_y , as shown by the second equality in Eq. (2). Furthermore, the term $F_e = P_e/A_g$ is the cross-section average axial stress at incipient elastic buckling, and γ_e may be considered as the ratio of this elastic buckling stress to the average required axial stress, $f_a = P_u/A_g$, as shown by the second equality in Eq. (3).

The calculations for a general nonprismatic member subjected to nonconstant internal axial force originate from the seminal research by Lee et al. (1981). For situations where the resistance is governed by elastic column buckling, the axial capacity ratio $P_u/\phi P_n$ in Eq. (1b) depends only on the ratio $\gamma_e = P_e/P_u = F_e/f_a$. This ratio is the same value for any cross-section along the member length. Given a general distribution or diagram of P_u along the member length, the elastic buckling load level is obtained simply by scaling up all the applied loads on the structure, and thus scaling the internal values of P_u , until elastic buckling of the member or structure occurs. Kaehler et al. (2011) discuss various methods for calculating the ratio γ_e for general members and frames.

For the more common situation where nominal yielding occurs along a portion of the member length (due to the applied load plus initial residual stresses), Eq. (1a) governs for the axial resistance. In this case, $P_u/\phi P_n$ depends on both γ_e and ρ_o . Lee et al. (1981) and White and Kim (2006) demonstrate that the axial capacity ratio ($P_u/\phi P_n$) may be calculated adequately for this case by mapping the nonprismatic nonuniformly-loaded member to an equivalent prismatic member that has:

1. The same γ_e , and
2. A ρ_o equal to the largest ρ_o value along the entire length of the physical member, $\rho_{o,max}$.

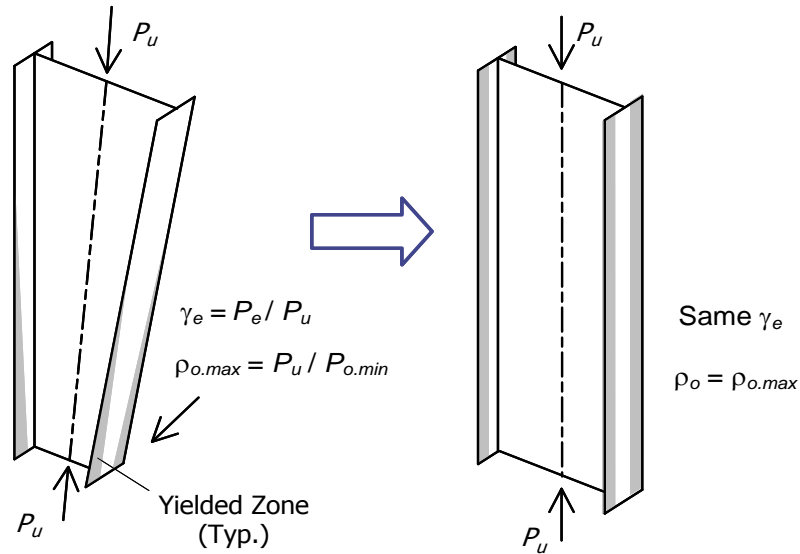


Figure 57 Conceptual mapping of a tapered-web I-section member subjected to constant axial compression to an equivalent prismatic member.

Figure 57 illustrates this approach for a tapered-web I-section member subjected to constant axial compression P_u . The equivalent prismatic I-section member has the same nominal extent of yielding along its entire length that the nonprismatic member has at its most highly stressed cross-section. For cases where the most highly stressed cross-section (the one with $\rho_{o,max}$) is located at a brace point, this approximation tends to be conservative. However, in situations where $\rho_{o,max}$ occurs at a cross-section within the member unsupported length (for example if $\rho_{o,max}$ occurs at the smaller cross-section at a section transition within the unsupported length), the approximation tends to be more accurate.

Based on the above concepts, the axial capacity ratio $P_u/\phi P_n$ may be determined generally as follows:

1. Calculate $\rho_o = P_u / P_o$ at the various cross-sections along the member length. At any cross-sections containing slender plate elements, P_o is determined using Eq. (5.2.4-14), Q_u in Eq. (5.2.4-14) is determined using $f = Q_s F_y$ in Eqs. (5.2.4-10) or (5.2.4-11), and Q_s in the expression for f is determined from Eq. (5.2.4-6).
2. Determine the maximum value of ρ_o , i.e., $\rho_{o,max}$, for all the cross-sections along the member length.
3. Determine the minimum ratio of the elastic buckling load to the factored axial load for the member

$$\gamma_{e,min} = \min(\gamma_{ex}, \gamma_{ey}, \gamma_{eTF}) \quad (5.2.6-4)$$

4. as appropriate, where γ_{ex} is the critical load ratio for elastic flexural buckling about the major axis of the cross-section, γ_{ey} is the critical load ratio for elastic flexural buckling about the minor axis, and γ_{eTF} is the critical load ratio for elastic torsional or torsional-flexural buckling.
5. Substitute $\rho_{o,max}$ and $\gamma_{e,min}$ for ρ_o and γ_e in Eqs. (1) to determine the axial capacity ratio $P_u/\phi P_n$.

Kaehler et al. (2011) detail a more complex procedure for I-section members that utilize the AISC (2010) approach from Eq. (5.2.4-16) for calculation of f . This approach is not recommended. The above recommended procedure simply calculates Q based on $f = Q_s F_y$ at the various member cross-sections. In addition to its relative simplicity, this approach is more accurate (see Section 5.2.4 of this module). In cases where the member is dominated by flexural rather than axial loading, the effect on the final beam-column resistance is typically quite small.

5.2.7 Composite Columns

5.2.7.1 AASHTO (2014) - AISC (1999) approach

AASHTO (2014) uses the AISC (1999) LRFD Specification approach to quantify the axial compressive resistance of concrete-filled sections and steel sections encased in concrete. This approach, developed based on the work of SSRC Task Group 20 (SSRC 1979), uses the steel column strength curve given by Eqs. (5.2.1-1) through (5.2.1-4) with the area of the steel section, $A_g = A_s$, and a modified yield strength, F_{my} , modulus of elasticity, E_m , and radius of gyration, r_m , to account for the effect of the concrete and longitudinal reinforcing bars. These modifications are as follows:

$$F_{my} = F_y + c_1 F_{yrs} \frac{A_{rs}}{A_s} + c_2 f'_c \frac{A_c}{A_s} \quad (5.2.7-1)$$

(AASHTO 6.9.5.1-4, AISC 1999 I2-1)

$$E_m = E + c_3 E_c \frac{A_c}{A_s} \quad (5.2.7-2)$$

(AASHTO 6.9.5.1-5, AISC 1999 I2-2)

$$r_m = \max(r_s, 0.3B_c) \quad (5.2.7-3)$$

where

A_c = area of the concrete,

A_{rs} = area of the continuous longitudinal reinforcing steel bars,

A_s = area of the encased steel section or the steel tube,

E = modulus of elasticity of the steel (29,000 ksi)

E_c = short-term modulus of elasticity of the concrete,

- F_y = specified minimum yield strength of the steel section or tube,
 F_{yrs} = specified minimum yield strength of the longitudinal reinforcing steel,
 f'_c = specified minimum 28-day compressive strength of the concrete,
 r_s = radius of gyration of the steel section or tube in the direction of buckling, and
 B_c = overall width of the composite section in the plane of bending

In addition, it should be noted that the AISC equation numbers in this sub-section correspond to the AISC (1999) Specification. The coefficients c_1 and c_2 account for the contributions of the reinforcing steel and concrete to the stub-column strength P_o , whereas the coefficient c_3 accounts for the contribution of the concrete to the stiffness of the overall section. In the context of Eqs. (5.2.1-1), the AASHTO (2014) - AISC (1999) approach specifically uses

$$P_o = F_{my} A_s \quad (5.2.7-4)$$

and

$$P_e = \frac{\pi^2 E_m}{(KL/r_m)^2} A_s \quad (5.2.7-5)$$

(AASHTO 6.9.6.1-6)

For encased sections, AASHTO (2014) and AISC (1999) use

$$c_1 = 0.7, c_2 = 0.6 \text{ and } c_3 = 0.2 \quad (5.2.7-6)$$

whereas for filled sections,

$$c_1 = 1.0, c_2 = 0.85 \text{ and } c_3 = 0.4 \quad (5.2.7-7)$$

If present in a filled section, the reinforcing steel is always supported sufficiently such that it can develop its full capacity ($c_1 = 1.0$). However, for encased sections, a reduced c_1 value is employed to account for the potential spalling of the concrete, leaving the steel bars exposed. The coefficient c_2 assumes that the concrete will at least reach a stress of $0.85 f'_c$ because of the confinement available in filled sections. However, for encased sections, the ACI (1977) reduction to 70 % of the capacity for components relying on unconfined concrete was applied, i.e., $c_2 = 0.7(0.85) \cong 0.6$. For the stiffness coefficient c_3 , SSRC (1979) adopted the ACI (1977) recommendations. For confined concrete, ACI (1977) recommended using only 40 % of the initial stiffness of the concrete, whereas for unconfined concrete, only 20 % was used (hence $c_3 = 0.2$ for encased sections and 0.4 for filled sections).

For the modified radius of gyration, r_m , SSRC (1979) noted that in members where the steel section provides the majority of the flexural resistance, the radius of gyration of the steel section, r_s , is appropriate, while if the concrete portion of the section provides the majority of the flexural resistance, the radius of gyration of the concrete section is appropriate. Therefore, the larger of

these two values was selected, with $0.3B_c$ being the radius of gyration of a square concrete cross-section (i.e., a square column is implicitly assumed in this development).

The AASHTO (2014) - AISC (1999) provisions are applicable only for members in which the area of the steel section, A_s , is greater than 4 % of the total composite section. For smaller A_s , the member must be designed as a reinforced concrete column. There is typically a significant discontinuity in the strength predicted by handling the member as a composite steel column versus a reinforced concrete column at this limit. Furthermore, the values for F_{yrs} and F_y used in calculating the resistance are restricted to 60 ksi. This is because the concrete stiffness reduces significantly at strains near 0.2 percent, and thus the concrete is considered potentially ineffective in stabilizing the steel for larger yield strengths. Concrete strengths $f'_c \leq 8$ ksi are required for normal weight concrete, since there was limited test data for larger strengths at the time of the original developments. Concrete strengths $f'_c \geq 3$ ksi are required to ensure good quality concrete. A number of requirements are specified for the longitudinal reinforcing bars, lateral ties and concrete cover in encased sections to ensure good performance of the concrete section. For rectangular filled sections, b/t is limited to $1.7(E / F_y)^{0.5}$ and for circular filled sections, D/t is limited to $2.8(E / F_y)^{0.5}$ to ensure that the steel section yields before the concrete crushes or significant local buckling occurs. These limits are the same as the AASHTO (2014) Article 6.9.4.1 limits for noncomposite rectangular and circular tubes.

5.2.7.2 AISC (2005) and (2010) approach

AISC (2005) provides substantially updated procedures for calculating the resistance of encased and filled composite columns. These procedures provide larger, more accurate resistances, and reduce the differences between the AISC and ACI design provisions. The corresponding AISC (2010) provisions are essentially unchanged from AISC (2005) for encased composite columns; however, a number of new enhancements have been implemented in AISC (2010) for filled composite columns that were not present in AISC (2005). The procedures are generally conservative, but still have a large coefficient of variation with respect to test data (Leon and Aho 2002). This results in a 12 % reduction in the ϕ_c factor relative to that used in AISC (1999). In the new AISC (2010) provisions, P_o is calculated more directly as

$$P_o = A_s F_y + A_{sr} F_{yrs} + 0.85 A_c f'_c \quad (5.2.7-8)$$

(AISC I2-4)

for encased sections, and as

$$P_o = A_s F_y + C_2 f'_c \left(A_c + A_{sr} \frac{E}{E_c} \right) \quad (5.2.7-9)$$

(AISC I2-9b)

for *compact* filled sections, where $C_2 = 0.85$ and 0.95 for rectangular and circular sections respectively. These equations recognize the full development of the continuous reinforcing bars for encased columns, and they account for the confinement effects on the concrete strength and the compatibility of the concrete and reinforcing steel strains in circular filled sections. Furthermore, the equivalent member elastic buckling load is calculated directly as

$$P_e = \frac{\pi^2 EI_{eff}}{(KL)^2} \quad (5.2.7-10)$$

(AISC I2-5)

where

$$EI_{eff} = EI_s + C_r EI_{sr} + C_c E_c I_c \quad (5.2.7-11)$$

(AISC I2-6 & I2-12)

I_s = moment of inertia of the steel section about the axis of buckling,

I_{sr} = moment of inertia of the reinforcing bars about the axis of buckling,

I_c = moment of inertia of the concrete section about the axis of buckling,

C_r = 0.5 for encased sections and 1.0 for filled sections, and

$$C_c = 0.1 + 2 \left(\frac{A_s}{A_c + A_s} \right) \leq 0.3 \text{ for encased sections,} \quad (5.2.7-12)$$

(AISC I2-7)

$$= 0.6 + 2 \left(\frac{A_s}{A_c + A_s} \right) \leq 0.9 \text{ for filled sections.} \quad (5.2.7-13)$$

(AISC I2-13)

In addition to the above, the AISC (2010) provisions improve upon the AISC (2005) provisions for filled sections by addressing the reduced column axial resistance for more slender HSS or box sections of uniform thickness or more slender circular hollow sections. AISC (2010) Chapter I provides its own set of tables for classification of these member types as compact, noncompact or slender. For rectangular HSS and box sections of uniform thickness, the compactness limit, which must be satisfied to use the above filled-section equations, is

$$b/t \leq \left[\lambda_p = 2.26 \sqrt{\frac{E}{F_y}} \right] \quad (5.2.7-14a)$$

and for filled circular sections, the corresponding compactness limit is

$$D/t \leq \left[\lambda_p = 0.15 \frac{E}{F_y} \right] \quad (5.2.7-14b)$$

AISC (2005) restricts the usage of its equations to the above limits, whereas AISC (2010) introduces the classification of compact, noncompact and slender steel elements in filled composite sections and provides additional equations that quantify the reduced axial resistance for sections where some of the steel elements are not compact. Although the same names are used, the implications of the AISC (2010) classification of filled composite sections are fundamentally different than the AISC (2010) and AASHTO (2014) classification of the steel

elements as compact, noncompact and slender in other cross-section types. In quantifying the axial resistance of filled composite section members:

“Compact” indicates that the section is able to develop a maximum “plateau” resistance of the concrete and reinforcing steel, including the influence of confinement from the steel section,

- “Noncompact” indicates that the steel section has sufficient thickness such that it can fully yield in the longitudinal direction, but it cannot adequately confine the concrete infill after it reaches $0.70f_c'$, at which point the concrete starts undergoing significant inelastic deformations and volumetric dilation (pushing against the wall of the steel section).
- “Slender” indicates that the steel section can neither develop full yielding on its area in the longitudinal direction, nor confine the concrete after it reaches $0.70f_c'$.

Furthermore, in quantifying the flexural resistance of filled composite section members:

- “Compact” indicates that the section can develop its full plastic moment capacity, M_p , in flexure,
- “Noncompact” indicates that the section can develop a moment capacity greater than the nominal first-yield moment of the section, M_{yt} , when the tension flange reaches first yielding, or greater than the moment corresponding to a maximum concrete compressive stress of $0.70f_c'$, but local buckling or inadequate confinement of the concrete in compression precludes the development of M_p , and
- “Slender” means that the flexural resistance of the member is limited to the smaller value of the first yield moment when the tension flange reaches first yielding and the moment corresponding to elastic response of the concrete and a maximum compressive stress of $0.70f_c'$.

Elsewhere in the AISC (2010) and AASHTO (2014) Specifications:

- A cross-section containing all “compact” compression elements is capable of developing *moments* equal to the fully-plastic flexural resistance M_p ,
- With the exception of the AASHTO (2014) provisions for composite sections in positive flexure, a cross-section containing “noncompact” compression elements is capable of developing *moments* larger than the nominal first yield flexural resistance in compression including residual stress effects, i.e., $M_{yr} = F_{yr}S_{xc}$, and
- With the exception of the AASHTO (2014) provisions for composite sections in positive flexure, a cross-section with “slender” compression elements has its strength generally limited by local buckling of compression elements prior to reaching M_{yr} .

- In the AASHTO (2014) provisions for composite sections in positive flexure, a “noncompact section” is one in which the maximum potential flexural resistance is limited to a compression flange stress of $R_b R_h F_{yc}$, corresponding to nominal yielding of the steel compression flange, neglecting residual stress effects but including the influence of load shedding from a slender and/or hybrid web, or a tension flange stress of $R_h F_{yt}$. For these sections, the reasons for limiting the maximum resistance to the above values include yield strength of the steel larger than 70 ksi, web slenderness, and/or limiting potential inelastic redistribution in curved bridge structural systems (see Sections 5.3.3 and 5.3.4 of this module).
- In the AASHTO (2014) provisions for composite sections in positive flexure, a “compact section” is one in which the maximum potential flexural resistance is the full plastic moment of the composite section (see Section 5.3.3).

The AISC (2005) and (2010) provisions for composite columns are applicable for A_s/A_c as small as 1 %. Furthermore, the specified minimum yield strength of the structural steel and reinforcing bars is increased to 75 ksi. The provisions are extended to concrete strengths up to $f'_c = 10$ ksi for normal weight concrete. Also, the required area for the transverse ties in encased sections is increased slightly relative to AISC (1999), from 0.007 to 0.009 in²/in of tie spacing, and a minimum reinforcement ratio for continuous longitudinal bars in these sections is relaxed slightly from 0.007 to 0.004. However, a minimum of four continuous longitudinal bars is required in encased columns. In addition, the above equations for encased sections are based on studies of doubly-symmetric composite columns. The commentary to Section I2.1b of AISC (2010) provides guidelines for the limited use of these equations with columns having non-symmetric cross-sections.

AISC (2010) specifies detailed rules for load transfer to the composite cross-section in encased and filled sections that are enhancements on prior AISC (1999) and AISC (2005) provisions.

5.2.7.3 Axial compression resistance of composite bridge girders

In some situations, steel bridge girders designed compositely with a concrete deck are subjected to combined flexure and axial compression. This occurs for instance in a cable-stayed bridge with a composite I- or box-girder deck system. Axial compression can also occur due to restraint of thermal expansion in stringer bridges, although these effects typically are rendered negligible by the movements permitted at integral abutments or deck joints. AASHTO (2014) Articles C6.10.6. 1 and C6.11.6.2.1 allow the Engineer to neglect a concentrically-applied axial force P_u in all types of I- and box-girder members whenever $P_u/\phi_c P_n$ is less than 0.1. However, for $P_u/\phi_c P_n > 0.1$, I- and box-girders must be checked in general as beam-columns. Any moments generated about the effective centroidal axis, due to eccentric application of axial loads, must be considered. An appropriate calculation of this effective axis is suggested below. Bending moments due to transverse loads and eccentricity of the applied axial loads are addressed separately in the flexural resistance calculations (see Sections 5.3.3 through 5.3.7 and 5.4.6 through 5.4.12 of this module).

In all of the above cases, the Engineer needs to calculate $\phi_c P_n$ for the composite girder. AISC (2010) provides substantial guidelines regarding the calculation of the resistance of flexural members subjected to combined axial load in the Commentary to its Section I7. However, this discussion is primarily directed at the calculation of the strength of collector components in building floor systems. Neither AASHTO (2014) nor AISC (2005) provide specific guidelines for this calculation, although the commentary of AISC (2005) does provide the following broad guidance in the context of composite I-section members:

“Adequate means to transmit axial loading to and from the steel section should be provided. Where shear connectors are used, the top flanges may be considered braced for compressive loading at the shear connector locations.... For load combinations resulting in compressive loading of the lower flange, length effects between brace points should be considered. Inflection points should not be considered as braced points for torsional buckling of the unbraced flange.”

Specifically, the axial compressive resistance of a composite I-girder may be governed either by flexural buckling about the major axis of bending, or by torsional buckling of the steel I-section about an enforced axis of rotation located at the depth of the shear connectors. The first of these limit states is expected to rarely control. It is suggested that it can be checked conservatively by using Eq. (11) for EI_{eff} , with C_c taken equal to the value of 0.2 implied in the AASHTO (2014) - AISC (1999) composite column provisions, then using Eq. (10) to calculate P_e . Since the composite cross-section is singly-symmetric, the Engineer will need to determine its effective centroidal axis for calculation of the separate contributions to the effective moment of inertia, I_{eff} . It is suggested that the full steel cross-section may be used for this calculation, consistent with the handling of slender-element cross-sections discussed in Section 5.2.4 of this module, and that a modular ratio of $n/0.2$ should be used for the concrete slab. The contribution of the longitudinal reinforcing steel in Eq. (11) usually will be quite small compared to the other terms, and thus it is suggested that this term should be neglected. Some judgment must be used in selecting the effective width of the slab concrete for use in Eqs. (4) and (11). Chen et al. (2005) suggest a lower bound effective width of 90 % of the full width for regions away from the towers and 70 % of the full width in regions close to the towers in cable-stayed bridges with two edge girders, two pylons, a semi-harp cable configuration with two planes of cables, a relatively thin concrete slab, cable spacing at approximately 10 % of the back span length, and floor beam spacing approximately one-third of the cable spacing.

Conversely, the load corresponding to the elastic torsional buckling of the steel I-girder about an enforced axis of rotation at the shear connectors is given by

$$P_{eT} = \left[\frac{\pi^2 E (C_w + I_y a_s^2)}{L_b^2} + GJ \right] \frac{1}{r_x^2 + r_y^2 + a_c^2} \quad (5.2.7-14)$$

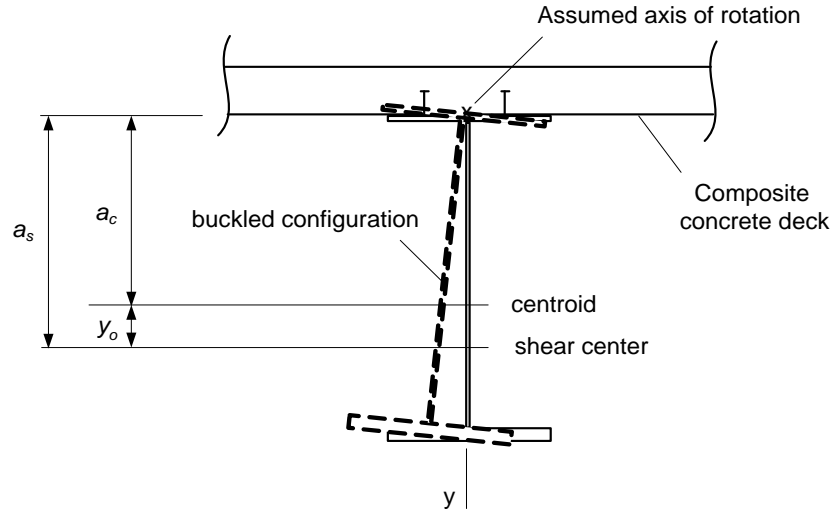


Figure 58 Cross-section displacements and relevant cross-section dimensions for torsional buckling about an enforced axis at the depth of the shear connectors.

where C_w is the warping constant of the steel section, a_s and a_c are the distances from the shear center and centroid of the steel cross-section to the fixed axis of rotation respectively, and L_b is the length between the locations where the cross-section is prevented from twisting (Timoshenko and Gere 1961; Bleich 1952). Figure 58 shows the typical case where the bottom flange is larger and $a_s > a_c$. Equation (14) gives a substantially larger buckling load than obtained based on the flexural buckling of the unrestrained steel I-section member about its minor principal axis.

Equation (14) neglects the torsional restraint potentially provided by the deck to the steel I-section member. The effect of this restraint is reduced substantially in many cases due to web distortion. Torsional restraint of the steel I-section is assumed only at the cross-frame locations, i.e., L_b is the spacing between the cross-frames. Equation (14) also neglects the axial force contribution from the deck at the incipient elastic torsional buckling of the steel section.

Given the above calculations of P_e and P_{eT} , it is desired to calculate P_n from Eqs. (5.2.1-1). As such, the Engineer is faced with a decision about the appropriate calculation of P_o . It is recommended that, with one exception, P_o may be calculated as

$$P_o = A_s(QF_y) + A_{sr}F_{yrs} + 0.85A_c f'_c \quad (5.2.7-15a)$$

where $Q = Q_s Q_a$ is determined as discussed in Section 5.2.4 of this module, using $f = F_y$ in calculating the effective width of the web. Since the top flange is connected compositely to the deck, it should always be considered as a nonslender element (i.e., $Q_s = 1$). For hybrid composite I-girders, the $A_s(QF_y)$ term in Eq. (15a) should be determined as discussed previously in Section 5.2.4. The exception to the use of Eq. (15a) is that, when calculating the ratio P_o/P_e for the torsional buckling limit state, P_e should be taken as P_{eT} from Eq. (14) and P_o should be determined as

$$P_o = A_s(QF_y) \quad (5.2.7-15b)$$

This accounts for the fact that P_{eT} does not include any axial force contribution from the deck.

Procedures similar to the above can be used to obtain P_e and P_o for a composite box girder. However, torsional buckling is not a consideration for these members. Therefore, P_e may be calculated based solely on flexural buckling about a horizontal axis through the effective centroid. This elastic buckling load usually will be quite large, and therefore P_n will be approximately equal to P_o .

The AISC (2005) commentary also discusses the potential need for a larger number of shear connectors for axial load transfer and added flexure. However, this statement is in the context of the typical use of partially-composite I-beams in building construction. In current design practice, bridge girders are usually designed as fully-composite and the shear connectors are designed for fatigue in addition to strength. Therefore, in most cases, no additional shear connectors will be necessary to handle combined axial loading and compression. Thus, no special detailing of the concrete deck is necessary beyond that required by AASHTO (2014) Chapter 9.

Equation (14) also can be used to calculate the compressive resistance of noncomposite I-girders when the top flange is embedded in the concrete deck. These types of members would be checked for flexural buckling about their major axis of bending using the corresponding KL/r to determine P_e , and using Eq. (14) to calculate $P_e = P_{eT}$ corresponding to torsional buckling about an enforced axis of rotation at the top flange.

5.3 I-Section Flexural Members

5.3.1 Introduction

The AASHTO (2014) Article 6.10 and Appendices A6 through D6 provisions for I-section flexure are central to the behavior and design of many of the bridge structural systems discussed in Section 2 of this module. Because of the large number of I-beam and I-girder stringer bridges used in highway construction, these provisions have possibly the greatest overall impact of all the AASHTO (2014) Specifications with respect to steel bridge construction. Furthermore, a number of the AASHTO (2014) Article 6.11 rules for box-girder design utilize or parallel specific I-section member provisions.

The calculation of the nominal flexural resistance of the various types of I-section members can be explained conceptually with just a few figures. However, numerous parameters must be considered for the wide range of I-section members utilized in design practice. Section 5.3.2 of this module initiates the discussion of I-section flexural members by outlining basic proportioning limits defined in AASHTO (2014) Article 6.10.2. Sections 5.3.3 and 5.3.4 then provide an overview of the AASHTO (2014) Article 6.10.7 provisions for composite members in positive major-axis bending. Most of the details for design of I-section members fall under the category of composite members in negative bending and noncomposite members. Section 5.3.5 outlines the key concepts and the basics of the calculations for the various design parameters pertaining to major-axis bending of these member types. All of the discussions of Sections 5.3.3 through 5.3.5 focus on prismatic member unbraced lengths. Section 5.3.6 explains how the

prismatic member rules are generalized to handle variable web depth I-section members and/or I-section members with cross-section transitions along their lengths. Section 5.3.7 then addresses the handling of combined major-axis bending, torsion and minor-axis bending in AASHTO (2014). Finally, Section 5.3.8 discusses the shear strength of I-section members, Section 5.3.9 addresses the strength of shear connectors for composite construction, and Section 5.3.10 discusses various “secondary” limit states such as web crippling and web yielding due to concentrated transverse loads.

5.3.2 Proportioning Limits

AASHTO (2014) Article 6.10.2 provides basic rules targeted at ensuring the economical and practical proportioning of I-section members in preliminary design. Also, these rules provide practical bounds on which the flexural resistance provisions are based. Article 6.10.2.1.1 requires that webs without longitudinal stiffeners shall satisfy the following depth-to-thickness limitation

$$D/t_w \leq 150 \quad (5.3.2-1)$$

(AASHTO 6.10.2.1.1-1)

This limit helps ensure ease of handling, permits simplification of resistance calculations for composite members (discussed subsequently in Section 5.3.3 of this module), and helps ensure adequate performance with respect to web distortion induced fatigue for members that do not have web longitudinal stiffeners. For longitudinally-stiffened I-section members, Article 6.10.2.1.2 requires

$$D/t_w \leq 300 \quad (5.3.2-2)$$

(AASHTO 6.10.2.1.2-1)

Equation (2) is simply a practical upper bound on the slenderness of webs with longitudinal stiffeners. I-girders with larger D/t_w values are more susceptible to secondary limit states such as transverse web crippling. Both of the above limits are expressed in terms of the total web depth to thickness, for ease of use in preliminary design.

Article 6.10.2.2 specifies limits on the flange dimensions. The half-width to thickness ratio is limited for both compression and tension flanges to

$$b_f / 2t_f \leq 12 \quad (5.3.2-3)$$

(AASHTO 6.10.2.2-1)

This limit is targeted predominantly at ensuring that the flanges of I-girders will not distort excessively when they are welded to the web. However, it also allows for some simplification of the flange local buckling resistance equations in AASHTO (2014) as discussed subsequently in Section 5.3.5. Article 6.10.2.2 also specifies

$$b_f \geq D/6 \quad (5.3.2-4)$$

(AASHTO 6.10.2.2-2)

$$t_f \geq 1.1 t_w \quad (5.3.2-5)$$

(AASHTO 6.10.2.2-3)

and

$$0.1 \leq I_{yc}/I_{yt} \leq 10 \quad (5.3.2-6)$$

(AASHTO 6.10.2.2-4)

where I_{yc} and I_{yt} are the moments of inertia about the plane of the web for the compression and tension flanges respectively. Few I-section member tests have been conducted with depths D larger than $6b_f$. Furthermore, a number of the available tests for deep narrow-flange members that violate Eq. (4) indicate significant degradation in the resistances relative to the prediction equations in AASHTO (2014) and AISC (2010) as well as in previous Specifications (White and Jung 2008; White and Kim 2008; White and Barker 2008; White et al. 2008). Also, I-sections with narrow flange widths violating Eq. (4) generally require bracing at close intervals to avoid significant reductions in their flexural resistance due to lateral-torsional buckling. Equation (5) requires that the flange thicknesses must be slightly larger than the web thicknesses in bridge I-section members. There is evidence of acceptable performance of I-section members with $t_f = t_w$; however, the requirement for the additional flange thickness in Eq. (5) helps ensure member robustness and does not appear to impose any practical or economic limitations on bridge construction. The combination of Eqs. (2) and (3) restricts the ratio of web-to-flange area for either flange, $A_w/A_f = Dt_w/b_f t_f$, to a maximum value of 5.4. Lastly, Eq. (6) ensures efficient relative flange proportions and prevents the use of extremely monosymmetric I-sections that may be difficult to handle during construction and for which the I-section member flexural resistance equations are generally not valid.

Article C6.10.3.4 recommends one additional limit on the minimum flange width, pertaining to constructability, that deserves mention in the context of general I-section proportioning limits. This article suggests

$$b_{fc} \geq L/85 \quad (5.3.2-7)$$

(AASHTO C6.10.3.4-1)

where L is taken as the length of a shipping piece. This limit helps alleviate potential problems due to out-of-plane distortion of the girder compression flange during fabrication, shipping and erection.

5.3.3 Compact Composite Sections in Positive Flexure

5.3.3.1 Section classification

AASHTO (2014) Article 6.10.6.2.2 defines composite sections in positive bending as compact sections when:

- The specified minimum yield strengths of all the flanges do not exceed 70 ksi
- $D/t_w \leq 150$

- $2D_{cp} / t_w \leq 3.76 \sqrt{E / F_{yc}}$ (5.3.3-1)

(AASHTO 6.10.6.2.2-1, AISC Section I3.2a)

and

- The bridge is straight (no horizontal curvature or kinked (chorded) continuous geometry).

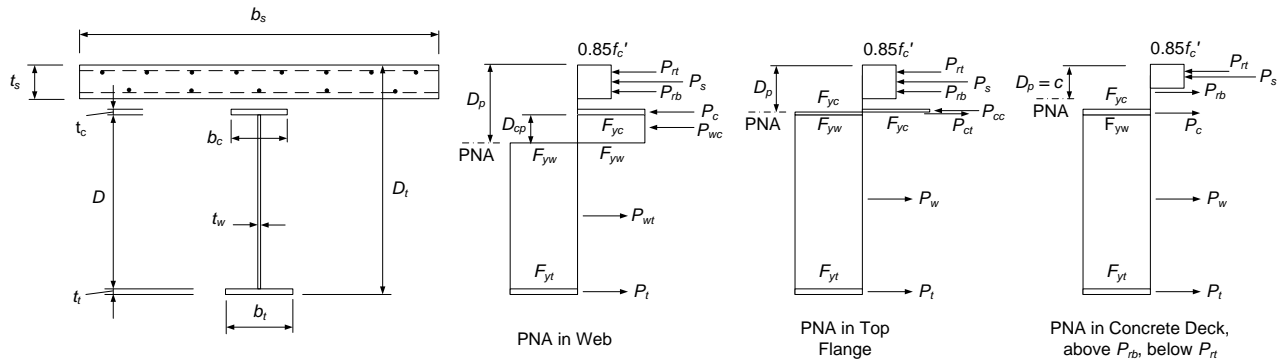


Figure 59 Illustrative plastic cross-section models for composite I-sections in positive bending. Cases for plastic neutral axis (PNA) in concrete deck below P_{rb} , concrete deck at P_{rb} , concrete deck at P_{rt} and concrete deck above P_{rt} are not shown.

This means that the fully-plastic cross-section models shown in Figure 59 may be used as the base for the member resistance calculations. The first of the above limits is specified to avoid potential crushing of the deck concrete prior to reaching the calculated flexural resistance. For $F_y = 70$ ksi, the yield strain of the steel $\epsilon_y = F_y/E = 0.0024$ is slightly beyond the level of strain corresponding to the peak compressive stress for typical deck concrete. For $F_y = 100$ ksi, the yield strain of the steel is 0.0034, which is somewhat beyond the nominal concrete crushing strain. The second limit is the Eq. 5.3.2-1 restriction on the web width-to-thickness ratio beyond which longitudinal stiffeners are required. Since longitudinally-stiffened sections tend to be deeper and are typically used in longer spans with corresponding larger dead load stresses, they often have large elastic $2D_c/t_w$ values. These large web slenderness values may result in significant web bend buckling prior to development of flexural yielding, even if the above third limit is satisfied at the theoretical plastic limit state. Furthermore, because of the relative size of the steel section to the concrete deck typical of these types of sections, and due to the thinness of the web, the plastic moment capacity M_p often is not significantly larger than the yield moment M_y (or the yield moment modified for hybrid web effects, $R_h M_y$). The third limit is the AASHTO (2014) - AISC (2010) web compactness limit corresponding to the plastic depth of web in compression, D_{cp} , in Figure 59. Webs more slender than this limit are nominally unable to develop the large inelastic strains necessary for the cross-section to reach its plastic moment M_p . The fourth limit has been discussed previously in Section 3 of this module. The above four limits are simple restrictions intended to limit the use of the plastic cross-section model of Figure 59 to designs where it is supported by test data. Future research may lead to some relaxation of a number of these limits.

5.3.3.2 Flexural resistance

The base model shown in Figure 59 is the same as the Whitney rectangular stress block model used in reinforced concrete design except that the concrete rectangular stress block is always taken as the full depth in compression above the plastic neutral axis (PNA) rather than a fraction of this depth. This simplification generally results in a negligible or only a slight increase of the calculated plastic moment. The effective width of the concrete slab is assumed to be stressed in compression at $0.85f'_c$, and all the reinforcing and structural steel elements are assumed to be stressed at their yield strengths F_y . AASHTO (2014) Article D6.1 gives equations for the PNA location and the corresponding M_p for all potential PNA positions in the slab or in the steel I-section. These equations are based simply on equilibrium of the fully-plastic stress distributions and the assumption of zero axial force. The concrete within the haunch over the girder flanges is neglected in the AASHTO (2014) equations for purposes of simplicity. However, the nominal height of the haunch is included. The reader is referred to Article D6.1 for the detailed equations.

AASHTO (2014) Article 6.10.7.1.2 does not necessarily use the full plastic moment M_p as the nominal flexural resistance for compact composite sections in positive bending. This Article specifies

$$M_n = M_p \quad (5.3.3-2)$$

(AASHTO 6.10.7.1.2-1)

when $D_p < 0.1D_t$, where D_p is the depth of the plastic neutral axis below the top of the deck (see Figure 59) and D_t is the total depth of the composite section. However, when $D_p/D_t > 0.1$, it specifies

$$M_n = M_p (1.07 - 0.7 D_p/D_t) \quad (5.3.3-3)$$

(AASHTO 6.10.7.1.2-2)

The AASHTO (2014) resistance factor for flexure is $\phi_f = 1.0$ for all types of composite and noncomposite members.

Equation (3) enforces a higher margin of safety for members with larger D_p/D_t , as first recommended by Wittry (1993). The increase in the margin of safety, relative to the theoretical resistance determined from a strain-compatibility analysis at crushing of the deck concrete, varies linearly from 1.0 at $D_p/D_t = 0.1$ to approximately 1.3 at $D_p/D_t = 0.42$. Strain-compatibility analyses of a wide range of practical composite sections indicate only a slight decrease in the cross-section moment below $M = M_p$ when the top of the slab reaches the theoretical crushing strain of 0.003 (Wittry 1993; White 2002). However, composite members with large D_p/D_t tend to have significantly smaller plastic curvature prior to crushing of the deck concrete and thus less ductility. Also, AASHTO (2014) specifies

$$D_p/D_t \leq 0.42 \quad (5.3.3-4)$$

(AASHTO 6.10.7.3-1)

to ensure significant yielding of the bottom flange prior to reaching the nominal crushing strain at the top of the deck. This limit is consistent with the former maximum reinforcement limit for concrete design given in AASHTO (2004) Article 5.7.3.3.

In addition to the above equations, AASHTO (2014) Article 6.10.7.1.2 limits the nominal flexural resistance to that given by Eq. (2) in continuous-span beams where the adjacent pier sections are not detailed to accommodate significant inelastic moment redistribution. The reader is referred to Section 3 of this module for discussion of this limit.

AASHTO (2014) generally requires that the separate effects of noncomposite, short-term composite and long-term composite loadings shall be considered in calculating the nominal flexural resistance. However, for compact composite sections in positive bending, the effect of these different types of loadings on the flexural stresses and on partial yielding of the cross-section need not be considered. Since these cross-section types are able to sustain inelastic curvatures sufficient to develop their nominal full plastic moment, the effect of the different loadings is negligible with respect to the section maximum strength. AASHTO (2014) Article 6.10.1.5 still requires an analysis of the structure separately for the noncomposite, short-term composite and long-term composite loadings. The relative proportion of the three types of loadings typically will have some effect on the distribution of the moments and forces in the structure.

5.3.3.3 Handling of creep and shrinkage effects

Stresses in the concrete deck due to permanent loads acting on the composite structure cause the concrete to creep. The effect of creep is to relieve the stresses in the concrete and increase the stresses in the steel. AASHTO (2014) Article 6.10.1.1.1a addresses the influence of creep on the steel stresses in a reasonable but approximate fashion by using three times the modular ratio, $3n = 3E_s/E_c$, when transforming the elastic concrete section to an equivalent steel section for analysis of the effects of permanent loads on the steel in composite bridges. Oehlers and Bradford (1999) discuss the accuracy of this type of approximation. AASHTO (2014) Article 6.10.1.1.1d requires the conservative use of the short-term modular ratio $n = E_s/E_c$ for calculation of longitudinal flexural stresses in the concrete due to all permanent and transient loads. This is important primarily for determining where sufficient longitudinal reinforcement should be provided in the concrete deck to control cracking (e.g., see AASHTO Articles 6.10.3.2.4 and 6.10.1.7).

Concrete slab shrinkage also has an effect on the detailed structural behavior. During the first several months after construction, the slab shrinks. In simple-span structures, this induces tensile stresses in the slab, compressive stresses in the top flanges of the steel I-sections and tensile stresses in the bottom flanges of the steel I-sections. Tests have indicated that the unit shrinkage of the slab in composite beams (i.e., the shrinkage strain adjusted for long-term relaxation effects) may be taken equal to 0.0002 (Viest et al. 1958). The corresponding stresses may be computed adequately by assuming that the shrinkage does not cause cracking. The steel stresses in straight simple spans may be approximated by considering the composite cross-section as an eccentrically loaded column with a load of $0.0002E_c n A_c$ applied at the centroid of the slab and using $n = E_s/E_c$ (Viest et al. 1958).

The shrinkage stresses in the concrete deck for simple spans, and in the positive moment regions of continuous spans, are counteracted by the composite dead and live load stresses. Furthermore, compact composite I-section members in positive bending develop maximum strengths that involve significant yielding and inelastic redistribution of the cross-section stresses. The steel section in noncompact composite members in positive bending (addressed in the next section) tends to be larger relative to the concrete slab, and hence the influence of the loading $0.0002E_c n A_c$ is smaller. Also, any strength beyond first yielding of the steel section is neglected in noncompact composite I-section members. Therefore, AASHTO (2014) neglects the additional incidental compression in the top of the steel I-sections in positive bending regions in all cases with one exception discussed below. In the negative moment regions of continuous beams, the slab concrete is neglected in all cases in determining the member flexural resistance. Also, due to minor slip at the shear connectors between the slab and the steel girders and minor cracking in the slab, the shrinkage forces are not likely to be fully effective. Hence, AASHTO (2014), with one exception, considers that the shrinkage stresses are not an important factor with respect to strength for all types of composite sections in negative bending.

The exception to the above simplifications is addressed in AASHTO (2014) Article 3.4.1 for composite girders where the slab is longitudinally post-tensioned. In this case, the AASHTO provisions indicate that the effect of shrinkage and long-term creep around the shear connectors should be evaluated to ensure that the composite girder is able to maintain the prestressing over the life of the bridge. This article also states that the contribution of long-term deformations in closure pours between precast deck panels that have been aged to reduce the shrinkage and creep may need evaluation. AASHTO (2014) Article C6.10.1.1.1a also indicates that for shored construction where close tolerances on the final girder cambers are important, the above handling of creep effects may not be appropriate. Refined analysis of shrinkage effects also may be important in other types of structures requiring close tolerances on girder cambers, e.g., in spans supporting elevated tracks for maglev trains (Frank 2005). Article C4.6.6 of AASHTO (2014) points out that general creep and shrinkage effects may be analyzed in the same fashion as strains due to temperature gradient through the bridge cross-section.

5.3.4 Noncompact Composite Sections in Positive Flexure

AASHTO (2014) classifies composite sections in positive bending as noncompact sections when any of the limits listed in Section 5.3.3 of this module are violated. The flexural resistance of these section types is defined by limiting the elastically computed compression and tension flange stresses to

$$F_{nc} = R_b R_h F_{yc} \tag{5.3.4-1}$$

(AASHTO 6.10.7.2.2-1)

and

$$F_{nt} = R_h F_{yt} \tag{5.3.4-2}$$

(AASHTO 6.10.7.2.2-2)

respectively, where R_b is the web load-shedding strength reduction factor specified in AASHTO Article 6.10.1.10.2 and R_h is the hybrid web strength reduction factor specified in AASHTO Article 6.10.1.10.1. These factors are discussed further in Section 5.3.5 of this module. AASHTO (2014) specifies the resistance of these types of sections in terms of the elastically computed flange stresses, rather than the stress-resultant moments, for the following reasons:

1. The separate effects of noncomposite, short-term composite and long-term composite loadings are considered explicitly in the strength assessment of these section types. For noncompact sections, the moments due to the above separate loading effects cannot be added together to determine the overall effect. The only rational way to address the separate loading effects is to consider the elastic cross-section stresses directly.
2. Bridge cross-sections such as those shown in Figure 3 through Figure 5 are more likely in longer-span structures where it may be desirable to violate one or more of the limits stated in Section 5.3.3. In these cases, the appropriate slab effective width for use with the main girders and/or with the secondary stringers potentially can be determined more rationally using a refined analysis that models the plate action of the concrete deck. The stress format for the cross-section resistances allows the Engineer to focus directly on the steel section stresses determined from this type of analysis. Conversely, the use of a moment format for the cross-section resistances requires further processing, including assumptions about the effective width of the deck that acts compositely with each of the steel members.

For compact composite sections in positive bending, the flexural resistances are potentially larger than the yield moment capacity of the cross-section. As a result, if the resistances are expressed in terms of elastically computed flange stresses, they can be larger than the corresponding flange yield stress. Furthermore, as noted at the end of Section 5.3.3, the elastic stresses are generally redistributed by inelastic deformations as the strength limit is approached in compact section members. Therefore, for compact section members, the resistances are expressed more naturally in terms of the total moment.

The elastically computed flange stresses used for checking of noncompact composite I-sections in positive bending are based generally on the assumption that the concrete stress-strain behavior is nominally linear. AASHTO (2004) considered that this assumption was valid without checking for all types of unshored composite construction, although it explicitly required that the longitudinal compressive stresses in the concrete deck should be limited to $0.6f'_c$ in shored composite noncompact section members subjected to positive bending, to ensure linear behavior of the concrete. AASHTO (2014) requires this check for all types of construction, and provides guidance regarding the unusual cases where this limit is apt to control.

5.3.5 Composite Sections in Negative Flexure and Noncomposite Sections

5.3.5.1 Key concepts

In AASHTO (2014), the flexural resistance of all types of composite I-section members in negative flexure, and of all types of noncomposite I-section members, is governed by the most critical of the three following limit states:

- Lateral-torsional buckling (LTB),
- Compression flange local buckling (FLB), and
- Tension flange yielding (TFY).

All of the AASHTO (2014) LTB and FLB resistance equations are based consistently on the logic of identifying the two anchor points shown in Figure 60 for the case of uniform major-axis bending. Anchor point 1 is located at the unbraced length $L_b = L_p$ for LTB or flange slenderness $b_{fc}/2t_{fc} = \lambda_{pf}$ for FLB corresponding to development of the maximum potential flexural resistance, labeled as F_{max} or M_{max} in the figure. Anchor point 2 is located at the length L_r or flange slenderness λ_{rf} at which the elastic LTB or FLB resistances are equal to $R_b F_{yr}$ in terms of stress or $R_b F_{yr} S_{xc}$ in terms of moment. The term F_{yr} is the nominal compression flange stress at the onset of significant yielding including residual stress effects, and R_b is the web load-shedding strength reduction factor (equal to 1.0 for sections with compact or noncompact webs). In most cases, F_{yr} is taken equal to $0.7F_{yc}$. The inelastic FLB and LTB resistances are expressed simply and accurately by linear interpolation between the above two anchor points. For $L_b > L_r$ or $b_{fc}/2t_{fc} > \lambda_{rf}$, the LTB and FLB resistances are governed by elastic buckling. The format shown in Figure 60, and all the underlying base equations, are with minor exceptions the same as in the AISC (2010) provisions for noncomposite I-section members.

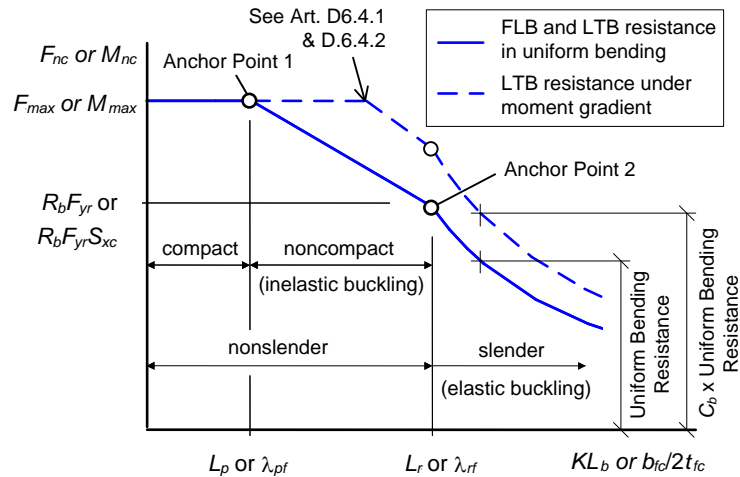


Figure 60 Basic form of flange local buckling (FLB) and lateral-torsional buckling (LTB) strength curves for all composite I-section members in negative bending and noncomposite I-section members (reprinted with permission from AASHTO (2004)).

For unbraced lengths subjected to moment gradient, the calculated LTB resistance is modified by the factor C_b as illustrated by the dashed line in Figure 60. In these cases, the uniform bending elastic and inelastic LTB strengths are simply scaled by C_b , with the exception that the resistance is capped by F_{max} or M_{max} . The FLB resistance for moment gradient cases is the same as that for uniform major-axis bending, neglecting the relatively minor influence of moment gradient on the FLB strengths.

AASHTO (2014) Article C6.10.8.2.3 indicates that for rehabilitation design or in extraordinary circumstances, the Engineer may consider modifying L_b in Figure 60 by an elastic effective length factor (K) for lateral torsional buckling. However, in most design situations, common practice is to take L_b as the actual unsupported length between the brace points corresponding to the compression flange-level bracing and/or the diaphragm or cross-frame locations. Article C6.10.8.2.3 recommends a simple hand method from Galambos (1998) and Nethercot and Trahair (1976) for determining LTB effective length factors K in cases where some additional calculation effort is merited. Ziemian (2010) also outlines this method. The application of this procedure to prismatic I-section members is explained in Section 5.3.5 of this module, after discussion of the more fundamental parameters illustrated in Figure 60.

The TFY flexural resistance addresses the general yielding of the tension flange as the name implies. However, depending on the slenderness of the web, the TFY resistance can be larger than just the moment corresponding to nominal first yielding of the tension flange. This aspect is addressed in more detail in Section 5.3.5.

The governing flexural resistance is generally taken as the smaller of the values calculated independently for each of the above idealized flexural limit states.

Depending on which of the three regions that the unbraced length L_b falls in, delineated by Anchor Points 1 and 2 in Figure 60, the unbraced length is referred to as compact, noncompact

or slender under flexure. Compact unbraced lengths are able to develop the maximum flexural resistance, F_{max} or M_{max} , in uniform bending, assuming that the FLB or TFY resistances are not smaller. The *uniform bending* resistance for noncompact unbraced lengths is reduced relative to F_{max} or M_{max} due to inelastic LTB. Lastly, for slender unbraced lengths *in uniform bending*, the LTB resistance is defined by the corresponding theoretical elastic LTB equations. However, it is important to note that the LTB resistance of unbraced lengths subjected to a moment gradient (i.e., nonuniform bending along the length) can be increased significantly due to the moment gradient effects. As such, F_{max} or M_{max} can be achieved at much larger unbraced lengths than the compact limit L_p . Thus, it is unwise in general to select unbraced lengths or a spacing of the cross-frames to enforce $L_b \leq L_p$.

Similar to the above discussion, cross-sections with compact compression flanges are able to develop F_{max} or M_{max} , cross-sections with noncompact compression flanges have their flexural resistance limited by inelastic FLB, and cross-sections with slender flanges have their flexural resistance governed by elastic FLB, assuming that the LTB or TFY resistances are not smaller. Actually, AASHTO (2014) does not explicitly provide any elastic FLB equations. This is because the proportioning limit $b_f/2t_f \leq 12$ in Article 6.10.2.2 (Eq. 5.3.2-3) precludes elastic FLB for all steel I-section members with $F_{yc} \leq 90$ ksi. AASHTO (2014) simply uses its inelastic FLB expressions into the elastic FLB range for the minor extent that $b_f/2t_f$ can potentially exceed λ_{rf} for $F_{yc} > 90$ ksi. This is justified given the approximations invoked in determining the flange local buckling resistance.

Also, as discussed in the following, the webs in I-section members are defined as either compact, noncompact or slender under flexure. The maximum potential resistance M_{max} is equal to the plastic moment capacity M_p for members with a compact web. However, the most economical welded composite I-girders in negative bending, and welded noncomposite I-girders in positive or negative bending, rarely have compact webs. In fact, welded I-section webs are often slender under flexural compression. The M_{max} of slender web members is generally smaller than the compression flange yield moment M_{yc} due to web bend buckling and shedding of load to the compression flange. The detailed influences of the web slenderness on M_{max} are discussed in Section 5.3.5 of this module.

All of the above definitions or classifications focus on separate member characteristics, i.e., the unbraced length or LTB slenderness, the compression flange slenderness and the web slenderness. This is slightly different from the classification of composite I-section members in positive flexure, where the entire cross-section is defined as either compact or noncompact. It is also somewhat different from prior AASHTO Specifications, which focused on the classification of entire cross-sections. The AASHTO (2014) emphasis on these separate member characteristics is consistent with the approaches in AISC (1999, 2005 and 2010).

The main LTB and FLB provisions in AASHTO (2014) Article 6.10.8.2 specify the flexural resistances in terms of elastically computed compression flange stresses. Also, the equations in this article are targeted specifically at the capacity of slender-web I-section members. The Engineer is allowed to use these equations conservatively for all I-section member types as a simplification. This simplification recognizes the fact that, with the exception of rolled I-section members, bridge I-sections predominantly have slender or nearly slender webs. However,

Appendix A6 of AASHTO (2014) specifies comparable and more liberal equations for I-section members in negative bending and noncomposite I-section members that have noncompact or compact webs. The Appendix A6 equations are a direct extension of the equations in Article 6.10.8.2, and with minor exceptions, are fundamentally the same as the equations for design of noncompact- and compact-web noncomposite I-section members in AISC (2010). AASHTO (2014) Articles C6.10.6.2.3 and C6.10.8.1.1 point out that the Engineer should give strong consideration to utilizing the provisions of Appendix A6 for I-sections with compact or nearly compact webs in straight bridges. In addition, the AASHTO (2014) equations in Article 6.10.8.2 are with minor exceptions fundamentally the same as the AISC (2010) flexural resistance equations for slender-web I-section members. White (2008) details the minor differences between the AASHTO (2014) and AISC (2010) provisions. Several of the most significant of these differences are outlined in the following Sections.

The Appendix A6 equations are expressed in terms of the section bending moment. The rationale for use of the flange stress format in Article 6.10.8.2 and the moment format in Appendix A6 is essentially the same as that discussed in Section 5.3.4 of this module for noncompact and compact composite I-sections in positive bending.

The coordinates of the anchor points shown in Figure 60 are (L_p, M_{max}) and $(L_r, R_b F_{yr} S_{xc})$ for LTB and (λ_{pf}, M_{max}) and $(\lambda_{rf}, R_b F_{yr} S_{xc})$ for FLB in terms of the bending moment. The specific terms associated with these anchor points are discussed in detail in the following Sections. Also, since the noncompact bracing limit, L_r , and the noncompact compression flange slenderness limit, λ_{rf} , are associated with the theoretical elastic buckling equations, the base elastic buckling formulas are also presented. The following discussions are targeted at providing an overall conceptual understanding of the AASHTO (2014) flexural resistance calculations. AASHTO (2014) Appendix C6 provides detailed flowcharts that capture the complete application of the flexural design provisions for I-section members. The Engineer is encouraged to consult these flowcharts for an efficient organization of the corresponding calculations. White (2008) gives similar flowcharts that emphasize the unified nature of the AASHTO (2014) Article 6.10.8 and Appendix A6 equations.

5.3.5.2 Maximum potential flexural resistance, M_{max} or F_{max}

5.3.5.2.1 Compact- and noncompact-web sections

As noted in the above, M_{max} is equal to the cross-section plastic moment capacity M_p for members with compact webs. However, for members with noncompact or slender webs, the ordinate of Anchor Point 1, M_{max} or F_{max} , decreases as a function of the web slenderness $2D_o/t_w$. For noncompact-web members, M_{max} decreases linearly as a function of $2D_o/t_w$ between the compact- and noncompact-web limits λ_{pw} and λ_{rw} , as shown in Figure 61. The noncompact-web limit is given by the equation

$$\lambda_{rw} = 5.7 \sqrt{\frac{E}{F_{yc}}} \quad (5.3.5-1)$$

(AASHTO 6.10.6.2.3-1, A6.2.1-3 & A6.2.2-3, AISC Table B4.1b)

This limit is the value of $2D_c/t_w$ at which an I-section is nominally able to develop $M_{max} = R_h M_{yc}$, or a compression flange yield stress $F_{max} = R_h F_{yc}$, just prior to the onset of local web buckling in flexure, referred to as web bend buckling. The theoretical background to this equation is discussed subsequently in Section 5.3.10 of this module. AASHTO (2014) defines the compact-web limit as

$$\lambda_{pw(D_c)} = \frac{\frac{D_c}{D_{cp}} \sqrt{\frac{E}{F_{yc}}}}{\left(0.54 \frac{M_p}{M_y} - 0.09\right)^2} \leq \lambda_{rw} \quad (5.3.5-2)$$

(AASHTO A6.2.2-6 & 6.2.1-2, AISC Table B4.1b)

Equation (2) accounts for the larger demands on the web required to develop the cross-section plastic moment in singly-symmetric cross-sections. The term D_c/D_{cp} in the numerator converts this equation from its fundamental form associated with the plastic depth of the web in compression, D_{cp} , to the form associated with the elastic depth of the web in compression, D_c . This is necessary so that a consistent web slenderness parameter, $2D_c/t_w$, may be employed for the linear interpolation between the anchor points (λ_{pw}, M_p) and $(\lambda_{rw}, R_h M_{yc})$ in Figure 61. For a homogeneous doubly-symmetric I-section with $D_c/D_{cp} = 1.0$ and an assumed $M_p/M_y = 1.12$, Eq. (2) reduces to the limit in Eq. (5.3.3-1). The requirement of $\lambda_{pw(D_c)} \leq \lambda_{rw}$ in Eq. (2) conservatively defines the compact-web limit as $\lambda_{pw(D_c)} = \lambda_{rw}$ for singly-symmetric sections with proportions such that the section is classified as slender based on the elastic depth of the web in compression and Eq. (1), but as compact based on the plastic depth of the web in compression D_{cp} and the fundamental form of Eq. (2) with the ratio D_c/D_{cp} removed from its numerator. This type of cross-section is possible in negative bending regions of continuous-span I-girders having a significantly larger bottom compression flange. White (2008) shows a practical cross-section for which $\lambda_{pw(D_c)} = \lambda_{rw}$.

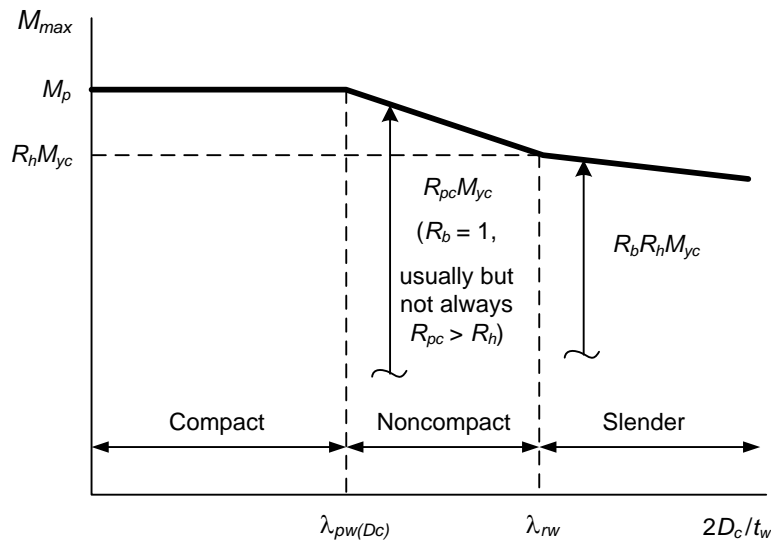


Figure 61 Variation of M_{max} for FLB and LTB versus the web slenderness $\lambda_w = 2D_c/t_w$.

The linear interpolation between $(\lambda_{pw}, M_{max} = M_p)$ and $(\lambda_{rw}, M_{max} = R_h M_{yc})$ shown in Figure 61 is represented by the *web plastification factor*, R_{pc} , in AASHTO (2014) (and in AISC (2010)). This parameter is simply equal to the cross-section shape factor, M_p/M_{yc} , for a compact-web section. It may be considered as an *effective shape factor* that varies linearly between M_p/M_{yc} and R_h for noncompact-web sections. One should note that R_{pc} is greater than one in most situations for girders with noncompact webs. However, M_{yc} can be greater than M_p for some extreme singly-symmetric sections having a large flange in compression and a neutral axis close to the compression flange (this is because earlier yielding in tension is generally neglected in the calculation of M_{yc}). In these cases, R_{pc} can be less than one. The resistance is more likely to be governed by tension flange yielding (TFY) in these situations.

5.3.5.2.2 Slender-web sections

For $2D_c/t_w > \lambda_{rw}$, the web is defined as slender and M_{max} is given by the expression $R_b R_h F_{yc} S_{xc}$ as shown in Figure 61 (i.e., $F_{max} = R_b R_h F_{yc}$). In this case, $R_b < 1$ accounts for the reduction in M_{max} or F_{max} due to shedding of flexural stresses to the compression flange associated with the post-bend buckling response of the web. The base AASHTO (2014) web load-shedding strength reduction factor is written as

$$R_b = \frac{a_{wc}}{1200 + 300a_{wc}} \left(\frac{2D_c}{t_w} - \lambda_{rw} \right) \leq 1.0 \quad (5.3.5-3)$$

(AASHTO 6.10.1.10.2-3, AISC F5-6)

where $a_{wc} = 2D_c t_w / A_{fc}$ and A_{fc} is the area of the compression flange (including cover plates, etc. as applicable). This equation is the more general and accurate form of two equations developed by Basler and Thurlimann (1961). For composite sections in negative bending, AASHTO (2014) Article 6.10.1.10.2 specifies the use of the depth of the web in compression D_c for the section consisting of the steel girder plus the longitudinal deck reinforcement within the slab effective width in determining R_b by Eq. (3).

If a more refined calculation is desired for R_b , AASHTO (2014) Article C6.10.1.10.2 suggests the use of F_{ncI} for F_{yc} in the λ_{rw} term of Eq. (3), where F_{ncI} is the smaller of:

1. The nominal flexural resistance of the compression flange F_{nc} computed assuming R_b and R_h are both equal to one, or
2. The elastic stress in the compression flange when the tension flange reaches a nominal elastic stress of $R_h F_{yt}$.

This accounts for the lesser influence of web post-bend buckling for members that reach their maximum resistance at a compression flange stress smaller than $R_b R_h F_{yc}$. Prior AASHTO Specifications have specified the substitution of the factored applied stress f_{bu} in similar equations for R_b . This gives a value for the strength reduction factor that is acceptable but is smaller than the actual R_b corresponding to the maximum flexural strength condition. More importantly, this practice can lead to subsequent difficulties in load rating, since the flexural resistance becomes a function of the applied load. AASHTO (2014) has eliminated dependencies

of the calculated flexural resistance on the applied load wherever possible to mitigate subsequent load rating difficulties. The calculation of D_c in determining R_b by Eq. (3) for composite sections in negative bending is another area where a dependency of the resistance on the applied loading has been eliminated. Since transversely-stiffened I-girders must satisfy Eq. (5.3.2-1), the differences in R_b based on the simple use of F_{yc} versus F_{ncI} in the λ_{rw} term of Eq. (3) are typically only a few percent for these member types. Therefore, the use of F_{yc} in Eq. (3) is recommended for routine practice.

AASHTO (2014) Article 6.10.1.10.2 gives a separate equation for a_{wc} that conservatively approximates the beneficial effect of the concrete composite deck for calculation of R_b in noncompact composite sections in positive bending. AASHTO (2014) Article C6.10.1.10.2 states that R_b may be taken equal to one for composite sections in positive bending that satisfy the proportioning limits of Article 6.10.2.2 as well as the ductility limit of Eq. (5.3.3-4), as long as Eq. (5.3.2-1) is also met such that longitudinal stiffeners are not required. Composite cross-sections in positive bending that satisfy these limits generally have R_b values equal to or close to 1.0. However, composite longitudinally-stiffened sections in positive bending, which are generally classified as noncompact sections based on the second requirement listed in Section 5.3.3(A) of this module, will sometimes have R_b values smaller than 1.0.

The calculation of R_b for longitudinally-stiffened sections in AASHTO (2014) hinges on an explicit check of whether web bend buckling is prevented up to the development of the compression flange yield strength F_{yc} . Longitudinally-stiffened sections that satisfy the limit

$$\frac{D}{t_w} \leq 0.95 \sqrt{\frac{Ek}{F_{yc}}} \quad (5.3.5-4)$$

(AASHTO 6.10.1.10.2-1)

where k is the local bend-buckling coefficient for webs with longitudinal stiffeners specified in Article 6.10.1.9.2, are able to develop the compression flange yield strength prior to nominal web bend buckling. In these cases, R_b is specified equal to 1.0. However, for longitudinally-stiffened sections that exhibit bend buckling at smaller compression flange stress levels, R_b must be calculated from Eq. (3). Equation (3) does not account for any influence of the longitudinal stiffeners on the load shedding from the post-buckled longitudinally-stiffened web. This is because the AASHTO (2014) Article 6.10.11.3 requirements for longitudinal stiffeners only target the development of the web bend buckling resistance. The longitudinal stiffener requirements generally are not sufficient to hold a line of near zero lateral deflection in a post-buckled web plate. The AASHTO (2014) approach of not including any influence of the longitudinal stiffeners in the calculation of R_b gives a practical slightly conservative calculation of the flexural resistance for cases where Eq. (4) is not satisfied. Proportioning of longitudinally-stiffened webs such that Eq. (4) is satisfied, or restricting the strength of longitudinally-stiffened sections to the web bend buckling resistance, is overly conservative relative to traditional practice. AISC (2010) does not address the design of longitudinally-stiffened I-girders.

5.3.5.2.3 Hybrid-web strength reduction factor

As noted above, the term R_h is the hybrid web strength reduction factor. This factor accounts for the reduced contribution of the web to the nominal flexural resistance at the first yielding of any

flange element, due to earlier yielding of a lower strength hybrid web. In AASHTO (2014), this factor is defined by the single equation,

$$R_h = \frac{12 + \beta(3\rho - \rho^3)}{12 + 2\beta} \quad (5.3.5-5)$$

(AASHTO 6.10.1.10.1-1)

for all types of composite and noncomposite members, where

$$\beta = 2D_n t_w / A_{fn} \quad (5.3.5-6)$$

(AASHTO 6.10.1.10.1-2)

ρ = smaller of F_{yw}/f_n and 1.0

A_{fn} = sum of the flange area and the area of any cover plates on the side of the neutral axis corresponding to D_n . For composite sections in negative bending, the area of the longitudinal reinforcement may be included in calculating A_{fn} for the top flange.

D_n = larger of the distances from the elastic neutral axis of the cross-section to the inside face of either flange. For sections where the neutral axis is at the mid-depth of the web, the distance from the neutral axis to the inside face of the flange on the side of the neutral axis where yielding occurs first.

f_n = for sections where yielding occurs first in the flange, a cover plate or the longitudinal reinforcement on the side of the neutral axis corresponding to D_n , the largest of the specified minimum yield strengths of each component included in the calculation of A_{fn} . Otherwise, the largest of the elastic stresses in the flange, cover plate or longitudinal reinforcement on the side of the neutral axis corresponding to D_n at first yield on the opposite side of the neutral axis.

These definitions account for all possible combinations associated with different positions of the elastic neutral axis and different yield strengths of the top and bottom flange elements. Equation (5) is adapted from a fundamental strength reduction equation, originally derived for doubly-symmetric I-sections (ASCE 1968; Schilling 1968; Frost and Schilling 1964), to handle singly-symmetric and composite sections. This is accomplished by focusing on the side of the neutral axis where yielding occurs first. This side of the neutral axis has the most extensive web yielding prior to first yielding of any flange element. All of the flange elements on this side of the neutral axis are conservatively assumed to be located at the edge of the web. The original equation is also adapted by assuming that the shift in the neutral axis due to the onset of web yielding is negligible. These assumptions are similar to those used in the development of a separate R_h equation for composite members in prior AASHTO and AISC Specifications. AISC (2010) does not address hybrid I-section members to simplify its design rules.

In lieu of the use of Eq. (5), AASHTO (2014) Article C6.10.1.10.1 allows the Engineer to determine R_h directly from an iterative strain-compatibility analysis. However, since the

computed R_h values from Eq. (5) are typically close to 1.0, this refined calculation will typically provide little benefit.

5.3.5.2.4 *Other considerations*

For sections with $2D_c/t_w < \lambda_{rw}$, AASHTO (2014) Articles 6.10.6.2.3 and A6.1 apply two restrictions on the use of M_{max} values larger than $R_h M_{yc}$ ($F_{max} > R_h F_{yc}$). If the compression flange of noncomposite I-sections is substantially smaller than the tension flange such that

$$I_{yc} / I_{yt} < 0.3 \quad (5.3.5-7)$$

(AASHTO 6.10.6.2.3-2 & A6.1-2)

the Engineer is required to calculate the flexural resistance conservatively based on the slender-web member equations of Article 6.10.8. This restriction guards against the use of extremely monosymmetric sections where analytical studies indicate a significant loss in the influence of the St. Venant torsional rigidity GJ on the LTB resistance due to cross-section distortion. If the flanges are of equal thickness, this limit is equivalent to $b_{fc} < 0.67b_{ft}$. AISC (2010) requires the use of $J = 0$ in the calculation of L_r and the elastic LTB resistance for singly-symmetric I-sections that satisfy Eq. (7), but expressed as $I_{yc}/I_y < 0.23$; otherwise, AISC (2010) permits the calculation of M_{max} as shown in Figure 61 for compact- and noncompact-web members. Based on the results from White and Jung (2007), the AASHTO restriction is considered more prudent. Also, AASHTO Article 6.10.6.2.3 requires the use of the slender-web member equations and disallows the use of Appendix A6 for all bridges with kinked (chorded) continuous or horizontally curved segments. As noted previously in Section 3 of this module, this restriction is based on the limited information about the influence of cross-section partial yielding on the response of curved bridge structural systems. The component studies on which the AASHTO (2014) curved I-girder resistances are based (White and Jung 2008; White and Kim 2008; White et al. 2008) fully support the use of Appendix A6 as well as Article 6.10.7.1 for composite and noncomposite curved I-girders. The studies by Beshah and Wright (2010) and Jung and White (2010) support the use of these Articles for curved I-girder bridges. However, as noted in Section 3, further studies are needed to address the influence of partial cross-section yielding on continuous-span curved I-girder bridges.

5.3.5.3 Tension flange yielding (TFY) resistance

Prior to considering the other parameters illustrated in Figure 60, it is useful to discuss the definition of the AASHTO (2014) TFY resistance. The AASHTO TFY resistance varies with the web slenderness in a fashion similar to the variation of M_{max} and F_{max} . However, the R_b factor is not applied in determining the TFY resistance of slender-web sections since the tension flange stress is not increased significantly by the shedding of the web compressive stresses (Basler and Thurlimann 1961). Figure 62 illustrates the variation of the TFY resistance as a function of the web slenderness $2D_c/t_w$. AASHTO (2014) Article 6.8.10.3 defines the TFY resistance of slender-web sections as the nominal first yielding of the tension flange reduced by any hybrid web effects, $R_h F_{yt}$ in terms of the tension flange stress, or $R_h F_{yt} S_{xt} = R_h M_{yt}$ in terms of the member bending moment. However, Articles A6.2 and A6.3 define a TFY resistance that varies linearly

from $R_h M_{yt}$ to the section plastic moment M_p as the web slenderness $2D_c/t_w$ varies from λ_{rw} to $\lambda_{pw(Dc)}$. Finally, for compact-web sections, the TFY resistance is equal to M_p .

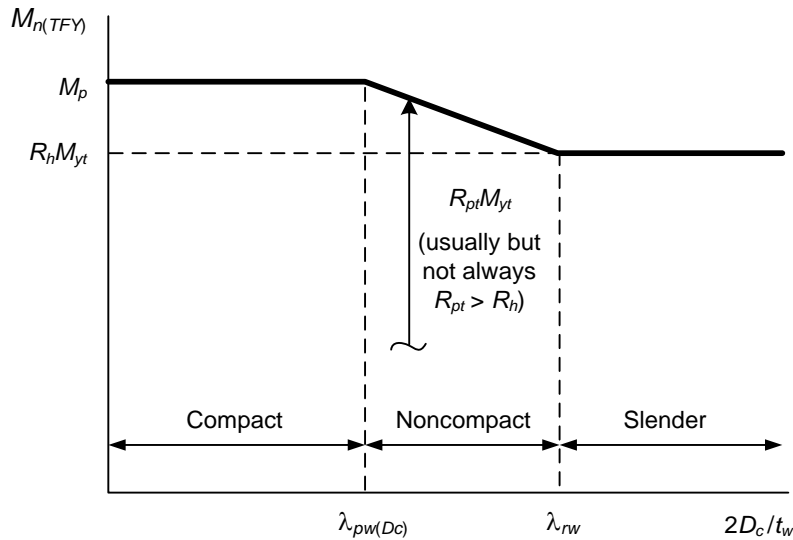


Figure 62 Variation of the tension flange yielding (TFY) resistance $M_{n(TFY)}$ versus the web slenderness $\lambda_w = 2D_c/t_w$.

Similar to the web plastification factor R_{pc} used in defining M_{max} for LTB and FLB of noncompact- and compact-web I-section members, AASHTO (2014) specifies a web plastification factor R_{pt} that corresponds to the TFY limit state. Similar to R_{pc} , R_{pt} is simply equal to the cross-section shape factor M_p/M_{yt} for compact-web sections, and it may be considered as an effective shape factor for noncompact-web sections. Also, similar to R_{pc} , R_{pt} can be less than one for extremely monosymmetric I-sections, basically sections that have a significantly larger tension flange causing the neutral axis to be very close to the tension flange (in these sections, M_{yt} can be greater than M_p due to the neglect of earlier yielding in compression). However, in these cases, R_{pc} will be greater than R_h and the LTB or FLB resistance equations will usually govern.

For sections in which $M_{yt} > M_{yc}$, TFY never governs and does not need to be checked.

5.3.5.4 Compact bracing limit, L_p

AASHTO (2014) specifies the equation

$$L_p = 1.0r_t \sqrt{\frac{E}{F_{yc}}} \tag{5.3.5-8}$$

(AASHTO 6.10.8.2.3-4 & A6.3.3-4)

as the compact bracing limit for all types of composite I-section members in negative bending and for all types of noncomposite I-section members. This equation is based on extensive analysis of experimental data by Yu and Sause (2002), White and Jung (2008) and White and

Kim (2008). These studies demonstrate that the inelastic LTB resistance is represented accurately using this single equation, with no variation in L_p as a function of web slenderness, etc. other than via the radius of gyration r_t , combined with the variable expressions for M_{max} or F_{max} discussed in Section 5.3.5 of this module. The radius of gyration in Eq. (8) can be calculated in all cases using the equation

$$r_t \cong \frac{b_{fc}}{\sqrt{12 \left(1 + \frac{1}{3} \frac{D_c t_w}{b_{fc} t_{fc}} \right)}} \quad (5.3.5-9)$$

(ASHTO 6.10.8.2.3-9 & A6.3.3-10)

This equation is precisely equal to the radius of gyration of the compression flange plus one-third of the depth of the web in compression. The web area term $D_c t_w$ in Eq. (9) accounts for the destabilizing effect of the compression in the web on the member lateral-torsional stability.

In prior Specifications, the L_p limit has been based on different radii of gyration for different types of sections, including r_t , the radius of gyration of solely the compression flange itself about the cross-section y -axis, r_{yc} , and the radius of gyration of the complete cross-section about its y axis, r_y . The radius of gyration r_{yc} is in general not appropriate because it neglects the destabilizing effect of the web compression. Also, the radius of gyration r_y is not appropriate for singly-symmetric and composite I-section members since it does not properly account for the influence of the cross-section monosymmetry on the LTB response. The radius of gyration r_t provides the best overall characterization for all I-section types not only within the context of Eq. (8), but also within the elastic LTB calculations discussed in Section 5.3.5 of this module. This statement is based on the simplicity of the equations as well as the accuracy of the predictions relative to experimental and refined analytical resistances.

Equation (8) generally gives somewhat smaller L_p values than in prior AISC and AASHTO Specifications. However, for slender-web members, if Eq. (8) is substituted into the original CRC based expression for the LTB resistance suggested by Basler and Thurlimann (1961) and summarized by Cooper et al. (1978), a strength of $0.97M_y$ is obtained for members with R_b and R_h equal to one. If L_p/r_t from Eq. (8) is substituted as an equivalent slenderness ratio into the column strength Eqs. (5.2.1-4) and (5.2.1-1a), a resistance of $0.96M_y$ is obtained.

The more liberal L_p equations in previous AASHTO and AISC Specifications are based largely on the studies by Yura et al. (1978), where the L_p limit

$$L_p = \frac{300r_y}{\sqrt{F_y}} = 1.76r_y \sqrt{\frac{E}{F_{yc}}} \quad (5.3.5-10)$$

was recommended for doubly-symmetric steel I-section members with compact webs and compact flanges. However, the original study by Galambos and Ravindra (1976) recommended

$$L_p = \frac{240r_y}{\sqrt{F_y}} = 1.41r_y \sqrt{\frac{E}{F_{yc}}} \quad (5.3.5-11)$$

for these member types. Table 1 of Yura et al. (1978) reports the same resistance factors ϕ based on predictions of experimental results as in Galambos and Ravindra (1976), although Yura et al. (1978) propose different L_p equations. The correct L_p expression corresponding to the ϕ factors in Yura et al. (1978) Table 1 is Eq. (11). Furthermore, the ratio r_t/r_y ranges from 1.12 to 1.28 for rolled wide-flange sections. Therefore, in terms of r_t , Eq. (11) may be expressed as

$$L_p = 1.10r_t \sqrt{\frac{E}{F_{yc}}} \quad \text{to} \quad 1.26r_t \sqrt{\frac{E}{F_{yc}}} \quad (5.3.5-12)$$

Cooper et al. (1978) specified

$$L_p = 0.86r_t \sqrt{\frac{E}{F_{yc}}} \quad (5.3.5-13)$$

in their final recommendations for load and resistance factor design of slender-web I-section members. These recommendations were subsequently changed to

$$L_p = \frac{300r_t}{\sqrt{F_{yc}}} = 1.76r_t \sqrt{\frac{E}{F_{yc}}} \quad (5.3.5-14)$$

for slender-web I-section members (referred to as plate girders) in AISC (1986), apparently to match the coefficient in Eq. (10) and to produce comparable compactly-braced results to the AISC (1978) Allowable Stress Design (ASD) equations. AISC (1986) also specified Eq. (10) for singly-symmetric I-section members, but AISC (1993 & 1999) subsequently changed the L_p limit for these members to

$$L_p = 1.76r_{yc} \sqrt{\frac{E}{F_{yc}}} \quad (5.3.5-15)$$

As discussed by White and Jung (2003b), r_{yc} can be substantially larger than r_y and r_t . Therefore, Eq. (15) liberalizes the AISC (1993 & 1999) L_p equations for singly-symmetric I-section members even further. The prior AASHTO equations for L_p were largely adopted from AISC, using the coefficient of 1.76 but with radii of gyration that in some cases differed from the AISC equations.

White and Jung (2008) show that Eq. (8) with a coefficient of 1.1 gives a nearly uniform reliability index throughout the compactly- and noncompactly-braced ranges for all types of I-section members. The results using a coefficient of 1.0 in Eq. (8) are essentially the same as those using a coefficient of 1.1 (the maximum difference in the resistance predictions is approximately one percent). AISC (2010) uses Eq. (8) with a coefficient of 1.1 except for

doubly-symmetric compact-web I-section members, where Eq. (10) is retained from AISC (1986, 1993 & 1999). White and Chang (2007) show that Eq. (8) with a coefficient of 1.1 gives resistances that are larger than the traditional AISC ASD values for most compact-web I-section members. The maximum difference in the predictions using Eq. (10) versus Eq. (8) with a coefficient of 1.1 is approximately six percent.

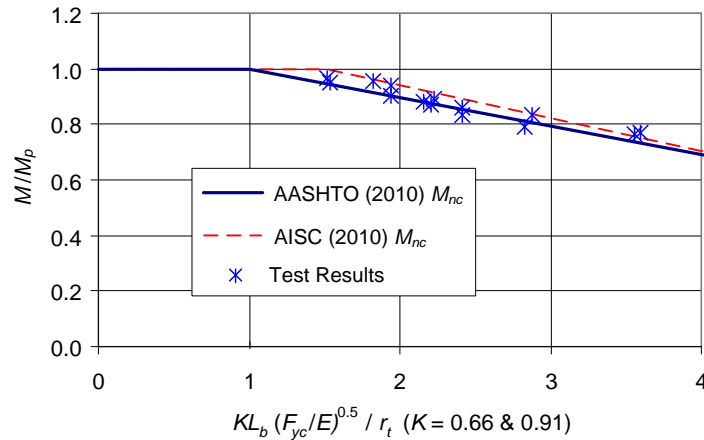


Figure 63 Comparison of rolled beam I-section uniform bending test results from Dux and Kitipornchai (1983) and Wong-Chung and Kitipornchai (1987) to the AASHTO (2014) and AISC (2010) flexural resistances ($F_{yc} = 41.3$ and 42.5 ksi, LTB effective length factors $K = 0.66$ and 0.91).

Figure 63 compares the predictions by AASHTO (2014) and AISC (2010) for a set of rolled I-beam tests in uniform bending conducted by Dux and Kitipornchai (1983) and Wong-Chung and Kitipornchai (1987). Figure 64 shows the AASHTO and AISC predictions for a suite of noncompact-web member tests in uniform bending conducted by Richter (1998). The unbraced lengths L_b are modified using the Nethercot and Trahair (1976) effective length factor K (discussed subsequently in Section 5.3.5 of this module) for the Dux and Kitipornchai (1983) and Wong-Chung and Kitipornchai (1987) tests. The Nethercot and Trahair (1976) K factors are equal to 1.0 in all cases for the Richter (1998) tests.

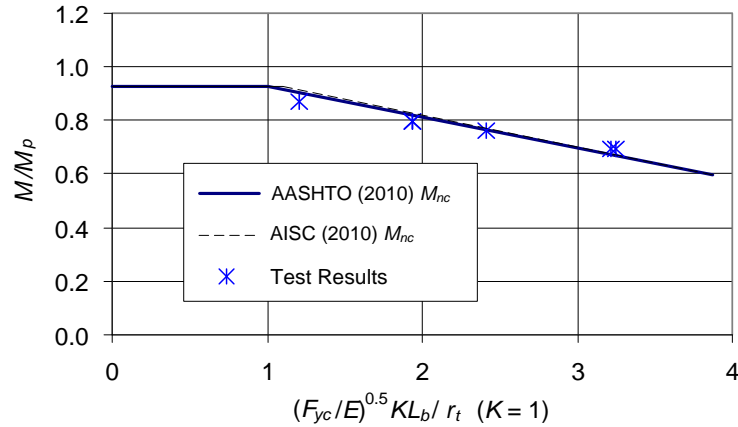


Figure 64 Comparison of compact-flange noncompact-web welded member test results for uniform bending, from Richter (1998), to the AASHTO (2014) and AISC (2010) flexural resistances ($b_{fc}/2t_{fc} = 8.0$ to 8.1 , $D/t_w = 110$, $D/b_{fc} = 3.6$, $F_{yc} = 48.4$ ksi).

Equation (8) provides the best combination of simplicity (one equation that applies to all I-section members) and accuracy (near uniformity of the reliability index throughout the compactly- and noncompactly-braced ranges for all I-section members). However, the differences in the results using the various incarnations of L_p are relatively small with the exception of the application of Eq. (15) to singly-symmetric I-section members. The use of r_t in Eq. (8) facilitates the assessment of LTB in composite I-section members subjected to negative bending, since r_t depends only on the characteristics of the portion of the cross-section subjected to flexural compression.

5.3.5.5 Compact flange slenderness limit, λ_{pf}

AASHTO (2014) and AISC (2010) define the compact-flange slenderness limit by the equation

$$\lambda_{pf} = 0.38 \sqrt{\frac{E}{F_{yc}}} \quad (5.3.5-16)$$

(AASHTO 6.10.8.2.2-4 & A6.3.2-4, AISC Table B4.1b)

for all types of I-section members. This equation is identical to the compact-flange limit in AISC (1989 & 1999) and is based largely on the original research by Lukey et al. (1969) as well as the subsequent studies by Johnson (1985).

5.3.5.6 Compression flange stress at the nominal onset of inelastic buckling, F_{yr}

AASHTO (2014) specifies $F_{yr} = 0.7F_{yc}$ with the exception of (1) highly monosymmetric compact-web and noncompact-web cross-sections with the larger flange in compression, where the neutral axis is so close to the compression flange that nominal tension flange yielding occurs prior to reaching a stress of $0.7F_{yc}$ at the compression flange and (2) hybrid web members in general where $F_{yw} < 0.7F_{yc}$. To address these cases, AASHTO (2014) Articles A6.3.2 and A6.3.3 specify

$$F_{yr} = \min\left(0.7F_{yc}, F_{yt} \frac{S_{xt}}{S_{xc}}, F_{yw}\right) \geq 0.5F_{yc} \quad (5.3.5-17)$$

The product $F_{yt}S_{xt}$ in the second term of this equation is the moment corresponding to nominal yielding at the tension flange. This value, divided by the section modulus to the compression flange, S_{xc} , is the compression flange stress corresponding to the onset of nominal yielding at the tension flange. The third term interprets the web yield stress as the limit corresponding to the onset of significant inelastic stability effects for hybrid sections with unusually low values for F_{yw} relative to F_{yc} . In extreme cases where $F_{yt}S_{xt}/S_{xc}$ or F_{yw} is less than $0.5F_{yc}$, AASHTO (2014) uses a minimum value of $F_{yr} = 0.5F_{yc}$.

For slender-web members, AASHTO (2014) Article 6.10.8.2 specifies

$$F_{yr} = \min(0.7F_{yc}, F_{yw}) \geq 0.5F_{yc} \quad (5.3.5-18)$$

That is, the second-term in Eq. (17) is not considered. This simplification is possible because the TFY resistance of slender-web members is defined as the nominal first yielding of the tension flange reduced by any hybrid web effects, $R_h F_{yt}$. However, since the TFY resistance for compact- and noncompact-web sections is generally larger than $R_h M_{yt}$, Eq. (17) is necessary to avoid significant violation of the assumption of elastic member behavior when using the AASHTO equations based on elastic LTB or FLB.

The limit $F_{yr} = 0.7F_{yc}$ is based on LTB and FLB experimental test data (White and Jung 2008; White and Kim 2008). This is a significant liberalization relative to the implicit use of $F_{yr} = 0.5F_{yc}$ for slender-web members in prior Specifications.

5.3.5.7 Elastic LTB stress, $F_{e.LTB}$

The AASHTO (2014) elastic LTB resistances are based on a single equation applicable for all types of I-section members. This equation gives the exact beam-theory solution for LTB of doubly-symmetric I-section members, and it gives an accurate to somewhat conservative approximation for singly-symmetric noncomposite members and composite members in negative bending (White and Jung 2003 a & b; White 2008). This equation may be written in terms of the compression flange flexural stress as

$$F_{cr} = F_{e.LTB} = C_b \frac{\pi^2 E}{(L_b / r_t)^2} \sqrt{1 + \frac{0.078}{X^2} (L_b / r_t)^2} \quad (5.3.5-19)$$

(AASHTO A6.3.3-8, AISC F2-4 & F4-5)

where

$$X^2 = \frac{S_{xc} h}{J} \quad (5.3.5-20)$$

r_t is approximately the radius of gyration of the compression flange plus one-third of the area of the web in compression, S_{xc} is the elastic section modulus to the compression flange, h is the distance between the centroids of the flange elements, and J is the St. Venant torsion constant of the steel I-section. Equation (20) is a simple ratio of the bending and torsional efficiencies of the cross-section. For a doubly-symmetric I-section, $X^2 \cong 2I_x/J$. This parameter ranges from 13 to 2500 for the complete set of ASTM A6 W shapes.

(Note that AASHTO (2014) uses the symbol F_{cr} rather than $F_{e.LTB}$ in Eq. (19). However, for slender-web members, AASHTO (2014) multiplies the beam-theory elastic LTB stress $F_{e.LTB}$, with J taken equal to zero, by the web load shedding parameter R_b to obtain the nominal flange stress at elastic LTB, i.e., $F_{cr} = R_b F_{e.LTB}$. The notation $F_{e.LTB}$ is used in this module for consistency with the notation for column buckling as well as to distinguish the beam-theory based $F_{e.LTB}$ from the nominal elastic LTB resistance for slender-web members $F_{cr} = R_b F_{e.LTB}$.)

The radius of gyration r_t may be calculated exactly as

$$r_t = \frac{(I_y C_w)^{1/4}}{S_x^{1/2}} \quad (5.3.5-21)$$

(AISC F2-7)

for doubly-symmetric I-sections (White and Jung 2003a). AISC (2010) gives this equation, but refers to the corresponding radius of gyration as r_{ts} , to avoid its potential erroneous use for singly-symmetric I-section members. Alternately, r_t may be calculated generally for any rectangular flange I-section as

$$r_t \cong \frac{b_{fc}}{\sqrt{12 \left(\frac{h}{d} + \frac{1}{3} \frac{D_c t_w}{A_{fc}} \frac{D^2}{hd} \left(1 + 6 \frac{A_{fillet}}{D_c t_w} \right) \right)}} \quad (5.3.5-22)$$

(AASHTO C6.10.8.2.3-1, AISC F4-10)

where d is the total depth of the member, D is the depth of the web, and A_{fillet} is the area of each of the web-to-flange fillets (White and Jung 2003a). (Note that A_{fillet} is generally taken equal to zero for welded I-section members.) If one assumes $d \cong h \cong D$ and $A_{fillet} \cong 0$, Eq. (22) reduces to Eq. (9) which is precisely the equation for the radius of gyration of the compression flange plus one-third of the depth of the web in compression. Equation (22) gives results that are within one percent of the exact Eq. (21) for all rolled I-sections. Due to compensating effects within the approximation of Eq. (22) by Eq. (9), Eq. (9) also tends to give an accurate but slightly conservative approximation of Eq. (21) for general doubly-symmetric I-shapes.

For column-type I-sections with $D/b_{fc} \cong 1$, D/t_w less than about 50 and compact flanges, the second term under the radical in Eq. (19) tends to be significantly larger than one. As such, it would be quite uneconomical to discount this major contribution to the resistance to obtain a simpler form for Eq. (19). However, in situations involving beam- or girder-type I-sections with D/b_{fc} greater than about two and $b_{fc}/2t_{fc}$ near the compact-flange limit λ_{pf} or larger, the contribution from the second term in Eq. (19) is relatively small (White and Jung 2003a).

For slender-web members, the contribution from the radical in Eq. (19) is neglected altogether, due to the reduction in the effective St. Venant torsional stiffness associated with web distortional flexibility (i.e., the deformation of the web into an S shape upon twisting of the cross-section, and the corresponding reduction in the twist rotation of the flanges) (White and Jung 2007). In this case, Eq. (19) reduces to the form

$$F_{e.LTB} = C_b \frac{\pi^2 E}{(L_b / r_t)^2} \quad (5.3.5-23)$$

(AASHTO 6.10.8.2.3-8, AISC F5-4)

used traditionally by AISC and AASHTO for slender-web members. Equation (23) is multiplied by the web load shedding strength reduction factor, R_b , to obtain the elastic LTB flexural resistance in terms of the compression flange stress for slender-web members.

5.3.5.8 Noncompact bracing limit, L_r

The noncompact bracing limit L_r is obtained by equating the base elastic LTB resistance for uniform bending ($C_b = 1$) to the compression flange stress at the nominal onset of yielding, F_{yr} . Equation (19) results in the following succinct expression for the noncompact lateral brace spacing,

$$L_r = \frac{1.95 r_t}{X} \frac{E}{F_{yr}} \sqrt{1 + \sqrt{1 + 6.76 \left(\frac{F_{yr}}{E} \right)^2}} X^4 \quad (5.3.5-24)$$

(AASHTO A6.3.3-5, AISC F2-6 & F4-8)

applicable for all types of compact- and noncompact-web I-section members, whereas Eq. (23) gives

$$L_r = \pi r_t \sqrt{\frac{E}{F_{yr}}} \quad (5.3.5-25)$$

(AASHTO 6.10.8.2.3-5, AISC F5-5)

White and Jung (2003b) give a closed-form alternative expression to Eq. (24) for compact- and noncompact-web singly-symmetric I-sections, based on the rigorous application of open-section thin-walled beam theory. Unfortunately, this equation is significantly longer than Eq. (24). Also, due to the larger effects of web distortion in singly-symmetric members, the rigorous beam-theory equation does not necessarily give a better representation of the physical buckling resistance (White and Jung 2007).

5.3.5.9 Elastic FLB stress, F_{el}

The elastic plate local buckling equation defined previously by Eq. (5.2.4-1) is also the base equation for the I-section FLB resistances in AASHTO (2014). Furthermore, the FLB

coefficients k_c defined by Cases 1 and 2 of Table 5 are employed for noncompact- and compact-web built-up and rolled I-sections in flexure. However, for slender-web I-section members, Article 6.10.8.2.2 implicitly assumes $k_c = 0.35$ as an accurate to conservative simplification. As noted in Section 5.2.4 of this module, the FLB coefficient for simply-supported edge conditions at the web-flange juncture is $k_c = 0.43$. Therefore, smaller values of k_c indicate that the web is tending to destabilize the flange. The equation for k_c in Case 1 of Table 5 was developed originally by equating the results from the AISC LRFD (1993) resistance equations to measured experimental strengths for a number of tests in which the flexural resistance was governed by FLB, then back-solving for k_c (Yura 1992). The data used in these developments was predominantly from Johnson (1985). White and Jung (2008) and White and Kim (2008) discuss the correlation of the AASHTO (2014) and AISC (2010) equations with a larger updated set of experimental test results. Case 1 of Table 5 may be considered as a simple but reasonable approximate lower-bound value for the FLB coefficient for general built-up I-section members.

5.3.5.10 Noncompact flange slenderness limit, λ_{rf}

Similar to the calculation of L_r , the noncompact flange slenderness limit λ_{rf} is obtained by equating the elastic FLB stress given by Eq. (5.2.4-1) to the compression flange stress at the nominal onset of yielding, F_{yr} . The resulting equation is

$$\lambda_{rf} = 0.95\sqrt{k_c E / F_{yr}} \quad (5.3.5-26)$$

(AASHTO A6.3.2-4, AISC Table B4.1a)

By substituting the implicitly assumed value of $k_c = 0.35$ into this equation, one obtains

$$\lambda_{rf} = 0.56\sqrt{E / F_{yr}} \quad (5.3.5-27)$$

(AASHTO 6.10.8.2.2-5)

for the noncompact flange slenderness limit within the main AASHTO (2014) provisions.

5.3.5.11 Moment gradient modifier, C_b

As illustrated previously in Figure 60, the effect of any variation in the moment along the unbraced length is accounted for in AASHTO (2014) and AISC (2010) via the moment gradient modifier C_b . The C_b modifier has a base value of 1.0 when the moment and the corresponding compression flange major-axis bending stresses are uniform along the length between the brace points. Furthermore, C_b may be conservatively taken equal to 1.0 for all cases, with the exception of:

- Situations involving significant top flange loading either on unbraced cantilevers or on members with no intermediate bracing in the entire span, and
- General unbraced cantilevers with less than essentially rigid warping restraint at their fixed end due to flexible end connections or continuity with a flexible back-span (Zieman 2010).

(For cases involving flexure in members other than in horizontal (i.e., in-plan) framing, the “top” flange may be considered as the flange opposite to the direction of the applied loads causing the major-axis bending, assuming that all the applied loads are in the same direction. Also, the “vertical” supports may be taken as the supports corresponding to the reactions associated with major-axis bending.)

The above exceptional cases are addressed after discussion of the more common situations. Whenever both ends of a cantilevered girder are prevented from twisting (by end cross-frames or diaphragms), the behavior is effectively the same as that of an ordinary span with vertical supports and twisting restrained at both ends. Therefore, if one or more intermediate braces are provided within either an ordinary span or a cantilever span in which the ends are prevented from twisting, load height effects do not need to be considered in the calculation of C_b . Helwig et al. (1997) discuss mitigating factors regarding load-height effects that justify this simplification. Cases in which the ends of a span are not prevented from twisting require specialized consideration regardless of the loading and span type.

For the above “common situations,” AASHTO (2014) and AISC (2010) specify different equations for C_b , both of which tend to give accurate to somewhat conservative solutions. AISC (2010) specifies the formula

$$C_b = \frac{12.5M_{\max}}{2.5M_{\max} + 3M_A + 4M_B + 3M_C} R_m \leq 3.0 \quad (5.3.5-28)$$

(AISC F1-1 & C-F1-3)

Where

M_{\max} = absolute value of the maximum moment in the unbraced segment

M_A = absolute value of the moment at the quarter point of the unbraced segment

M_B = absolute value of the moment at the mid-length of the unbraced segment

M_C = absolute value of the moment at the three-quarter point of the unbraced segment

R_m = cross-section monosymmetry parameter

= 1.0 for doubly-symmetric members

= 1.0 for singly-symmetric members subjected to single-curvature bending

$$= 0.5 + 2 \left(\frac{I_{y,top}}{I_y} \right)^2 \quad (5.3.5-29)$$

for singly-symmetric members subjected to reverse-curvature bending.

Conversely, AASHTO (2014) Article 6.10.8.2.3 specifies

$$C_b = 1.0 \quad (5.3.5-30a)$$

(AASHTO 6.10.8.2.3-6)

for members where $f_{mid}/f_2 \geq 1$ or $f_2 = 0$, and

$$C_b = 1.75 - 1.05 \frac{f_1}{f_2} + 0.3 \left(\frac{f_1}{f_2} \right)^2 \leq 2.3 \quad (5.3.5-30b)$$

(AASHTO 6.10.8.2.3-7)

for all other common situations, where

f_2 = absolute value of the largest factored compressive major-axis bending stress at either end of the unbraced length of the flange under consideration, determined from the critical moment envelope value. If the stress is zero or tensile in the flange under consideration at both ends of the unbraced length, f_2 is taken equal to zero.

f_{mid} = factored major-axis bending stress at the middle of the unbraced length of the flange under consideration, calculated from the moment envelope value that gives the largest compression at this point, or the smallest tension if this point is never in compression, taken as positive in compression and negative in tension.

$$f_1 = f_o \quad (5.3.5-31)$$

(AASHTO 6.10.8.2.3-10)

when the variation in the flange stress between the brace points is concave in shape, and otherwise

$$f_1 = 2f_{mid} - f_2 \geq f_o \quad (5.3.5-32)$$

(AASHTO 6.10.8.2.3-11)

f_o = factored major-axis bending stress at the brace point opposite to the one corresponding to f_2 , calculated from the moment envelope value that gives the largest compression at this point in the flange under consideration, or the smallest tension if this point is never in compression, taken as positive in compression and negative in tension.

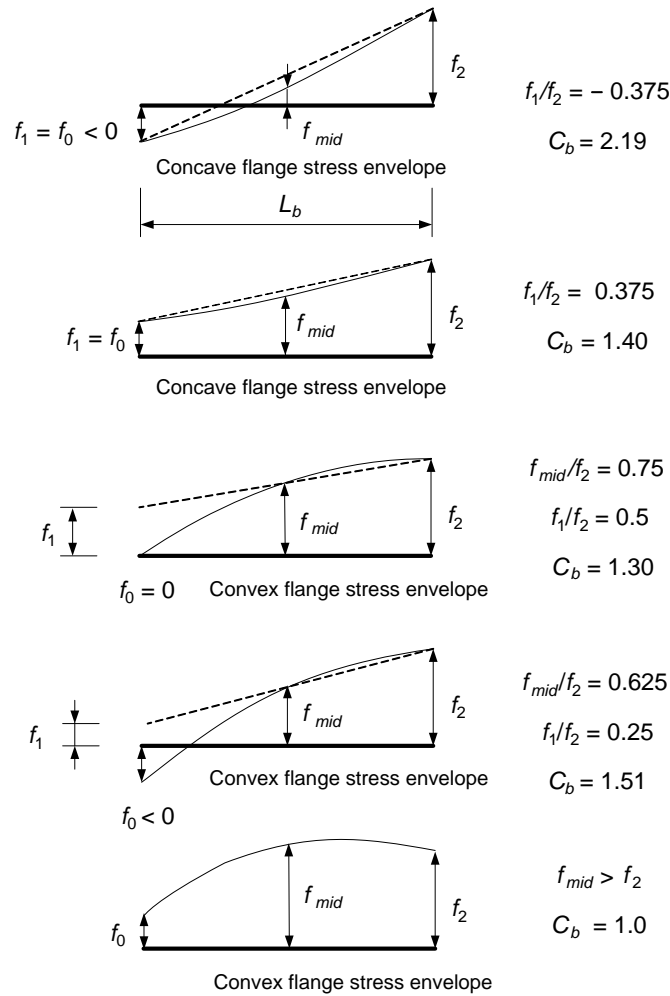


Figure 65 Sample cases for calculation of the AASHTO (2014) moment gradient modifier, adapted from AASHTO (2014) Article C6.4.10.

Figure 65 shows several sample cases that illustrate the application of the AASHTO procedure. The first two cases involve a concave flange stress envelope, that is, $|f_{mid}|$ is smaller than the absolute value of the average of f_2 and f_0 . For these cases, f_1 is taken equal to f_0 and the application of Eq. (30b) is the same as in prior AASHTO Specifications. However, the second two cases involve a convex flange stress envelope. The prior usage of Eq. (30b) results in significant unconservative error in many of these cases. For example, the prior AASHTO Specifications would use $f_1 = 0$ in the third case, resulting in $C_b = 1.75$. The above AASHTO (2014) equations effectively define f_1 as the ordinate of a straight line that goes from f_2 at the opposite end of the unbraced length through f_{mid} at the mid-length. This definition gives $C_b = 1.30$, which is a more accurate representation of analytical solutions (Ziemian 2010). Other sample cases are illustrated in AASHTO (2014) Article C6.4.10.

For reverse-curvature bending, both the AISC and AASHTO procedures require the Engineer to check LTB considering the base resistance for uniform bending, scaled by the appropriate C_b value for each of the member flanges. In the AISC method, one C_b factor is calculated and

applied to both flanges. In the AASHTO method, a separate C_b factor is calculated using Eqs. (30) to (32) for each flange.

Figure 66 illustrates the C_b calculations for several representative examples by both of the above procedures. The results are compared to the exact LTB solutions for the two I-girder cross-sections shown in Figure 67. An unbraced length-to-depth ratio of $L_b/h = 12.5$ ($L_b = 75$ ft) is assumed for the first four examples, and an unbraced length-to-depth ratio of 8.0 ($L_b = 48$ ft) is assumed for the last example. The cross-sections shown in Figure 67 are similar in terms of behavioral characteristics to those used by Helwig et al. (1997) in their studies. Both cross-sections satisfy the AASHTO (2014) Article 6.10.2 proportioning requirements and, for the 150 and 144 ft continuous-span examples in Figure 66 (the fourth and fifth ones), these sections are representative of I-girder designs using the AASHTO Specifications. The singly-symmetric cross-section shown in Figure 67 is a representative extreme case with $I_{yc}/I_{yt} = 0.22$ (for positive bending), which is smaller than the Eq. (7) limit but satisfies Eq. (5.3.2-6).

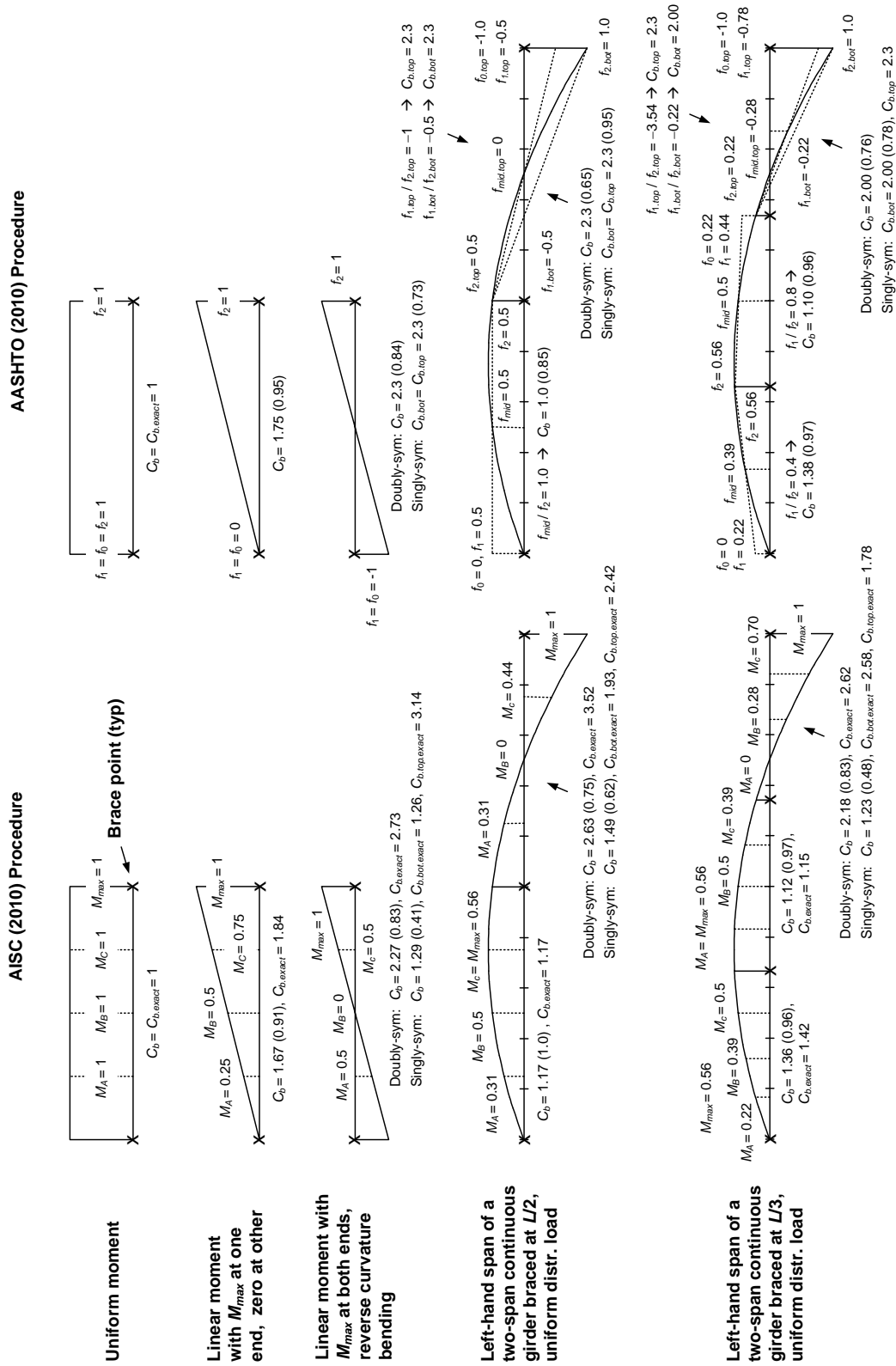


Figure 66 Calculation of C_b by AISC (2010) and AASHTO (2014) for several representative design examples.

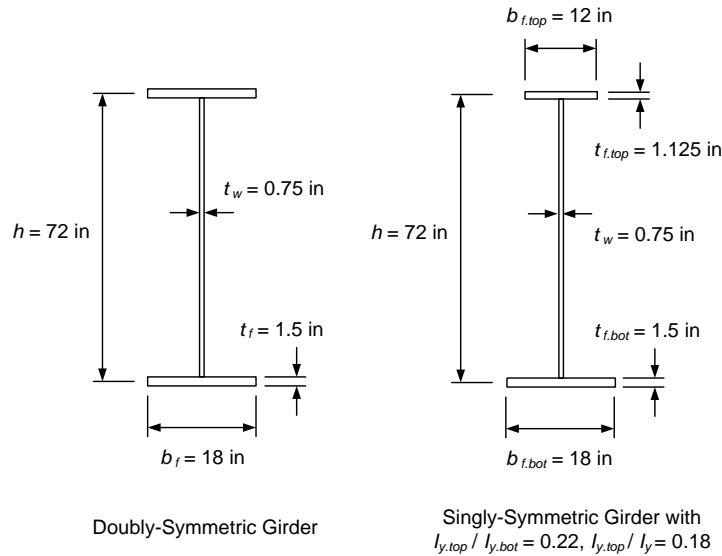


Figure 67 Cross-sections used in the example C_b calculations.

For demonstration purposes, non-moving loads are assumed in Figure 66 such that the moment envelopes and the moment diagrams are the same. Also, noncomposite members are assumed since Eq. (28) is not applicable for composite members. In the case of noncomposite members, the distribution of the flange stresses along the unbraced length is the same as the distribution of the member bending moments. However, for composite members, the distribution of the flange stresses and the bending moments are different due to the influence of the separate noncomposite, short-term composite and long-term composite loadings, and due to the different effective cross-sections in positive and negative bending. Equations (28) and (29) are neither derived nor intended for composite I-girders in negative bending.

The exact solutions are determined using the open-section thin-walled beam element in GT-Sabre (Chang and White 2010). These solutions are determined by analyzing the various unbraced lengths as isolated segments assuming torsionally simply-supported end conditions (i.e., the flange lateral bending and warping are unrestrained at the ends of the isolated unbraced segments, neglecting any continuity effects with adjacent unbraced lengths). The “exact” C_b values are calculated as

$$C_{b,exact} = M_{cr} / M_{cro} \quad (5.3.5-33)$$

where

M_{cr} = buckling moment corresponding to the cross-section with the largest compression stress in the flange under consideration for any of the loadings causing non-uniform moment along the unbraced length, and

M_{cro} = buckling moment corresponding to uniform compression in the flange under consideration.

This is the same as the calculation of $C_{b,exact}$ by Helwig et al. (1997). The exact C_b values are presented only with the AISC (2010) calculations in Figure 66, to simplify the figure. Both the AISC and the AASHTO design values are compared to these exact solutions. The number contained in the parentheses after the reported design C_b values is the ratio of the design C_b value to the relevant $C_{b,exact}$. As noted above, for the reverse-curvature bending cases, one C_b value is applied to both flanges in the AISC procedure. The LTB strength prediction is governed by the flange that has the smallest ratio of $C_b / C_{b,exact}$. In the AASHTO procedure, separate C_b values are determined for each flange in cases involving reverse curvature bending. The ratio of the predicted to exact LTB resistance is governed by the flange that has the smallest ratio of $C_b / C_{b,exact}$.

For all the unbraced lengths subjected to single-curvature bending in Figure 66, the exact solutions are presented only for the doubly-symmetric cross-section to simplify the figure. The reader is referred to Helwig et al. (1996) for examples that show that Eq. (28) with $R_m = 1$ gives accurate results for singly-symmetric beams in single-curvature bending.

The following observations can be drawn from the results shown in Figure 66:

- The AASHTO (2014) procedure involves fewer calculations. In cases where the flange stress diagram is concave (e.g., the bottom flange stress distribution in the right-most unbraced lengths of the two-span continuous beam examples), f_1 and f_2 in Eqs. (30) are simply the flange stresses at the ends of the unbraced segment under consideration. That is, f_1 and f_2 are the same as in the traditional usage of Eq. (30b). In other cases, the Engineer only needs to determine the maximum compressive flange stress, f_2 , and the flange stress at the middle of the unbraced length, f_{mid} , from the structural analysis. The stress f_1 is simply the ordinate of a straight line that goes from f_2 at the opposite end of the unbraced length through f_{mid} at the mid-length. By using Eq. (32) to define f_1 in these cases, the accuracy of Eq. (30b) is significantly improved relative to the traditional usage of just the end values for f_1/f_2 . Equation (32) gives the same result as the traditional definition of f_1/f_2 when the moment diagram is linear or concave.
- The AASHTO (2014) procedure is more accurate and liberal for the linear moment diagram cases. For these cases, Eq. (30b) is still a lower bound compared to analytical solutions (Salvadori 1956). Helwig et al. (1997) state that Eq. (28) is quite conservative for cases with linear moment diagrams in reverse curvature bending and smaller values of $I_{y,top}/I_y$. They refer to Kitipornchai et al. (1986) for more accurate estimates of C_b in these situations. Equations (30) give accurate to somewhat conservative calculations relative to the more complex equations presented by Kitipornchai et al. (1986) for linear moment diagrams.
- For longer unbraced lengths, nonlinear moment diagrams (i.e., transverse loading within the unbraced length) and single-curvature bending, Eq. (28) often gives more accurate estimates than Eqs. (30). For example, for the left-most unbraced length in the first continuous-span example of Figure 66, Eq. (28) gives $C_b = 1.17$ (versus $C_{b,exact} = 1.17$) while Eqs. (30) give $C_b = 1.0$. However, for the unbraced lengths in single-curvature bending in the second continuous-span example, which still has only two internal brace

points, the C_b values calculated using Eq. (30b) are essentially the same as those calculated using Eq. (28). Both of the design C_b calculations are only slightly conservative compared to the exact values for the specific doubly-symmetric I-girder considered in this study.

- For the continuous-span beam segments subjected to reverse-curvature bending, Eqs. (28) and (30b) both give accurate to somewhat conservative results for the doubly-symmetric cross-section. However, for the singly-symmetric cross-section, Eq. (28) is quite conservative relative to the exact elastic LTB solutions. For cases with a smaller top flange ($I_{y,top}/I_y < 0.5$), Eq. (29) gives an abrupt drop in the calculated C_b value regardless of the length of the top flange subjected to compression. Also, the terms M_A , M_B and M_C in Eq. (28) are blind to the sign of the bending moment. This is appropriate for doubly-symmetric I-section members, but the accuracy of Eq. (28) is limited for reverse-curvature bending of singly-symmetric I-section members due to this simplification.
- For all the cases involving reverse-curvature bending and a singly-symmetric cross-section in Figure 66, Eq. (28) gives a more accurate estimate of $C_{b,exact}$ if R_m is taken equal to 1.0 (such that the C_b calculation is the same as that for a doubly-symmetric cross-section member). For the third example (the linear moment diagram with M_{max} at both ends and reverse-curvature bending) the resulting C_b is 2.27 versus $C_{b,top,exact} = 3.14$, giving a ratio of the design estimate to the exact buckling calculation of $2.27/3.14 = 0.72$ rather than the ratio 0.41 shown in the figure. For the right-most unbraced length in the fourth example, the resulting C_b is 2.63 versus $C_{b,top,exact} = 2.42$, giving a ratio of $2.63/2.42 = 1.09$. This is within the range of the $C_b/C_{b,exact}$ ratios for the examples studied by Helwig et al. (1997). For the right-most unbraced length in the fifth example, the resulting C_b is 2.18 versus $C_{b,bot,exact} = 2.58$, giving a ratio of $2.18/2.58 = 0.84$ rather than 0.48. However, for more extreme reverse-curvature bending cases on singly-symmetric cross-section members, such as when there are no intermediate braces within the span, the calculation of R_m by Eq. (29) is necessary to obtain an adequate solution using Eq. (28) (Helwig et al. 1997).

In addition to the above observations, White et al. (2001) show that the AASHTO (2014) approach, when used with the most critical moment envelope values as specified in the definitions of f_2 , f_{mid} and f_o , always gives an accurate to conservative representation of the moment gradient effects associated with the actual concurrent loadings. There does not appear to be a way to prove this useful property for Eqs. (28) and (29). Also, Eqs. (30) focus solely on the flange under consideration. For unbraced lengths subject to single-curvature negative bending or for reverse-curvature bending in composite I-section members, Eq. (30b) is applied by focusing solely on the bottom flange stresses, without the need to consider any properties of the top flange. For composite sections in positive bending, AASHTO (2014) considers the compression flange to be continuously braced. If the right-most unbraced lengths in examples 4 and 5 of Figure 66 were composite I-girders, the C_b calculations for the bottom flange would be the same as illustrated in the figure. No calculations would be required for the composite top flange. As noted above, Eqs. (28) and (29) are not intended for composite I-section members. Section 5.3.5 of this module discusses the overall logic and rationale behind the AASHTO (2014) LTB calculations for composite I-girder segments in negative bending. Lastly, it is important to

recognize that in most practical design situations, even with relatively large unbraced lengths, the base uniform bending resistance, F_{nc} or M_{nc} , shown by the solid curve in Figure 60 is often not significantly smaller than F_{max} or M_{max} . For example, if $L_b = L_r$, F_{nc} is typically equal to $0.7F_{yc}$. Therefore, for slender-web members, a C_b value of $1/0.7 = 1.43$ is sufficient to raise the flexural resistance to F_{max} .

The discussion at the beginning of this section indicates that in unusual cases involving significant top flange loading either on unbraced cantilevers or on members with no intermediate bracing in the entire span, the influence of the load height must be considered. Loads applied to the top flange cause destabilizing (tipping) effects, whereas loads applied to the bottom flange enhance the member LTB resistance. When twisting of the cross-section is prevented at the ends of a cantilever or ordinary span, these effects are approximated with reasonable accuracy by the equation

$$C_b^* = 1.4^{2y/h} C_b \quad (5.3.5-34)$$

where C_b is the base moment gradient factor determined without considering load height effects (e.g., via Eq. (28) or Eqs. (30)), y is the load height above the mid-depth of the cross-section, negative for load applied above the mid-depth, and h is the distance between the flange centroids (Helwig et al. 1997; Ziemian 2010). Helwig et al. (1997) show that the definition of y in Eq. (34) as the distance from the mid-depth gives an accurate representation of the effect of the load height. They show that if the C_b values are derived using the cross-section shear center as the origin for y , they are quite sensitive to the shear center location. However, with the origin for y taken at the cross-section mid-depth, Eq. (28) gives an accurate representation of the C_b values for loadings applied at the mid-depth, regardless of the shear center location. Equation (28) generally gives a more accurate and more liberal estimate of the effects of moment gradient relative to Eqs. (30) for spans with no internal bracing but where twisting is restrained at the ends of the span.

The discussion at the beginning of this section also indicates that C_b may not necessarily be taken equal to 1.0 in general unbraced cantilevers with less than essentially rigid warping restraint at their fixed end. Ziemian (2010) suggests recommended procedures for determining the buckling load of these types of members. The reader is referred to Ziemian (2010), Dowswell (2002), Yura and Helwig (1996) and Anderson and Trahair (1972) for a range of LTB solutions applicable for unbraced cantilevers.

5.3.5.12 Other considerations specific to composite I-section members in negative bending

The AASHTO (2014) equations discussed in the above sections provide one single consistent representation of the FLB and LTB resistance of both noncomposite I-section members as well as composite I-section members in negative bending. The application of these equations to composite I-girders in negative bending is based on the following simple concept that has been used extensively for the design of experimental tests to study the behavior in the negative moment regions of composite beams. Numerous research studies have shown that the resistance of composite beams in negative bending can be approximated accurately to conservatively by

using a large steel tension flange or a cover-plated tension flange. These tension flange elements provide a force equivalent to that developed by the slab reinforcing steel in the prototype composite member (White and Barth 1998; Barth and White 1997; Kemp 1996; Grubb and Carskaddan 1981 & 1979; Climenhaga and Johnson 1972). The AASHTO (2014) approach considers the contribution to the cross-section moment from the reinforcing steel as a tension flange element, but otherwise focuses on the compressed region of the steel I-section for the stability assessment. The lateral and torsional restraint that the concrete deck provides to the steel I-section is neglected. The effects of this restraint are reduced in general by web distortion, and for typical I-girder bridges, the benefits of this restraint are judged not to be worth the additional effort associated with the distortional buckling solution. This is because, for the majority of cases in bridge I-girders, the C_b values calculated as discussed in the previous section will place the negative bending LTB capacity on the plateau of the dashed flexural resistance curve shown in Figure 60.

In calculating the radius of gyration r_t from Eq. (9) for composite I-section members, AASHTO (2014) specifies that D_c should be determined using the cross-section composed of the steel I-section member plus the longitudinal reinforcing steel. For composite I-sections in negative bending, this value of D_c tends to be slightly conservative relative to the actual D_c under the combined composite and noncomposite loadings. This calculation also removes another dependency of the LTB resistance on the applied loadings.

For composite I-section members in negative bending, the Appendix A6 LTB and FLB resistances, which are written in terms of member moments, depend in general on the elastic section modulus to the compression flange, S_{xc} . Also, the TFY resistance depends in general on the elastic section modulus to the tension flange elements, S_{xt} . These elastic section moduli are calculated as

$$S_{xc} = M_{yc}/F_{yc} \quad (5.3.5-35a)$$

and

$$S_{xt} = M_{yt}/F_{yt} \quad (5.3.5-35b)$$

where M_{yc} and M_{yt} are the cross-section yield moments. The yield moments are in turn calculated using a procedure detailed in Article D6.2.2 that accounts for the separate influence of noncomposite and composite loadings on the cross-section elastic stresses. The yield moment M_{yt} is based on the first yielding of any top-flange elements of the steel section or of the slab reinforcing steel.

For negative bending of composite I-section members with compact or noncompact webs, the AASHTO Appendix A6 flexural resistance depends on the loading type only in the places where the elastic section moduli, S_{xc} or S_{xt} , or the yield moments, M_{yc} or M_{yt} , enter into the calculations. The composite cross-section is handled as fully cracked in the section-level calculations, and hence the long-term and short-term section moduli are identical.

Article A6.3.3 specifies equations for C_b that parallel Eqs. (30) but are written in terms of the member moments rather than the flange stresses. This is consistent with the practice of neglecting the separate influence of noncomposite and composite loadings on the resistance in the limit that the I-section web, flange and unbraced length are compact. Article C6.8.10.2.3 points out that the overall effect of the different types of loading on the C_b calculation is considered negligible for compact- and noncompact-web composite I-sections in negative bending. This article also permits the use of the total moments in calculating C_b for slender-web members if it is felt in the judgment of the Engineer that the effect on the final calculated value of C_b is insignificant.

5.3.5.13 LTB effective lengths

As noted in Section 5.3.5 of this module, ordinary practice is to take L_b as the actual unsupported length between the brace points corresponding to compression flange level bracing and/or the diaphragm or cross-frame locations. That is, a LTB effective length factor of $K = 1.0$ is assumed for all the unbraced lengths. However, substantial restraint can exist at the ends of a critical unbraced length when the adjacent segments are less critically loaded, resulting in an effective length $KL_b < L_b$ for the critical segment. AASHTO (2014) allows this smaller KL_b to be used in place of L_b to increase the calculated member LTB resistance, F_{nc} or M_{nc} , in its Articles 6.10.8.2.3 and A6.3.3 and/or to reduce the calculated amplification of the compression flange lateral bending stresses in Article 6.10.1.6. Article C6.10.8.2.3 recommends a simple hand method from Galambos (1998) and Nethercot and Trahair (1976) for estimating K . A generalized form of this procedure, which is applicable for singly- and doubly-symmetric I-section members and includes the consideration of moving live loads, is outlined below. The method is based on an analogy between the buckling of a continuous beam and the buckling of an end-restrained column. As such, it uses the alignment chart for nonsway columns to determine a K factor for the critical unbraced length.

The suggested procedure involves the following steps:

1. Determine C_b for each unbraced segment in the member as discussed in Section 5.3.5.
2. Identify the critical segment. This segment is the one that buckles elastically at the smallest multiple of the design loadings, using the largest moment envelope value in each unbraced segment, and using the actual unbraced length L_b in the applicable elastic LTB resistance equation for each segment. The multiple of the design loadings associated with the buckling of the critical segment is denoted by γ_m . Also, the multiples of the design loadings associated with the buckling of the adjacent segments (should they exist) are denoted by γ_{rL} and γ_{rR} respectively. For all of these segments, the following equation applies:

$$\gamma = \frac{F_{e.LTB}}{f_{bu}} \tag{5.3.5-36}$$

where $F_{e.LTB}$ is the governing elastic LTB resistance determined using Eq. (19) for compact- or noncompact-web members or Eq. (23) for slender-web I-section members, and f_{bu} is the largest value of the compression flange stress in the segment under consideration.

3. Calculate a stiffness ratio, α , for each of the above three segments. The stiffness ratio for the critical segment is determined as

$$\alpha_m = \frac{2(b_{fc}t_{fc} + \frac{1}{3}D_c t_w)r_t^2}{L_{bc}} \quad (5.3.5-37)$$

and the stiffness ratio for each of the adjacent “restraining” segments is determined as

$$\alpha_r = \frac{n(b_{fc}t_{fc} + \frac{1}{3}D_c t_w)r_t^2}{L_b} \left(1 - \frac{\gamma_m}{\gamma_r} \right) \quad (5.3.5-38)$$

where $n = 2$ if the far end of the adjacent segment is continuous, $n = 3$ if it is simply-supported (torsionally), and $n = 4$ if it is torsionally fixed. If the critical segment has a simply-supported end and no adjacent unbraced length, $\alpha_r = 0$. Also, for cases involving monosymmetric I-girders and reverse curvature bending in any one of the above segments, the area $(b_{fc}t_{fc} + D_c t_w / 6)$ and r_t terms in Eqs. (37) and (38) are the values corresponding to the governing elastic LTB resistance.

4. Determine the ratios $G = \alpha_m / \alpha_r$ for each end of the critical segment.
5. Substitute the above G values into the sidesway-inhibited column alignment chart (AISC 2010; AASHTO 2010; Kavanagh 1962) to obtain the effective length factor K . As noted previously in Section 5.2.2 of this module, AASHTO (2014) Article C4.6.2.5 gives closed form equations that provide a close fit to the alignment chart results.

The above procedure is a very practical approach in that steps 1 and 2 are a by-product of the ordinary design calculations, where K is implicitly taken equal to 1.0 and the actual unsupported length L_b is used within the LTB resistance equations. Therefore, steps 3 through 5 are basically an “add-on” to the ordinary design procedures that the Engineer can utilize when he or she deems the additional calculations to be useful to justify a more liberal calculation of the resistance. Also, the Engineer should note that in the special case where the adjacent unbraced lengths are equally critical (e.g., if all three unsupported segments have the same length L_b , the same cross-section, each segment subjected to the same uniform bending moment and $n = 2$ in the adjacent segments), $\alpha_r = 0$ and $G = \infty$ at each end of the critical segment. This gives $K = 1.0$ from the sidesway-inhibited column alignment chart. The above method is conservative because it is based on the assumption that the largest moment-envelope values in the adjacent segments are taken from the concurrent loadings associated with buckling of the critical unbraced length.

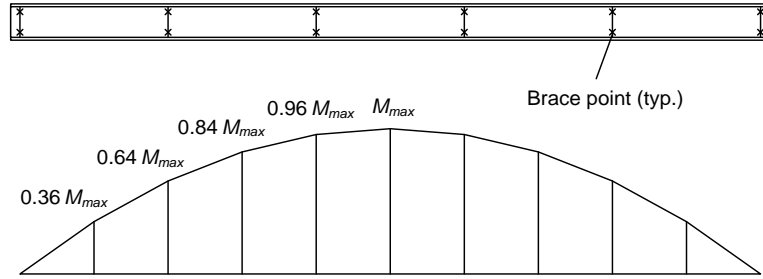


Figure 68 Simple-span I-girder and critical moment envelope for example calculation of LTB effective length factor K .

The application of the above procedure can be understood best by working a representative example. Consider the prismatic simple-span girder with four equally-spaced intermediate brace points shown in Figure 69. The middle unbraced length of this beam is clearly the most critical since it contains the largest moment and all of the unbraced lengths are equal. In step 1 of the above procedure, the moment envelope values for the middle unbraced segment give $f_{mid}/f_2 > 1$. As a result, $C_b = 1.0$ for this segment from Eq. (30a). The moment envelope values for the unbraced lengths adjacent to the central segment give $f_{mid}/f_2 = 0.875$ and thus $f_1/f_2 = 0.75$ using Eq. (32). This gives, $C_b = 1.13$ for these segments from Eq. (30b). For the end segments, $f_{mid}/f_2 = 0.56$, giving $f_1/f_2 = 0.12$ and $C_b = 1.63$.

If the Engineer deems that the additional effort of calculating $K < 1$ is not worthwhile, he or she can stop at this stage and use the above C_b values along with $K = 1$ for the design. For that matter, the Engineer could base the design on $C_b = 1$ and $K = 1$ and avoid the calculations in step one. However, if the additional benefits of using $K < 1$ are potentially significant, the Engineer may wish to continue to step 2. One of the excellent attributes of the suggested (Nethercot and Trahair 1976) procedure is that the subsequent steps utilize the C_b values that the Engineer has already determined based on ordinary practice.

If the Engineer continues to step 2 for the example girder in Figure 69, he or she would observe that since the central segment has $C_b = 1$ and the girder is prismatic (no section transitions) with equal unbraced lengths, the central unbraced length is the most critical one. If the applied load level on the beam associated with the buckling of this segment is taken as $\gamma_m = 1.00$, the corresponding applied load level at the buckling of the adjacent segments (using $K = 1$), are simply $\gamma_r = C_b = 1.13/0.96 = 1.18$. (Note that one has to divide by 0.96 because at the applied load level of $\gamma_m = 1.00$, the maximum moment in the adjacent segments is only $0.96M_{max}$.) If α_m from Eq. (37) is normalized to a value of 2, then

$$\alpha_r = 2 \left(1 - \frac{1}{1.18} \right) = 0.301 \quad (5.3.5-39)$$

from Eq. (38). This completes step 3. In step 4, the value of $G = \alpha_m/\alpha_r$ is $2/0.301 = 6.64$ at both ends of the critical segment. Given these G values, one enters the sidesway-inhibited column alignment chart (step 5) to obtain $K \cong 0.94$. This K factor can now be used to obtain a slightly higher LTB resistance (roughly 13 % higher if the elastic LTB equations govern the strength) as

well as a slightly smaller amplification of the elastic compression flange lateral bending stresses. This is a relatively small benefit in this example. However, the benefit can be larger in some cases.

When checking the resistance of the unbraced lengths adjacent to the critical segment, it is essential to account for the fact that the more critical segment tends to destabilize the less critical ones if the critical segment is assumed to be restrained such that its K is less than one. This is addressed by calculating the K factor for the adjacent segments as

$$K = \sqrt{\frac{\gamma_r}{\gamma_m^*}} \quad (5.3.5-40)$$

where γ_m^* is the load parameter at elastic buckling of the critical unbraced, based on the above computed $K < 1$, i.e., $\gamma_m^* = (1/0.94)^2 = 1.13$. Equation (40) gives $K = [1.18 / 1.13]^{0.5} = 1.02$ for the segments adjacent to the central unbraced length in Figure 69. As illustrated here, the effective length factor for the adjacent segments will actually exceed 1.0; however, these segments are the less critical ones, and the overall calculated elastic LTB capacity of the girder is always increased by using the above procedure.

An effective length factor of $K = 1$ should be used for other unbraced lengths that are not adjacent to the critical segment. The above procedure focuses only on the critical segment and the unbraced lengths adjacent to this segment. The more remote unbraced lengths are assumed not to have any significant buckling interaction with the critical segment.

In cases where one or more of the unbraced lengths contains a cross-section transition, but the members are otherwise prismatic, the transition to a smaller section may be neglected in determining the γ value for the segment containing the transition, and the above procedure may be used to determine the LTB effective lengths, when:

- The critical segment or either of its adjacent segments has a cross-section transition within 20 % of the corresponding unbraced length L_b , and
- The changes in the flange moments of inertia about the plane of the web at the cross-section transition(s) are less than a factor of two for both flanges (i.e., $I_1/I_2 \geq 0.5$ where I_1 and I_2 are the moments of inertia of the smaller and larger flanges respectively).

The calculation of the LTB resistances for more general cases involving stepped, variable web-depth and other nonprismatic I-section members is addressed in Section 5.3.6 of this module.

5.3.5.14 Inelastic redistribution of interior pier moments in continuous-span bridges

Minor yielding over the interior supports of continuous spans results in a redistribution of the girder moments. For straight continuous-span flexural members that satisfy requirements intended to ensure adequate ductility and robustness of the girder segments adjacent to the interior piers, AASHTO (2014) Appendix B6 may be used to calculate the redistribution

moments at the SERVICE II and/or Strength load levels. These provisions replace the former 10 % redistribution allowance as well as former inelastic analysis procedures. They provide a simple calculated percentage redistribution from the interior-pier sections. The calculated redistribution moments are akin to internal moments generated by the following pre-stressing procedure:

1. The slab is cast and/or cover plates are welded to the bottom flange of pier sections with the interior supports jacked to an elevation higher than their final positions, and
2. The interior supports are lowered to their final positions after the construction is complete and the slab has attained sufficient strength.

However, the redistribution moments are generated by minor inelastic rotations in the girders over the interior supports rather than the above construction operations. The interior pier sections are designed to exhibit ductile moment-rotation responses and to shake down elastically after a few passages of the maximum design loads.

Appendix B6 utilizes the elastic moment envelopes and does not require any direct use of inelastic analysis. As such, these updated procedures are substantially simpler and more streamlined than the inelastic analysis procedures of previous AASHTO Specifications. For the types of bridges and girder requirements where they are allowed, these provisions make it possible to potentially use prismatic sections along the entire length of the bridge or between field splices without requiring excess material. This practice can improve the overall fatigue resistance and provide significant fabrication economies. The development of the Appendix B6 provisions is documented in a number of comprehensive reports (Barker et al. 1997; Schilling et al. 1997; White et al. 1997) and in a summary paper by Barth et al. (2004).

The provisions of Appendix B6 account for the fact that the compression flange slenderness, $b_{fc}/2t_{fc}$, and the cross-section aspect ratio, D/b_{fc} , are the predominant factors that influence the ductility of the moment-rotation response at adequately braced interior-pier sections. As such, these provisions apply to all compact compression-flange pier sections with compact, noncompact or slender webs up to $D/t_w = 150$, as long as the following restrictions are satisfied:

- The bridge must be straight.
- The bearing lines shall not be skewed more than 10 degrees.
- None of the cross-frame lines may be staggered.
- The largest girder specified minimum yield strength in the unbraced lengths immediately adjacent to the interior piers shall not exceed 70 ksi.
- The tension flange shall not have any holes over a distance of two times the web depth on each side of interior pier sections from which moments are redistributed.

- Moments shall be redistributed only from interior pier sections that have bearing stiffeners at the interior pier sections and for which the immediately adjacent unbraced lengths are prismatic and satisfy the requirements

$$\frac{2D_c}{t_w} \leq 6.8 \sqrt{\frac{E}{F_{yc}}} \quad (5.3.5-41)$$

(AASHTO B6.2.1-1)

$$D_{cp} \leq 0.75D \quad (5.3.5-42)$$

(AASHTO B6.2.1-3)

$$b_{fc} \geq \frac{D}{4.25} \quad (5.3.5-43)$$

(AASHTO B6.2.2-2)

$$L_b \leq \left[0.1 - 0.06 \frac{M_1}{M_2} \right] \frac{E}{F_{yc}} r_t \quad (5.3.5-44)$$

(AASHTO B6.2.4-1)

And

$$V_u \leq \phi_v V_{cr} \quad (5.3.5-45)$$

(AASHTO B6.2.5-1)

Where

M_1 = the bending moment at the brace point with the smaller moment due to the factored loads, taken as the value from the moment envelope that produces the smallest permissible unbraced length,

M_2 = the bending moment at the brace point with the larger moment due to the factored loads, taken as the critical moment envelope value,

V_u = the shear in the web due to the factored loads, and

V_{cr} = the shear buckling resistance specified in AASHTO (2014) Article 6.10.9.2 for unstiffened webs and in AASHTO (2014) Article 6.10.9.3 for transversely-stiffened webs.

The above limits ensure that the pier sections exhibit significant ductility and limit the application of the Appendix B6 procedures to designs supported by the background research. The main provisions of Articles B6.3 and B6.4 utilize the concept of an effective plastic moment

$$M_{pe} \leq M_n \quad (5.3.5-46)$$

(AASHTO B6.5.1-3 & B6.5.2-2)

at the interior pier sections, where M_n is the pier section flexural resistance calculated as discussed in Section 5.3.5 of this module, and the reduction in M_{pe} relative to M_n is based on

simplified lower-bound estimates of the pier section inelastic moment-rotation responses. The differences between the maximum moments from the factored elastic moment envelopes, M_e , and the effective plastic moments, M_{pe} , are redistributed from the pier sections to the positive moment regions up to a maximum of $0.2M_e$.

5.3.6 Stepped, Variable Web Depth and Other Nonprismatic I-Section Members

Section 5.2.6 of this module outlines a generalization of the AASHTO (2014) and AISC (2010) column resistance equations, from Kaehler et al. (2011), for handling of nonprismatic members loaded in nonuniform axial compression. Kaehler et al. also address the generalization of the AASHTO (2014) and AISC (2010) flexural resistance equations to members with nonprismatic cross-section geometry. The following is a summary of the basic concepts and procedures from this reference.

The equations for composite members in positive bending, discussed in Sections 5.3.3 and 5.3.4 of this module, as well as the FLB and TFY equations for composite members in negative bending and noncomposite members, outlined in Section 5.3.5, are effectively cross-section based checks. Hence, these equations may be applied directly for all types of members on a cross-section-by-cross-section basis. One determines the required moment, M_u , or the required flange stress, f_{bu} , at all the cross-sections along the member length. These required moments or stresses are then compared against the corresponding cross-section design resistances. Of course, when performing manual calculations, the Engineer can often identify by inspection one or only a few potentially critical sections that need to be checked. However, for automated design assessment, one would typically check the cross-sections at a selected interval along the member lengths.

In contrast to the above limit state checks, the LTB resistance cannot be assessed solely on a cross-section-by-cross-section basis. This is because the LTB resistance depends on the cross-section properties along the entire unbraced length as well as the loading configuration (e.g., moment gradient) and the end conditions (e.g., continuity with adjacent unbraced lengths). These factors are very similar to the factors that influence the member out-of-plane resistance in axial compression. As such, similar to the approach outlined in Section 5.2.6 of this module, the LTB resistance of a general nonprismatic I-section member may be determined by focusing on:

1. The ratio of the moments (or compression flange stresses) at elastic LTB to the corresponding factored moments (or stresses)

$$\gamma_{e.LTB} = \frac{M_{e.LTB}}{M_u} = \frac{F_{e.LTB}}{f_{bu}} \quad (5.3.6-1)$$

And

2. The largest ratio of the factored moment (or compression flange stress) to the section yield strength

$$\rho_{o,max} = \left(\frac{M_u}{M_{yc}} \right)_{\max} = \left(\frac{f_{bu}}{F_{yc}} \right)_{\max} \quad (5.3.6-2)$$

from all the cross-sections along the unbraced length.

Elastic LTB governs for unbraced lengths in which

$$\left(F_{e.LTB} = \gamma_{e.LTB} f_{bu,max} = \gamma_{e.LTB} \frac{M_{u,max}}{S_{xc,max}} \right) \leq F_{yr} \quad (5.3.6-3a)$$

or

$$\frac{F_{e.LTB}}{F_{yc}} \leq \frac{F_{yr}}{F_{yc}} \quad (5.3.6-3b)$$

where

$f_{bu,max}$ and $M_{u,max}$ = the required compression flange flexural stress and the corresponding moment at the most highly stressed cross-section, relative to the compression flange yield strength (i.e., at the location of $\rho_{o,max}$),

$S_{xc,max}$ = elastic section modulus to the compression flange at the location of $\rho_{o,max}$,
and

$\gamma_{e.LTB}$ = the ratio of the elastic LTB load level to the factored load level defined above.

In this case, the nominal flexural resistance may be written simply as

$$F_{nc} = F_{cr} = R_b F_{e.LTB} \quad (5.3.6-4a)$$

for slender-web members or

$$M_{nc} = M_{e.LTB} = S_{xc} F_{e.LTB} \quad (5.3.6-4b)$$

for noncompact- or compact-web members.

(The symbols $F_{e.LTB}$ and $M_{e.LTB}$ represent the elastic LTB resistances obtained from beam theory. As indicated by Eq. (4a), the nominal elastic LTB resistance for slender-web members is reduced, relative to the beam theory solution, by the web load-shedding factor, R_b . AASHTO (2014) denotes this flange LTB stress by the symbol F_{cr} . The term $F_{e.LTB}$ is used in this module for consistency with the terms in the column resistance equations and to distinguish the nominal flange LTB stress from the beam theory LTB stress.)

Similar to the column buckling calculations discussed in Section 5.2.6 of this module, there is only one $\gamma_{e.LTB}$ for a given unbraced length, although the compression flange stresses and the corresponding moments vary in general from cross-section to cross-section along the member length. The above equations give the elastic LTB resistance at the most highly stressed cross-

section. However, if $F_{e.LTB} = \gamma_{e.LTB} f_{bu}$ and $M_{e.LTB} = \gamma_{e.LTB} M_u$ were calculated at any of the other cross-sections, the ratio $f_{bu} / F_{e.LTB} = M_u / M_{e.LTB}$ is still the same value, $1 / \gamma_{e.LTB}$.

For unbraced lengths where

$$\left(F_{e.LTB} = \gamma_{e.LTB} f_{bu,max} = \gamma_{e.LTB} \frac{M_{u,max}}{S_{xc,max}} \right) > F_{yr} \quad (5.3.6-5)$$

nominal yielding occurs before the member reaches its full flexural resistance, and thus inelastic LTB resistance governs. In this case, similar to the calculation of the inelastic column resistance in Section 5.2.6, the inelastic LTB resistance is determined by mapping the nonprismatic member to an equivalent prismatic member that has:

1. The same $\gamma_{e.LTB}$, and
2. A ρ_o equal to the above $\rho_{o,max}$.

This is illustrated by Figure 69.

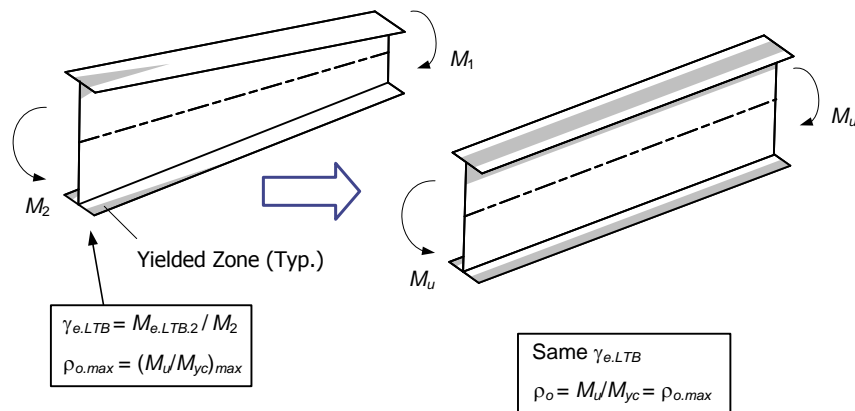


Figure 69 Conceptual mapping of a tapered-web I-section member subjected to bending moment to an equivalent prismatic member.

Since the St. Venant torsional constant J typically has little influence on the elastic LTB resistance for $L_b \leq L_p$, Eq. (5.3.5-23) can be employed to solve for the unbraced length L_b corresponding to a given $F_{e.LTB}$ in uniform bending ($C_b = 1$). The result is

$$L_b = \pi r_t \sqrt{\frac{E}{F_{e.LTB}}} \quad (5.3.6-6)$$

This unbraced length may be equated to Eq. (5.3.5-8) to determine the following elastic critical stress to yield stress ratio corresponding to the compact bracing condition:

$$\frac{F_{e.LTB}}{F_{yc}} \geq \pi^2 \quad (5.3.6-7)$$

That is, whenever Eq. (7) is satisfied, the inelastic LTB resistance corresponds to the plateau

$$M_{nc} = M_{max} \text{ or } F_{nc} = F_{max} \quad (5.3.6-8)$$

illustrated in Figure 60. Furthermore, for $\frac{F_{yr}}{F_{yc}} < \frac{F_{e.LTB}}{F_{yc}} < \pi^2$, one can substitute Eq. (6) and a similar equation for $L_b = L_r$ into the AASHTO (2014) expressions describing the linear interpolation between Anchor Points 1 and 2 in Figure 60 to obtain

$$F_{nc} = R_b R_h F_{yc} \left[1 - \left(1 - \frac{F_{yr}}{R_h F_{yc}} \right) \left(\frac{\pi \sqrt{\frac{F_{yc}}{F_{e.LTB}}} - 1}{\pi \sqrt{\frac{F_{yc}}{F_{yr}}} - 1} \right) \right] \leq R_b R_h F_{yc} \quad (5.3.6-9a)$$

for slender-web members and

$$M_{nc} = R_{pc} M_{yc} \left[1 - \left(1 - \frac{F_{yr} S_{xc}}{R_{pc} M_{yc}} \right) \left(\frac{\pi \sqrt{\frac{F_{yc}}{F_{e.LTB}}} - 1}{\pi \sqrt{\frac{F_{yc}}{F_{yr}}} - 1} \right) \right] \leq R_{pc} M_{yc} \quad (5.3.6-9b)$$

for noncompact- and compact-web members (White and Kim 2006; Kaehler et al. 2011).

The Engineer should note that the ratio $\frac{F_{e.LTB}}{F_{yc}} = \frac{M_{e.LTB}}{M_{yc}}$ in Eqs. (7) and (9) is analogous to the ratio P_e/P_o in the general column resistance equations of Section 5.2.1 of this module. Similar to the developments in Section 5.2.6 of this module, this ratio may be expressed as follows in terms of the parameters $\rho_{o,max}$ and $\gamma_{e.LTB}$:

$$\frac{F_{e.LTB}}{F_{yc}} = \frac{M_{e.LTB}}{M_{yc}} = \rho_{o,max} \gamma_{e.LTB} \quad (5.3.6-10)$$

The design calculations corresponding to the above concepts start by testing the result from Eq. (10) against the limits for the above equations, then calculating M_{nc} or F_{nc} based on the applicable of Eqs. (4), (8) or (9).

Although the derivation of Eqs. (7) and (9) is conducted in the context of uniform bending of prismatic members and is based on the assumption of $J = 0$, these equations provide an accurate to slightly conservative approximation of the nominal flexural resistance for all types of prismatic and nonprismatic members subjected to general loading (moment gradient) conditions. One only needs to determine the elastic LTB load ratio $\gamma_{e.LTB}$ and the maximum ratio of the factored moment to the yield moment $\rho_{o.max} = (M_u/M_{yc})_{max} = (f_{bu}/F_{yc})_{max}$. This conceptual extension of the Specification LTB resistance equations is the same as that invoked originally by Lee et al. (1981) in the context of AISC Allowable Stress Design.

Based on the above concepts, the LTB flexural capacity ratio $f_{bu,max}/\phi F_{nc}$ or $M_{u,max}/\phi M_{nc}$ for a given unbraced length is determined as follows:

1. Calculate $\rho_o = f_{bu}/F_{yc}$ or M_u/M_{yc} at the various cross-sections along the unbraced length.
2. Determine the maximum value of ρ_o , i.e., $\rho_{o.max}$.
3. Calculate the ratio of the elastic LTB load level to the factored load level $\gamma_{e.LTB}$. If the web is slender at any location along the unbraced length, $F_{e.LTB}$ is to be calculated using $J = 0$. (This is because the AASHTO (2014) and AISC (2010) resistance equations are based on $J = 0$ for slender web members. Members with slender or nearly slender webs tend to exhibit only a minor difference between the $F_{e.LTB}$ obtained using the actual J or using $J = 0$. Furthermore, the LTB resistance tends to be reduced significantly due to web distortion effects in these types of members, particularly in cases with heavy flanges (Bradford 1992; White and Jung 2007).)
4. Determine the flexural capacity corresponding the most highly stressed cross-section by substituting $\gamma_{e.LTB}$ and $\rho_{o.max}$ into Eq. (10), and then using Eq. (4), Eq. (8) or Eq. (9) as applicable based on the value of $F_{e.LTB}/F_{yc} = M_{e.LTB}/M_{yc}$ calculated from Eq. (10). If the web is slender at any position along the unbraced length under consideration, the unbraced length is considered as a slender-web member. The parameters R_b for slender-web members and R_{pc} for noncompact- or compact-web members, are calculated at the most highly stressed cross-section (i.e., the one corresponding to $\rho_{o.max}$), but using the largest $2D_c/t_w$ throughout the segment length. The parameter R_h is taken as the smallest value of R_h from the different cross-sections along the member length.
5. Calculate the flexural capacity ratio for the unbraced length under consideration as $f_{bu,max}/\phi F_{nc}$ or $M_{u,max}/\phi M_{nc}$.

(It should be noted that the calculation of R_b and R_{pc} in step 4 involve conservative simplifications. Alternatively, one can calculate $F_{yc}/F_{e.LTB}$, R_b and R_h for slender-web cross-sections, or $F_{yc}/F_{e.LTB}$ and R_{pc} for noncompact- or compact-web cross-sections, separately for all the cross-sections along the unbraced length, where $F_{e.LTB}$ is defined as the compression flange stress at the cross-section under consideration at incipient elastic LTB. The governing $f_{bu}/\phi F_{nc}$ or $M_u/\phi M_{nc}$ is obtained as the largest value from all of these cross-section based checks. The member length effects are handled properly at each cross-section via the calculation of $F_{e.LTB}$ considering the member loading and geometry.)

Kaehler et al. (2011) provide a range of design example calculations and discuss various methods for determining the ratio $\gamma_{e.LTB}$ for different member geometries. Potentially, $\gamma_{e.LTB}$ can be calculated most reliably using software tools. Unfortunately, few analysis programs give accurate elastic LTB solutions for singly-symmetric and/or nonprismatic members. Furthermore, there are a number of complexities associated with the proper definition of elastic LTB models, and most programs that have reliable capabilities for elastic LTB analysis are somewhat difficult to use in setting up these models. Even when this state of practice is eventually improved, Engineers will still have a need for reliable simplified approximate solutions.

The following very simple and useful approximate solution for practical unbraced lengths with linearly-tapered web depths uses a procedure suggested by Yura and Helwig (1996) for the calculation of $\gamma_{e.LTB}$:

1. Calculate C_b using any appropriate equation, but for C_b equations written in terms of member moments, use the stresses in the flange under consideration rather than the cross-section moments.
2. Estimate the elastic LTB stress at the cross-section having the largest $f_{bu}/F_{yc} = M_u/M_{yc}$ as

$$F_{e.LTB} = C_b F_{e.mid} \quad (5.3.6-11)$$

where $F_{e.mid}$ is the elastic LTB stress calculated from the AASHTO-AISC elastic LTB equations for a prismatic member using the cross-section properties at the middle of the unbraced length.

3. Calculate $F_{e.LTB}/F_{yc}$ as the ratio of the above $F_{e.LTB}$ to the compression flange yield strength at the above cross-section with the largest f_{bu}/F_{yc} , or alternatively, determine $\gamma_{e.LTB}$ by substituting $F_{e.LTB}$ and f_{bu} at the most highly stressed cross-section into Eq. (1), determine $\rho_{o,max}$ by substituting the elastic flange stress and the compression flange yield strength at this cross-section into Eq. (2)
4. Use the above $F_{e.LTB}/F_{yc}$ ratio to determine the nominal flexural resistance based on the applicable Eq. (4), (8) or (9).

White and Grubb (2003) give another approximate solution for unbraced lengths composed of prismatic segments with a single cross-section transition within the unbraced length. This solution is adapted from Carskaddan and Schilling (1974) and Dalal (1969):

1. Calculate C_b using Eqs. (5.3.5-30) and assuming that the unbraced length is prismatic.
2. Calculate the elastic LTB stress corresponding to the section with the largest end moment M_2 as

$$F_{e.LTB.2} = \chi \frac{C_b \pi^2 E}{(L_b / r_{1.2})^2} \quad (5.3.6-12)$$

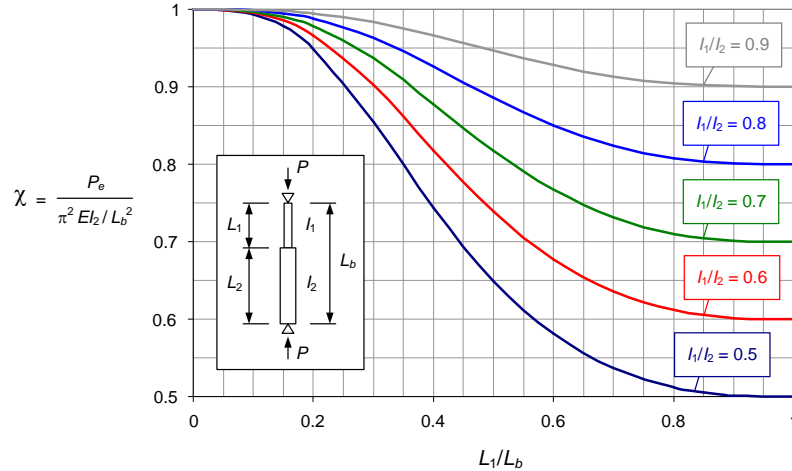


Figure 70 Ratio of elastic LTB stress at the section with the largest moment M_2 to the LTB stress determined assuming that the member is prismatic with the larger cross-section throughout the unbraced length (adapted from Carskaddan and Schilling (1974) and Dalal (1969)).

where $r_{t,2}$ is the radius of gyration of the compression flange plus one-third of the depth of the web in compression for the cross-section corresponding to M_2 and χ is determined from the chart shown in Figure 70. (This procedure assumes M_2 is the largest moment within the unbraced length under consideration, and that this moment occurs in the larger of the two cross-sections.)

3. Calculate $\gamma_{e.LTB}$ as $F_{e.LTB,2}/f_{bu,2}$, where $f_{bu,2}$ is the compression flange factored stress at the cross-section corresponding to M_2 .
4. Calculate $\rho_{o,max}$ as the larger of $f_{bu,s}/F_{yc,s}$ and $f_{bu,2}/F_{yc,2}$, where $f_{bu,s}$ is the compression flange factored stress at the smaller section at the cross-section transition, $F_{yc,s}$ is the corresponding compression-flange yield stress, and $F_{yc,2}$ is the compression flange yield stress at the cross-section corresponding to M_2 .
5. Calculate $F_{e.LTB}/F_{yc}$ from Eq. (10), and use this ratio for determining the nominal flexural resistance from the applicable Eq. (4), (8) or (9).

The parameter χ is the ratio $P_e/(\pi^2 EI_2/L_b^2)$ for the stepped column shown in Figure 70. This ratio gives a slightly conservative estimate of the elastic LTB resistance for a stepped I-section member subjected to moment gradient with the larger moment applied to the larger end cross-section. Based on the behavior illustrated in Figure 70, AASHTO (2014) Articles C6.10.8.2.3 and CA6.3.3 effectively allow transitions to a smaller cross-section to be neglected in determining F_n (or M_n) for unbraced lengths having a step in the cross-section with

- $L_1/L_b \leq 0.2$,
- $I_1/I_2 \geq 0.5$ and

- maximum f_{bu}/F_{yc} in the unbraced length corresponding to the larger cross-section.

where L_I is the length of the segment with the smaller cross-section, and I_1 and I_2 are the individual compression flange moments of inertia about the plane of the web for the smaller and larger flanges respectively (to be checked for both flanges). The reader is referred to Kaehler et al. (2011) for other elastic LTB solutions.

5.3.7 Combined Major-Axis Bending, Minor-Axis Bending and Torsion

5.3.7.1 General

AASHTO (2014) Article 6.10 and its Appendices A6 and B6 provide a unified approach for consideration of I-girder major-axis bending, minor-axis bending and torsion from any source. Similar to prior Guide Specifications for curved steel bridge design such as AASHTO (2003), the AASHTO (2014) provisions focus on the flange lateral bending caused by the warping (i.e., cross-bending) of the flanges as the primary response associated with the torsion of I-section members. Significant flange lateral bending may be caused by wind, by eccentric concrete deck overhang loads acting on forming brackets placed along exterior girders, and by the use of discontinuous cross-frame lines in bridges with skew angles larger than about 20° . For the majority of straight non-skewed bridges, flange lateral bending effects tend to be the most significant during construction and tend to be insignificant in the final constructed condition. However, for horizontally curved bridges, in addition to the effects from the above sources, flange lateral bending due to the curvature must be considered at all limit states and during construction. The intent of the Article 6.10 provisions is to provide a straightforward approach for the Engineer to account for the above effects in design in a direct and rational manner whenever these effects are nonnegligible. When the various flange lateral bending effects are judged negligible or incidental, the provisions reduce the design of I-section members subjected to major-axis bending alone (outlined in Sections 5.3.5 and 5.3.6 of this module).

The basic form of the AASHTO (2014) resistance equations that account for the combined effects of major-axis bending and flange lateral bending is

$$f_{bu} + \frac{1}{3} f_\ell \leq \phi_f F_n \quad (5.3.7-1)$$

(AASHTO 6.10.3.2.1-2, 6.10.3.2.2-1, 6.10.7.2.1-2, 6.10.8.1.1-1 & 6.10.8.2-1)

for members in which the major-axis bending resistance is expressed in terms of the corresponding flange stress and

$$M_u + \frac{1}{3} f_\ell S_x \leq \phi_f M_n \quad (5.3.7-2)$$

(AASHTO 6.10.7.1.1-1, A6.1.1-1 & A6.1.2-1)

for members in which the major-axis bending resistance is expressed in terms of the bending moment, where

- f_{bu} = the elastically-computed flange major-axis bending stress,
- f_ℓ = the elastically-computed flange lateral bending stress,
- $\phi_f F_n$ = the factored flexural resistance in terms of the flange major-axis bending stress,
- M_u = the member major-axis bending moment,
- S_x = the elastic section modulus about the major-axis of the section to the flange under consideration, taken as the short-term section modulus for composite members in positive bending or the section modulus of the composite section for composite members in negative bending, and
- $\phi_f M_n$ = the factored flexural resistance in terms of the member major-axis bending moment.

Equations (1) and (2) are referred to in AASHTO (2014) as the one-third rule. These equations are simple, yet they do an excellent job of characterizing the various strength limit states that can govern the resistance of I-section members. Equations (1) and (2) address the combined major-axis and flange lateral bending effects basically by handling the flanges as equivalent beam-columns.

Equation (1) is targeted specifically at checking of slender-web noncomposite members, slender-web composite members in negative bending, and noncompact composite members in positive bending. Also, as discussed previously in Section 3 of this module, the resistance of I-section members generally to $f_{bu} \leq \phi_f F_n$. In the limit that the flange lateral bending stress f_ℓ is equal to zero, Eq. (1) reduces to this basic member check for major-axis bending alone. The maximum potential value of F_n is the flange yield strength F_{yf} , but F_n can be less than F_{yf} due to slender-web bend buckling and/or hybrid-web yielding effects, or due to compression flange lateral-torsional (LTB) or local buckling (FLB) limit states.

Equation (2) may be used for checking the strength limit states of straight noncomposite members or composite members in negative bending that have compact or noncompact webs, and for checking of compact composite members in positive bending. For these member types, $\phi_f M_n$ can be as large as $\phi_f M_p$, where M_p is the section plastic moment resistance. The reader is referred to Sections 5.3.3 through 5.3.5 of this module for definitions of the terms slender, noncompact and compact and for an overview of the calculation of $\phi_f F_n$ and $\phi_f M_n$. Equation (1) may be used as a simple conservative resistance check for all types of I-section members. AASHTO (2014) Article 6.10 emphasizes this fact by relegating the use of Eq. (2) for straight compact and noncompact web noncomposite members and composite members in negative bending to its Appendix A6. The definition of S_x as the short-term modulus for composite sections in positive bending, and as the section modulus of the composite section for composite sections in negative bending, is a conservative simplification. This simplification is consistent with the precedent of neglecting the influence of the different types of loading on the resistance for compact composite members in positive bending, and with the limited dependency of the

different loading types for compact- and noncompact-web composite members in negative bending, as discussed previously in Sections 5.3.3 and 5.3.5 of this module.

In the application of Eqs. (1) and (2), the stresses f_ℓ and f_{bu} , and the moment M_u , are taken as the largest values throughout the unbraced length when checking against the base flexural resistance $\phi_f F_n$ or $\phi_f M_n$ associated with lateral-torsional buckling. This is consistent with the application of the AASHTO and AISC interaction equations for a general beam-column subjected to combined axial load and bending. The stress f_{bu} in Eq. (1) and the moment M_u in Eq. (2) are analogous to the axial load in a general beam-column, and the stress f_ℓ is analogous to the beam-column bending moment. The moment M_u is analogous to axial loading since it produces axial stresses in the flanges. When checking compression flange local buckling or tension flange yielding, f_ℓ , f_{bu} and M_u may be determined as the corresponding values at the cross-section under consideration. Generally, Eq. (1) or (2), as applicable, must be checked for each flange, and both the FLB and LTB based resistances must be checked for the compression flange in calculating F_{nc} or M_{nc} . The check providing the largest ratio of the left-hand side to the right-hand side of these equations governs.

The Engineer is permitted to use $f_\ell = 0$ when checking the top flange of composite I-girders, once the section is composite, since the composite slab tends to restrain the top flange lateral bending. AASHTO (2014) Article 6.10.7.2.1 requires that the concrete slab flexural stress shall be checked in addition to the use of Eq. (1). However, except in shored construction and in unusual cases of unshored construction discussed in the commentary to this article, the concrete flexural is typically much less than f_c' at the Eq. (1) strength limit, and therefore the concrete stress check does not govern.

As noted above, for curved bridges, AASHTO (2014) restricts the I-girder design in all cases to the use of Eq. (1). This restriction is due to the lack of a comprehensive understanding of the implications of significant member yielding and the concomitant inelastic redistribution on the forces and moments in curved bridge structural systems at the time that these provisions were implemented. Otherwise, Eqs. (1) and (2) are valid generally for all types of I-section members that satisfy the limits

$$L_b/R \leq 0.1 \tag{5.3.7-3}$$

(AASHTO 6.7.4.2-1)

within the final constructed configuration, where L_b is the unsupported length between the cross-frame locations and R is the horizontal radius of curvature,

$$L_b \leq L_r \tag{5.3.7-4}$$

(AASHTO 6.7.4.2-1)

where L_r is the unbraced length limit beyond which the base lateral-torsional buckling limit state is elastic, and

$$f_\ell \leq 0.6 F_{yf} \tag{5.3.7-5}$$

(AASHTO 6.10.1.6-1)

The first of these limits is a practical upper bound for the subtended angle between the cross-frame locations (for constant R). It ensures that the I-girder webs will not have a d_o/R larger than 0.1, where d_o is the spacing of the transverse stiffeners. Equations (1) and (2) have been observed to perform adequately in a number of cases with L_b/R larger than 0.2 (White et al. 2001). However, the development of these equations as well as the validation of the AASHTO (2014) Article 6.10.9.3 tension-field action shear strength equations for curved web panels has focused predominantly on members designed up to the limit specified by Eq. (3). Equation (4) is a practical upper bound for the unbraced length L_b beyond which the second-order amplification of the flange lateral bending stresses tends to be particularly severe. The reason for Eq. (5) is discussed in Section 5.3.7 of this module.

Prior AASHTO Specifications have required L_b to be less than 25 ft. Article C6.7.4.1 explains that this requirement has been replaced by the requirement for a rational analysis. Nevertheless, typical curved I-girders will not have unbraced lengths exceeding this former limit.

5.3.7.2 Calculation of flange lateral bending stresses

Various methods may be used for calculating the flange elastic lateral bending stresses f_ℓ . AASHTO (2014) Article 6.10.1.6 gives simple equations for estimating the first-order lateral bending stresses due to the torsion associated with horizontal curvature (see Eq. (2.2.1-1) and AASHTO (2014) Article 4.6.1.2.4b), the torsion from eccentric concrete deck overhang loads acting on cantilever forming brackets placed along exterior girders (see AASHTO (2014) Article C6.10.3.4), and due to wind load (see AASHTO (2014) Article 4.6.2.7). These equations are based on the assumption of unbraced lengths other than at the ends of the bridge, where the flange is continuous with adjacent unbraced lengths, as well as equal lengths of the adjacent segments. Based on these idealized assumptions, the ends of the unbraced lengths are effectively torsionally and laterally fixed due to approximate symmetry boundary conditions. The Engineer should consider other more appropriate idealizations, or the use of computer analysis methods, when these assumptions do not approximate the actual conditions. Implications of various types of computer analysis on the calculation of f_ℓ are addressed by Jung et al. (2005) and Chang et al. (2005).

Similar to the amplification of internal bending moments in beam-column members, flange lateral bending stresses are generally amplified due to stability effects. However, it is impractical to calculate second-order live load stresses for moving live loads. Therefore, when Eq. (1) is applied for checking the compression flange, AASHTO (2014) Article 6.10.1.6 provides the following simple lateral bending amplification equation to account in an approximate fashion for these second-order effects:

$$f_\ell = \left(\frac{0.85}{1 - \frac{f_{bu}}{F_{e.LTB}}} \right) f_{\ell 1} \geq f_{\ell 1} \quad (5.3.7-6)$$

(AASHTO 6.10.1.6-4 & 6.10.1.6-5)

where

- $F_{e.LTB}$ = the compression flange elastic lateral-torsional buckling resistance from Eq. (5.3.5-19) for compact- or noncompact-web members or Eq. (5.3.5-23) for slender-web members,
- f_{c1} = the first-order compression flange lateral bending stress at the section under consideration (for checking of FLB), or the largest first-order compression flange lateral bending stress within the unbraced length (for checking of LTB), and
- f_{bu} = the largest value of the compression flange major-axis bending stress within the unbraced length under consideration.

Amplification of the tension flange lateral bending stresses is not required, since this effect on the girder strength tends to be relatively minor compared to the compression flange response. White et al. (2001) show that Eq. (6) gives accurate to conservative estimates of the flange second-order lateral bending stresses. The purpose of Eq. (6) is to guard conservatively against large unbraced lengths in which second-order lateral bending effects are significant. The Engineer should be particularly mindful of the amplified compression flange lateral bending in exterior girders due to eccentric concrete deck overhang loads during construction. In situations where the amplification given by these equations is large, the Engineer may wish to consider using an effective length factor $K < 1$ in the calculation of $F_{e.LTB}$ (using the procedure outlined in Section 5.3.5 of this module). In cases where the amplification of construction stresses is large, a second alternative is to conduct a direct geometric nonlinear analysis to determine the second-order effects within the superstructure more accurately. In the final constructed condition, the above amplification typically is applied only to the bottom flange in negative moment regions of continuous spans. In this case, $F_{e.LTB}$ is increased significantly due to the moment gradient in these regions, via the moment gradient modifier C_b (see Section 5.3.5).

5.3.7.3 One-third rule concept

Figure 71 compares the result from Eq. (2) to the theoretical fully plastic resistance for several doubly-symmetric noncomposite compact-flange, compact-web cross-sections. Figure 72 shows a sketch of a typical fully plastic stress distribution on this type of cross-section. The equations for the fully plastic cross-section resistances are based on the original research by Mozer et al. (1971) and are summarized by White and Grubb (2005). The specific stress distribution shown in Figure 72 is associated with equal and opposite lateral bending in each of the equal-size flanges (i.e., warping of the flanges due to nonuniform torsion). However, the solution is the same if one considers equal flange lateral bending moments due to minor-axis bending.

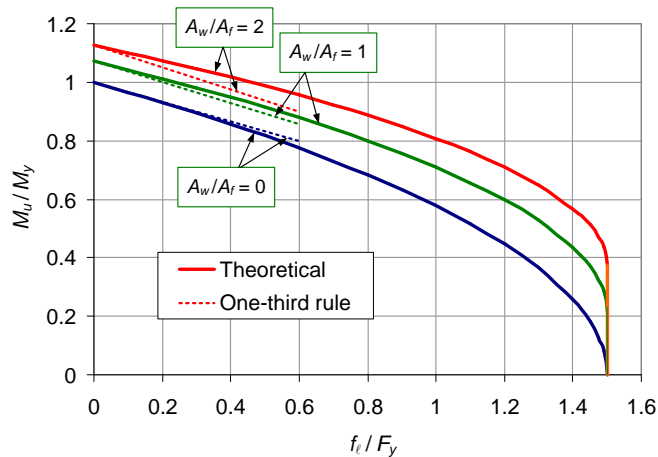


Figure 71 Comparison of the AASHTO (2014) one-third rule equation to the theoretical fully-plastic cross-section resistance for several doubly-symmetric noncomposite compact-flange, compact-web I-sections (adapted from White and Grubb (2005)).

One can observe that, within the limit given by Eq. (5), the one-third rule equation (Eq. (2)) provides an accurate to somewhat conservative estimate of the theoretical cross-section resistances for the different web-to-flange area ratios, A_w/A_f , shown in Figure 71. In the limit that A_w/A_f is taken equal to zero, the same approximation is provided by both Eq. (2) and Eq. (1). The comparison of the theoretical and approximate equations shown in Figure 70 is useful for gaining a conceptual understanding of the one-third rule equations in the limit of compact-flange, compact-web, compactly-braced noncomposite members. Also, Schilling (1996) and Yoo and Davidson (1997) present other useful cross-section yield interaction relationships. However, cross-section yield interaction equations are limited in their ability to fully characterize the combined influence of distributed yielding along the member lengths along with the various stability effects (FLB, LTB and web bend buckling). Furthermore, yield interaction equations generally do not reduce to the resistance equations for straight members subjected only to major-axis bending in the limit that $f_\ell = 0$.

Equations (1) and (2) are a basic extension of the one-third rule approximation of the above theoretical cross-section resistances to address the influence of general yielding and stability limit states on the member resistance. The basic extension is accomplished simply by changing the flange yield strength, F_{yf} , to $\phi_t F_n$ in Eq. (1) and by changing the section plastic moment resistance, M_p , to $\phi_t M_n$ in Eq. (2). The 1/3 coefficient accurately captures the strength interaction including the various yielding and stability effects (White et al. 2001). The extension from cross-section equations to member equations is ad hoc, but it is similar in many respects to the development of the AISC (2010) and AASHTO (2014) general beam-column interaction relationships. The shape of the interaction (i.e., the slope of the line relating f_{bu} and f_ℓ in Eq. (1) or M_u and f_ℓ in Eq. (2)) is based on curve fitting. Equations (1) and (2) are thus semi-analytical and semi-empirical. White and Grubb (2005) provide a summary of the correlation of Eqs. (1) and (2) with analytical, numerical and experimental results.

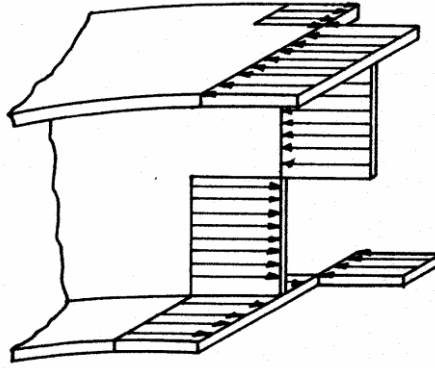


Figure 72 Sketch of a fully plastic stress distribution, including flange lateral bending.

5.3.8 Shear Strength

5.3.8.1 General

AASHTO (2014) Article 6.10.9.3 bases the I-section member shear resistance either on the web shear buckling capacity or an idealized additive contribution of the web shear buckling and postbuckling resistances. The web elastic shear buckling capacity may be expressed as

$$V_{cr} = \tau_{cr} Dt_w = \frac{\pi^2 Ek}{12(1-\nu^2) \left(\frac{D}{t_w}\right)^2} Dt_w = \frac{0.90Ek}{\left(\frac{D}{t_w}\right)^2} Dt_w \quad (5.3.8-1)$$

which is the classical plate buckling equation multiplied by the web area, Dt_w , but with the buckling coefficient, k , corresponding to pure shear loading. This coefficient is taken as

$$k = 5 + \frac{5}{\left(\frac{d_o}{D}\right)^2} \quad (5.3.8-2a)$$

(AASHTO 6.10.9.3.2-7)

for stiffened webs, i.e., webs with transverse stiffeners (referred to as transversely-stiffened) or with transverse and longitudinal stiffeners (referred to as longitudinally-stiffened) and in which the transverse stiffeners are spaced within certain maximum limits, and it is taken as

$$k = 5 \quad (5.3.8-2b)$$

for unstiffened webs. These equations are a simple approximation of analytical buckling solutions for isolated panels with ideal simply-supported edge conditions subjected to pure shear loading (Ziemian 2010). They are applied to the average shear stress in the context of I-girder webs. Therefore, the ratio of the AASHTO (2014) elastic shear buckling strength to the web plastic shear capacity may be written as

$$C_{el} = \frac{\tau_{cr}}{\tau_{yw}} = \frac{V_{cr}}{V_p} = \frac{1.57Ek}{\left(\frac{D}{t_w}\right)^2 F_{yw}} \quad (5.3.8-3)$$

Where

$$V_p = \tau_{yw} D t_w = \frac{F_{yw}}{\sqrt{3}} D t_w = 0.58 F_{yw} D t_w \quad (5.3.8-4)$$

(AASHTO 6.10.9.2-2)

is the fully plastic resistance of the web based on the von Mises yield criterion and $\tau_{yw} = F_{yw} / \sqrt{3}$. Similar to the developments for plates in uniform axial compression discussed in Section 5.2.4 of this module, inelastic buckling is assumed to occur when the web average shear stress reaches a certain fraction of the strength τ_{yw} corresponding to full yielding. Inelastic buckling is assumed for $C_{el} > 0.8$, which is higher than for uniform compression because the effect of residual stress is less. The resulting AASHTO (2014) Article 6.10.9.3 web shear buckling resistance (elastic or inelastic) is expressed as a fraction of the fully plastic shear strength (C) as follows:

$$\text{For } C_{el} \leq 0.8 \text{ or } \frac{D}{t_w} \geq 1.40 \sqrt{\frac{Ek}{F_{yw}}} \text{ (elastic buckling)}$$

$$C = C_{el} \quad (5.3.8-5a)$$

(AASHTO 6.10.9.3.2-6)

and for $C_{el} > 0.8$

$$C = \sqrt{0.8C_{el}} = \frac{1.12}{\frac{D}{t_w}} \sqrt{\frac{Ek}{F_{yw}}} \text{ (inelastic buckling)} \quad (5.3.8-5b)$$

(AASHTO 6.10.9.3.2-5)

Lastly, the above inelastic shear buckling equation gives

$$C = 1 \text{ (full web plastification)} \quad (5.3.8-5c)$$

(AASHTO 6.10.9.3.2-4)

$$\text{at } C_{el} \geq 1.25 \text{ or } \frac{D}{t_w} \leq 1.12 \sqrt{\frac{Ek}{F_{yw}}} .$$

AASHTO (2014) requires that webs with transverse stiffeners spaced at $d_o > 3D$ or webs with one or more longitudinal stiffeners and transverse stiffeners spaced at $d_o > 1.5D$ shall be considered as unstiffened. In these cases, the shear resistance is limited to the shear buckling design resistance

$$\phi_v V_n = 1.0 C V_p \quad (5.3.8-6)$$

(AASHTO 6.10.9.2-1)

However, webs with closer transverse stiffener spacing are considered as stiffened. The resistance for these types of webs is taken as the additive combination of the above shear buckling resistance with a representation of the shear postbuckling strength from Basler's (1961) seminal research. For members where the ratio of the web area to the average flange area is smaller than 2.5, i.e.,

$$\frac{2Dt_w}{(b_{fc}t_{fc} + b_{ft}t_{ft})} \leq 2.5 \quad (5.3.8-7)$$

(AASHTO 6.10.9.3.2-1)

the sum of the web buckling and postbuckling design resistances is expressed as

$$\phi_v V_n = 1.0 \left[C + \frac{0.87(1-C)}{\sqrt{1 + \left(\frac{d_o}{D}\right)^2}} \right] V_p \quad (5.3.8-8)$$

(AASHTO 6.10.9.3.2-2)

whereas for members that have smaller flanges relative to the web area, this sum is written as

$$\phi_v V_n = 1.0 \left[C + \frac{0.87(1-C)}{\sqrt{1 + \left(\frac{d_o}{D}\right)^2 + \frac{d_o}{D}}} \right] V_p \quad (5.3.8-9)$$

(AASHTO 6.10.9.3.2-8)

The second term inside the square brackets in each of the above equations is the web postbuckling strength based on Basler's (1961) theory. Both of the above equations are based on the assumption that the web develops tensile postbuckling stresses (i.e., a tension field) along a diagonal in each of the web panels as shown in Figure 73, in addition to the shear buckling stresses. In determining the slope of this tension field, θ , Basler assumes that only an effective band, s , takes part in transmitting the additional tension (i.e., the flanges are assumed to provide zero anchorage to the theoretical tension field). The maximum resistance is obtained when yielding occurs due to the combination of the tension field stress plus the initial web shear buckling stress. The angle θ is determined to maximize the predicted postbuckling contribution. However, when the ultimate shear force given by Eq. (8) is determined, a complete tension field is assumed at the orientation θ throughout the entire web. Basler (1963) acknowledges this inconsistency, and illustrates that the flanges are actually not loaded to the extent required by his theory in physical tests. Nevertheless, he argues that his theory still provides an acceptable characterization of I-girder shear strengths.

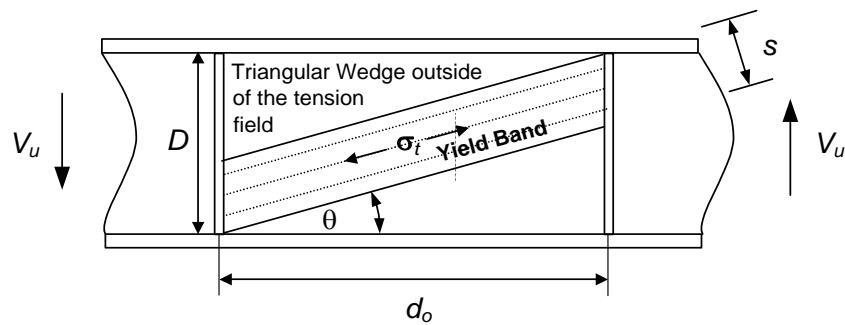


Figure 73 Assumed tension field used in determining the angle θ implicit in Basler's (1961) shear postbuckling strength (Eq. (8)), and used in determining the "true Basler" shear resistance (Eq. (9))

Equation (9) is referred to in the literature as the "true Basler" shear resistance (e.g., see Porter et al. (1975) and Wolchuk and Mayrbaur (1980)). This equation is determined by consistently applying the idealization shown in Figure 73 throughout the formulation. (There is a typographical error in the equation for the true Basler shear strength in Porter et al. (1975); the correct expression is as provided in Eq. (9).)

It should be obvious to the reader that the above idealizations are only a very simplified representation of the true web response. Numerous additional web shear failure theories have been postulated since Basler's original research (e.g., see Ziemian (2010)). The large number of these idealizations in itself is evidence of the fact that the corresponding behavior is complex and tends to defy explanation by basic strength of materials models. Recent studies such as Jung and White (2010b), Yoo and Lee (2006) and Kim et al. (2007) have provided further insight into the detailed force transfer mechanisms associated with the web ultimate shear resistance. These studies show that the force transfer mechanisms can differ substantially from the various failure theories. Nevertheless, the ability of Eqs. (8) and (9) to provide a reasonable prediction of experimental test results is irrefutable. White and Barker (2008) have recently studied the predictions by 12 different models using a data set of 129 experimental high-shear low-moment tests, including 30 hybrid and 11 horizontally curved I-girders. They conclude that Basler's model provides the best combination of accuracy and simplicity of the models considered.

White et al. (2008) study the predictions for the above 129 tests plus an additional 57 tests involving combined high-shear and high-moment, including 21 additional hybrid girders. Their results indicate that within the constraint of Eq. (7) plus the AASHTO (2014) proportioning limits discussed in Section 5.3.2 of this module, the combination of Eq. (8) for the shear resistance and the AASHTO (2014) equations outlined in Sections 5.3.3 through 5.3.5 for the flexural resistance gives a sufficient representation of the high-shear high-moment resistance without the consideration of moment-shear strength interaction. In other words, the same resistance factor $\phi_v = 1.0$ is justified for both high-shear low-moment and high-shear high-moment, and the same resistance factor $\phi_f = 1.0$ is justified for both high-moment low-shear and high-moment high-shear. Also, White et al. (2008) show that for girders with small flanges that violate Eq. (7), the capacities tend to be smaller but are predicted adequately when Eq. (9) is

used for the shear resistance. Extensive finite element parametric studies have been conducted by Hash (2001), White et al. (2001), Aydemir et al. (2004), Jung and White (2006), Kim et al. (2007) and others that support the above conclusions and help address the complete range of potential I-girder designs including hybrid and curved I-girders with combined high-moment and high-shear.

One important condition associated with the above conclusions is that the members must be checked in general using the maximum shear within a given web panel for V_u , the maximum moment (or flange stress) within the web panel for M_u or f_{bu} when the flexural resistance is governed by FLB or TFY, and the maximum moment (or flange stress) within the unbraced length under consideration for M_u or f_{bu} when the flexural resistance is governed by LTB. Some of the developments in the past have suggested that the moment should be checked at the smaller of $D/2$ or $d_o/2$ from a transverse stiffener location. The use of M_u at $\min(D/2, d_o/2)$ in plotting the experimental results leads to a false indication of significant M-V interaction. At regions of high shear, the moment drops rapidly as one moves away from the peak moment position. This drop is required for equilibrium, i.e., $dM/dx = V$. It is not due to M-V interaction. Use of the maximum moment or flange stress for the flexural resistance check in regions of combined high-moment and high-shear is consistent with the established procedures for checking of regions subjected to high-moment low-shear (White et al. 2008).

5.3.8.2 Longitudinally-stiffened members

The contribution of the longitudinal stiffeners to the shear resistance is neglected in AASHTO (2014). Longitudinal stiffeners divide a web panel into sub-panels. Cooper (1967) calculates the full web shear resistance for these member types by summing the shear resistance of the subpanels. However, when a single longitudinal stiffener is located near its optimum position for flexure, the corresponding enhancement of the shear capacity is relatively small. Furthermore, as noted previously in Section 5.3.5 of this module, the longitudinal stiffener requirements in AASHTO (2014) Article 6.10.11.3 are not sufficient to develop the general postbuckling resistance of the web panels. Neglecting the contribution of the longitudinal stiffeners to the web shear capacity is consistent with neglecting their contribution to the flexural capacity in cases where f_{bu} is larger than the longitudinally-stiffened web bend buckling resistance. These conservative assumptions make it possible to neglect moment-shear interaction for longitudinally-stiffened I-girders.

5.3.8.3 Variable web depth members

Falby and Lee (1976) address the shear design of I-section members with linearly tapered webs. They indicate that the Basler shear resistance model can be used, with the average web depth replacing the uniform depth, as long as the angle between the flanges is less than about 4 degrees. Also, they suggest a simple modification to Basler's model for moderate tapers larger than 4 degrees, as well as a more conservative model based on an assumed lower-bound tension-field stress distribution for tapers larger than about 7 degrees. It appears that no studies have been conducted to ascertain the shear capacity of I-girders with parabolic or fish-belly haunches. Conservative approximations can be made using concepts similar to those discussed by Falby and Lee (1976).

AASHTO (2014) Article C6.10.1.4 discusses the positive or negative contribution of the force within an inclined flange to the I-girder shear resistance. Falby and Lee (1976) do not consider this contribution. Also, Article C6.10.1.4 suggests that this flange contribution is difficult to calculate in general, since numerous sets of concurrent moments and shears must be evaluated to determine the critical combination. Therefore, this contribution is commonly neglected. However, the vertical component of the inclined flange force can provide a substantial contribution to the overall shear resistance, reducing the shear force that the web must resist near the interior supports in continuous-span I-girders. In turn, the bottom flange normal stress is increased due to the bottom flange slope within a haunch. Article C6.10.1.4 suggests that this increase can be estimated as

$$f = P_h / A_f \cos \theta \quad (5.3.8-10a)$$

(AASHTO C6.10.1.4-1)

Where

$$P_h = \frac{M_u}{S_x} A_f \quad (5.3.8-10b)$$

(AASHTO C6.10.1.4-2)

is the horizontal component of the flange force required to develop the bending moment M_u ,

A_f = area of the inclined bottom flange

θ = angle of inclination of the bottom flange, and

S_x = elastic section modulus to the inclined bottom flange

Equation (10b) assumes zero axial force in the horizontal direction. If this force is non-zero, the corresponding girder axial stress should also be included in the calculation of P_h .

5.3.8.4 Web transverse stiffeners

AASHTO (2014) Article 6.10.11.1 addresses the design requirements for web transverse stiffeners. Numerous research studies have observed that the bending rigidity is the dominant parameter that governs the performance of transverse stiffeners. This is true both for developing the shear buckling as well as the combined shear buckling and postbuckling resistance of stiffened webs (Kim et al. 2007; Yoo and Lee 2006; Lee et al. 2003; Stanway et al. 1996; Rahal and Harding 1990; Horne and Grayson 1983). Although there is some evidence of axial stresses in the transverse stiffeners due to tension field loading, these effects are relatively minor compared to the lateral loading on the stiffeners due to the postbuckling response of the web panels. Furthermore, several research studies have shown that prior AASHTO stiffener area requirements were more than adequate in certain cases and less than adequate in others in maintaining a line of near zero lateral deflection along the line of the stiffener (Kim et al. 2007; Lee et al. 2003; Xie 2000). Also, the studies show that different types of transverse stiffeners

with comparable moments of inertia, but with widely different areas, have essentially the same strength performance. Webs with transverse stiffeners attached such that the stiffeners only provide lateral restraint perform similarly to webs in which a load path exists to transfer tension-field axial forces into the stiffeners. Lastly, Kim et al. (2007) observe that the demands on the transverse stiffeners are very similar in comparable straight and curved I-girders that satisfy the AASHTO (2014) proportioning requirements. Based on these research results, AASHTO (2014) Article 6.10.11.1 no longer specifies any area requirement for transverse stiffeners in stiffened webs. Rather, several equations are specified for the transverse stiffener lateral rigidity that apply equally to straight and curved I-section members.

For stiffeners adjacent to web panels in which neither panel supports shear forces larger than the shear buckling resistance, the stiffener moment of inertia, taken about the edge in contact with the web for single stiffeners and about the mid-thickness of the web for stiffener pairs, is required to satisfy the *smaller* of the following limits:

$$I_t \geq bt_w^3 J \quad (5.3.8-11)$$

(AASHTO 6.10.11.1.3-1)

$$I_t \geq \frac{D^4 \rho_t^{1.3}}{40} \left(\frac{F_{yw}}{E} \right)^{1.5} \quad (5.3.8-12)$$

(AASHTO 6.10.11.1.3-2)

where

b = the smaller of d_o and D ,

$$J = \frac{2.5}{(d_o/D)^2} - 2.0 \geq 0.5 \quad (5.3.8-13)$$

(AASHTO 6.10.11.1.3-3)

ρ_t = the larger of $F_{yw}/F_{e\ell,s}$ and 1.0,

$$F_{e\ell,s} = \frac{0.31E}{(b_t/t_p)^2} \leq F_{ys} \quad (5.3.8-14)$$

(AASHTO 6.10.11.1.3-4)

b_t = the width of a rectangular plate stiffener,

t_p = the thickness of a rectangular plate stiffener,
and

F_{ys} = the specified minimum yield strength of the stiffener.

Equation (11) is the fundamental stiffener rigidity necessary to develop the calculated AASHTO web shear buckling resistance. For webs proportioned to develop their full plastic shear capacity (i.e., $C = 1$ in Eq. 5.3.8-5c), the rigidity requirement based on this equation becomes excessive as the web is made more and more stocky. Equation (12) generally gives a required rigidity that is slightly larger than that required by Eq. (11) at the web slenderness D/t_w just sufficient to achieve $C = 1$. For webs in which the I_t requirement from Eq. (11) is larger than that from Eq. (12), the requirement from Eq. (12) is sufficient to develop the web plastic shear capacity ($C = 1$) (Kim et al. 2007). For webs in which the nominal shear buckling capacity is less than V_p (i.e., $C < 1$), Eq. (11) typically governs. The rigidity requirement defined by this equation is constant for $d_o/D > 1.0$, but increases substantially for $d_o/D < 1$ as shown by Figure 74.

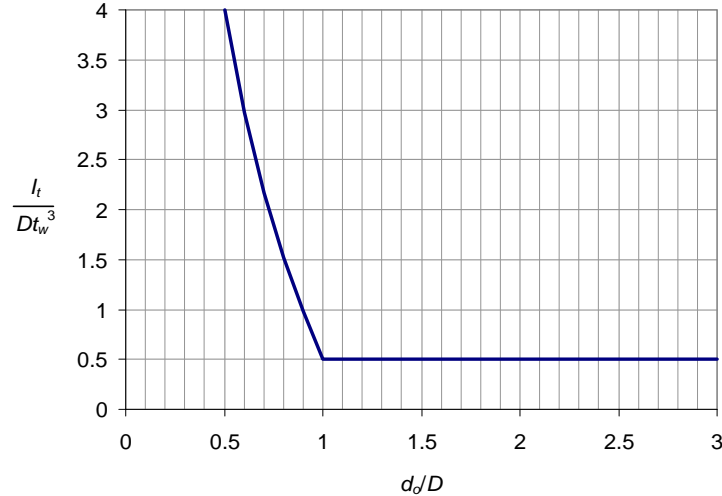


Figure 74 Normalized transverse stiffener bending rigidity I_t / Dt_w^3 necessary to develop the AASHTO (2014) web shear buckling resistance V_{cr} .

That is, the demand on the transverse stiffeners to hold a line of near zero lateral displacement at the web shear buckling load is substantially larger when the stiffeners are spaced at $d_o < D$.

For transverse stiffeners adjacent to web panels in which the shear force is larger than the shear buckling resistance, such that the web tension-field resistance is required in one or both panels, AASHTO (2014) specifies that the moment of inertia of the transverse stiffeners must satisfy Eq. (12). As noted above, Eq. (12) generally requires a stiffener size slightly larger than that necessary to develop the web fully plastic shear capacity, were the web to be made thick enough such that $C = 1$ for a given panel aspect ratio d_o/D , web yield strength F_{yw} and web depth D . Kim et al. (2007) observe that this stiffener size is always accurate to somewhat conservative compared to the size necessary to develop the web shear postbuckling resistance for thinner webs. Kim and White (2013) provide additional discussion of the background to these provisions.

The term ρ_t in Eq. (12) accounts conservatively for the effect of early yielding in transverse stiffeners with $F_{ys} < F_{yw}$ and for the effect of potential local buckling of plate stiffeners having a relatively large width-to-thickness ratio b_f/t_p . The definition of the stiffener local buckling stress $F_{e,s}$ is retained from AASHTO (1998).

For longitudinally-stiffened girders, Article 6.10.11.1.3 also requires that the transverse stiffeners satisfy

$$I_t \geq \left(\frac{b_t}{b_\ell} \right) \left(\frac{1}{3(d_o/D)} \right) I_\ell \quad (5.3.8-15)$$

(AASHTO 6.10.11.1.5)

This equation is retained from prior AASHTO Specifications. It is a liberalization (by a factor of three) of the transverse stiffener section modulus recommended by Cooper (1967). Equation (15) tends to govern the transverse stiffener size only for horizontally curved I-girders with

longitudinal stiffeners, relatively large d_o/R values (such that the curvature parameter Z in the Article 6.10.11.3.3 provisions for the longitudinal stiffener requirements is at its maximum value of 10), d_o/D close to 1.5, and D/t_w less than about 175.

Equation (12) facilitates the selection of a single size for all the transverse stiffeners in a given girder or set of girders, since it is independent of D/t_w and d_o/D . AASHTO (2014) also specifies several other transverse stiffener dimensional requirements that ensure that the stiffener width is not overly small relative to the widest compression flange or the largest web depth within the field section under consideration. These basic dimensional requirements govern in a number of practical cases.

5.3.9 Shear Connectors

AASHTO (2014) Article 6.10.10 addresses the design of the shear connectors between the deck and the steel I-sections for composite construction. Both fatigue and strength limit states must be considered in selecting the number, type and size of the shear connectors. This section focuses on the strength behavior of the shear connectors in horizontally curved I-girders. In horizontally curved girders, the shear connectors can be subjected to significant lateral (i.e., radial) shear forces in addition to longitudinal shear forces. In the limit that the girder is straight, the lateral shear forces are relatively small and are generally neglected. The calculation of the longitudinal shear forces is the same in both straight and curved I-girders. Therefore, the behavior of the shear connectors in straight composite I-girders may be considered as a special case of the behavior in curved I-girders.

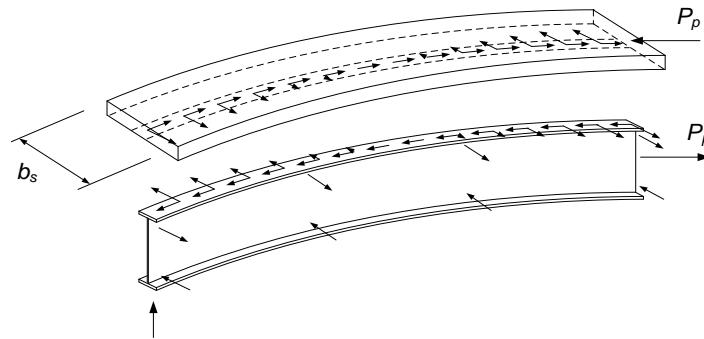


Figure 75 Idealized free-body diagrams of the slab and the steel I-section for a single I-girder taken from approximately one-half of the span of a hypothetical simple-span composite I-girder bridge.

Figure 75 shows idealized free-body diagrams of the slab and the steel I-section for a single I-girder taken from approximately one-half of the span of a hypothetical simple-span composite I-girder bridge. All the forces acting on each of the elements are indicated in the figure, with the exception of:

1. Dead loads and vertical live loads applied directly to the I-girder,
2. Slab membrane and plate bending forces and moments transferred from adjacent I-girders along the circumferential cuts made through the slab thickness to isolate the effective

width of the slab over the I-girder being considered, b_s , from the remainder of the slab, and

3. Vertical forces transferred between the slab and the I-girder, including any vertical forces associated with the torsional restraint of the I-girder provided by the slab.

The force labeled P_p in the figure is the total force developed in the slab by a maximum positive major-axis bending moment equal to the corresponding cross-section plastic moment M_p . Article 6.10.10.4.2 assumes that the maximum positive bending moment is located approximately at the position of the maximum positive live load plus impact moment. This position is selected because it is easier to locate than the position of the total maximum dead- plus live-load moment. The force P_p is calculated as

$$P_p = \min \left(0.85 f'_c b_s t_s, \right. \\ \left. F_{yw} D t_w + F_{yt} b_{ft} t_{ft} + F_{yc} b_{fc} t_{fc} \right) \quad (5.3.9-1)$$

(AASHTO 6.10.10.4.2-2 & 6.10.10.4.2-3)

Any reduction in the cross-section major-axis positive bending moment from Eqs. (3-2), (5.3.3-3), (5.3.4-1 & 2), (5.3.7-1) and/or (5.3.7-2) is neglected.

For *straight I-girders*, Article 6.10.10.4.2 requires that the shear connectors located between the maximum moment cross-section and the simply-supported end of the girder must develop the total force P_p . No other forces acting on the shear connectors need to be considered for these member types. Furthermore, only a slight deformation around more heavily stressed shear connectors is needed to redistribute the horizontal shear forces to less heavily stressed connectors. Therefore, the total required number of connectors within the above I-girder length may be calculated as

$$n = \frac{P_p}{Q_r} \quad (5.3.9-2)$$

(AASHTO 6.10.10.4.1-2)

Where

$$Q_r = \phi_{sc} Q_n = 0.85 Q_n \quad (5.3.9-3)$$

(AASHTO 6.10.10.4.1-1)

is the factored shear resistance of a single connector.

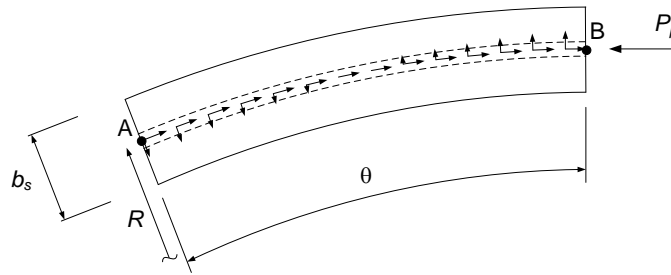


Figure 76 Plan view of the slab in the idealized free-body diagram of Figure 75.

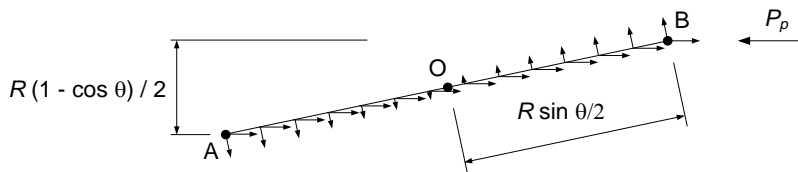


Figure 77 Plan view simplification of the free-body diagram of the slab in Figure 76.

For the horizontally curved I-girder illustrated in Figure 75, potentially significant radial shear forces must be accounted for in addition to the above longitudinal forces. Colville (1972) suggests the simplified model for calculation of these forces illustrated in Figure 76 and Figure 77. Figure 76 is a plan view of the slab free-body diagram from Figure 75. Figure 77 is an idealization of this free-body diagram explained below. One can observe that the force P_p developed at the maximum moment cross-section is not collinear with the shear connectors. This creates a secondary radial loading effect on the connectors. The connector radial loads may be estimated by making the following assumptions:

1. The influence of the slab forces and moments within the circumferential cut through the slab thickness to isolate the effective width b_s from the remainder of the slab are neglected. That is, the shear connectors are assumed to be the only components available to equilibrate the force P_p within the plan view of Figure 76.
2. Any differences in the slab stresses across the cut at the maximum moment location, which would give an eccentricity to the force P_p on this cross-section, are neglected.
3. The shear connectors are assumed to be spaced uniformly along a straight chord between the ends A and B shown in Figure 76. This idealization is illustrated in Figure 77. The shear connectors are actually located along the curved axis AB in Figure 76. By assuming that they are located along the straight chord AOB (see Figure 77), the equations are simplified and the resulting connector forces are estimated conservatively. Also, since the radius R is typically large compared to the length $R\theta$, the error caused by this assumption is small.
4. The radial forces in the shear connectors are normal to the line AOB in Figure 77 and are proportional to the distance of the connectors from point O.

Based on the above assumptions, the resultant of the connector forces may be taken as a force P_p acting at the centroid of the group of connectors (taken as point O), plus a moment about a vertical axis through point O equal to $PR(1 - \cos \theta) / 2$. The force in each of the extreme connectors is equal to the vector sum of the two components, namely

$$\bar{P} = P_p / n \quad (5.3.9-4)$$

where n is the total number of connectors along the girder length under consideration, and the lateral force (perpendicular to AOB)

$$\bar{F} \cong \frac{1.5 P_p (1 - \cos \theta)}{(n/n^* - 1) n^* \sin \theta / 2} \quad (5.3.9-5a)$$

where n^* is the number of shear connectors placed at each cross-section. If n/n^* is assumed to be large compared to one, Eq. (5a) simplifies to

$$\bar{F} \cong \frac{1.5 P_p (1 - \cos \theta)}{n \sin \theta / 2} \quad (5.3.9-5b)$$

Furthermore, for all practical values of the subtended angle θ between the maximum moment location and the simply-supported end of the girder, Eq. (5b) is closely approximated by

$$\bar{F} \cong \frac{1.5 P_p \theta}{n} \quad (5.3.9-5c)$$

where θ is expressed in radians. AASHTO (2014) Article 6.10.10.4.2 neglects the 1.5 coefficient in Eq. (5c). This is equivalent to assuming that the radial shear forces are the same magnitude in all of the connectors, and is justified by the conservative nature of the assumption that the connectors are all located along AOB. Also, Article 6.10.10.4.2 assumes that \bar{F} is perpendicular to \bar{P} in writing the vector sum of the shear forces. This leads to a total force

$$P = \sqrt{P_p^2 + F_p^2} \quad (5.3.9-6)$$

(AASHTO 6.10.10.4.2-1)

that replaces P_p in Eq. (2), where

$$F_p = n \bar{F} = P_p \theta \quad (5.3.9-7)$$

(AASHTO 6.10.10.4.2-4)

Colville (1972) discusses other contributions to the shear connector radial forces that come from the uniform St. Venant and nonuniform warping torsion of the composite I-girder between the brace points, where the brace points are indicated by the larger radial arrows on the free-body diagram of the steel I-section in Figure 75. He concludes that these forces are small compared to

the above forces \bar{P} and \bar{F} . Nevertheless, the assumption that the connector radial forces increase linearly with their distance from point O in Figure 77 is inconsistent with Colville's open-section thin-walled beam theory analysis of the composite I-section member to determine the connector forces due to St. Venant and warping torques. The above calculation of the connector radial loading effect from Eqs. (6) and (7) should be considered as no more than a reasonable but coarse approximation of the true radial loading effects on the shear connectors. The above equations are based on a constant radius of curvature R between the maximum moment location and the simply-supported girder ends. For more general girder geometries, R may be taken conservatively as the minimum girder radius over the length under consideration.

A more conservative estimate of the shear connector radial force is used in Article 6.10.10.1.2 for calculating the connector radial fatigue shear range for horizontally curved bridges and in straight bridges with skews exceeding 20°. If written in terms of the forces under strength load conditions, these estimates would be

$$\bar{F} \cong A_{bot} f_{bu.bot} \frac{L_b}{R} \frac{1}{n_w} \quad (5.3.9-8)$$

(AASHTO 6.10.10.1.2-4)

and

$$\bar{F} \cong \frac{F_c}{n_w} \quad (5.3.9-9)$$

(AASHTO 6.10.10.1.2-5)

where

A_{bot} = area of the bottom flange,

$f_{bu.bot}$ = elastically computed bottom flange stress,

L_b = distance between brace points,

R = horizontal radius of curvature at the brace point under consideration,

F_c = cross-frame or diaphragm force at the top flange, taken as the total radial force transferred to the I-girder from all the components of the cross-frames or diaphragms on each side of the girder at the location under consideration (the assumption associated with this calculation is that this total radial force must be balanced by a shear that is transferred to the slab by the shear connectors), and

n_w = number of shear connectors within an effective length of the deck over which the total radial force from the cross-frames is developed, taken as 48 inches at interior locations and 24 inches at end supports for calculation of the connector radial fatigue shear range in Article 6.10.10.1.2.

AASHTO (2014) Article 6.10.10.4 takes Eqs. (6) and (7) as a sufficient estimate of the shear connector radial loads under strength conditions. It uses formulas analogous to Eqs. (8) and (9)

only for checking the fatigue shear range in horizontally curved bridges and in bridges with skews exceeding 20°.

Colville (1972) also discusses a conservative calculation of the vertical (uplift) forces on shear connectors due to the restraint provided to twisting of the steel I-girders from the bridge deck. His equations for estimating these forces tend to be small compared to the vector sum of the longitudinal and radial forces. Furthermore, the downward dead and live loads located above the I-girder-to-slab interface counteract these local uplift forces. Therefore, AASHTO (2014) Article 6.10.10 does not require any consideration of uplift forces on the shear connectors. Article 6.10.10.1.1 simply specifies that the connectors shall be capable of resisting both horizontal and vertical movement between the concrete and the steel.

AASHTO (2014) Article 6.10.10.4.3 specifies the nominal shear resistance of a single stud shear connector embedded in a concrete deck as

$$Q_n = 0.5A_{sc}\sqrt{f'_c E_c} \leq A_{sc}F_u \quad (5.3.9-10)$$

(AASHTO 6.10.10.4.3-1, AISC I3-3)

where

A_{sc} = cross-sectional area of the stud shear connector,

E_c = modulus of elasticity of the deck concrete,

f'_c = compressive strength of the deck concrete,

F_u = specified minimum tensile strength of the stud shear connector.

Also, an alternate equation is specified for the strength of less commonly used channel shear connectors. Channel shear connectors should not be used in curved bridges or bridges with skews larger than 20° due to the combined longitudinal and radial loading effects.

The above calculations of P_p and F_p apply only to simple span bridges, and to the length between the position of the maximum positive moment (taken as the maximum live load plus impact moment) and the adjacent point of zero moment in continuous-span bridges that are noncomposite for negative flexure in the final condition. For I-girders in continuous-span bridges that are composite for negative flexure in the final condition, a larger total longitudinal force must be developed in the length between the maximum positive moment position and the centerline of an adjacent interior support. This is handled by replacing P_p in Eqs. (1), (2), (6) and (7) by

$$P_T = P_p + P_n \quad (5.3.9-11)$$

(AASHTO 6.10.10.4.2-6)

where P_n is an estimate of the total force developed in the negative moment cross-section of the concrete deck over the interior support. That is, the model of Figure 76 is replaced by the one shown in Figure 78. The force P_n is calculated as

$$P_n = \min \left(0.45 f'_c b_s t_s, \right. \\ \left. F_{yw} D t_w + F_{yt} b_{ft} t_{ft} + F_{yc} b_{fc} t_{fc} \right) \quad (5.3.9-12)$$

(AASHTO 6.10.10.4.2-7 & 6.10.10.4.2-8)

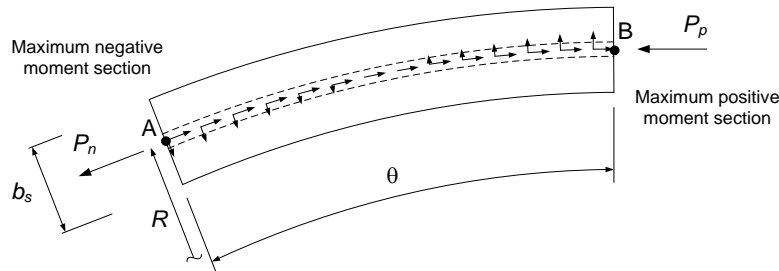


Figure 78 Plan view free-body diagram of the slab between the maximum positive moment and maximum negative moment positions.

at the interior support cross-section. The first term in this equation is intended as a conservative estimate of the combined contribution of both the longitudinal reinforcement and the concrete that remains effective in tension at the maximum negative moment cross-section.

5.3.10 Secondary Limit States

This section highlights a number of strength limit states pertaining to I-section flexural members that are somewhat separate from the overall flow and logic of the behavioral considerations discussed in the previous sections. Nevertheless, all strength limit states are essential to the proper structural performance.

5.3.10.1 Net section fracture

AASHTO (2014) Article 6.10.1.8 addresses the potential fracture through the net section of tension flanges containing holes typically used for connectors such as bolts. This article implements the check

$$f_t \leq 0.84 \frac{A_n}{A_g} F_u \leq F_{yt} \quad (5.3.10-1)$$

(AASHTO 6.10.1.8-1)

where

f_t = the elastically computed stress on the gross area of the tension flange, not including flange lateral bending but presumably including the stress due to tensile axial force if it exists,

A_n = the net tension flange area at the holes, calculated as discussed in Section 5.1.1 of this module,

A_g = the gross area of the tension flange, and

F_u = the specified minimum tensile strength of the tension flange.

By multiplying each of the expressions in Eq. (1) by A_g and noting that $0.84 \cong \phi_u / \phi_y = 0.80 / 0.95$, one can observe that this equation effectively handles the tension flange as a tension member according to AASHTO Article 6.8 (discussed in Section 5.1.1) and ensures that tension yielding will govern relative to tension fracture based on these provisions. Dexter and Altstadt (2004) indicate that due to the constraint provided by the web, net section fracture of the tension flange is less critical than the tension member equations imply. However, the splice design provisions of Article 6.13.6.1.4 do not consider the contribution of substantial web yielding to the flexural resistance. Therefore, potential liberalization of Eq. (1) should also include the consideration of substantial web yielding in the splice design provisions.

5.3.10.2 Web bend buckling

The web bend buckling resistance does not enter directly into the flexural resistance of I-section members at strength load levels except in the context of influencing when the web load-shedding parameter R_b is less than one, via Eqs. (5.3.5-1) and (5.3.5-4). However, the AASHTO Article 6.10.3 and 6.10.4.2 provisions for constructability and for the SERVICE II permanent deflection limit states directly restrict the elastically computed compression flange stress to the nominal web bend buckling stress as a simple device to help limit web plate bending and transverse displacements under these conditions. Also, as noted in AASHTO Article 6.10.5.3 on special fatigue requirements for webs, the Article 6.10.4.2 provisions with respect to web bend buckling always govern relative to a comparable check for the fatigue load combinations of this article. Therefore, theoretical web bend buckling is effectively prevented also under the AASHTO (2014) factored fatigue loading.

AASHTO Article 6.10.1.9.1 defines the web bend buckling resistance as

$$F_{crw} = \frac{0.9Ek}{(D/t_w)^2} \quad (5.3.10-2)$$

(AASHTO 6.10.1.9.1-1)

which is again the classical elastic plate buckling equation shown previously as Eqs. (5.2.4-1) and (5.3.8-1), but with another expression for the buckling coefficient k . AASHTO Article 6.10.1.9.1 defines the web bend buckling coefficient as

$$k = \frac{9}{(D_c/D)^2} \quad (5.3.10-3)$$

(AASHTO 6.10.1.9.1-2)

for webs without longitudinal stiffeners, and Article 6.10.1.9.2 defines the web bend buckling coefficient as

$$k = \frac{5.17}{(d_s/D)^2} \geq \frac{9}{(D_c/D)^2} \quad (5.3.10-4a)$$

(AASHTO 6.10.1.9.2-1)

for longitudinally-stiffened webs with $d_s/D_c \geq 0.4$ and by

$$k = \frac{11.64}{\left(\frac{D_c - d_s}{D}\right)} \quad (5.3.10-4b)$$

(AASHTO 6.10.1.9.2-2)

for other longitudinally-stiffened webs, where d_s is the depth between the compression flange and the longitudinal stiffener. One can observe that the web bend buckling resistance for webs without longitudinal stiffeners is actually based on the slenderness $2D_c/t_w$, and that the corresponding bend buckling coefficient is $k = 36$. The Eq. (2) form is specified so that a single equation can be applied for webs with and without longitudinal stiffeners. For a doubly-symmetric I-section without longitudinal stiffeners, the above constant $k = 36$ is approximately equal to $k_{ss} + 0.8(k_{sf} - k_{ss})$, where $k_{ss} = 23.9$ and $k_{sf} = 39.6$ are the bend buckling coefficients for simply-supported and fully-restrained longitudinal edge conditions respectively (Timoshenko and Gere 1961). For singly-symmetric I-sections with $D_c \neq D/2$, Eqs. (2) and (3) provide a reasonably accurate approximation of the theoretical bend buckling resistance (Ziemian 2010) consistent with $k = k_{ss} + 0.8(k_{sf} - k_{ss})$.

For webs without longitudinal stiffeners, Eqs. (2) and (3) predict $F_{crw} = F_{yc}$ at $2D_c/t_w = \lambda_{rw}$ given by Eq. (5.3.5-1). The potential use of $F_{crw} > F_{yw}$ in hybrid members is justified since the flange tends to restrain the longitudinal and plate bending strains associated with web bend buckling for nominal compression flange stresses up to $R_h F_{yc}$. ASCE (1968) recommends that web bend buckling does not need to be considered in hybrid sections with F_{yc} up to 100 ksi as long as the web slenderness does not exceed $5.87(E/F_{yc})^{0.5}$. AASHTO Article 6.10.1.9 adopts a more conservative approach than recommended by ASCE (1968) for $F_{yw}/F_{yc} < 0.7$ by limiting F_{crw} to the smaller of $R_h F_{yc}$ and $F_{yw}/0.7$ in its explicit web bend buckling checks.

Equation (2) generally gives $F_{crw} = F_{yc}$ at $D/t_w = 0.95(Ek/F_{yc})^{0.5}$ as defined by Eq. (5.3.5-4). Equations (4), developed by Frank and Helwig (1995), account for the effect of the location of a single longitudinal stiffener with respect to the compression flange on the web bend buckling resistance. The optimum stiffener position is given by $d_s/D_c = 0.4$, in which case both Eqs. (4a) and (4b) give $k = 129$ for a doubly-symmetric girder. For longitudinally-stiffened webs with $d_s/D_c \geq 0.4$, the web bend buckling deformations occur predominantly within the height d_s between the longitudinal stiffener and the compression flange. Eq. (4a) results in a web bend buckling stress that is constant with respect to d_s/t_w in this case. For longitudinally-stiffened webs with $d_s/D_c < 0.4$, the web bend buckling deformations occur predominantly within the height $(D - d_s)$ between the longitudinal stiffener and the tension flange. Equations (4) assume simply-supported boundary conditions at the flanges. Equation (4a) is limited to a minimum value equal to the k for webs without longitudinal stiffeners (Eq. (3)) to recognize the nominal restraint from

the flanges in the limit that Eq. (4a) would otherwise predict a smaller F_{crw} than if the web did not have a longitudinal stiffener.

Aside from its implicit use in determining when load shedding due to the postbuckling actions of the web must be considered via the R_b factor, the theoretical web bend buckling stress given by Eq. (2) has little significance with respect to the maximum flexural resistance. Article C6.10.1.9.1 emphasizes:

“In many experimental tests, noticeable web plate bending deformations and associated transverse displacements occur from the onset of load application due to initial web out-of-flatness. Because of the stable postbuckling behavior of the web, there is no significant change in the rate of increase of the web transverse displacements as a function of the applied loads as the theoretical web bend-buckling stress is exceeded (Basler et al. 1960). Due to unavoidable geometric imperfections, the web bend-buckling behavior is a load-deflection rather than a bifurcation problem. The theoretical web-buckling load is used in these Specifications as a simple index for controlling the web plate bending strains and transverse displacements.”

5.3.10.3 Longitudinal stiffeners

The AASHTO (2014) Article 6.10.11.3 provisions specify the following requirements for the design of web longitudinal stiffeners in I-girders subjected to flexure:

1. Web longitudinal stiffeners nominally must not yield when subjected to the idealized stress due to major-axis bending, i.e.,

$$f_s \leq \phi_f R_h F_{ys} \tag{5.3.10-5}$$

(AASHTO 6.10.11.3.1-1)

where

f_s = the elastic stress at the longitudinal stiffener due to major-axis bending, calculated assuming a linear variation in the flexural stress through the depth of the web and

F_{ys} = the specified minimum yield strength of the stiffener.

The yield strength of the stiffener is multiplied by the hybrid strength reduction factor to account conservatively for the influence of early web yielding on the stiffener stress in hybrid members. Article C6.10.11.3 suggests that R_h in Eq. (5) should be taken as the value applied to the flanges at the strength limit state. Lateral bending of longitudinal stiffeners due to eccentricity of the stiffener with respect to the web plate, and/or due to horizontal curvature, is neglected in Eq. (5).

2. Web longitudinal stiffeners must not buckle locally prior to reaching their yield strength in uniform axial compression. This is achieved by satisfying the following slenderness limit, assuming rectangular plate longitudinal stiffeners

$$b_s \leq 0.48t_s \sqrt{\frac{E}{F_{ys}}} \quad (5.3.10-6)$$

(AASHTO 6.10.11.3.2-1)

which is Eq. (5.2.4-4) with an assumed plate local buckling coefficient of $k_c = 0.56$.

3. Web longitudinal stiffeners and a portion of the web adjacent to them, acting as an equivalent column, must not fail by flexural buckling prior to development of the yield strength of the compression flange. This is achieved by:
- Assuming that the equivalent column fails by inelastic buckling,
 - Using the traditional CRC column inelastic buckling formula, and
 - Assuming a linear variation in the flexural stress through the depth of the web as in the first requirement above.

These combined idealizations give

$$R_h F_{ys} \left[1 - \frac{1}{4} \left(\frac{d_o}{r} \right)^2 \left(\frac{F_{ys}}{E} \right) \frac{1}{\pi^2} \right] \geq \left(1 - \frac{d_s}{D_c} \right) F_{yc} \quad (5.3.10-7a)$$

The stiffener yield strength is multiplied by the hybrid factor, R_h , on the left-hand side of this equation, but the hybrid factor is not included in the reduction for column inelastic buckling in the square brackets on the left-hand side. The longitudinal stiffener is taken as a simply-supported column with an effective length equal to the spacing between the transverse stiffeners, d_o , within the reduction for column inelastic buckling. The right-hand side of this equation is simply the elastic stress at the location of the longitudinal stiffener when the compression flange reaches its yield strength F_{yc} . If Eq. (7a) is solved for the required radius of gyration of the equivalent column, one obtains

$$r \geq \frac{0.16d_o \sqrt{\frac{F_{ys}}{E}}}{\left[1 - \left(1 - \frac{d_s}{D_c} \right) \frac{F_{yc}}{R_h F_{ys}} \right]} \quad (5.3.10-7b)$$

The Engineer is required to include an effective width of the web of $18t_w$ with the longitudinal stiffener in calculating the radius of gyration r . Also, it is required that the radius of gyration shall be calculated about the neutral axis of the combined effective cross-section (one is not allowed to assume that the neutral axis is located at the edge of the stiffener in contact with the

web, as specified for transverse stiffeners). This requirement is based on the recommendations by Cooper (1967). Cooper recommended the use of a mean effective width of $20t_w$ based on the results of strain measurements reported by Massonnet (1960). The effective width of $18t_w$ is specified to conform to traditional assumptions in American bridge design, as discussed by Vincent (1969). Lastly, AASHTO (2014) invokes one additional simplification that is justified given all the above idealizations and assumptions utilized in arriving at Eq. (7b). Rather than make the required radius of gyration a function of d_s/D_c , AASHTO Article 6.10.11.3 addresses the influence of the location of the longitudinal stiffener solely via Eq. (5) and assumes the optimum location $d_s/D_c = 0.4$ in Eq. (7b) to obtain

$$r \geq \frac{0.16d_o \sqrt{\frac{F_{ys}}{E}}}{\left[1 - 0.6 \frac{F_{yc}}{R_h F_{ys}}\right]} \quad (5.3.10-7c)$$

(AASHTO 6.10.11.3.3-2)

4. Web longitudinal stiffeners must be stiff enough to maintain a line of near zero lateral deflection at their juncture with the web plate for load levels up to the calculated bend buckling resistance of the web. This is achieved by satisfying

$$I_\ell \geq Dt_w^3 \left[2.4 \left(\frac{d_o}{D} \right)^2 - 0.13 \right] \beta \quad (5.3.10-8)$$

(AASHTO 6.10.11.3.3-1)

where

I_ℓ = moment of inertia of the longitudinal stiffener including an effective width of the web equal to $18t_w$ taken about the neutral axis of the combined section. If F_{yw} is smaller than F_{ys} , the strip of the web included in the effective section shall be reduced by the ratio F_{yw}/F_{ys} .

β = correction factor for horizontal curvature, taken as 1.0 for straight I-girders.

Equation (8) with $\beta = 1$ gives a reasonably good fit to the results from Dubas (1948) for the required lateral rigidity of longitudinal web stiffeners in doubly-symmetric I-girders with $0.5 \leq d_o/D \leq 1.6$, a single longitudinal stiffener located at the optimum position $d_s = D/5$, an effective width of the web acting with the stiffener of $20t_w$, and an upper-bound stiffener-to-web area ratio $A_s/A_w = A_s/Dt_w$ of 0.1. Dubas (1948) accounts for the fact that the necessary rigidity depends not only on the panel aspect ratio d_o/D , but also on the ratio of the stiffener area to the total web area A_s/A_w . The required I_ℓ is smaller for lesser values of A_s/A_w , and hence Eq. (8) may be considered as a reasonable upper bound for the necessary moment of inertia of the combined stiffener and web effective width (conservatively taken as $18t_w$).

It is important to recognize that the true web bend buckling resistance is a continuous function of the longitudinal stiffener properties. For stiffener I_ℓ values larger than specified by Eq. (8), the web bend buckling resistance asymptotes gradually to a maximum value as I_ℓ approaches infinity. For I_ℓ values somewhat smaller than specified by Eq. (8), the web bend-buckling resistance starts to reduce significantly due to increasing participation of stiffener lateral deformations in the web buckling mode. Also, it is important to note that the theoretical web bend buckling stress is not necessarily the maximum limit of the flexural resistance. For cases where the web violates Eq. (5.3.5-4) and thus the web bend buckling resistance is exceeded, the AASHTO (2014) flexural resistance is generally larger, although $R_b < 1$ is then calculated neglecting any benefit of the longitudinal stiffening. However, with respect to strength, the longitudinal stiffener should be adequate to ensure the validity of Eqs. (2), (4) and (5.3.5-4).

Equation (8) neglects any influence of the stiffener location, d_s/D , or the fraction of the web depth in compression, D_c/D , on the required I_ℓ . Frank and Helwig (1995) show that Eqs. (2) and (4) give an accurate to slightly conservative estimate of F_{crw} values determined from finite element analysis for a wide range of doubly- and singly-symmetric web panels with $d_o/D = 1$ using minimum-size longitudinal stiffeners based on the AASHTO (1998) requirements. For $\beta = 1$, Eqs. (6) and (8) are identical to the AASHTO (1998) requirements except that AASHTO (1998) specified that I_ℓ should be calculated about the edge of the stiffener in contact with the web. AASHTO (2014) specifies that I_ℓ is to be calculated about the true neutral axis for the combined stiffener and effective width of the web ($18t_w$) based on Cooper (1967). For $F_{ys} = F_{yc}$ and $R_h = 1$, Eq. (7c) requires an eight percent larger radius of gyration, r , relative to d_o , as well as the calculation of $r = [I_\ell / (b_s t_s + 18t_w^2)]^{0.5}$ using I_ℓ determined as specified above. Therefore, the minimum size longitudinal stiffeners studied by Frank and Helwig (1995) have I_ℓ values that range from 72 to 81 percent of the AASHTO (2014) requirement from Eq. (8), and they have r values that range from 64 to 131 percent of the AASHTO (2014) requirement from Eq. (7c). Frank and Helwig (1995) point out that one source of conservatism in their study is the fact that the longitudinal stiffeners participate in resisting the overall bending applied to the I-girder. That is, they do not apply flexural stresses directly to the longitudinal stiffeners in their study, but the longitudinal stiffeners tend to attract stress due to their compatibility with the web plate. On this basis, it is suggested that the longitudinal stiffeners should not be included in calculating the moment of inertia I_x and section moduli S_{xc} and S_{xt} for longitudinally-stiffened I-girders.

It is important to note that Eq. (8) and the results from Dubas (1948) are based only on linear buckling analysis. Therefore, Eq. (8) gives an I_ℓ that guarantees only the development of the web bend-buckling resistance given by Eqs. (2) and (4). Longitudinal stiffener rigidities as much as seven times larger have been found to be necessary to ensure the integrity of the longitudinal stiffeners within the postbuckling range of the web response, e.g., see Ziemian (2010) and Owen et al. (1970).

For horizontally curved girders, AASHTO requires an increase in the required I_ℓ to account for the tendency of the web to bow and the tendency of the longitudinal stiffeners to bend laterally. This is accomplished via the parameter β , given by

$$\beta = Z/6 + 1 \quad (5.3.10-9a)$$

(AASHTO 6.10.11.3.3-3)

for cases where the longitudinal stiffener is on the side of the web away from the center of curvature, and

$$\beta = Z/12 + 1 \quad (5.3.10-9b)$$

(AASHTO 6.10.11.3.3-4)

for cases where the longitudinal stiffener is on the side of the web toward the center of curvature, where

$$Z = \frac{0.95d_o^2}{Rt_w} \quad (5.3.10-10)$$

(AASHTO 6.10.11.3.3-5)

is referred to as the curvature parameter. This parameter is limited to a maximum value of 10. When a longitudinal stiffener is placed on the side of the web away from the center of curvature, the eccentricity of the stiffener with respect to the web plate gives a bending effect that is additive with the effect of the horizontal curvature. Conversely, when the longitudinal stiffener is placed on the side of the web toward the center of curvature, the eccentricity of the stiffener gives a bending effect that counteracts the effect of the horizontal curvature.

Equations (9) are a simplification of the Hanshin (1988) provisions for longitudinal stiffeners developed by Hall et al. (1999). The reader is referred to Nakai and Yoo (1988) for a summary of the Hanshin (1988) equations. A comparison of the AASHTO (2014) and Hanshin (1988) requirements gives the following results:

- For $d_o/D = 0.5$, Eqs. (8) through (10) give a net I_t requirement ranging from about 0.3 to 1.0 of that from the Hanshin provisions.
- For $d_o/D = 1.0$, the AASHTO equations give a net requirement ranging from about 1.0 to 2.0 times that from the Hanshin provisions.
- For $d_o/D = 1.5$, Eqs. (8) through (10) give a net requirement ranging from about 1.0 to 3.0 times that of the Hanshin provisions.

The Hanshin provisions are based on preventing nominal yielding of the longitudinal stiffener and a portion of the web acting together as a beam-column. These provisions assume that longitudinal stiffeners are continuous across the transverse stiffener locations; hence, it is imperative that the detailing of the longitudinal stiffeners is consistent with this assumption. The reason for the more liberal nature of the AASHTO equations for small d_o/D stems predominantly from the fact that the Hanshin provisions require a larger I_t for straight I-girders with small d_o/D .

The behavior of stiffened plate assemblies is one of the areas of greatest complexity in the analysis and design of steel structures. The AASHTO (2014) Article 6.10.11.3 provisions for longitudinal stiffeners are a basic set of criteria for proper proportioning of longitudinal stiffeners in the webs of I-girders subjected solely to flexure. These provisions are not intended for members that are subjected to combined flexure and axial compression. The reader is referred to Ziemian (2010) for discussion of the broader problem of combined flexure and axial compression in members with longitudinally-stiffened webs.

5.3.10.4 Bearing stiffeners

AASHTO (2014) Article 6.10.11.2 addresses the design of bearing stiffeners. AASHTO Article 6.10.11.2.1 requires full-depth bearing stiffeners on built-up sections at all bearing locations. This is consistent with the AISC (2010) provisions for unframed ends of beams and girders, and helps ensure adequate member torsional restraint at support locations. At bearing locations on rolled shapes and at other locations on built-up sections or rolled shapes where the concentrated loads are not transmitted through a deck or deck system, either bearing stiffeners must be provided or the web must satisfy the provisions of Article D6.5 (discussed below).

Bearing stiffeners are designed using the AASHTO Article 6.9.2.1 column strength equations and assuming an effective length equal to $0.75D$. Also, bearing stiffeners are required to satisfy the same limit as Eq. (5.3.10-6) to ensure against local buckling, the areas at the ends of the stiffeners (where the stiffeners are clipped to clear the web-to-flange fillet weld) must be sufficient to accept the bearing loads, and the connection of the stiffeners to the web must be sufficient to transmit the full bearing force to the web. AASHTO Article 6.10.11.2.1 requires plates or angles bolted or welded on both sides of the web, the intent being that the bearing stiffeners should be symmetric about the plane of the web.

With the exception of the restrictions described below, a strip of the web extending not more than $9(F_{yw}/F_{ys}) t_w \leq 9 t_w$ on each side of the stiffener elements may be included as part of the effective column area. If multiple stiffener pairs are used, the effective column section may include the web area extending up to $9(F_{yw}/F_{ys}) t_w \leq 9t_w$ on each side of the outer projecting elements of the web. If the stiffeners are bolted to the web or if F_{yw} is less than 70 % of the specified minimum yield strength of the higher strength flange at interior supports of continuous-span members, only the stiffener elements may be included in the effective column cross-section. The first restriction guards against the loss of compatibility between the web and the stiffeners due to slip within the bolted connection. The second restriction guards against the loss of effectiveness of a hybrid web due to early yielding caused by longitudinal flexural stresses.

5.3.10.5 Web yielding and web crippling

Webs of built-up sections and rolled shapes subjected to concentrated loads at locations that do not have bearing stiffeners, and where the loads are not transmitted through a deck or deck system, must be designed to prevent transverse web yielding or web crippling at the concentrated loads. If the loads are transmitted through a deck or deck system, they are assumed to be adequately distributed to the web such that these failure modes do not occur. AASHTO (2014) Article D6.5 specifies the same web yielding and web crippling limit state equations as in AISC

(2010) to guard against these secondary failure modes. The web yielding and web crippling limit states can be important in some cases during construction, for example during incremental launching over supports, where temporary concentrated loads may be applied to the members at locations that do not have bearing stiffeners.

5.4 Box-Section Flexural Members

5.4.1 Introduction

The design of box-girder bridges is generally more involved than the design of I-girder bridges. AASHTO (2014) Articles 6.7.4.3, 6.7.5.3 and 6.11 address various considerations specific to box-girder bridge design. Coletti et al. (2006 and 2005) provide useful summaries of the broad analysis and design considerations for tub girder bridges, which as noted in Section 2.3 of this module are the predominant type of box-girder construction in the United States. Box-girder bridges require a number of unique considerations tied to the design of the individual girder elements. Also, they contain a number of components beyond the box girders themselves, components that are essential to the behavior of the girders and the corresponding overall structural system. These include:

- Diaphragms inside the individual box girders at points of support, to transmit the girder vertical reactions and torques to the support bearings, which generally are not located directly under the girder webs.
- Intermediate cross-frames inside the individual boxes at certain intervals along their span to maintain the shape of the cross-section, and in tub girders, to help brace the narrow top flanges prior to placement of the deck.
- External diaphragms between the box girders at supports to transmit the torsional reactions across the entire bridge width between the inside and outside bearings, and to restrain individual girder torsional rotations at the bearing lines (such rotations tend to impact the girder torsional rotations throughout the span length). Also, at end bearing lines, these diaphragms provide support for an expansion joint.
- For tub girders, lateral bracing inside the individual boxes near the top flanges to make the girders act as a closed section prior to composite action of the slab. After composite slab action is achieved, the slab itself acts predominantly as the top flange of the box, rendering the lateral bracing redundant for subsequent loading. Nevertheless, the top lateral bracing system still can be an important element during future redecking.

In spite of the unique attributes of box girders and box-girder bridges, many of the requirements for their design can be taken directly from the requirements for I-girder bridges. For instance, the general requirements for analysis of the composite structure and for consideration of slab reinforcing in negative bending regions, hybrid webs, variable web depth, lateral bending stresses in the top flanges of tub girders during construction, net section fracture at cross-sections containing holes in a tension flange, and web bend buckling are largely the same as the I-girder

requirements. As such, Article 6.11 refers back to Article 6.10 in numerous places rather than duplicate the I-girder provisions.

AASHTO (2014) specifies several broad restrictions intended to limit its scope to the most common types of box-girder bridges:

- Only single-cell box girders are addressed. Multiple-cell box girders require additional considerations.
- Only moderate span lengths less than or equal to 350 ft are considered. Article C6.11.1 states that the AASHTO provisions may be applied to larger spans “based on a thorough evaluation of the application of the bridge under consideration consistent with basic structural fundamentals.” This article also references the proposed Wolchuk and Mayrbaur (1980) straight box-girder specification for information regarding the design of long-span steel box-girder bridges.
- Only box-girder bridges that have a composite concrete deck throughout their length in their final constructed configuration are addressed. Articles 2.5.2.6, 4.6.2.6.4, 6.14.3 and 9.8.3 address the design of orthotropic steel decks and orthotropic deck superstructures in general. However, AASHTO (2014) does not address the design of the other components of box girders in combination with the use of an orthotropic deck. Orthotropic deck box-girder bridges are typically longer than the above moderate length definition.
- Only composite top flanges are addressed. The behavior and design of composite bottom flanges is not considered.

Section 5.4 of this module provides an overview of the behavior of box-girder bridges and the corresponding AASHTO (2014) box-girder bridge design provisions. Section 5.4.2 first focuses on several overriding system behavioral considerations. AASHTO (2014) categorizes box-girder bridges into two main groups, one for which various analysis and design simplifications are allowed and a second for which more detailed analysis and design procedures are necessary. Section 5.4.2 summarizes the restrictions applied to bridges classified in the first of these groups as well as the specific simplified analysis and design procedures allowed for these types of bridges. Section 5.4.2 then summarizes the more detailed procedures required for bridges not satisfying the restrictions listed in Section 5.4.2. Sections 5.4.3 and 5.4.4 then outline additional general AASHTO (2014) requirements applicable to all types of box-girder bridges as well as requirements for several specific box-girder bridge types respectively. The remaining sections of Section 5.4 focus on the strength behavior and design of the box girders themselves. The discussions in these sections largely parallel those in the previous Sections 5.3.2 through 5.3.9 on I-section flexural members. In places where the I-girder provisions are applicable, Sections 5.4.5 through 5.4.14 refer back to the previous discussions. Section 5.4.15 closes the discussion of box-girder bridges by highlighting and explaining a number of key differences between the AASHTO (2014) box-girder provisions and previous proposed Wolchuk and Mayrbaur (1980) specifications for straight long-span steel box-girder bridges.

Prior to discussing the behavior and design of box girders in detail, it is useful to establish the following definitions, adapted from AASHTO Article 6.2:

Tub section – An open-top steel girder composed of a bottom flange plate, two inclined or vertical web plates, and an independent top flange attached to the top of each web. The Specification requires that the top flanges of straight tub girders must be connected with either a partial- or a full-length lateral bracing system, with due consideration of the lateral stability of the top flanges and the overall stability of the members. A full-length lateral bracing system is required for curved tub girders.

Closed-box section – A member having a closed cross-section composed of two vertical or inclined webs and top and bottom stiffened or unstiffened steel plate flanges. In the context of Article 6.11, the top flange of a closed-box section is always composite with a concrete deck in the final constructed configuration.

Box flange – A flange that is connected to two webs. The flange may be a flat unstiffened plate, a stiffened plate or a top flat plate with reinforced concrete attached with shear connectors. The terms “unstiffened” and “stiffened” here have a different meaning than these terms in the prior discussions of plate local buckling in Section 5.2.4 of this module and in AASHTO Article 6.9.4.2. In this section, “stiffened” means that longitudinal and/or transverse stiffeners are attached to the plate, whereas “unstiffened” means that the plate does not have any longitudinal or transverse stiffeners.

Diaphragm – A vertically oriented solid-web transverse member connecting adjacent longitudinal flexural members, or placed inside of a closed-box or tub section to transfer and distribute vertical and lateral loads, to provide stability to the compression flanges, and to limit the cross-section distortion to acceptable levels.

Cross-frame – A transverse truss assembly connecting adjacent longitudinal flexural members, or placed inside of a closed-box or tub section to transfer and distribute vertical and lateral loads, to provide stability to the compression flanges, and/or to limit the cross-section distortion to acceptable levels.

5.4.2 Categorization of Box-Girder Bridges in AASHTO (2014)

5.4.2.1 Straight multiple-box-girder bridges satisfying the restrictions in Article 6.11.2.3 and having fully effective flanges

Article 6.11.2.3 specifies the following restrictions that are first stated as being necessary for the applicability of line girder analysis using the live-load lateral distribution factor equation of Article 4.6.2.2.2 for multiple steel box girders with a concrete deck. However these restrictions, combined with additional limits, also form the basis for a number of other analysis and design simplifications. The additional limits and the corresponding analysis-design simplifications are discussed subsequently. The specific requirements for use of the above basic live-load distribution factor are:

- The bridge cross-section must consist of two or more single-cell box sections.
- The bridge should not have any horizontally curved segments (the influence of horizontal curvature generally extends beyond the horizontally curved segments and into other straight spans of the structure).
- The bridge shall not have any support skew.
- At midspans, $0.8w \leq a \leq 1.2w$, where w is the center-to-center distance between the top flanges of the box girders and a is the center-to-center distance between the flanges of adjacent box sections (see Figure 21).
- For nonparallel box girders, $0.65w \leq a \leq 1.35w$ must be satisfied at the supports.
- The value of w must be the same for all of the girders.
- The inclination of the webs with respect to a plane normal to the bottom flange shall not exceed 1 to 4.
- The width of concrete deck cantilever overhangs, w_o , including curbs and parapets, shall satisfy $w_o \leq \min(0.6 a_{avg}, 6 \text{ ft})$, where a_{avg} is the average a dimension along the span length.

These restrictions are based on the range of bridge characteristics considered in the original development of the box-girder lateral load distribution factors by Johnston and Mattock (1967).

In addition to the above restrictions, AASHTO Article 6.11.1.1 specifies that a box flange may be considered to be fully effective in resisting flexure (i.e., no reduction in resistance due to shear lag effects) when $b_f \leq L/5$, where L is taken as the span length for simple spans and the distance between points of permanent load contraflexure or between a simple support and a point of permanent load contraflexure for continuous spans. For negative moment regions in continuous-span box girders, L is taken as the distance between the points of permanent load contraflexure on each side of the support.

The above simplified rule comes from studies of simple-span bridges with L/b_f ranging from 5.65 to 35.3 (Goldberg and Leve 1957). The effective flange width ranged from 0.89 for the bridge with the smallest L/b_f to 0.99 for the bridge with the largest L/b_f in these studies. Dowling and Harding (1992) also indicate that box flanges may be considered as fully effective except in cases with particularly large aspect ratios (i.e., large b_f/L), or cases with particularly slender edge panels or stiffeners. AASHTO 4.6.2.6.4 gives different effective width rules developed by Moffatt and Dowling (1975 and 1976) for orthotropic steel decks. These effective width definitions, which are applicable to stiffened or unstiffened box flanges, are discussed subsequently in Article 5.4.15.

Various AASHTO (2014) articles specify analysis and design simplifications for box-girder bridges that: satisfy all of the above requirements for (1) use of the simple live-load distribution

factor equation and (2) consideration of the box flange or flanges as fully effective. These analysis and design simplifications are as follows:

- Stresses due to distortion of the box cross-section (when it is subjected to torsion) may be neglected (Article C6.11.2.3). These are the shear, warping and plate bending stresses illustrated previously in Figure 20. AASHTO (2014) allows these stresses to be neglected both for consideration of strength as well as for consideration of fatigue (see Article 6.11.5).
- If several other requirements are also satisfied (discussed subsequently), sections in positive flexure may be designed as compact sections using the provisions of Article 6.11.7.1 (this is specified in Article 6.11.6.2.2).
- Shear stresses due to St. Venant torsion may be neglected (Article C6.11.2.3).
- The shear connectors between the slab and the steel girders need be designed only for flexural shear (Article 6.11.10).
- The Engineer may consider reducing the number of intermediate internal cross-frames to a minimum of: (1) points of maximum moment in the span, (2) points adjacent to field splices, and (3) points required to avoid excessive stresses during transportation and lifting of shipping pieces (Article 6.7.4.3). Article C6.7.4.3 also indicates that internal bracing members inserted for transportation, lifting and/or construction may be handled as temporary members. Nevertheless, Article C6.7.4.3 also states that additional cross-frame members may be required for construction. This statement either requires Engineers to use their judgment about potential construction conditions, such as eccentric loading causing torsion, and/or to perform analyses of potential construction conditions to check the St. Venant shear and distortional stresses and deformations. Furthermore, Article C6.7.4.3 also states that in tub sections with inclined webs, additional intermediate cross-frames, diaphragms or struts may be required to reduce the lateral bending in the discretely-braced top flanges during construction. Lastly, Article C6.11.1.3 states that at least two intermediate internal cross-frames or diaphragms are necessary to reduce the magnitude of the secondary stresses due to distortion of the cross-section at the web-to-flange welds to an extent (i.e., by more than 80 %) such that fillet welds on both sides of the web designed according to Article 6.13.3.4 may be assumed to be adequate. In short, although it is possible to reduce the number of internal cross-frames in bridges satisfying the above restrictions, there are a number of additional considerations that must be addressed.

5.4.2.2 Box-girder bridges not satisfying one or more of the above requirements

AASHTO (2014) specifies the following more detailed analysis and design procedures for box-girder bridges not satisfying one or more of the above requirements:

- The bridge should be analyzed using a refined analysis, i.e., an analysis that captures the three-dimensional responses of the structure (Article C6.11.2.3).

- For wide bridges in which the box flanges are not considered fully effective, the box-flange width is to be taken as $L/5$ in calculating the major-axis bending stresses (Article 6.11.1.1). However, the full box flange width is to be used in the applicable resistance equations.
- Internal diaphragms or cross-frames shall be provided to control the cross-section distortion, with the spacing not to exceed 40 ft (Article 6.7.4.3). Article C6.7.4.3 elaborates that internal diaphragms and cross-frames: (1) “must” be spaced to limit the plate bending stresses due to distortion (see Figure 20) to 20 ksi at the strength limit state (this is stated as a requirement in Article 6.11.1.1), and (2) should be spaced to limit the longitudinal warping stresses (see Figure 20) to 10 % of the normal stresses due to major-axis bending at the strength limit state (Article 6.11.1.1 states that these stresses may then be ignored at the strength limit state). These plate bending stresses may be estimated using a beam-on-elastic-foundation (BEF) analogy developed by Wright and Abdel-Samad (1968). In this method, the internal cross-braces are analogous to intermediate supports and the resistance to distortion provided by the box cross-section is analogous to a continuous elastic foundation. Sample calculations using this method are presented by Heins and Hall (1981) and in AASHTO (2003). The longitudinal warping stresses due to cross-section distortion also can be determined using the BEF analogy. Given the provision of adequate internal diaphragms and cross-frames using these rules, AASHTO (2014) neglects the influence of the plate bending and warping stresses due to cross-section distortion for checking of strength limit states.

As noted subsequently in Section 5.4.3 of this module, Article C6.7.4.3 also states that in tub sections with inclined webs, additional intermediate cross-frames, diaphragms or struts may be required to reduce the flange lateral bending in discretely-braced top flanges. Furthermore, the following statement from Article C6.11.1.3 still applies: at least two intermediate internal cross-frames or diaphragms are necessary to reduce the magnitude of the secondary stresses due to distortion of the cross-section at the web-to-flange welds to an extent (i.e., by more than 80 %) such that fillet welds on both sides of the web designed according to Article 6.13.3.4 may be assumed to be adequate.

- In designing the webs for shear, the web shear force shall be taken as the sum of the forces due to flexure and due to the St. Venant torsional shears (Article 6.11.9).
- The top flange shear connectors shall be designed for the sum of the shear forces due to flexure and due to the St. Venant torsion (Article 6.11.10).
- Web splices shall be designed for the sum of the above shears (Article 6.13.6.1.4b).
- The longitudinal warping stresses due to cross-section distortion shall be considered when checking bolted flange splices for slip and for fatigue (Article 6.13.6.1.4c).
- The need for a bottom transverse member within internal cross-frames shall be considered (Article 6.7.4.3). Article 6.7.4.3 indicates that this member may be needed to

limit the plate bending stress range for fatigue in the bottom box flange at the termination of fillet welds connecting cross-frame connection plates to the flange. In addition, Article 6.11.11.2 indicates that for rare cases where a box flange is exceptionally wide and more than two longitudinal stiffeners may be required, transverse flange stiffeners should be considered to reduce the required size of the longitudinal stiffeners. AASHTO does not suggest any other conditions requiring a transverse member or transverse stiffener attached to a box flange.

Where provided, the transverse member shall be attached to the box flange unless longitudinal flange stiffeners are used, in which case the transverse member shall be attached to the longitudinal stiffeners by bolting. Article 6.7.4.3 also states that the cross-sectional area and stiffness (implying flexural stiffness) of the top and bottom cross-frame members shall be greater than or equal to that of the diagonal members. The intent of these provisions is to ensure that the shape of the cross-section is maintained, i.e., to limit the transverse bending of the bottom flange due to cross-section distortion at the internal cross-frame locations.

5.4.3 Other General Requirements Applicable to All Types of Box-Girder Bridges

In addition to the above rules and procedures, which differ depending on whether the bridge satisfies the restrictions for simplified analysis and design listed in Section 5.4.2 of this module or not, AASHTO (2014) specifies other general requirements that apply to all types of box-girder bridges. These requirements are summarized in the following subsections.

5.4.3.1 Diaphragm requirements at supports (Article 6.7.4.3)

Article 6.7.4.3 specifies the following diaphragm requirements at the bridge supports:

- Internal diaphragms or cross-frames shall be provided at each support to resist transverse rotation, displacement and cross-section distortion and shall be designed to transmit the torsional moments and lateral forces from the box to the bearings.
- External cross-frames or diaphragms shall be used between the boxes at end supports.
- Where box or tub girders are supported on only one bearing, the need for external cross-frames between girders at interior supports should be evaluated to ensure torsional stability (these components are also key in controlling the torsional rotations of the individual girders, particularly during construction).
- Diaphragms that are provided for continuity or to resist torsion shall be connected to the webs and flanges of the box section. (It should be noted that recent studies by Zhou (2006) and Helwig et al. (2007) indicate that it is not essential to connect the diaphragms to the girder flanges when the length to depth ratio of the diaphragm is less than five; fit-up of external diaphragms with the girders during construction is facilitated by not providing a connection to the flanges,)

- The effect of access holes on the stresses in diaphragms should be investigated to determine if reinforcement is required

5.4.3.2 Bearing requirements (Article 6.11.1.2)

Article 6.11.1.2 specifies the following requirements at bearings:

- Single or double bearings may be used. Double bearings provide a restoring couple on each box, whereas single bearings require bearings on other girders to provide the torsional reactions required for equilibrium.
- Single bearings shall be aligned with the shear center of the box.

Furthermore, Article 6.11.11.1 states that stiffeners are to be designed using the I-girder provisions of Article 6.10.11.2 plus the following additional requirements:

- The bearing stiffeners should be attached to the diaphragms and not to the inclined webs, so that the stiffeners are perpendicular to the sole plate.
- At expansion bearings, the bearing stiffeners and diaphragms should be designed for eccentricity due to the thermal movement. This may be handled by designing the bearing stiffener assembly as a beam-column.

5.4.3.3 Top lateral bracing requirements in tub girders (Article 6.7.5.3)

Article 6.7.5.3 addresses the top lateral bracing system requirements for tub girders. This article requires a full-length lateral bracing system for curved boxes. Its commentary suggests that a full-length system should be provided for all straight boxes with spans greater than about 150 ft, and for general cases in which the torques acting on the steel section are deemed particularly significant (e.g., tubs in which the deck is unsymmetrically placed, and tub girders with skewed supports). Article 6.7.5.3 indicates that the objective is to ensure that the overall stability of the girders is provided and the deformations of the tub sections are adequately controlled during erection and placement of the concrete deck. For the other very limited situations, the Engineer is allowed to consider providing a partial length lateral bracing system. However, if the bracing system is partial length, the local and global stability of the top flanges and the tub-girder members must be investigated for the Engineer's assumed construction sequence. Also, Article C6.7.5.3 states that for spans less than about 150 ft, at least one panel of horizontal lateral bracing should be provided on each side of a lifting point. Furthermore, this article indicates that cross-section distortion and additional top-flange lateral bending stresses due to warping of the cross-section may need to be considered when a tub with a partial-length bracing system is subjected to a net torque.

Article C6.7.5.3 suggests the following equation as a guideline to ensure that a reasonable minimum area is provided for the diagonal bracing members:

$$A_d \geq 0.03w \quad (5.4.3-1)$$

(AASHTO C6.7.5.3-1)

Where

A_d = the minimum required cross-sectional area of one diagonal, expressed in inches². and

w = the center-to-center distance between the top flanges, expressed in inches.

This equation was recommended by Heins (1978) based on studies of straight and curved steel composite box-girder bridges with spans between 50 and 250 ft. Tub sections with vertical webs and ratios of the section width-to-depth between 0.5 and 2.0, and an X-type top lateral bracing system with the diagonals placed at an angle of 45° relative to the longitudinal axis of the flanges were assumed in these studies. Heins found that an equivalent solid plate thickness for the top lateral bracing system of

$$t_{eq} = 0.05 \text{ in} = \frac{E}{G} \frac{2A_d}{w} \cos^2 \alpha \sin \alpha \quad (5.4.3-2)$$

was sufficient to limit the section warping stresses to less than 10 % of the major-axis bending stresses in all cases, where α is the angle of the X-bracing diagonals with respect to the plane of the box cross-section. Eq. (2) is obtained from Kollbrunner and Basler (1969) by assuming rigid truss chords (i.e., the tub girder top flanges) relative to the diagonal members. By substituting $\alpha = 45^\circ$ into this equation and solving for A_d , one obtains Eq. (1).

AASHTO (2014) Article C6.7.5.3 acknowledges that Eq. (1) is not necessarily applicable to general bracing configurations and cross-section geometries. However, it suggests that this equation may be used as a guide to ensure that a reasonable minimum area is provided for the bracing members. If the underlying $t_{eq} = 0.05$ in. were generally applicable, the equations given by Kollbrunner and Basler (1969) could be used to determine the necessary bracing member areas for various bracing configurations. It is suggested that the requirement of $t_{eq} = 0.05$ in. should be revisited to ascertain its applicability for a complete range of modern tub girder designs, including spans up to 350 ft. In the meantime, $t_{eq} = 0.05$ in. may be used as an implementation of the Article C6.7.5.3 suggestion to ensure that a reasonable minimum area is provided for top flange bracing members.

Lastly, Article 6.7.5.3 requires that the top lateral bracing system shall be designed for the combined forces due to the shear flow in the pseudo-box section plus the force associated with the flexure of the tub due to the factored loads before the concrete deck has hardened or is made composite.

5.4.4 Additional Requirements for Specific Box-Girder Bridge Types

In addition to the above general requirements, specific types of box girders are addressed by different Articles of the AASHTO (2014) provisions. These requirements are summarized below.

5.4.4.1 Horizontally curved boxes (multiple or single)

Article C6.11.1 emphasizes that for horizontally curved tub girders, top flange lateral bending due to curvature must be considered during construction. Also, it points out that the effects of the St. Venant torsional shear must always be considered at all limit states and during construction in horizontally curved boxes.

5.4.4.2 Single boxes

The following specific requirements pertain to single box section bridges:

- Article 6.11.1 states that single box sections shall be positioned in a central location with respect to the cross-section, and that the center of gravity of the dead load shall be as close to the shear center of the box as possible. This requirement is intended to minimize the torsion that must be resisted by the box.
- Article C6.11.1 indicates that items such as sound barriers on one side of the bridge may be critical on single-box sections.
- should be positioned to evaluate both the maximum flexure and the maximum torsion in single-box-girder bridges, since the loads causing the critical torsion may be different than those causing the critical flexure.
- Article C6.11.1.2 emphasizes that the bearing arrangement dictates how torsion is resisted at supports and is especially critical for single box sections.
- Article 6.11.5 states that for single box sections, box flanges in tension shall be considered fracture critical unless analysis shows that the section can support the full dead load and an appropriate portion of the live load after sustaining a hypothetical complete fracture of the flange and the webs at any point.

5.4.4.3 Closed boxes

The following specific requirements pertain to closed-box section bridges:

- Article 6.11.3.2 states that for loads applied to a composite box flange before the concrete has hardened or is made composite, the flange shall be designed as a noncomposite box flange.
- Article 6.11.3.2 states that the maximum vertical deflection of a noncomposite box flange relative to its edges due to the unfactored permanent loads plus the unfactored construction loads is limited to $b_f/360$.
- Article 6.11.3.2 specifies that the through thickness bending stress in the noncomposite box flange due to the factored permanent loads plus the factored construction loads shall not exceed 20 ksi. The box flange may be assumed to be simply supported at the webs in making this calculation and the above calculations.

5.4.5 Proportioning Limits

AASHTO (2014) Article 6.11.2 defines the following proportioning limits unique to box girders:

- A 1 to 4 limit on the inclination of the web plates is recommended relative to an axis normal to the bottom flange. Larger web inclination is allowed, but the effects of changes in the St. Venant and/or flexural web shears on lateral bending of the top flanges will be larger during construction (see the discussion in Section 2.3 of this module). Also, highly inclined webs are generally less efficient in transmitting shear. However, the width of the bottom flange may be reduced by using a larger web inclination.
- The webs shall be attached to the mid-width of the top flanges. Attachment of the webs other than at the top flange mid-widths would cause additional flange lateral bending that would require special investigation.
- Extension of the box flanges at least one inch beyond the outside of each web is recommended to facilitate welding of the webs to the flange.

Otherwise, the web and top flange proportioning requirements for box girders are the same as those for I-girders (discussed previously in Section 5.3.2 of this module), with the exception that Eq. (5.3.2-6) is not applicable. Article 6.11.2 specifies that the inclined distances along the web are to be used in checking the web proportioning limits as well as all other pertinent design requirements.

Although it is discussed in Article 6.11.3.2 on Constructability, AASHTO (2014) provides one additional limit that deserves mention with the above proportioning limits. This article suggests

$$b_f \geq L/85 \quad (5.4.5-1)$$

for the top flanges of tub girders, in cases where a full-length lateral bracing system is not provided within a tub section, with L taken as the larger of the distances between panels of lateral bracing, or between a panel of lateral bracing and the end of the piece. This limit is similar in intent to Eq. (5.3.2-7) discussed previously for I-section flexural members.

5.4.6 Compact Composite Sections in Positive Flexure

The Article 6.11.6.2.2 requirements for composite sections in positive flexure to be considered as compact are the same as in Article 6.10.6.2.3 for I-sections (see Section 5.3.3 of this module), except that the bridge must also satisfy the requirements of Article 6.11.2.3 for use of the simplified live load distribution factor (see Section 5.4.2(A)) and the box flange must be fully effective based on the provisions of Article 6.11.1.1 (also discussed in Section 5.4.2).

The corresponding Article 6.11.7.1 resistance calculations and ductility requirements are the same as for compact composite I-sections in positive flexure (see Section 5.3.3) except that, for continuous spans, the nominal flexural resistance is always subject to the limitation of Eq. (3-2,

AASHTO 6.10.7.1.2-3). Either Eq. (3-2) or Eq. (5.3.3-3, AASHTO 6.10.7.1.2-2) will usually govern, thus limiting the nominal flexural resistance to a value less than the full plastic moment of the cross-section but larger than the cross-section yield moment.

5.4.7 Noncompact Composite Sections in Positive Flexure

AASHTO Article 6.11.6.2.2 specifies that all box sections in positive bending that do not meet the restrictive requirements discussed above must be designed as noncompact composite sections. As such, the flexural resistance is always less than or equal to the cross-section yield moment. Similar to the procedures for noncompact composite I-sections in positive flexure, discussed previously in Section 5.3.4 of this module, the resistances are expressed in terms of the elastically computed flange stresses.

For tub sections, the Article 6.11.7.2 calculation of the resistance based on the top flange stress is the same as that for noncompact composite I-sections in positive flexure (see Section 5.3.4). However, for closed-box sections, the nominal resistance of the top (compression) flange is taken as

$$F_{nc} = R_b R_h F_{yc} \Delta \quad (5.4.7-1)$$

(AASHTO 6.11.7.2.2-2)

Where

$$\Delta = \sqrt{1 - 3 \left(\frac{f_v}{F_{yc}} \right)^2} \quad (5.4.7-2)$$

(AASHTO 6.11.7.2.2-3)

f_v = the St. Venant torsional shear stress in the flange due to the factored loads at the section under consideration, calculated as

$$f_v = \frac{T}{2A_o t_{fc}} \quad (5.4.7-3)$$

(AASHTO 6.11.7.2.2-4)

R_b = the web load-shedding strength reduction factor specified in Article 6.10.1.10.2, with the top flange area taken as one-half of the effective area of the box flange, including the contribution of the concrete deck, and

R_h = the hybrid web strength reduction factor specified in Article 6.10.1.10.1, with the bottom flange area taken as one-half of the effective area of the box flange. (Note that yielding will practically always occur first in the bottom flange of these section types.)

Also, in Eq. (5.4.7-3),

T = the torque due to the factored loads and

A_o = the enclosed area within the box section.

Equation (2) reduces the effective yield resistance of the top flange accounting for the influence of the St. Venant torsional shear stress via the von Mises yield criterion. The participation of the concrete deck in transferring the shear stresses is neglected by using just the thickness of the steel top flange for t_{fc} in Eq. (3). Also, the flange shear stress due to flexure is considered negligible and is not included in Eq. (2).

The term Δ appears in many places in the different box flange resistance equations presented in this Section. In all cases, this term gives a reduction in the effective yield strength under longitudinal tension or compression due to the St. Venant torsional shear stress.

Similar to the above, the nominal resistance of the bottom tension flange is taken as

$$F_{nt} = R_h F_{yt} \Delta \quad (5.4.7-4)$$

(AASHTO 6.11.7.2.2-5)

Article 6.11.1.1 requires that box flanges also must generally satisfy

$$f_v \leq 0.75 \phi_v \frac{F_{yf}}{\sqrt{3}} \quad (5.4.7-5)$$

(AASHTO 6.11.1.1-1)

This magnitude of torsional shear stress is rarely, if ever, encountered in practical box girder designs. However, this limit ensures that Δ (Eq. (2)) will never be smaller than 0.66.

The Article 6.11 provisions imply that box flange shear stresses associated with flexure do not need to be considered in any situation. However, for cases with t_f only slightly larger than t_w , consideration of these shear stresses is prudent. The elastic shear flow $f = VQ/I$ in a box flange at the web-flange junctures is essentially the same as the corresponding elastic shear flow in the webs at these locations.

As a refinement on Eq. (3), for composite box flanges, the St. Venant torsional shear in the steel plate may be determined by multiplying the shear on the top of the composite box section by the ratio of the transformed concrete deck to the total thickness of the top flange plus the transformed deck. The St. Venant torsional shear in the concrete deck may be determined similarly. Adequate transverse reinforcing should be provided in the concrete deck to resist the shear forces due to St. Venant torsion.

The requirements for checking the slab stresses in shored construction are the same as those for I-section members

5.4.8 Noncomposite Sections

AASHTO (2014) Article 6.11 assumes that box-girder bridges always have a composite concrete deck throughout their length in their final constructed condition. Design using a noncomposite orthotropic steel plate deck is not explicitly addressed. Therefore, the resistance of box sections under noncomposite loadings is addressed only within Article 6.11.3, Constructability. This article requires the checking of noncomposite box flanges in tension as well as continuously-braced (top) box flanges in tension or compression using Eq. (5.4.7-4) but with the yield strength of the flange under consideration substituted for F_{yt} . Noncomposite box flanges in compression are checked under the factored construction loads for

$$f_{bu} \leq \phi_f F_{nc} \quad (5.4.8-1)$$

(AASHTO 6.11.3.2-1)

where

f_{bu} = the longitudinal flange stress due to the factored loads at the section under consideration, calculated without consideration of cross-section warping, and

F_{nc} = the nominal compressive resistance, defined in the Article 6.11.8.2 provisions for sections in negative flexure (discussed in the next section of the module).

The top flanges of tub-girders are checked in their noncomposite condition under construction loadings using the I-section member provisions of Articles 6.10.3.2.1 through 6.10.3.2.3. As such, the design of these elements in tub and I-girders is handled in the same unified fashion across all of the AASHTO (2014) provisions. The top flange unbraced length is taken as the distance between the panel points of the top lateral bracing system. The flange strength check under construction loadings is given by Eq. (5.3.7-1), which includes the influence of flange lateral bending due to any source. The following actions contribute generally to the lateral bending of the top flanges in tub girders in their noncomposite condition prior to the concrete slab becoming composite:

- forces from overall action of top lateral bracing system in resisting major-axis flexure and torsion,
- changes in shear along the length of the girder, causing a horizontal distributed load on the top flanges of the tub,
- eccentric loads from cantilever overhangs acting on forming brackets,
- horizontal curvature, and
- typically to a minor extent, wind.

The top flanges of tub girders are assumed to be continuously braced after the concrete slab has hardened or is made composite. As such, the top flange lateral bending effects are negligible and are no longer considered once the flanges have reached this state.

5.4.9 Composite Sections in Negative Flexure

As noted in the previous section, AASHTO (2014) Article 6.11 assumes that box-girder bridges always have a composite concrete deck in their final constructed condition. As a result, resistance checks for flange lateral bending and/or member lateral torsional buckling are no longer a consideration once the slab has hardened or is made composite. Flange lateral bending is not a consideration because the top flange elements are continuously supported by the concrete deck. Sufficient internal cross-frames and diaphragms are required such that lateral bending stresses due to warping are negligible in box flanges at the strength limit states during construction and after the completion of the structure. Lateral torsional buckling is not a consideration for composite boxes because of their large torsional stiffness and lateral torsional buckling resistance.

For the continuously braced top flanges of box girders in the final constructed condition, Articles 6.11.8.1.2 and 6.11.8.3 specify

$$f_{bu} \leq \phi_f R_h F_{yt} \quad (5.4.9-1)$$

(AASHTO 6.11.8.1.2-1 and 6.11.8.3-1)

for tub sections and Eq. (5.4.7-4) for closed box sections. For the bottom box flange in compression under negative flexure, Article 6.11.8.1.1 specifies

$$f_{bu} \leq \phi_f F_{nc} \quad (5.4.9-2)$$

(AASHTO 6.11.8.1.1-1)

where F_{nc} is the nominal compressive resistance defined in Article 6.11.8.2. Article 6.11.8.2 is subdivided into two subarticles addressing the cases of unstiffened box flanges and longitudinally stiffened box flanges. The resistance equations for box flanges in compression are specified in Article 6.11.8.2.1 along with the plate buckling coefficients k and k_s for uniform axial compression and uniform shear on unstiffened flanges respectively. Article 6.11.8.2.2 utilizes the same resistance equations, but uses the panel width (defined below) rather than the total flange width in its definition of the flange slenderness. Also, this article redefines the plate buckling coefficients k and k_s accounting for the influence of the flange stiffeners.

The resistance of box flanges in compression is based on local buckling of the flange under combined uniform axial compression and shear. The resistance curves, illustrated in Figure 79, are fitted to two anchor points similar to the handling of compression flange local buckling and lateral torsional buckling in I-section members. For flange slenderness values

$$\left[\lambda_f = \frac{b}{t_f} \right] \leq R_1 \sqrt{\frac{kE}{F_{yc}}} \quad (5.4.9-3)$$

the flange is taken to provide a constant maximum potential resistance, for

$$\left[\lambda_f = \frac{b}{t_f} \right] > R_2 \sqrt{\frac{kE}{F_{yc}}} \quad (5.4.9-4)$$

the flange resistance is governed by elastic local buckling, and for

$$R_1 \sqrt{\frac{kE}{F_{yc}}} < \left[\lambda_f = \frac{b}{t_f} \right] \leq R_2 \sqrt{\frac{kE}{F_{yc}}} \quad (5.4.9-5)$$

the flange resistance is governed by inelastic local buckling, where

$b = b_f$ for unstiffened flanges and

$b = w =$ larger of the width between flange longitudinal stiffeners or the distance from a web to the nearest flange longitudinal stiffener for stiffened flanges.

However, the box flange inelastic local buckling resistance is represented by a sinusoidal function rather than by a linear interpolation between the two anchor points as in the I-section member equations. The selection of a sinusoidal function for the inelastic transition curve originates from the straight box girder developments by Vincent (1969) and Mattock and Fountain (1967).

The maximum potential resistance associated with Anchor Point 1 in Figure 79,

$$F_{max} = R_b R_h F_{yc} \Delta \quad (5.4.9-6)$$

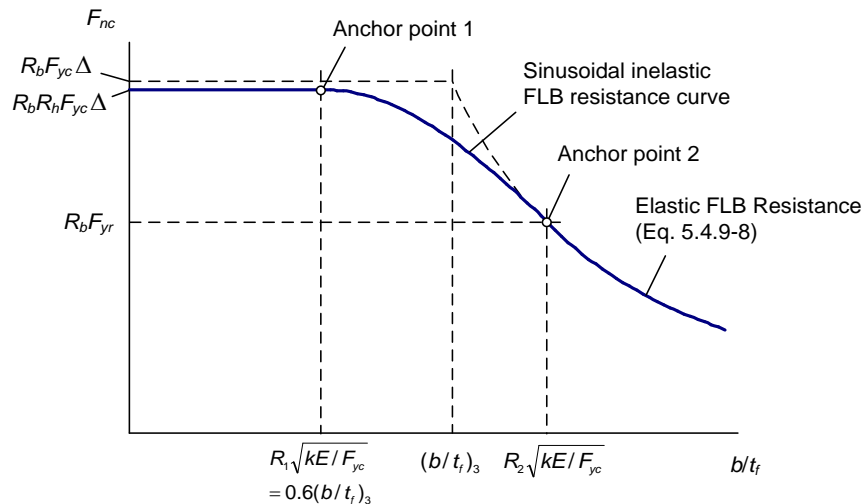


Figure 79 Flange local buckling resistance for box flanges in compression.

is the flange full-yielding resistance, reduced by the shedding of flexural stresses from the web due to bend buckling (via R_b), the use of a hybrid web (via R_h) and the influence of the St. Venant torsional shear stresses (via Δ , Eq. (5.4.7-2)). The abscissa of Anchor Point 1 is taken at 0.6 of the flange slenderness λ_f at which the elastic local buckling resistance is equal to $R_b F_{yc} \Delta$. Correspondingly, the ordinate of Anchor Point 2 is taken as $R_b F_{yr}$, where F_{yr} is the base flange stress corresponding to the nominal onset of yielding. This is taken as

$$F_{yr} = (\Delta - 0.3) F_{yc} \leq F_{yw} \quad (5.4.9-7)$$

(similar to AASHTO 6.11.8.2.2-13)

The abscissa of Anchor Point 2 is the value of λ_f at which the flange elastic local buckling resistance is equal to $R_b F_{yr}$. The elastic local buckling resistance is expressed as

$$F_{nc} = R_b \frac{0.9Ek}{(b_{fc}/t_{fc})^2} \left[1 - \frac{f_v^2}{\left(\frac{0.9Ek_s}{(b_{fc}/t_{fc})^2} \right)^2} \right] \quad (5.4.9-8)$$

The term within the square brackets in Eq. (8) gives an accurate to somewhat conservative estimate of the influence of a uniform applied shear stress on the elastic buckling resistance of flat plates in uniform axial compression (Ziemian 2010). The applied St. Venant torsional shear stress f_v is taken as the sum of the contributions from the different torques applied to the noncomposite and composite cross-sections.

For unstiffened flanges, k is taken equal to 4.0 and k_s is taken as 5.34 in Eqs. (3), (4), (5) and (8). These are the theoretical values for elastic buckling of an infinitely long flat plate with simply-supported edge conditions. For the case of $f_v = 0$, and thus $\Delta = 1$, AASHTO (2014) Article 6.11.8.2.2 gives a value of 0.57 for R_1 in Eq. (3). This, combined with $k = 4.0$ in Eq. (3), is practically equivalent to the AISC (2010) compactness requirement for the compression flange of a rectangular box section. For $F_{yc} = 50$ ksi, the corresponding Anchor Point 1 value for b/t_f is 27.5. Also for this basic case, Article 6.11.8.2.2 gives $R_2 = 1.23$. For $F_{yc} = 50$ ksi, the corresponding Anchor Point 2 value for b/t_f is 59.2.

For stiffened flanges, k and k_s are typically smaller than the above values due to the finite rigidity (i.e., flexibility) of the longitudinal stiffeners. In this case, the AASHTO (2014) equations are formulated in terms of the longitudinal stiffener moment of inertia I_s necessary to develop a certain value of $k \leq 4.0$. The base equation is

$$I_s \geq \psi w t_{fc}^3 \quad (5.4.9-9)$$

(AASHTO 6.11.11.2-2)

Where

$$\psi = 0.125k^3 \text{ for } n = 1 \quad (5.4.9-10a)$$

$$= 1.120k^3 \text{ for } n = 2 \quad (5.4.9-10b)$$

I_s is taken as the moment of inertia of the longitudinal flange stiffener about an axis parallel to the flange located at the base of the stiffener, and n is the number of equally spaced longitudinal flange stiffeners.

AASHTO (2014) Articles 6.11.8.2.3 and 6.11.11.2 require I_s to be large enough to develop a value of at least $k = 1.0$, although a value of at least $k = 2.0$ is recommended. Equations (10), which originate from Vincent (1969), are approximate equations that give values close to theoretical elastic buckling solutions for infinitely long, longitudinally stiffened plates from Goldberg and Levy (1957). In Article 6.11.8.2.3, the above equations are solved algebraically for the k values corresponding to a given I_s . Article C6.11.11.2 suggests that the number of longitudinal flange stiffeners should not exceed one for maximum economy in boxes of typical proportions.

AASHTO (2014) Article C6.11.11.2 gives the following more general equation for ψ , from Vincent (1969), applicable for $n = 2, 3, 4$ and 5:

$$\psi = 0.07k^3n^4 \quad (5.4.9-10c)$$

For $n > 2$, the required moment of inertia from Eqs. (9) and (10c) is excessive. This is due to the fact that these equations are based on the idealization of an infinitely long plate. Therefore, for the rare cases where an exceptionally wide box flange is required and n may need to exceed 2, Article C6.11.11.2 suggests that transverse flange stiffeners be provided to reduce the required size of the longitudinal stiffeners to a more practical value. This Article also suggests that transverse flange stiffeners should be considered for $n = 2$ if a k value larger than about 2.5 is needed and it is desired to reduce the required size of the longitudinal stiffeners relative to that given by Eq. (9). Article C6.11.11.2 provides equations for the proportioning of the transverse and longitudinal stiffeners as well as the resulting value of the plate buckling coefficient k applicable for these exceptional cases. The longitudinal stiffeners are sized using $\psi = 8.0$ in these situations, which is approximately the same as the requirement to develop $k = 2.0$ in Eq. (10b). Transverse and longitudinal flange stiffeners sized by these requirements give a value of $k \cong 4.0$ when the transverse flange stiffeners are spaced at a distance less than or equal to $4w$ for $n \leq 5$.

Furthermore, the coefficient for the elastic shear buckling of a stiffened flange is specified as

$$k_s = \frac{5.34 + 2.84 \left(\frac{I_s}{wt_{fc}^3} \right)^{1/3}}{(n+1)^2} \leq 5.34 \quad (5.4.9-11)$$

(AASHTO 6.11.8.2.3-3)

in AASHTO (2014) Article 6.11.8.2.3. This equation, as well as the general extension of Vincent's (1969) straight-box girder equations in Figure 79, and Eqs. (3) through (10) originate from Culver (1972).

The longitudinal stiffeners act integrally with the flange in resisting flexural compression in stiffened box flanges. Also, AASHTO (2014) generally does not count upon any postbuckling resistance of box flange elements. Therefore, the area of these stiffeners generally should be included in calculating the moment of inertia, elastic section modulus and other properties of the box section. Conversely, the web longitudinal stiffeners are sized using the same philosophy as for I-section members (see Section 5.3.10 of this module). That is, the web longitudinal stiffeners are sized to maintain a line of near zero lateral deflection at their juncture with the web plate for load levels up to the calculated bend buckling resistance of the web. As discussed previously in Section 5.3.10 of this module, based on the derivation of the web longitudinal stiffener rigidity requirements and the design of the webs generally including their postbuckling resistance, it is recommended that the web longitudinal stiffeners should not be included in determining the member cross-section properties.

Article 6.11.11.2 requires that the specified minimum yield strength of the flange longitudinal stiffeners shall not be less than the specified minimum yield strength of the box flange to which they are attached. This is similar to the previously discussed requirement of Eq. (5.3.10-5). Also, this article specifies that the projecting widths of the flange longitudinal stiffener elements must satisfy the same limit as defined by Eq. (5.3.10-6). As noted in Section 5.3.10, this limit is intended to prevent local buckling of the flange longitudinal stiffeners. For structural tee stiffeners, this limit is to be applied to one-half of the tee flange width.

5.4.10 Bottom Box Flange at Interior Pier Sections

Article C6.11.8.1.1 addresses the complex biaxial stress conditions in bottom box flanges at interior pier sections. At these locations, the bottom flange is subjected to the stresses from major-axis bending of the box section as well as major-axis bending of the internal diaphragm over the bearings. In addition the flange is subjected to shear stresses due to the internal diaphragm vertical shear as well as, when it is non-negligible, the St. Venant torsional shear in the box section. The flexural and shear stresses due to the bending of the internal diaphragm can be particularly significant for boxes supported on single bearings. Article C6.11.8.1.1 provides the following equation for checking the bottom box flange at interior pier sections under the strength limit states

$$\sqrt{f_{bu}^2 - f_{bu}f_{by} + f_{by}^2 + 3(f_d + f_v)^2} \leq \phi_f R_b R_h F_{yc} \quad (5.4.10-1)$$

(AASHTO C6.11.8.1.1-1)

Where

f_{bu} = the longitudinal flange stress due to major-axis bending of the box section,

f_{by} = the flexural stress in the flange caused by major-axis bending of the internal diaphragm over the bearings,

f_d = the shear stress in the flange caused by the internal diaphragm vertical shear, and

f_v = the St. Venant torsional shear stress in the box flange.

Equation (1) is simply a statement of the von-Mises yield criterion (Ugural and Fenster 2003) for a plate subjected to biaxial normal stress plus shear. Article C6.11.8.1.1 suggests the use of a flange width equal to $18t_f$ with the internal diaphragm for simplified calculation of the stresses f_{by} and f_d . The shear stress f_d may be estimated as

$$f_d = \frac{VQ}{I_{t_{fc}}} \quad (5.4.10-2)$$

(AASHTO C6.11.8.1.1-2)

Where

V = the maximum vertical shear in the internal diaphragm,

Q = the first moment of one-half of the effective box flange area ($9t_f^2$) about the neutral axis of the effective internal diaphragm section, and

I = the moment of inertia of the effective internal diaphragm section.

The shear stress f_v may be estimated using Eq. (5.4.7-3).

Article C6.11.8.1.1 points out that for a box supported on two bearings, f_{by} and f_d in Eq. (1) are typically small and can often be neglected. In these cases, Eq. (5.4.9-2) will govern the resistance of the bottom box flange at an interior support. Theoretically, in cases where the bottom box flange is governed by Eq. (1), the top flange (i.e., the concrete slab in a tub girder or the top composite box flange in a closed-box section girder) should also be checked for its adequacy under the related biaxial and shear loading conditions.

5.4.11 Concrete Slab

AASHTO (2014) Article 6.11.1.1 states that the shear due to St. Venant torsion should be considered when designing the reinforcing steel for the concrete slab. Article 6.11.10 suggests a simple method for determining the torsional shear in the slab of closed box sections. For tub sections, Article 6.11.1.1 indicates that the slab should be considered to resist all the torsional shear acting on the top of the composite box section.

5.4.12 Stepped, Variable Web Depth and Other Nonprismatic Box-Section Members

With the exception of:

1. Potential overall lateral torsional buckling of tub girders during construction, and

2. Potential lateral-torsional buckling of the top flanges between their brace points for tub girders subjected to positive bending under construction conditions (prior to the hardening or the concrete slab or the slab being made composite),

all of the resistance checks for box section members are effectively cross-section based. For stepped, variable web depth and other general nonprismatic box-section members, the above two cases can be handled as discussed for I-section members in Section 5.3.6 of this module. For other cases, the resistance calculations for stepped, variable web depth and other nonprismatic box-section members are handled as discussed in the above Sections 5.4.6 through 5.4.11.

5.4.13 Web Shear Strength

The provisions of Article 6.10.9 are applied separately for checking each of the webs of box girders. These provisions have been discussed previously in Section 5.3.8 of this module. In applying these provisions, D is taken as the depth of the web along the slope of the web for inclined webs. Also, the factored shear force in each web is determined generally as

$$V_{ui} = V_u / \cos \theta \quad (5.4.13-1)$$

(AASHTO 6.11.9-1)

Where

V_u = vertical shear due on the inclined web under consideration and

θ = the angle of inclination of the web plate with respect to the vertical direction.

For box girders in bridges not satisfying the requirements of Article 6.11.2.3, or with box flanges that are not fully effective according to the provisions of Article 6.11.11.1, V_u is to be taken as the sum of the flexural and St. Venant torsional shears.

In checking Eq. (5.3.8-7) to determine whether the full or true Basler shear resistance is applicable for transversely stiffened webs designed utilizing the web postbuckling shear strength, the effective flange width b_{fc} or b_{ft} of box flanges should be taken as the smaller of:

- One-half the flange width between the webs plus the outside extension of the flange beyond the centerline of the web, or
- $18t_f$ plus the outside extension of the flange beyond the centerline of the web.

The above $18t_f$ limit ensures that the I-section member web shear postbuckling resistance equations of Article 6.10.9 may be applied equivalently to box-section members.

Articles 6.11.9 and 6.11.11.1 require that intermediate transverse web stiffeners shall be designed using the I-girder provisions of Article 6.10.11.1 (see Section 5.3.8).

5.4.14 Shear Connectors

Article 6.11.10 points to the I-girder provisions of Article 6.10.10 for design of the shear connectors and provides the following additional supplementary requirements:

- Shear connectors are required in negative moment regions. This is because these components are necessary to resist any significant St. Venant torsional shears that exist in composite box sections. Also, the simplified live load distribution factors of Article 4.6.2.2.2b were developed for straight box sections that had shear connectors throughout the negative flexure regions.
- For box girders in bridges not satisfying the requirements of Article 6.11.2.3 (for use of the simplified live load distribution factors), or with box flanges that are not fully effective according to the provisions of Article 6.11.11.1, the shear connectors are to be designed for the sum of the flexural and St. Venant torsional shears. For tub girders, the St. Venant shear increases the connector force on one flange and decreases it on the other. Article 6.11.10 requires that the same connector pitch shall be used on both flanges. Article C6.11.10 points out the conservatism of adding both the maximum flexural and torsional shears, since these are typically not produced by concurrent loads, but indicates that the calculation of the critical concurrent shear forces is not practical using current analysis tools.
- The total area of the steel box section and the effective area of the concrete deck associated with that box are to be used in calculating the longitudinal force requirements in Eqs. (5.3.9-1) and (5.3.9-12).
- The shear connectors on composite box flanges shall be distributed uniformly across the width of the flange. The transverse spacing between shear connectors on composite box flanges, s_t , shall satisfy

$$\frac{s_t}{t_f} \leq R_1 \sqrt{\frac{kE}{F_{yf}}} \quad (5.4.14-1)$$

to help prevent local buckling of the flange plate subjected to compression. This limit is equal to the value of $\lambda_f = b/t_f$ corresponding to Anchor Point 1 in Figure 79.

- In composite box flanges, in addition to satisfying the requirements of Article 6.10.10, which require consideration of a radial force component in the shear connectors due to horizontal curvature, the vector sum of the longitudinal and St. Venant torsional shears must be considered. The St. Venant torsional shear may be determined by multiplying the shear on the top of the composite box section by the ratio of the transformed concrete deck to the total thickness of the top flange plus the transformed deck.

5.4.15 Comparison to the Wolchuk and Mayrbaurl (1980) Proposed Specifications for Long-Span Steel Box-Girder Bridges

As discussed previously, AASHTO (2014) references the proposed Wolchuk and Mayrbaurl (1980) straight box-girder specification for information regarding the design of long-span steel box-girder bridges. This section highlights and explains a number of key differences between the AASHTO (2014) box-girder provisions and the above proposed FHWA provisions. One of the most important differences is that the FHWA specification does not address the special requirements necessary for horizontally curved bridges and bridges with skewed bearing lines. The AASHTO (2014) provisions address these considerations. As such, all of the discussions in this section pertain to straight box-girder bridges in which the bridge cross-section is subjected to minor torsion. Other differences discussed in the following subsections include the assumed effective widths for box flanges, the flexural resistance calculations for unstiffened and stiffened box flanges, and the web shear resistance calculations.

5.4.15.1 Box flange effective widths

Figure 80 is reproduced from AASHTO (2014) Article 4.6.2.6.4-1. This figure contains the approach recommended for calculation of flange effective widths in Wolchuk and Mayrbaurl (1980) and is based on research by Moffatt and Dowling (1975 and 1976). The particular adaptation in this figure is from Wolchuk (1997). The following discussion focuses on the effective width of the box flange between the webs within the positive moment regions and in the negative moment regions in the vicinity of interior supports. The reader is referred to Wolchuk and Mayrbaurl (1980) for the complete application of Figure 80.

The effective width of a box flange is expressed as $b_{eff} = \psi B$ in Figure 80, where B is the total width between the webs. Curves (1) and (2) in the figure apply to the maximum positive moment region of simply-supported girders and continuous girders. The distance $L = L_1$ is taken as the simple-span length or the distance between the points of inflection in determining the value of ψ for these regions. Curve (1) applies to unstiffened box flanges while Curve (2) applies to stiffened box flanges with a ratio of the stiffener area to the box flange area $A_s/Bt = 1$. The values of ψ are to be determined for intermediate values of A_s/Bt by interpolation. One can observe that even for the extreme case of $A_s/Bt = 1$, ψ is approximately equal to 0.9 at $L/B = 5$ (the length to width ratio at which AASHTO (2014) assumes that the box flanges are fully effective. This supports the use of the AASHTO effective width rule within the positive moment regions (see the prior discussion in Section 5.4.2 of this module).

Curves (5) and (6) in the figure apply to the cross-section over interior supports in continuous-span girders. In this case, $L = L_2$ is taken as the distance between points of inflection on each side of the support. If the distances between the support and the points of inflection on each side, C_1 and C_2 , are unequal, ψ is determined as the average of the values of ψ for $L_2 = 2C_1$ and $L_2 = 2C_2$. One can observe that at $L/B = L_2/B = 5$, curves (5) and (6) indicate a range of ψ values of only 0.55 to 0.62. This implies that the effective width assumptions in AASHTO (2014) Article 6.11.1.1 are overly optimistic at continuous-span interior supports.

Curves (3) and (4) in the figure apply at the inflection points or simple-support locations. In Wolchuk and Mayrbaur (1980), the value of ψ taken as a constant based on the value from Curves (1) and (2) within the middle $L/2$ of the span, and is varied linearly between this value and the inflection point or simple support values, and linearly between the inflection point values and the interior support values. Obviously, this level of refinement in the assumed effective width may not be necessary.

Dowling and Harding (1992) take a much more optimistic view regarding box flange effective widths than indicated from the earlier research by Moffatt and Dowling (1975 and 1976). They indicate that

“Tests [Dowling et al. 1977] have shown, however, that for most practical cases shear lag can be ignored in calculating the ultimate compressive strength of stiffened or unstiffened flanges. This conclusion has been supported by the numerical studies of Lamas and Dowling [1980], Burgan and Dowling [1985], Jetteur et al. [1984] and Hindi [1991]. Thus a flange may normally be considered to be loaded uniformly across its width. Only in the case of flanges with particularly large aspect ratios [large L/B], or particularly slender edge panels or stiffeners [Burgan and Dowling 1985; Hindi 1991] is it necessary to consider the flange stability in greater detail.”

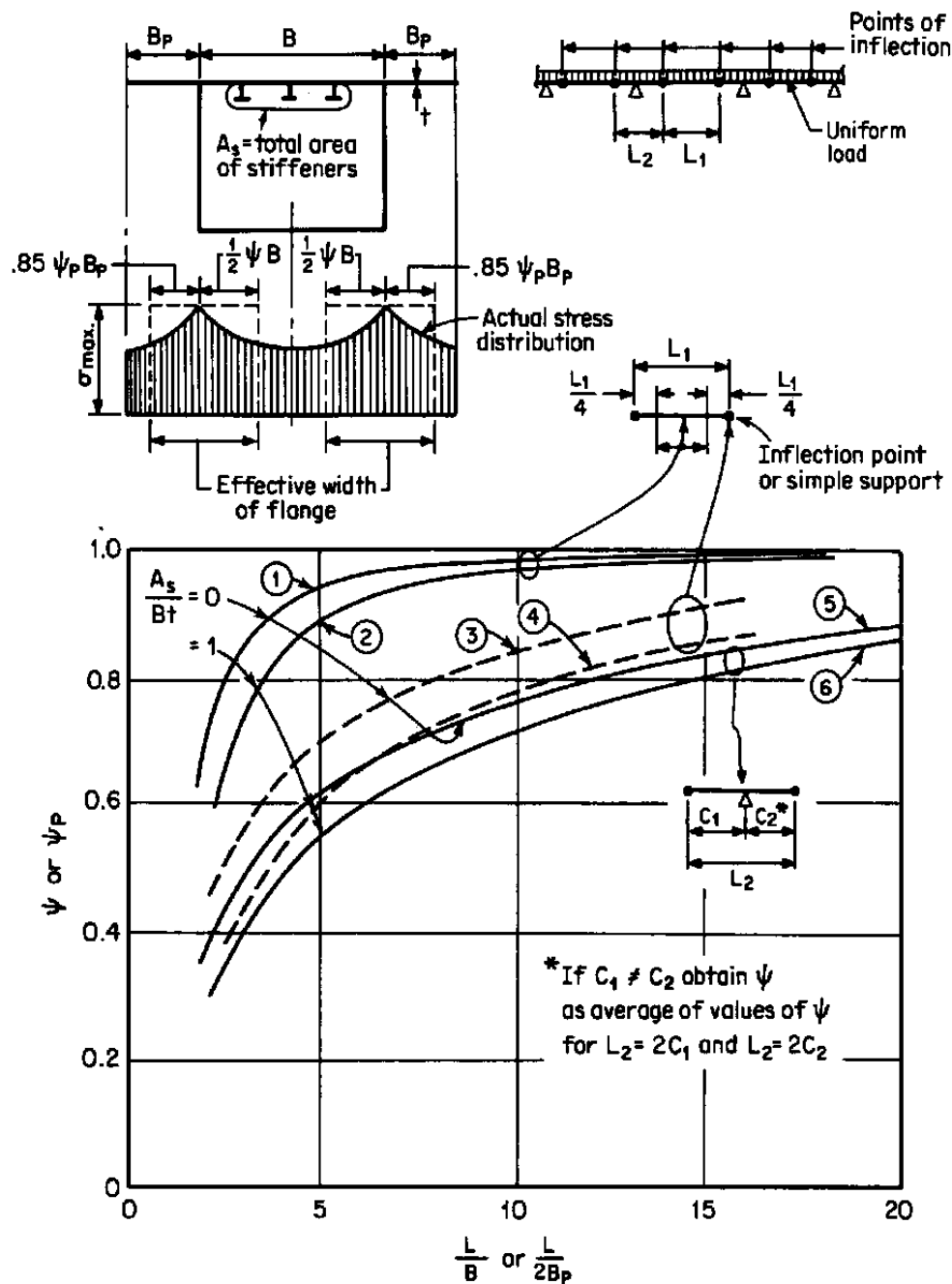


Figure 80 Flange effective widths, reproduced with permission from AASHTO (2014) and Wolchuk (1997).

Results from recent studies by Chen et al. (2005), which included several tub-girder bridges, have already been summarized in Section 2.2.1. Based on these results, the highly simplified AASHTO (2014) Article 6.11.1.1 rule for the box flange effective widths is considered acceptable.

5.4.15.2 Resistance of unstiffened box flanges in compression

As discussed in Section 5.4.9, the AASHTO (2014) provisions for the resistance of unstiffened box flanges are based on the theoretical elastic buckling for slender flange elements, i.e., plates satisfying Eq. (5.4.9-4). They are based on a sinusoidal transition curve and a plateau region developed based on an assumed analogy between column and plate buckling for stockier plates. The AASHTO (2014) equations are based in large part on the prior AASHTO Specifications that originate from the developments by Vincent (1969) and Mattock and Fountain (1967). Various studies of the behavior of geometrically imperfect plates containing different representative initial residual stresses indicate that the strength curve shown previously in Figure 79 is somewhat optimistic within the inelastic buckling range while it is somewhat conservative for highly slender flange plates.

Figure 81 compares the range of plate strengths determined by Dwight and Little (1974) to the FHWA strength curve recommended by Wolchuk and Mayrbaurl (1980) and the AASHTO (2014) Article 6.11.8.2 curve previously illustrated in Figure 79, but using R_b , R_h and Δ equal to 1.0. Wolchuk (1997) provides a detailed discussion of the background to these different curves. One can observe that a linear transition between Anchor Points 1 and 2 provides a reasonable fit to both the FHWA strength curve as well as the upper-bound strength curve for unwelded plates determined by Dwight and Little (1974) within the inelastic buckling region of the response. The more conservative predictions by AASHTO (2014) for highly slender flanges governed by elastic buckling is due to the substantial postbuckling resistance of these types of elements. It would appear that a linear transition curve between Anchor Points 1 and 2 is more appropriate to describe the nominal inelastic local buckling resistance of unstiffened box flanges. Although larger resistances are possible for slender flange plates, slender flange plates are generally an inefficient use of the material.

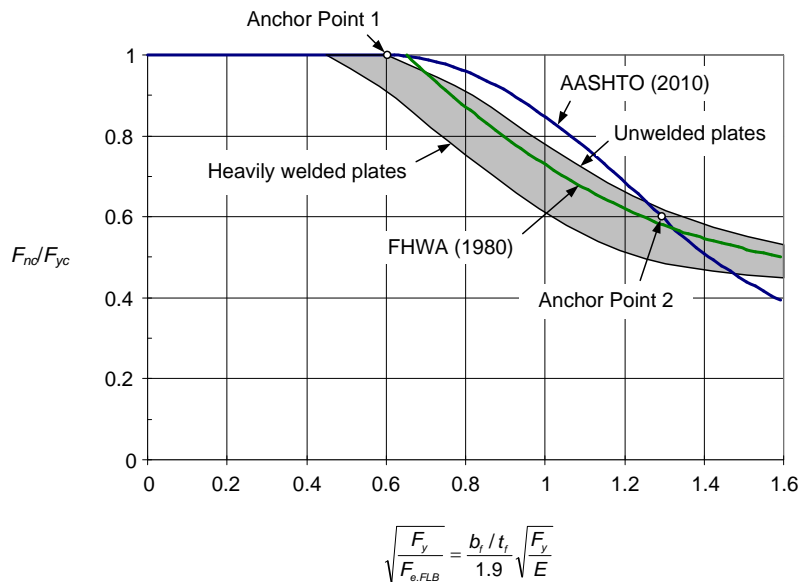


Figure 81 Resistance curves for unstiffened box flanges.

Regarding the broader application of the AASHTO (2014) flange resistance equations to cases involving combined axial compression and shear, Dowling and Harding (1992) indicate

“The weakening effect of both types of initial imperfection [geometric imperfections and residual stresses], separately and together is now well understood and has been incorporated into the various design methods produced to predict the inelastic buckling strength of plated structures. The weakening effect of these imperfections is most pronounced in the range of intermediate slenderness, that is those slendernesses at which the critical buckling stress and the yield stress are roughly equal. The knockdown in strength is most marked for plates of intermediate slenderness subjected to compressive stress and is least pronounced for shear-loaded cases, being practically negligible for rectangular plates in pure shear.”

Based on these observations, one can surmise that the handling of the effects of shear on the flange resistance in AASHTO Article 6.11 is accurate to somewhat conservative.

5.4.15.3 Resistance of stiffened box flanges in compression

The considerations regarding the local buckling strength of stiffened box flanges in compression are similar to those discussed in the previous section for unstiffened flanges. The AASHTO Article 6.11.8.2 provisions are based on the elastic buckling resistance of the stiffened flange assembly, and they map this resistance to an inelastic buckling resistance based on the sinusoidal transition curve discussed in the previous sections. Wolchuk and Mayrbaurl (1980) suggest a different approach in which the flange resistance is calculated based on the slenderness ratios L/r of the longitudinal stiffeners and w/t_f of the flange plates between the stiffeners. This approach treats the plate stiffened by several equally-spaced longitudinal stiffeners as a series of unconnected struts, each of which consists of a stiffener acting together with an associated width of plate that represents the plate between the stiffeners. The solutions are expressed as a design interaction chart. The influence of the rigidity of transverse stiffeners is not included. Where transverse stiffeners are present, they are designed to be sufficiently stiff to ensure that they provide nodal lines acting as simple supports to the ends of the longitudinal stiffeners. The effective length of the longitudinal stiffeners, L , is taken as the distance between the transverse elements.

It appears that direct comparisons of the predictions by the AASHTO (2014) approach versus the results from tests and refined numerical studies are not available. Dowling and Harding (1992) and Galambos (1998) show results from various Japanese tests that imply a linear transition for stiffened flange resistances. However, the definitions used for the flange local buckling coefficient are somewhat different than those in AASHTO (2014). Further studies are needed to carefully ascertain the relationship between the AASHTO (2014) curves and test results. Furthermore, Galambos (1998) indicates, “Design rules are needed for flanges stiffened by one or two stiffeners. The strut approach may not be appropriate in such cases, as it neglects the transverse stiffness of the plate and is a poor model for a single stiffener.” For the moderate length box girders targeted by the AASHTO (2014) provisions, the greatest economy is expected with only one or two longitudinal stiffeners at most. Ziemian (2010) indicates:

“For most stiffened flanges the strut approach is sufficiently accurate and is suitable for design purposes... The discretely stiffened plate approach is of interest mainly for plates with one or two stiffeners. For such flanges Eurocode 3 Part 1-5 offers a simple design method that considers the restraint from the plate to the buckling of the stiffeners... A more rational ultimate load method for the design of transversely loaded flanges needs to be evolved.”

Section 7.3.3 of Ziemian (2010) provides a summary of the discretely stiffened plate approach from Eurocode 3, which is based on a theoretical model for buckling of a strut on an elastic foundation.

5.4.15.4 Shear resistance

Dowling and Harding (1992) state,

“The key difference between plate and box girders which may influence the shear strength of the webs is the use of relatively thin flanges in box girders at the boundaries of the webs. Caution is needed in applying available tension field models, derived and verified in the context of plate girder webs, to the design of webs of box girders. Of major concern is the relatively small amount of support against in-plane movement which may be afforded to the web by the thin flange of a box girder, compared with the restraint offered by the thicker and narrower flange of a corresponding plate girder.”

Wolchuk and Mayrbaur (1980) express similar concerns and suggest the use of the true Basler shear strength formula, Eq. 5.3.8-9, in all cases for box-section members. In addition, Ziemian (2010) indicates:

“Further research is needed into the buckling strength of transversely stiffened webs and their stiffeners.”

However, recent studies by Yoo and Lee (2006) have demonstrated in detail that an external anchorage system is not necessary for the development of substantial web postbuckling shear strength. These investigators show that the diagonal compression continuously increases near the edges of panels after buckling. Due to this increase, tractions normal to the edges of the panels are not necessary for equilibrium. Similarly, numerous investigators, e.g., Yoo and Lee (2006), Kim et al. (2007), Stanway et al. (1996), Rahal and Harding (1990) and Horne and Grayson (1983) have shown that intermediate transverse stiffeners are not subjected to significant axial compression due to tension field action. Furthermore, the definitions of b_{fc} or b_{ft} for use in Eq. (5.3.8-7) to check the limits of applicability of the full Basler tension-field model (Eq. (5.3.8-8)) versus the true Basler model (Eq. (5.3.8-9)), explained in Section 5.4.13 of this module, appear to be sufficient to ensure the equivalent application of the I-section member web shear postbuckling resistance equations to box-section members.

5.5 Miscellaneous Flexural Members

5.5.1 Introduction

Article 6.12 of AASHTO (2014) addresses the flexural resistance of various rolled or built-up noncomposite or composite members used primarily in trusses and frames or in miscellaneous applications subjected to bending, often in combination with axial loads. In many cases, the Article 6.12 provisions are based on the AISC (2010) Specification provisions. However, there are some significant differences. This section provides a succinct overview of the corresponding AASHTO (2014) and AISC (2010) provisions.

5.5.2 I-Section Members in Weak-Axis Bending

The nominal flexural resistance of I-section members subjected to weak-axis bending is defined by AASHTO (2014) Article 6.12.2.2.1 as the corresponding fully-plastic resistance

$$M_n = M_p = F_{yf} Z_y \quad (5.5.2-1)$$

(AASHTO 6.10.2.2.1-1)

for cross-sections in which the largest flange slenderness $b_f/2t_f$ is less than or equal to the compact-flange limit λ_{pf} given by Eq. (5.3.5-16). For unusual cases where the flanges have different yield strengths, the smaller of these yield strengths should be used in checking the flange compactness and in calculating M_p . The web contribution to M_p is generally small, and hence hybrid web effects are ignored. For cross-sections with the largest flange slenderness greater than λ_{pf} but less than the noncompact flange limit λ_{rf} given by Eq. (5.3.5-26), with F_{yr} taken equal to the smaller F_{yf} and k_c taken equal to 0.76, the flexural resistance is assumed to be governed by inelastic flange local buckling (FLB). For $F_{yr} = F_{yf}$ and $k_c = 0.76$, Eq. (5.3.5-26) becomes

$$\lambda_{rf} = 0.83 \sqrt{\frac{E}{F_{yf}}} \quad (5.5.2-2)$$

(AASHTO 6.10.2.2.1-5)

The theoretical elastic FLB coefficient for a linear stress distribution across the flange width, with the maximum compressive stress at the flange tip and zero stress at the web-flange juncture, is 0.57 for simply-supported edge conditions and 1.61 for fixed edge conditions at the web-flange juncture (Ziemian 2010). The value $k_c = 0.76$ is taken as a reasonable value given some restraint from the web and from the portion of the flange loaded in flexural tension on the opposite side of the web. In setting $F_{yr} = F_{yf}$, the influence of residual stresses is neglected. This is justified due to the strain gradient across the flange width, as well as the relatively small value of $k_c = 0.76$ compared to potential theoretical values. Therefore, the moment capacity corresponding to $F_{yr} = F_{yf}$ is the nominal yield moment $M_y = F_{yf} S_y$, where S_y is the elastic section modulus for minor-axis bending. If the above values are substituted into the linear equation representing the inelastic buckling resistance between Anchor Points 1 and 2 in Figure 60 (with R_b taken equal to 1.0 since the web flexural stress is zero), one obtains

$$M_n = M_p - (M_p - M_y) \left(\frac{\lambda_f - \lambda_{rf}}{0.45 \sqrt{E / F_{yf}}} \right) \quad (5.5.2-3)$$

(AASHTO 6.12.2.2.1-2)

where λ_f = larger $b_f/2t_f$ of the two flanges. Equation (2) gives $\lambda_{rf} = 14.1$ for $F_{yf} = 100$ ksi, which is larger than the maximum $b_f/2t_f = 12$ permitted for I-sections in AASHTO Article (6.10.2.2) (see Eq. 5.3.2-3). Therefore, Article 6.12.2.2 does not define a weak-axis bending resistance based on elastic FLB.

The inelastic FLB resistance is slightly different in AISC (2010). AISC (2010) uses $k_c = 0.76$ and $F_{yr} = 0.7F_y$ in its calculation of λ_{rf} . The resulting AISC inelastic FLB resistance approaches AASHTO FLB resistance as the flange slenderness approaches the compact limit given by Eq. (5.3.5-16). However, it tends to be significantly more conservative than the AASHTO resistance for more slender flanges.

It is important to note that for I-section members subjected to major-axis bending combined with flange lateral bending due to minor-axis flexure or torsion, the one-third rule equations discussed in Section 5.3.7 of this module apply as long as Eq. (5.3.7-5) is satisfied. The one-third rule equations provide a more accurate representation of the resistance and should be utilized rather than the above equations in these cases.

5.5.3 Noncomposite Box-Section Members

AASHTO (2014) Article 6.12.2.2.2 addresses the flexural resistance of noncomposite box-section members. The provisions in this article assume that the flexural resistance $\phi_f M_n$ is unaffected by flange or web local buckling.

For general box-section members, the validity of neglecting of flange local buckling at $M_u = \phi_f M_n$ is ensured conservatively by the Article 6.9.4.2 limits on the flange slenderness (see Eq. (5.2.4-4) and Table 5 and Table 6), as long as the applied stresses $f_a + f_b$ are not substituted for F_y as permitted at the end of this article. For box-sections used as arch ribs, the validity of neglecting flange local buckling is often but not necessarily always ensured by the Article 6.14.4.3 flange slenderness limits, Eqs. (5.2.4-20) and (5.2.4-21)). The validity of neglecting flange local buckling is ensured if Eq. (5.2.4-4) is satisfied for the rib flanges and flange overhangs with k_c taken equal to 4.8 and 0.50 respectively (see Table 5 and Table 6).

Web bend buckling at $M_u = \phi_f M_n$ generally is not precluded for webs proportioned by the Article 6.14.4.2 web slenderness requirements (see Eqs. (5.2.4-18) and (5.2.4-19) and the discussions in Section 5.2.4 of this module). Equation (5.3.10-2) must be satisfied to ensure that web local buckling will not influence the calculation of the AASHTO (2014) $\phi_f M_n$ in general box-section members, including solid-web arch ribs.

Section 5.6.3 discusses the appropriate calculation of beam-column resistances for cases of combined axial compression and bending when flange or web local buckling is not precluded at $M_u = \phi_f M_n$.

Based on the assumption that flange and web local buckling is precluded at the limit of the flexural resistance, the AASHTO (2014) Article 6.12.2.2.2 expression for the flexural resistance of noncomposite box-section members is derived as follows. The derivation starts with the traditional CRC inelastic column strength equation (Ziemian 2010) written in terms of moments, i.e.,

$$M_n = M_{yc} \left[1 - \frac{M_{yc}}{4M_{e.LTB}} \right] \quad (5.5.3-1)$$

(AASHTO C6.12.2.2.2-5)

where

$$M_{e.LTB} = \frac{\pi}{L_b} \sqrt{EI_y GJ} \quad (5.5.3-2)$$

(AASHTO C6.12.2.2.2-1)

is the theoretical elastic LTB bending resistance for uniform bending (i.e., the beneficial effects of moment gradient are neglected).

If one substitutes $G = E/2(1 - \nu) = E/2.6$ and

$$J = \frac{4A^2}{\Sigma(b/t)} \quad (5.5.3-3)$$

(AASHTO C6.12.2.2.2-3)

into Eq. (2), where

A = the area enclosed within the centerlines of the plates,

b = the clear distance between the plates, and

t = thickness of the plates.

and then substitutes Eq. (2) into Eq. (1), the nominal flexural resistance may be expressed as

$$M_n = M_{yc} \left[1 - \frac{0.064M_{yc}L_b}{AE} \sqrt{\frac{\Sigma(b/t)}{I_y}} \right] \quad (5.5.3-4)$$

(AASHTO 6.12.2.2.2-1)

after some algebraic manipulation.

Equation (5.5.3-4) is not intended for checking of closed-box section girders in their noncomposite condition during construction. It is intended for checking of homogeneous doubly-

symmetric box-section members in trusses, frames, arches, and other miscellaneous applications. The checking of closed-box section girders in their noncomposite condition is addressed previously in Section 5.4.8 of this module. For these sections, noncomposite stiffened or unstiffened box-flanges in compression are checked for a flange local buckling limit state as illustrated in Figure 79, and the box-flanges in tension are checked for the tension yielding limit state represented by Eq. (5.4.7-4). The lateral-torsional buckling limit state is assumed not to govern, and no LTB check is required. Of course, the b/t ratios for the web and flange plates of box girders can be significantly larger than the b/t limits required for the miscellaneous box-section members for which Article 6.12.2.2.2 applies.

AISC (2010) takes a different approach in quantifying the flexural resistance of homogeneous doubly-symmetric noncomposite box-section members. The AISC (2010) box-section member provisions address cases with compact, noncompact or slender unstiffened flanges (i.e., no longitudinal stiffeners) and compact or noncompact webs. The AISC rules neglect the LTB limit state, partly because of the minor reduction in the LTB resistance obtained for uniform bending (but using a linear transition equation for the inelastic buckling region rather than the CRC Eq. (1)), and partly because a moment modifier C_b only slightly greater than one makes this reduction nonexistent. Furthermore, AISC (2010) allows the calculation of resistances larger than M_y and gives $M_n = M_p$ if the compression flange and the web of the section are compact. The AISC (2010) Section F7 provisions define the FLB resistance as

$$M_n = M_p - (M_p - M_{yc}) \left(3.57 \frac{b_{fc}}{t_{fc}} \sqrt{\frac{F_{yc}}{E}} - 4.0 \right) \leq M_p \quad (5.5.3-5)$$

(AISC F7-2))

for box-section members with noncompact flanges. This equation gives $M_n = M_p$ for

$$\frac{b_{fc}}{t_{fc}} \leq \left[\lambda_{pf} = 1.12 \sqrt{\frac{E}{F_{yc}}} \right] \quad (5.5.3-6)$$

where the above λ_{pf} is the AISC compactness limit for box flanges. It gives $M_n = M_{yc}$ for

$$\frac{b_{fc}}{t_{fc}} = \left[\lambda_{rf} = 1.40 \sqrt{\frac{E}{F_{yc}}} \right] \quad (5.5.3-7)$$

where λ_{rf} is the general AISC limit for a noncompact box flange. For larger flange slenderness values, the AISC FLB resistance is expressed as

$$M_n = F_{yc} S_{eff} \quad (5.5.3-8)$$

(AISC F7-3)

where S_{eff} is the effective section modulus determined using the effective width of the compression flange from Eq. (5.2.4-10) with $f = F_{yc}$.

Section F7 of AISC (2010) handles the influence of a noncompact web by requiring an independent web local buckling (WLB) limit state check:

$$M_n = M_p - (M_p - M_{yc}) \left(0.305 \frac{D}{t_w} \sqrt{\frac{F_{yc}}{E}} - 0.738 \right) \leq M_p \quad (5.5.3-9)$$

(AISC F7-5)

This equation gives $M_n = M_p$ for

$$\frac{D}{t_w} \leq \left[\lambda_{pw} = 2.42 \sqrt{\frac{E}{F_{yc}}} \right] \quad (5.5.3-10)$$

where λ_{pw} is the AISC web compactness limit for box sections, and it gives $M_n = M_y$ for

$$\frac{D}{t_w} \leq \left[\lambda_{rw} = 5.7 \sqrt{\frac{E}{F_{yc}}} \right] \quad (5.5.3-11)$$

which is the noncompact limit for box-section member webs in AISC (same as the noncompact limit for I-section member webs).

The AISC (2010) equations generally give $M_n \geq M_{yc}$ as long as the compression flange is not slender. However, the AASHTO (2014) Eq. (4) generally gives M_n slightly less than M_{yc} . The AISC (2010) equations provide the most representative characterization of the flexural resistance of straight box sections having compact or noncompact webs without longitudinal stiffeners. Conversely, the AASHTO (2014) Article 6.11.3 provisions are the most appropriate for checking of box girders in their noncomposite condition, since these types of members often have slender webs and are horizontally curved. Equation (4) from AASHTO (2014) Article 6.12.2.2.2 is recommended for box-section arch ribs, particularly for arch ribs with longitudinally-stiffened webs. This is because the web and web longitudinal stiffener requirements of AASHTO Article 6.14.4.2 do not address the development of flexural capacities larger than M_{yc} (see Section 5.2.4 of this module), and Eq. (4) provides some additional conservatism with respect to potential LTB limit states for these types of members. Equation (4) is generally conservative compared to the AISC (2010) provisions for box-section members where both the AASHTO and the AISC rules are applicable.

5.5.4 Circular Tubes

AASHTO (2014) adopts the following equations directly from AISC (2010) for the nominal flexural resistance of noncomposite circular tubes having D/t ratios less than $0.45E/F_y$:

$$M_n = M_p \quad \text{for } D/t \leq 0.07 E/F_y \quad (5.5.4-1)$$

(AASHTO 6.12.2.2.3-1, AISC F8-1)

$$M_n = \left(\frac{0.021E}{D/t} + F_y \right) S \quad \text{for } 0.07 E/F_y < D/t \leq 0.31 E/F_y \quad (5.5.4-2)$$

(AASHTO 6.12.2.2.3-2, AISC F8-2)

$$M_n = \frac{0.33ES}{D/t} \quad \text{for } D/t \leq 0.31 E/F_y \quad (5.5.4-3)$$

(AASHTO 6.12.2.2.3-3 & 6.12.2.2.3-4, AISC F8-3 & F8-4)

The failure modes and postbuckling behavior of these types of members can be grouped into the following three categories (Sherman 1992; Ziemian 2010):

1. For D/t less than about $0.05E/F_y$, a long inelastic plateau occurs in the moment-rotation curve. The cross-section gradually ovalizes, then local wave buckles eventually form, after which the moment resistance slowly decays. The flexural resistance may exceed the theoretical plastic moment due to strain hardening.
2. For $0.05E/F_y \leq D/t \leq 0.10E/F_y$, the plastic moment is nearly achieved but a single local buckle develops and the moment decays slowly with little or no inelastic plateau.
3. For $D/t > 0.10E/F_y$, multiple buckles form suddenly with little ovalization, and the bending moment drops rapidly to a more stable level.

The above equations reflect the above regions of behavior for specimens with long constant moment regions and little restraint against ovalization at the failure location. They are based on five North American studies involving hot-formed seamless pipe, electric-resistance-welded pipe and fabricated tubing (Sherman 1992; Ziemian 2010).

5.5.5 Tees and Double Angles in Strong-Axis Bending

AASHTO (2014) uses the AISC (2010) equations in large part for calculation of the flexural resistance of tees and double angles. For bridges, one of the most important practical usage of the AISC equations is in determining the capacity of Tee-section members subjected to eccentric axial tension or compression (due to the attachment of the Tee flange to end gusset plates). The AISC (2010) and AASHTO (2014) provisions utilize a simplified elastic LTB equation developed by Kitipornchai and Trahair (1980). Ellifritt et al. (1992) review this equation and other prior AISC equations for tees and compare the results to experimental tests. The AISC (2010) and AASHTO (2014) LTB resistances are expressed as

$$M_n = \frac{\pi \sqrt{EI_y GJ}}{L_b} \left[B + \sqrt{1 + B^2} \right] \leq M_{\max} \quad (5.5.5-1)$$

(AASHTO 6.12.2.2.4-2, AISC F9-4)

where

$$B = \pm 2.3 \frac{d}{L_b} \sqrt{\frac{I_y}{J}} \quad (5.5.5-2)$$

(AASHTO 6.12.2.2.4-3, AISC F9-5)

d is the total depth of the section, the plastic moment capacity is defined as

$$M_{max} = F_y Z_x \leq 1.6M_y \quad \text{for stems in tension} \quad (5.5.5-3a)$$

$$\leq M_y \quad \text{for stems in compression} \quad (5.5.5-3b)$$

(AASHTO 6.12.2.2.4-1, AISC F9-1 to F9-3)

M_y = the yield moment of the cross-section, based on the distance to the tip of the tee stem,

and the other parameters have been defined previously. The plus sign in Eq. (2) applies when the stem is in tension and the minus sign applies when the stem is in compression. If the tip of the stem is in compression anywhere along the unbraced length, the provisions require the use of the negative value of B . The $1.6M_y$ limit on M_{max} for cases with the stem in tension is intended indirectly to eliminate situations where significant yielding of the stem would occur at service load levels. Also, the AISC and AASHTO provisions require checking of flange local buckling (FLB) when the flange is subjected to flexural compression. The FLB resistance may be expressed as

$$M_n = M_p - (M_p - 0.7M_y) \left(\frac{b_{fc}/2t_{fc} - 0.38\sqrt{E/F_y}}{0.62\sqrt{E/F_y}} \right) \leq 1.6M_y \quad (5.5.5-3)$$

(AASHTO 6.12.2.2.4-4, 5 & 6, AISC F9-6)

for tee section flanges with slenderness values ranging between the compact and noncompact limits, which are the same limits as for rolled I-section members (see Eqs. (5.3.5-16) and (5.3.5-26)). AISC (2010) also provides a resistance equation for tee sections with slender flanges. However, none of the ASTM A6 tee sections have slender flange elements and the corresponding $b_f/2t_f$ values for elastic FLB are larger than the AASHTO Article 6.10.2.2 limit for I-sections. This limit is assumed as an intended AASHTO (2014) maximum for tee sections.

Equation (1) does not contain any C_b factor. The C_b factor used for I-section members is unconservative for tees with the stem in compression (AISC 2010). For these cases, $C_b = 1.0$ is appropriate. For reverse curvature bending, the portion with the stem in compression may govern the LTB resistance even though the corresponding moments may be small relative to other portions of the unbraced length. This is because the LTB strength of a tee with the stem in compression is substantially smaller than that for the stem in tension. Since the LTB strength is sensitive to the moment diagram, AISC (2010) conservatively takes $C_b = 1.0$ for all cases. The commentary of AISC (2010) also cautions that in cases where the stem is in tension, the connection details should be designed to minimize end restraining moments that may cause the stem to be in flexural compression.

AASHTO (2014) does not provide any λ_p or λ_r limits for local buckling of tee stems loaded in flexural compression. This is because the above LTB equations give the stem local buckling strength in the limit of $L_b = 0$. By substituting $L_b = 0$ into Eqs. (1) and (2), one obtains $M_n = 0/0$. However, by using L'Hospital's rule, the following equation is obtained in the limit of zero unbraced length (AISC 2005):

$$M_n = \frac{\pi EJ \sqrt{G/E}}{4.6d} = 0.424 \frac{EJ}{d} \leq M_y \quad (5.5.5-4)$$

(AISC C-F9-1)

The 2010 AISC Specification provides explicit equations for the local buckling strength of Tee stems in flexural compression. The AISC (2010) Commentary indicates that the former approach was correct, but that additional explicit equations are provided in the latest Specification to alleviate confusion among users of the Specification. The 2010 Commentary provides a derivation of these updated explicit equations, which strictly speaking, are unnecessary.

The AISC (2010) Commentary also provides guidelines for calculating the resistance of tees and double-angles bent about the y-axis. This case is not addressed in this module, since it is expected to be rare for bridge applications.

5.5.6 Channels in Strong- and Weak-Axis Bending

AASHTO (2014) adopts the AISC (2010) provisions for calculation of the flexural resistance of channels. AISC (2010) uses a generalized form of the compact I-section member equations for channels subjected to major-axis bending. This generalized form simply uses

$$X^2 = \frac{S_x h}{J c} \quad (5.5.6-1)$$

where

$$c = \begin{cases} 1 & \text{for doubly-symmetric I-shapes} \\ \frac{h}{2} \sqrt{\frac{I_y}{C_w}} & \text{for channels} \end{cases} \quad (5.5.6-2)$$

in place of Eq. (5.3.5-20). This equation simply allows a conversion from the implicit warping constant C_w for doubly-symmetric I-section members to the C_w for channel sections. This generalized form also uses Eq. (5.3.5-21) for the radius of gyration term r_t . The LTB resistance equations, i.e., Eqs. (5.3.5-19), (5.3.5-24), etc., are otherwise unchanged. The AISC (2010) equations for channels assume compact flanges and webs. All of the ASTM A6 channels have compact flanges and webs for $F_y \leq 65$ ksi. As such, the flanges and webs of fabricated channels must satisfy Eqs. (5.3.5-16) and

$$\frac{D}{t_w} \leq 3.76 \sqrt{\frac{E}{F_y}} \quad (5.5.6-3)$$

respectively.

The AISC (2010) resistance equations for channels in major-axis bending are based on the assumption that the other members that frame into the channel are sufficient to restrain the twisting of the member (Johnston 1976; McGuire 1968). Based on this assumption, bending without twisting occurs between the supports.

AASHTO (2014) also bases its provisions for weak-axis bending of channels on the corresponding AISC (2010) Section F6 provisions. For channel-section members subjected to minor-axis flexure, AISC (2010) uses its equations for minor-axis flexure of I-section members (see Section 5.5.2 of this module). AISC (2010) places a limit of $1.6F_yS_y$ on the maximum minor-axis bending flexural resistance. For I-section members, the shape factor Z_y/S_y is nearly always less than 1.6 (only four ASTM A6 W-shapes have a $Z_y/S_y > 1.6$). However, for channel-sections, Z_y/S_y is generally greater than 1.6. Similar to the $M_{max} = 1.6M_y$ limit for tee-sections with the stem in tension, the use of $M_{max} = 1.6F_yS_y$ for channel sections is intended to indirectly prevent substantial yielding at service load levels. Interestingly, the AISC (2010) Section F6 provisions do not give any restriction on the slenderness of the web for channels in weak-axis bending. However, if the web is loaded in flexural compression, the AISC Section F6 provisions are based implicitly on a compact web response. The slenderness limit

$$\frac{D}{t_w} \leq 1.12 \sqrt{\frac{E}{F_y}} \quad (5.5.6-4)$$

may be taken as a sufficient requirement to ensure the compact behavior of the web in this case. AASHTO (2014) specifies Eq. (5.5.6-3) instead, which is in error since this equation is for a web bent about an axis normal to its plane.

5.5.7 Rectangular Bars and Rounds

In addition, AASHTO (2014) uses the AISC (2010) for calculation of the flexural resistance of rectangular bars and rounds. For rectangular bars bent about their major-axis, the AISC (2010) resistances are based on lateral-torsional buckling and have the same form as shown previously in Figure 60. For these member types, the maximum potential resistance is

$$M_{max} = M_p \quad (5.5.7-1)$$

(AASHTO 6.12.2.2.7-1, AISC F11-1)

Anchor Point 1 has the abscissa

$$L_p = 0.08 \frac{t^2 E}{d F_y} \quad (5.5.7-2)$$

where d and t are the section depth and width respectively, and Anchor Point 2 has the abscissa

$$L_r = 1.9 \frac{t^2 E}{d F_y} \quad (5.5.7-3)$$

and an ordinate of M_y (i.e., residual stress effects are neglected at the elastic-to-inelastic LTB transition point). Furthermore, the nominal elastic LTB capacity may be expressed for these sections in terms of the bending moment or in terms of the maximum bending stress, respectively, as:

$$M_{e.LTB} = C_b \frac{\pi}{L_b} \sqrt{EI_y GJ} = C_b \frac{\pi}{L_b} \frac{E}{\sqrt{2.6}} \sqrt{\frac{dt^3}{12} \frac{dt^3}{3}} = 0.32 C_b E \frac{dt^3}{L_b} \quad (5.5.7-4)$$

$$F_{e.LTB} = \frac{M_{e.LTB}}{S_x} = C_b \frac{1.9E}{L_b d / t^2} \quad (5.5.7-5)$$

(AASHTO 6.12.2.2.7-3, AISC F11-3 & F11-4)

For solid rounds and rectangular bars bent about their minor axis, AISC and AASHTO give the flexural resistance as

$$M_n = M_p \leq 1.6M_y \quad (5.5.7-6)$$

One might note that AISC (2010) and AASHTO (2014) also specify the limit of $1.6M_y$ with Eq. (5.5.7-1). However, since the shape factor for a rectangular bar is equal to 1.5, the limit $1.6M_y$ is never reached for these sections.

5.5.8 Single Angles

Single angles are generally not intended as flexural members in bridge construction. Furthermore, the practical condition of flexure due to eccentric axial compression is addressed via the equivalent slenderness, KL/r , expressions discussed in Section 5.2.3 of this module, and the practical condition of flexure due to eccentric axial tension is addressed via the shear lag coefficient U (see Section 5.5.1). Therefore, the calculation of the flexural resistance of single-angle members is not addressed in this document. The reader is referred to AISC (2010) and the references provided in the commentary of the AISC Specification for flexural resistance equations and discussion of the flexural behavior of single-angle members.

5.5.9 Concrete-Encased and Filled Members

5.5.9.1 AASHTO (2014) - AISC (1999) approach

For concrete-encased shapes that satisfy specific detailing requirements on the lateral and longitudinal reinforcement, AASHTO (2014) Article 6.12.2.3.1 defines the flexural resistance for members that are not subjected to any axial compression as the smaller of:

1. The plastic moment resistance of the steel section alone, M_{ps} , and
2. The yield moment of the composite section, M_{yc} , determined accounting for the different moments applied to the noncomposite, long-term composite, and short-term composite cross-sections, and neglecting any of the concrete loaded in tension.

The concrete is assumed to prevent local buckling of the steel, and hence concrete-encased shapes are not subject to the width/thickness limitations of Article 6.9.4.2 (discussed in Section 5.2.4 of this module).

Furthermore, for concrete-encased shapes subjected to combined compression and flexure with $P_u/\phi_c P_n \geq 0.3$, Article 6.12.2.3.1 specifies that the flexural resistance may be calculated as

$$M_n = M_{ps} + \frac{(H_c - 2c)A_{rs}F_{yrs}}{3} + \left(\frac{H_c}{2} - \frac{A_w F_y}{1.7 f'_c B_c} \right) A_w F_y \quad (5.5.9-1)$$

(AASHTO 6.12.2.3.1-3)

Where

A_{rs} = total area of the longitudinal bar reinforcement in the composite column cross-section,

A_w = the web area of the structural steel section, $d t_w$,

B_c = the width of the composite cross-section perpendicular to the plane of flexure,

F_y = the yield strength of the structural steel section,

F_{yrs} = the yield strength of the reinforcing steel,

H_c = the depth of the composite cross-section in the plane of flexure,

M_{ps} = the fully-plastic resistance of the steel section,

c = the average distance from the compression face to the longitudinal reinforcement adjacent to that face and the distance from the tension face to the longitudinal reinforcement adjacent to that face,

f'_c = the specified minimum 28-day compressive strength of the concrete.

Equation (1) gives a simplified estimate of the appropriate fully-plastic flexural resistance for use with the AASHTO (2014) beam-column strength interaction equations. The first, second and third terms of this equation are the estimated plastic moment contributions from the steel shape, the reinforcing bars, and the reinforced concrete respectively. In the second term, it is assumed that at least one-third of the longitudinal bars in the cross-section can be considered to be located at the distance c from the tension and compression faces of the cross-section. To obtain the third term, the web of the encased shape is taken as a tension reinforcement for a concrete cross-section with a flexural depth equal to half the overall depth of the composite section in the plane of bending.

If $P_u/\phi_c P_n$ is less than 0.3, AASHTO Article 6.12.2.3.1 requires that the flexural resistance shall be determined by a straight-line transition between the value obtained from Eq. (1) at $P_u/\phi_c P_n = 0.3$ and the flexural resistance at $P_u = 0$.

The above approach is supported by comparisons to 44 beam-column tests with concrete-encased steel shapes (Galambos and Chapuis 1980). This approach is essentially the same as the method

detailed in AISC (1999). The only difference is that the AASHTO procedure does not allow for any consideration of the influence of shear connectors. The AISC (1999) provisions allow the flexural resistance at $P_u = 0$ to be taken as the corresponding beam fully-plastic composite section resistance if adequate shear connectors are provided and the concrete longitudinal and lateral bars meet specific requirements. Also, when shear connectors are not provided, AISC (1999) specifies that either the steel section plastic moment resistance or the composite section yield resistance at $P_u = 0$ may be used in determining the nominal flexural capacity.

For concrete-filled sections, AASHTO (2014) assumes the use of circular tubes and uses the following flexural resistance equations. These are the former AASHTO (2005) equations for noncomposite circular tube sections:

$$M_n = M_{ps} \quad \text{for } \frac{D}{t} < 2\sqrt{\frac{E}{F_y}} \quad (5.5.9-2, \text{ AASHTO 6.12.2.3.2-1})$$

and

$$M_n = M_y \quad \text{for } 2\sqrt{\frac{E}{F_y}} \leq \frac{D}{t} \leq 8.8\sqrt{\frac{E}{F_y}} \quad (5.5.9-3, \text{ AASHTO 6.12.2.3.2-2})$$

This appears to be a simplification of the AISC (1999) provisions. For filled sections, AISC (1999) specifies the use of the same approach as defined above for encased sections, but with A_w taken equal to zero in Eq. (1). This approach is supported by comparisons to 48 beam-column tests of concrete-filled pipe and tubing (Galambos and Chapuis 1980).

AISC (1999) Section I2.4 specifies a number of shear connector requirements for transfer of the axial force from the steel to the concrete or vice-versa, to ensure that the steel and the concrete work compositely. For concrete-encased members, AISC (1999) Section I2.4 requires that an adequate number of shear connectors must be provided along the length of the member to develop the axial forces into the composite cross-section. The maximum spacing of these connectors is not allowed to exceed 16 in, and connectors are required on at least two faces of the steel shape in a configuration symmetrical about the cross-section. The commentary of AISC (1999) indicates that force transfer by bond is generally disregarded in encased members, but is commonly used in concrete-filled HSS members as long as the connections are detailed to limit local deformations. However, it notes that no guidelines are available for structures other than fixed offshore platforms. No specific guidelines are provided for the shear connector requirements in concrete-filled members in the AISC (1999) Specification. Also, no specific shear connector requirements are provided for development of the bending moments into the composite cross-section of concrete-encased or filled members.

5.5.9.2 AISC (2010) Approach

The AISC (2010) provisions for the nominal flexural resistance of concrete-encased and compact filled members are essentially the same as AISC (1999) for the case of $P_u = 0$. Also, presumably, Eq. (1) and the linear interpolation between this equation and the strength at $P_u = 0$ is still allowed for concrete encased members where the shear transfer between the concrete and the

steel is not provided according to the Specification requirements. However, AISC (2010) emphasizes a direct plastic stress distribution based approach that provides significantly enhanced strength estimates for members that have adequate shear transfer between the concrete and the steel. Section 5.6.3 of this module explains this enhanced procedure. In addition, AISC (2010) provides additional equations that quantify a reduced flexural resistance for filled composite sections where the steel section is classified as noncompact or slender in flexural compression (see Section 5.2.7 for a description of these and other definitions of “compact,” “noncompact,” and “slender” in the AISC (2010) and AASHTO (2014) Specifications).

AISC (2010) provides substantial new information about force transfer mechanisms and concrete anchorage and shear connector requirements for composite members.

5.6 Combined Flexure and Axial Load

5.6.1 Introduction

Section 5.1 of this module addresses the resistance of members under concentric axial tension, Section 5.2 addresses the resistance of members under concentric axial compression, and Sections 5.3 through 5.5 address the flexural resistance of I- and box-section members and members with other miscellaneous cross-section profiles respectively. For members subjected to combined bending and axial load, commonly referred to as beam-columns, the AASHTO (2014) and AISC (2010) Specifications define the resistance by interaction equations that reduce to the above resistances in the limit of pure axial loading (with zero flexure) or flexure about a single principal axis (with zero axial load). Section 5.6.2 summarizes the strength interaction equations defined in AASHTO (2014) and in the primary AISC (2010) beam-column provisions. Section 5.6.3 then discusses the physical interaction between the axial and flexural resistances for various types of noncomposite steel members. Finally, Section 5.6.4 outlines these interaction relationships for composite steel-concrete beam-columns. Section 5.6.5 provides concluding remarks.

5.6.2 AASHTO (2014) and Primary AISC (2010) Beam-Column Interaction Equations

AASHTO (2014) Articles 6.8.2.3 and 6.9.2.2 and the primary AISC (2010) Section H1 provisions specify the following bilinear relationship to define the resistance of members subjected to combined axial loading and flexure

$$\frac{P_u}{2\phi_c P_n} + \frac{M_{ux}}{\phi_f M_{nx}} + \frac{M_{uy}}{\phi_f M_{ny}} \leq 1.0 \quad \text{for } \frac{P_u}{\phi_c P_n} < 0.2 \quad (5.6.2-1a)$$

(AASHTO 6.8.2.3-1 & 6.9.2.2-1, AISC H1-1b)

$$\frac{P_u}{\phi_c P_n} + \frac{8}{9} \left(\frac{M_{ux}}{\phi_f M_{nx}} + \frac{M_{uy}}{\phi_f M_{ny}} \right) \leq 1.0 \quad \text{for } \frac{P_u}{\phi_c P_n} \geq 0.2 \quad (5.6.2-1b)$$

(AASHTO 6.8.2.3-2 & 6.9.2.2-2, AISC H1-1a)

Where

P_u = the maximum axial force along the member unbraced length under consideration

resulting from the factored loads,

M_{ux} and M_{uy} = the maximum second-order elastic moments along the member unbraced length under consideration, taken respectively about the cross-section x- and y-axes,

$\phi_c P_n$ = the factored tensile or compressive axial resistance corresponding to the unbraced length under consideration,

$\phi_f M_{nx}$ and $\phi_f M_{ny}$ = the factored flexural resistance about the cross-section x- and y-axes corresponding to the unbraced length under consideration.

The above definitions are strictly applicable only for prismatic members. For nonprismatic members, P_u and $\phi_c P_n$ are based on the cross-section having the largest value of $P_u/QP_y = f_a/QF_y$ combined with the governing member elastic buckling load ratio for the unbraced segment $\gamma_e = P_e/P_u = F_e/f_a$ (see Section 5.2.6). Similarly, M_{ux} , M_{uy} , $\phi_f M_{nx}$ and $\phi_f M_{ny}$ are based on the cross-section having the largest values of M_{ux}/M_{ycx} and M_{uy}/M_{yey} for checking the lateral-torsional buckling limit state (in cases where this limit state is applicable), combined with the member elastic buckling load ratio $\gamma_{e.LTB} = F_{e.LTB}/f_{bu.max}$ (see Section 5.3.6). In the above expressions, M_{ycx} and M_{yey} are the nominal yield moments corresponding to the extreme fiber in compression for flexure about the cross-section x- and y-axes respectively. For checking of flange local buckling or tension flange yielding limit states, in cases where these limit states are applicable, the ratios $M_{ux}/\phi_f M_{nx}$ and $M_{uy}/\phi_f M_{ny}$ are checked at all the cross-sections along the unbraced length under consideration. The largest values of $M_{ux}/\phi_f M_{nx}$ and $M_{uy}/\phi_f M_{ny}$ from all the applicable flexural limit state checks are inserted into Eqs. (1) for checking the member resistance under the combined loading conditions.

The largest value of $P_u/\phi_c P_n$ from all the applicable axial resistance limit states (i.e., tension yielding, tension fracture, flexural buckling about the cross-section x-axis, flexural buckling about the cross-section y-axis, torsional buckling or torsional-flexural buckling) is inserted in Eqs. (1) for checking the strength interaction. Similarly, the largest values of $M_{ux}/\phi_f M_{nx}$ and $M_{uy}/\phi_f M_{ny}$ from all the applicable flexural resistance limit states (i.e., local buckling, yielding or lateral-torsional buckling) also are inserted in Eqs. (1). It should be noted that the largest values of $P_u/\phi_c P_n$, $M_{ux}/\phi_f M_{nx}$ and $M_{uy}/\phi_f M_{ny}$ may occur at different cross-sections along the length of the unbraced segment under consideration. This is in general a conservative simplification. The buckling limit states strictly do not correspond to an individual cross-section. They depend on the loadings, properties and boundary conditions along the full x- and y-axis unbraced lengths. For bridge engineering, the applied moments, M_{ux} and M_{uy} , are obtained in the vast majority of cases by applying amplification factors to first-order elastic moments obtained from structural analysis at the various required factored loadings.

Strictly speaking, the $P_u/\phi_c P_n$, $M_{ux}/\phi_f M_{nx}$ and $M_{uy}/\phi_f M_{ny}$ ratios used in Eqs. (1) should be concurrent values taken from the same factored loading combination. However, this requires that the above process be applied separately for each factored load combination, including all the appropriate positions of live load on the structure. Although this is theoretically not a problem in theory for computerized assessment, such an approach can be prohibitive. This is particularly true when one realizes that the concurrent loadings giving the maximum value of the unity check in Eqs. (1) may actually occur for a situation where none of the above strength ratios are at their

individual maximum values. The maximum envelope values of $P_u/\phi_c P_n$, $M_{ux}/\phi_f M_{nx}$ and $M_{uy}/\phi_f M_{ny}$ may be combined conservatively for practical checking of the members.

With one minor restriction (discussed subsequently), Eqs. (1) are applicable for all doubly- and singly-symmetric section members, including rolled I-sections, channels, tee-shapes, round, square and rectangular HSS, solid rounds, squares or rectangles, and any of the many possible combinations of doubly- or singly-symmetric members fabricated from plates and/or shapes by welding or bolting (AISC 2010). They also, except for one restriction, give an accurate to conservative characterization of the resistance of composite members subjected to combined axial loading and flexure (i.e., encased I-section members, concrete filled tubes, and I-members with a composite concrete slab). Nevertheless, Eqs. (1) were developed predominantly based on studies of noncomposite compact I-section members subjected to combined axial loading and flexure. Therefore, in the following, the relationship between these equations and the physical responses of compact I-section beam-columns is summarized first. This is followed by a discussion of the predictions from Eqs. (1) versus the physical responses for other member types.

5.6.3 Noncomposite Members

5.6.3.1 In-plane resistance of doubly-symmetric I-section members subjected to axial load and major- or minor-axis bending

Figure 82 shows representative nominal first-yield and “exact” fully-plastic axial force-moment strength envelopes for two short compact doubly-symmetric I-section members subjected to major-axis bending moment. These envelopes are identical for either axial tension or compression or for positive or negative bending moment. Therefore, only one quadrant of the strength envelopes is shown. One of the sections considered is a W40x167, which is representative of a “beam-type” wide-flange section (deep web and relatively narrow flanges). The other section is a W14x257, which is representative of a “column-type” wide-flange section (web depth and flange width nearly the same). The fully-plastic strength envelope is slightly less convex for the column-type section. However, the normalized initial-yield envelopes are essentially the same.

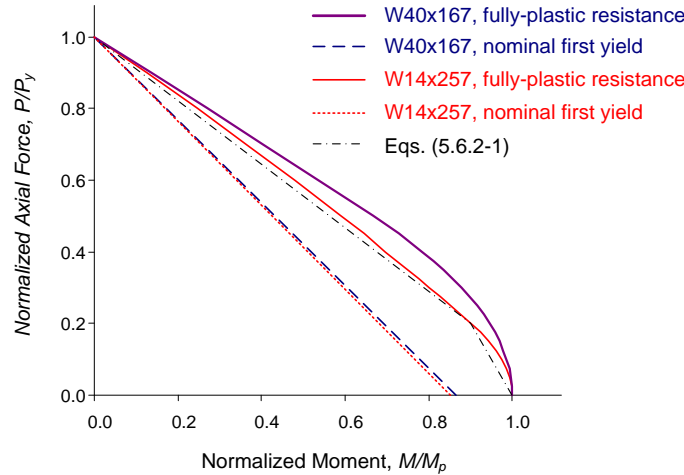


Figure 82 Representative first-yield and fully-plastic axial force-moment strength envelopes for short compact doubly-symmetric I-section members subjected to major-axis bending.

The figure also shows the result from Eqs. (5.6.2-1) with ϕ_c and ϕ_f taken equal to 1.0. For these ideal short compact-section members, the nominal axial resistance P_n is equal to the cross-section yield load P_y (assuming that net section fracture does not govern the resistance in tension) and the nominal flexural resistance is equal to the section plastic moment capacity M_p (again assuming that the tension flange fracture flexural limit state does not govern the resistance). One can observe that Eqs. (5.6.2-1) provide a reasonable lower-bound fit to the exact fully-plastic strength envelopes.

The nominal first yield curves in Figure 82 may be expressed simply as

$$\frac{P_u}{P_y} + \frac{M_u}{M_y} = 1 \quad (5.6.3-1a)$$

in terms of the axial force and moment, or equivalently

$$\frac{f_a}{F_y} + \frac{f_{bu}}{F_y} = 1 \quad (5.6.3-1b)$$

in terms of the corresponding additive elastic axial and flexural stresses, neglecting residual stress effects. If nominal residual stresses of F_r are assumed in compression at the flange tips and in tension at the mid-width of the flanges, the corresponding first yield condition is given by these equations with P_y , M_y and F_y replaced by $(1-F_r/F_y)P_y$, $(1-F_r/F_y)M_y$ and F_y-F_r .

Figure 83 compares the nominal first yield and fully-plastic axial force-moment strength envelopes for the same two short compact doubly-symmetric I-section members to Eqs. (5.6.2-1) for the case of combined axial loading and weak-axis flexure. The W40x167 fully-plastic strength curve is again more convex than the corresponding W14x257 curve. However, the

normalized first-yield envelope is slightly smaller for the W40x167 compared to that for the W14x257. In this case, one can observe that both of the theoretical fully-plastic resistance envelopes are significantly more convex than Eqs. (5.6.2-1), and that Eqs. (5.6.2-1) appear to provide a rather conservative estimate of the true capacity. Although this observation is correct, it only applies to short “stub-columns” or to members loaded in weak-axis flexure and axial tension. Figure 84 compares the maximum in-plane strength envelopes for strong- and weak-axis bending and axial compression on representative finite-length column-type wide-flange members with $L/r = 80$, taken from Maleck (2001), to the nominal resistance predictions from Eqs. (5.6.2-1). Although the stub-column (i.e., cross-section) strength envelope for weak-axis bending is significantly more convex than either of the Eqs. (5.6.2-1), or the exact fully-plastic strength envelopes for *strong-axis* bending, the beam-column resistances for all but very short members are similar regardless of the axis of bending. This is because the weak-axis flexural rigidity of an I-section reduces dramatically once yielding starts at the flange tips. The spread of yielding through the flanges has a less dramatic effect on the flexural rigidity as the first-yield strength is exceeded and the cross-section fully-plastic resistance is approached in major-axis bending. However, the larger reduction in the member stiffness that occurs for combined compression and weak-axis bending leads to larger inelastic stability ($P-\delta$) effects, which in turn reduces the finite-length member resistance to a strength envelope far below the idealized stub-column strength.

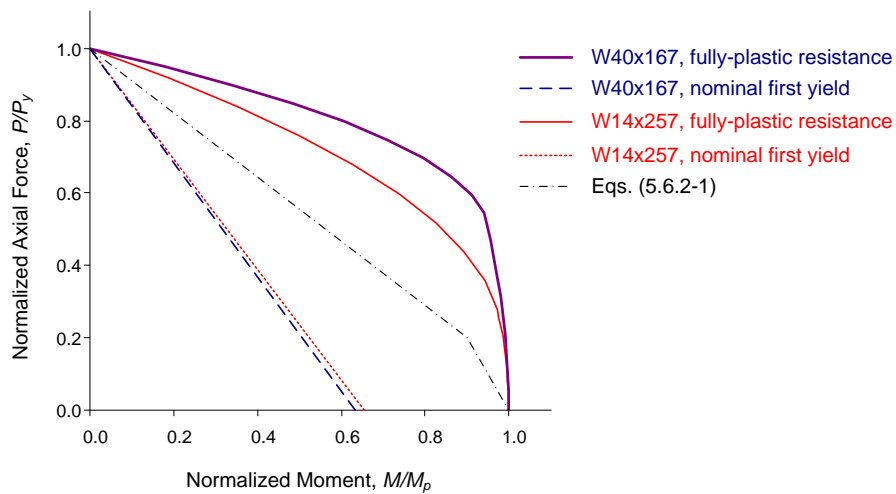


Figure 83 Representative first-yield and fully-plastic axial force-moment strength envelopes for short compact doubly-symmetric I-section members subjected to minor-axis bending.

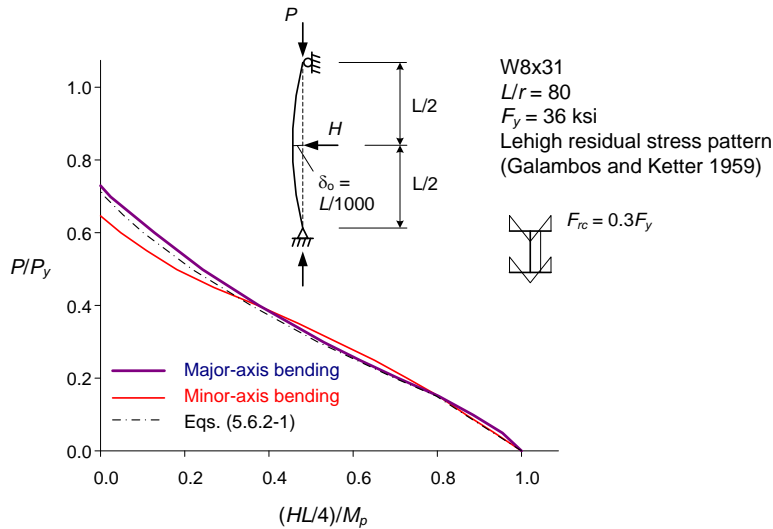


Figure 84 Representative maximum in-plane strength envelopes for strong- and weak-axis bending and axial compression on finite length column-type wide-flange members, from Maleck (2001).

Figure 85 illustrates the behavior for the above weak-axis bending example in greater detail. This figure shows the strength envelope from Figure 84, where the moment is defined as the first-order moment $M_1 = HL/4$ at the maximum load capacity of the member, the corresponding internal maximum *second-order inelastic* moment at the midspan of the member, $M_{2.inelastic} = M_1 + P\delta_{2.inelastic}$, and the corresponding internal maximum *second-order elastic* moment $M_{2.elastic} = M_1 + P\delta_{2.elastic} = AF M_1$. In these expressions, $\delta_{2.inelastic}$ is the “true” second-order inelastic lateral deflection relative to a straight chord at the midspan of the beam-column at the maximum load capacity of the member, including a nominal initial out-of-straightness of $\delta_o = L/1000$ as well as the influence of initial residual stresses, $\delta_{2.elastic}$ is the idealized second-order elastic displacement at the midspan for the nominally-elastic ideally-straight member, obtained from any legitimate second-order elastic analysis (e.g., a first-order elastic analysis combined with a second-order elastic amplification factor), and AF is the second-order elastic amplification factor for the member internal maximum moment.

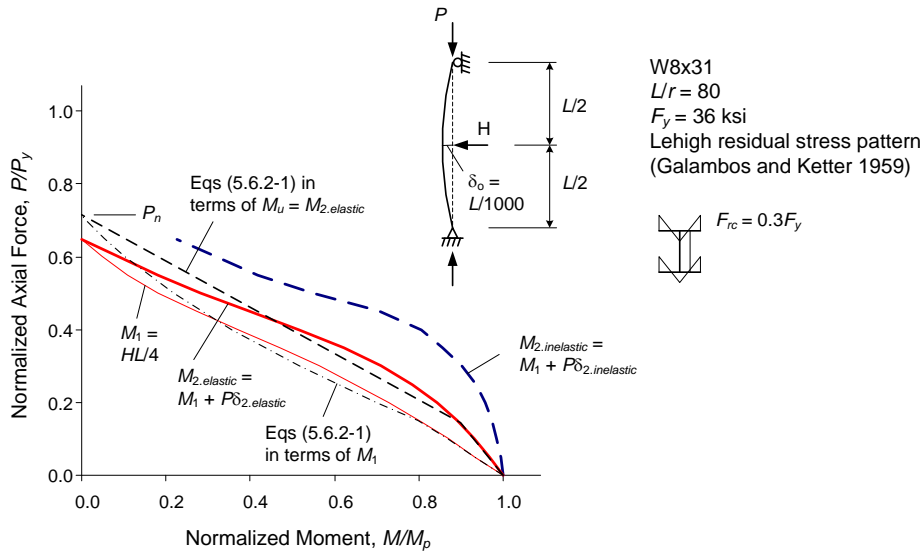


Figure 85 Strength interaction curves in terms of different calculated moments, $M_1 = HL/4$, $M_u = M_{2,elastic} = M_1 + P\delta_{2,elastic}$ and $M_{2,inelastic} = M_1 + P\delta_{2,inelastic}$ for the Figure 84 example beam-columns subjected to minor axis bending.

The P - M_1 and P - $M_{2,inelastic}$ curves in Figure 85 are obtained from refined distributed plasticity analyses of the beam-column. This type of analysis tracks the spread of yielding through the cross-sections and along the length of the member, including residual stress and initial geometric imperfections effects, and the corresponding gradual reduction in the member stiffness, with increases in the applied loads. Conversely, the P - $M_{2,elastic}$ curve is obtained by applying the second-order elastic amplification factor AF to the member maximum first-order moments $M_1 = HL/4$. The P - $M_{2,inelastic}$ curve falls inside of the bounds of the fully-plastic strength curve for the cross-section (not shown but similar to the W14x257 fully-plastic resistance curve in Figure 83). This is because the maximum load capacity of the member is reached due to a combination of yielding and stability effects prior to full plastification of the midspan cross-section. Part of the differences between the curves based on Eqs. (5.6.2-1) and the “exact” strength curves in Figure 84 and Figure 85 is due to the use of a single column strength equation for P_n . In general, the P_n from the Specification column strength equations tends to fall between the major- and minor-axis column strengths obtained from distributed plasticity analysis (see Figure 84). The accuracy of the fit by Eqs. (5.6.2-1) is generally improved if P_n is set to the corresponding column strength obtained from the distributed plasticity solutions.

The AASHTO (2014) - AISC (2010) Eqs. (5.6.2-1) were established in large part based on curve fitting to the results from a large number of beam-column solutions similar to those illustrated in Figure 85. Based on the definition of the internal moment M_u as the maximum second-order elastic moment within the unbraced length under consideration, determined from an analysis of the nominally-elastic ideally-straight member (i.e., $M_u = M_{2,elastic}$), the P - $M_{2,elastic}$ curve in Figure 85 is the appropriate “exact” curve that the beam-column strength interaction equation represents. The AASHTO (2014) - AISC (2010) Eqs. (5.6.2-1) provide an accurate to conservative fit to the rigorous P - $M_{2,elastic}$ curves for all of the strong- and weak-axis bending cases studied in their development (LeMessurier 1985; Liew et al. 1992; ASCE 1997; Maleck

and White 2003). In general, Eqs. (5.6.2-1) give a superb fit for strong-axis bending and L/r from 0 to 100. They are increasingly conservative for the weak-axis case when L/r is less than about 40. This is due to the large shape factor and significant convexity of the cross-section fully-plastic strength for weak-axis bending of I-shapes. They are moderately conservative for both axes when L/r is greater than 120. Also, for sidesway-inhibited cases, Eqs. (5.6.2-1) tend to be somewhat more conservative for beam-columns subjected to reversed-curvature bending than for cases involving single-curvature bending (Clarke and Bridge 1992). This is due to the fact that Eqs. (5.6.2-1) do not account for the influence of moment gradient on the shape of the strength envelope.

A few attributes of Eqs. (5.6.2-1) deserve highlighting:

- By curve fitting to the $P-M_{2,elastic}$ strength envelopes, the calculation of second-order effects via structural analysis (or by amplification of the first-order elastic internal moments) is clearly separated from the calculation of the member internal resistances P_n and M_n . Many prior steel design standards do not provide a clear separation between the consideration of second-order effects in the elastic structural analysis and the calculation of the member resistances. The separation of these two calculations facilitates the use of an explicit second-order elastic analysis to achieve a more accurate characterization of stability effects in cases where these effects are significant.
- The bilinear form given by Eqs. (5.6.2-1), which provides an accurate characterization of the fully-plastic resistance for a short I-section member subjected to major-axis bending, also provides an accurate fit to the majority of the strong- and weak-axis $P-M_{2,elastic}$ strength envelopes.
- The bilinear form given by Eqs. (5.6.2-1) combines the consideration of “member strength” and “member stability” into one single beam-column interaction curve. Many other prior and current steel design standards worldwide quantify the in-plane strength of steel beam-column members by a combination of two curves, one that addresses a member stability (or strength) limit and the other which addresses a member cross-section strength limit. However, all beam-columns of finite length fail physically by a combination of inelastic bending and stability effects. Equations (5.6.2-1) provide a simpler representation of member strengths that is truer to the fundamental attributes of the beam-column resistance (at least for members that fail by in-plane bending).

The reader is referred to Liew et al. (1992), ASCE (1997), and Maleck and White (2003) for further discussion of the in-plane strength interaction behavior of doubly-symmetric I-section members subjected to axial loading and major- or minor-axis bending.

The application of Eqs. (5.6.2-1) to other types of beam-column members and other types of strength limit states is generally ad hoc. Nevertheless, as noted in the previous section, within certain restrictions, these equations provide an accurate to conservative characterization of the member strength envelopes for all types of beam-column members. For instance, the in-plane beam-column resistance of compact square and rectangular welded box or HSS sections is very similar to that for I-section members in major-axis bending. The in-plane behavior of these types

of members is much the same as an I-section member with a single web thickness equal to the sum of the box or HSS section web thicknesses. The next section discusses the relationship between Eqs. (5.6.2-1) and the true in-plane and out-of-plane strength interaction curves for singly-symmetric members and/or members with noncompact or slender cross-section elements.

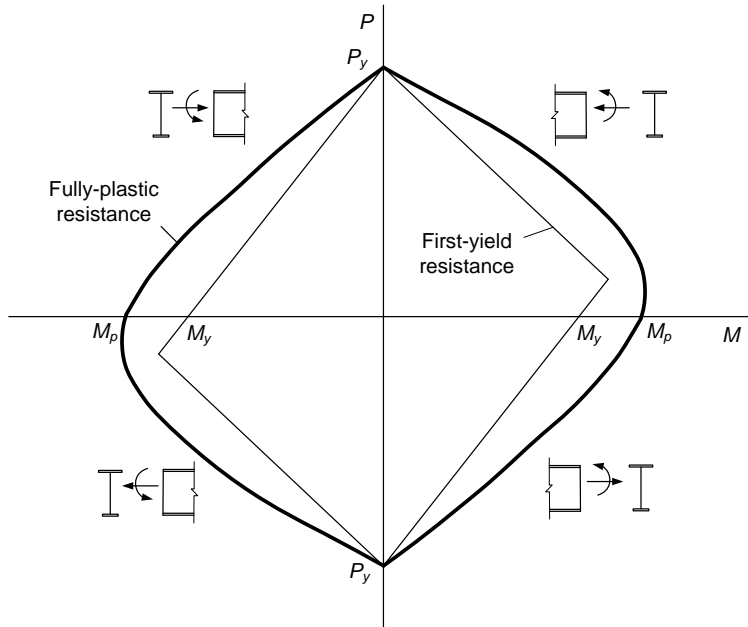


Figure 86 Representative first-yield and fully-plastic axial force-moment strength envelopes for a short compact singly-symmetric I-section member.

Figure 86 shows representative first-yield and fully-plastic axial force-moment strength envelopes for a short compact singly-symmetric I-section member. Interestingly, these envelopes are not symmetric. The strength interaction curves have a bulge in the quadrants where the axial and flexural stresses are additive either in compression or in tension on the larger flange. Of course, similar to the above results for doubly-symmetric I-section members, the fully-plastic cross-section strength is only an upper-bound theoretical limit. The actual resistance for a general singly-symmetric finite-length beam-column can be influenced by a combination of yielding, overall member stability and/or local member and cross-section distortional stability effects.

The dark solid curve in Figure 87 shows a representative strength envelope for a hypothetical simply-supported finite-length beam-column with noncompact and/or slender cross-section elements and a singly-symmetric cross-section profile. Also shown as dashed lines in the figure are the base AASHTO (2014) - AISC (2010) strength interaction curves given by Eqs. (5.6.2-1). White and Kim (2003) discuss the behavior of various strength interaction equations and review the limited experimental test results for prismatic doubly- and singly-symmetric I-section beam-columns with noncompact and/or slender webs and compact, noncompact and slender flanges. They conclude that the bilinear strength curves given by Eqs. (5.6.2-1) provide an accurate to conservative characterization of the in-plane and out-of-plane resistances from the available tests. Galambos (2001a & b) proposes a refined procedure for determining the resistance of prismatic singly-symmetric compact I-section members and makes similar observations

pertaining to Eqs. (5.6.2-1). Generally, Eqs. (5.6.2-1) provide an accurate to slightly conservative characterization of the in-plane resistance of singly-symmetric I-section members when the smaller flange is subjected to additive flexural and axial stresses. However, these equations tend to be somewhat conservative relative to the physical beam-column in-plane and out-of-plane resistances in many cases involving singly-symmetric I-section members when the larger flange is subjected either to additive axial and flexural compression or tension. The studies by Lee and Hsu (1981) provide evidence of this conclusion for tapered web singly-symmetric I-section members.

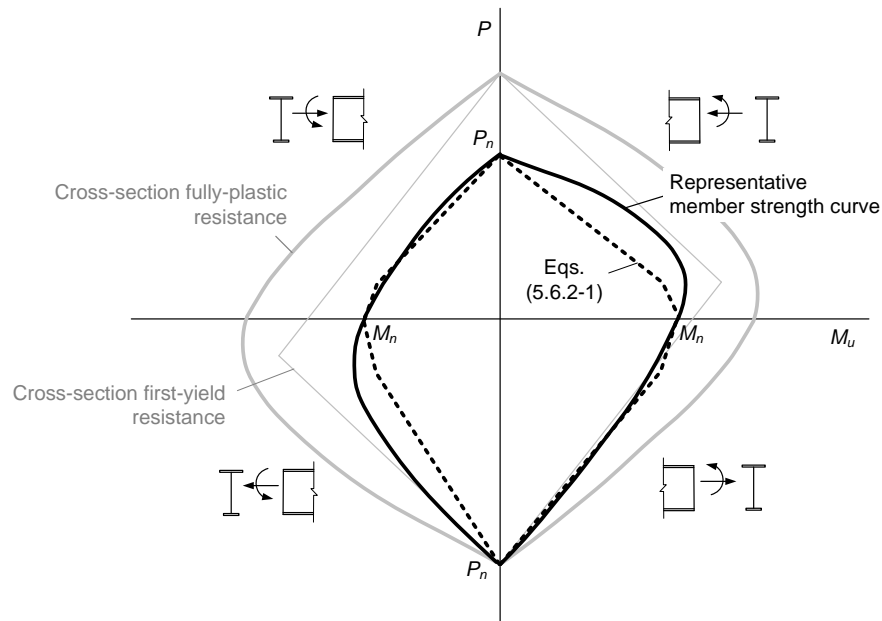


Figure 87 Comparison of a representative strength envelope for a hypothetical simply-supported finite-length beam-column with noncompact and/or slender cross-section elements, the AISC (2010) strength interaction curves (Eqs. (5.6.2-1)), and the cross-section yield and fully-plastic strength.

The behavior for finite-length Tee- and double-angle beam columns is similar to that shown in Figure 87. However, particularly for members of these types with intermediate and longer lengths, the non-symmetry of the interaction curves is highly accentuated. Figure 88 illustrates this behavior along with the corresponding AASHTO (2014) - AISC (2010) strength for a representative simply-supported Tee-section member considered by Galambos (2001a). The two different solid curves in the figure denote capacities based on the in-plane strength limit states. The two dashed curves denote out-of-plane strength envelopes. Furthermore, the heavy lines illustrate the results obtained by the refined calculations from Galambos (2001a) whereas the thin lines indicate the resistances calculated by the AASHTO (2014) - AISC (2010) equations. One can observe that the bulge in the upper-right and lower-left quadrants is substantial for this member, and that the true strength along a radial line taken from the origin of the plot can be more than two times the strength estimate based on Eqs. (5.6.2-1) for some of the combinations of axial force and bending moment. However, in the lower-right and upper-left quadrants, where

the stem of the Tee-section is loaded in additive axial and flexural tension or compression, Eqs. (5.6.2-1) provide an accurate estimate of the “true” member strength.

Unfortunately, practical connections for typical Tee-section struts used as bracing or cross-frame members are typically made to the flange. The corresponding bending moment due to the eccentricity of the connection generally places the member design in the upper-right or lower-left quadrants of Figure 88. Furthermore, the moment due to the eccentricity often places the design in the region of the strength envelopes that exhibit the largest bulge relative to Eqs. (5.6.2-1).

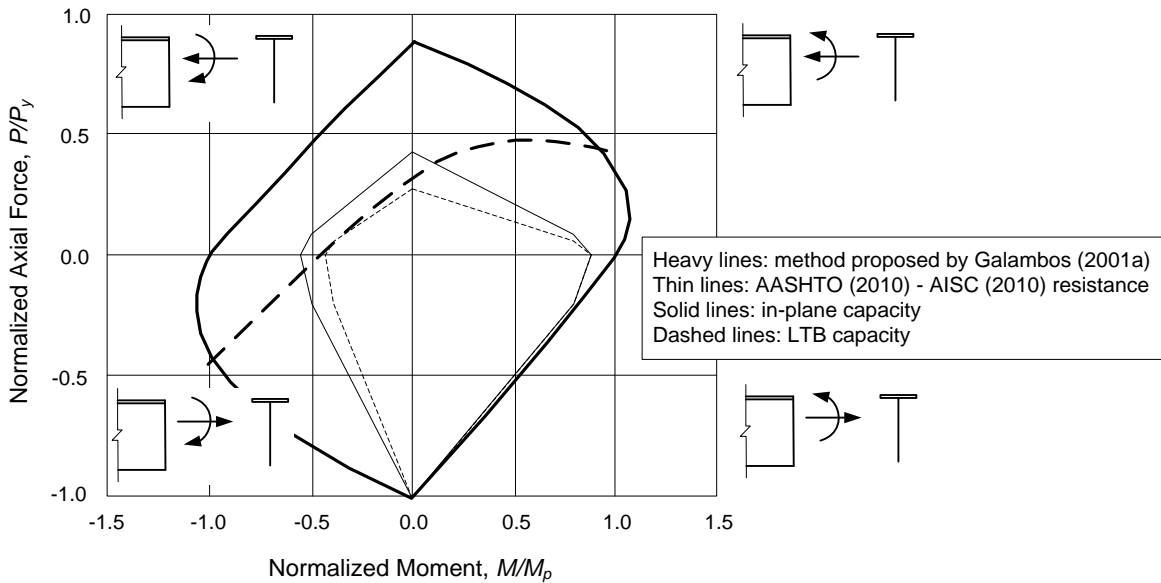


Figure 88 Representative simply-supported Tee-section member considered by Galambos (2001a) (WT18x67.5, $F_y = 50$ ksi, $L = 20$ ft).

Although Figure 88 indicates substantial additional capacity compared to that predicted by the AASHTO (2014) - AISC (2010) procedures in the upper-right and lower-left quadrants of the response, one must be careful in applying these additional strengths. The conservatism in the lower-left quadrant is largely due to the fact that AISC (2010) limits the maximum flexural resistance to $M_n = M_y$ (where M_y corresponds to first yielding at the tip of the stem, neglecting residual stress effects) for cases where the stem is loaded in flexural compression (see Section 5.5.5 of this module). For typical eccentric connections on Tee-struts, the compressive elastic flexural stress at the tip of the stem, M/S_x , is larger than the corresponding axial tension, P/A_g . Therefore, some conservatism may be merited to protect against significant inelastic LTB distortion of the tee stem. Also, in the upper-right quadrant, the axial compressive resistance P_n is reduced due to local buckling effects (via the Q factor, see Section 5.2.4) for a large number of rolled Tee-sections. This is the case for the WT18x67 member considered in Figure 88. However, in the upper-right quadrant, if the elastic flexural stress due to the eccentric loading, $M/S_x = Pe/S_x$, is larger than the corresponding axial compression stress, P/A_g , the Tee stem is completely in tension. As such, the influence of the slenderness of the stem, d/t_w , on the beam-column resistance is expected to be minor. Furthermore, the AISC (2010) and AASHTO (2014)

flexural resistances in this quadrant are limited to $M_n = 1.6M_y$ to avoid potential significant yielding at service load levels (see Section 5.5.5).

Unfortunately, no simple method has been established at the present time (2010) for determining the strength envelopes for singly-symmetric members, accounting for the bulges in the upper-right and lower-left quadrants illustrated in Figure 86 and Figure 87. In fact, it is probably fair to say that no simple manual method will ever exist for this calculation.

5.6.3.1.1 Enhanced strength interaction curves for singly-symmetric members loaded in their plane of symmetry

AISC (2010) Section H2 gives a separate beam-column interaction equation, which can be written for the case of bending within the plane of symmetry of a singly-symmetric member as

$$\left| \frac{f_a}{F_a} + \frac{f_b}{F_b} \right| \leq 1.0 \quad (5.6.3-2)$$

(AISC H2-1)

This equation is intended to capture some of the bulge in the upper right and lower left quadrants of Figure 88. The term f_a in this equation is the required axial stress, F_a is the axial capacity in terms of stress, f_b is the required flexural stress at the point under consideration, and F_b is the flexural capacity in terms of stress at the point under consideration, taken as $\phi_f M_n / S$ in LRFD where S is the corresponding elastic section modulus corresponding to the specific point in the cross-section under consideration.

The implied advantage of Eq. (2) is that the Engineer is allowed to consider the sign of the axial and flexural stresses, which are additive on one side of the cross-section and subtractive on the other. Unfortunately, this equation does not provide any advantage relative to Eqs. (5.6.2-1) for singly-symmetric members subjected to bending in the plane of symmetry. This is because, generally, the Engineer must check all the applicable points within the cross-section. Hence, *the extreme fiber where the axial and flexural stresses are additive always governs the resistance* when the axial and flexural resistance terms F_a and F_b are calculated as specified in AISC (2010), i.e., $F_a = \phi_c P_n / A$ or $\phi_t P_n / A$ and $F_b = \phi_f M_c / S$.

White and Kim (2006) discuss a variation on Eq. (5.6.3-2), proposed by Sherman (2005), that provides some of the intended benefits for cases where the M_n associated with yielding or buckling of the smaller flange (or Tee stem) is substantially smaller than M_p . However, Eqs. (5.6.2-1) always provide a more liberal estimate of the capacities for members where $M_n = M_p$.

The commentary to AISC (2010) Section H2 acknowledges the above problem and then discusses several ad hoc checks, similar to but different from Eq. (2). The AISC commentary points out that these checks are justified by the statement, “A more detailed analysis of the interaction of flexure and tension is permitted in lieu of Equation H2-1.”

Galambos (2001a) details a procedure that accomplishes the intended objective of Eq. (2), i.e., capturing the bulge in the upper-right and lower-left quadrants of the strength envelope, for

prismatic singly-symmetric compact-section members loaded in their plane of symmetry. Galambos' procedure also is applicable for doubly-symmetric I-section members as a special case. In these cases, it provides an enhanced assessment of the out-of-plane resistance for members subjected to major-axis bending. Galambos uses separate formulations for the in-plane and out-of-plane resistance to achieve these objectives. For the nominal in-plane resistance, Galambos uses the theoretical cross-section fully-plastic strength curve, but with an adjusted yield strength that varies from F_y at $P = 0$ to F_n at $P = P_n$, where F_n is the in-plane column resistance in terms of the axial stress and P_n is the in-plane column resistance in terms of the axial load. For the nominal out-of-plane strength, Galambos uses the fundamental equation for the elastic torsional-flexural buckling of a singly-symmetric member under combined axial load and uniform major-axis bending,

$$(P_{ey} - P_e)(\bar{r}_o^2 P_{ez} - \bar{r}_o^2 P_e + \beta_x M) = (M + P_e y_o)^2 \quad (5.6.3-3)$$

to solve for the value of P_e at elastic torsional-flexural buckling corresponding to a given applied moment M . He then calculates the ordinate (i.e., the axial resistance) for the nominal out-of-plane strength curve at this moment by substituting $P_e/P_o = P_e/P_y$ into Eqs. (5.2.1). The terms P_{ey} , \bar{r}_o , P_{ez} and y_o are defined in Section 5.2.3 of this module. The term β_x is a cross-section monosymmetry parameter (Galambos 2001a; Ziemian 2010; White and Jung 2003b).

The above approach works well for characterizing the resistance of prismatic compact doubly- and singly-symmetric I-section, Tee and double-angle members in cases where $M_n = M_p$ at $P = 0$. However, for longer unbraced lengths, this approach predicts a lateral-torsional buckling resistance equal to the elastic critical moment $M_{e,LTB}$ in the limit of $P = 0$. For compact Tee and double-angle members, this approximation is consistent with the AISC (2010) nominal flexural resistance equations (see Section 5.5.5). However, for I-section members, this prediction is overly optimistic with respect to the Specification inelastic LTB flexural resistance (see Figure 60). Galambos (2001b) suggests capping the nominal flexural resistance at $M = M_n$ in these cases, where M_n is calculated using the applicable inelastic LTB resistance equations. This adjustment assumes that the member inelastic LTB resistance is unaffected by the presence of axial load, either positively for axial tension or negatively for axial compression.

The AISC (2010) Specification provides simplified procedures that accomplish the objective of the above approach for doubly-symmetric rolled compact-element I-section members with $KL_z \leq KL_y$ subjected to major-axis bending and axial tension or compression, i.e., an enhanced characterization of the out-of-plane resistance. Section 5.6.3 of this module summarizes these procedures.

Ultimately, the simplest and most reliable determination of the strengths for the above types of beam-columns may be the use of carefully validated numerical procedures that give explicit maximum strength solutions, including the influence of appropriate nominal residual stresses and geometric imperfections. Such calculations are explicitly permitted by Appendix 1 of the AISC (2010) Specification. However, these types of analysis tools are not readily available for professional practice at the present time (2010).

5.6.3.1.2 Usage of the AASHTO (2014) and primary AISC (2010) bilinear interaction equations with relaxed flange and/or web compactness limits

The last paragraph of Article 6.9.4.2 in AASHTO (2014) states that for members designed for combined axial compression and flexure using Eqs. (5.6.2-1), the plate slenderness requirements summarized previously by Eq. (5.2.4-4) and Table 5 and Table 6 may be relaxed. These previously discussed requirements ensure that local buckling of the cross-section plate elements will not influence the behavior prior to developing the full yield strength of the member in uniform axial compression. Obviously, if the member compressive resistance in terms of the axial stress, F_n , is smaller than F_y , the plate slenderness limits necessary to prevent local buckling prior to reaching the column axial resistance should not need to be as stringent. Also, if the applied elastic stress level due to axial load plus bending in a given cross-section plate element is smaller than F_y , one might expect that the Eq. (5.2.4-4) requirements could be relaxed. Based on this logic, the last paragraph of Article 6.9.4.2 allows the Engineer to replace F_y in Eq. (5.2.4-4) by $f_a + f_b$, where $f_a = P_u/A_g$, $f_b = M_u/S$, A_g is the gross area of the cross-section and S is the applicable elastic section modulus to the extreme fiber of the plate element under consideration.

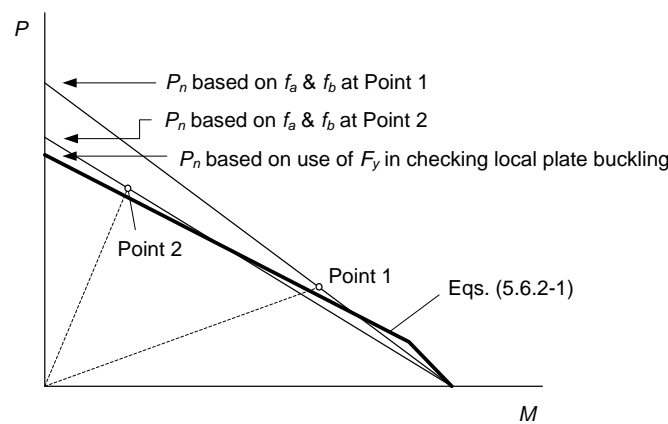


Figure 89 Effect of relaxing the plate slenderness limits by use of $f_a + f_b$ rather than F_y in Eqs. (5.2.4-4), (5.2.4-19) and (5.2.4-20) (the use of f_a in Eq. (5.2.4-17) and $f_a + f_b/3$ in Eq. (5.2.4-19) has a similar effect)

Also, as previously discussed in Section 5.2.4 of this module, Article 6.14.4.2 specifies similar criteria for the plate elements in solid-web arch ribs. The only difference between the Article 6.14.4.2 provisions and the above Article 6.9.4.2 rule is that Article 6.14.4.2 allows the Engineer to replace F_y by f_a when checking the plate slenderness of the webs of solid-web arch ribs, and by $f_a + f_b/3$ when checking the b/t of web longitudinal stiffeners (see Eqs. (5.2.4-18) and (5.2.4-19)).

As noted in Section 5.2.4, if the above plate slenderness limits are relaxed, AASHTO (2014) Article 6.9.4.2.1 requires the use of a linear axial force-moment interaction equation rather than Eqs. (5.6.2-1). This is because the validity of Eqs. (5.6.2-1) for members containing slender cross-section elements under uniform axial compression is tied to the calculation of the resistance P_n based on the loading of the member as a column up to its maximum resistance in

uniform axial compression. If the plate slenderness requirements in Eqs. (5.2.4-4), or (5.2.4-18) through (5.2.4-21) are relaxed by the use of applied stresses rather than F_y , the calculated P_n is larger for smaller ratios of axial load to bending as shown in Figure 89. The bilinear shape given by Eqs. (5.6.2-1) already accounts approximately for this effect. The calculations are simpler and exhibit comparable accuracy to the use of a linear interaction equation with the above variable P_n if one simply uses Eqs. (5.6.2-1) with a single calculation of P_n determined as the “true” resistance of the member under uniform axial compression. Nevertheless, the effect of replacing F_y by $f_a + f_b$ is typically small since the factored $f_a + f_b$ is often close to F_y .

5.6.3.2 Out-of-plane strength of doubly-symmetric rolled nonslender-element I-section members with $KL_z \leq KL_y$ subjected to axial load and major-axis bending

AISC (2010) specifies the following equation as an enhanced description of the out-of-plane resistance of doubly-symmetric rolled nonslender-element I-section beam-columns subjected to major-axis bending and axial compression:

$$1.5 \frac{P_u}{\phi_c P_{ny}} - 0.5 \left(\frac{P_u}{\phi_c P_{ny}} \right)^2 + \left(\frac{M_{ux}}{C_b \phi_b M_{nx(Cb=1)}} \right)^2 \leq 1.0 \quad (5.6.3-4)$$

(AISC H1-2)

where P_{ny} is the nominal column strength for weak-axis flexural buckling in the out-of-plane direction, and $M_{nx(Cb=1)}$ is the governing major-axis flexural resistance of the member based on the idealized case of uniform bending. The analytical basis for this equation comes from the solution of the differential equations of equilibrium for a simply-supported elastic member subjected to axial compression and unequal end moments (McGuire 1968). This solution yields the equation

$$\frac{M^2}{C_b^2 r_o^2 P_{ey} P_{ez}} = \left(1 - \frac{P}{P_{ey}} \right) \left(1 - \frac{P}{P_{ez}} \right) \quad (5.6.3-5)$$

where P_{ey} is the out-of-plane column flexural buckling load (see Eq. (5.2.3-3)), P_{ez} is the column torsional buckling load (see Eq. (5.2.3-1)) and

$$r_o = \sqrt{\frac{I_x + I_y}{A_g}} \quad (5.6.3-6)$$

is the polar radius of gyration of the cross-section. The term in the denominator on the left side of Eq. (5) is the square of the elastic lateral-torsional buckling resistance of the member, i.e.,

$$M_e = \sqrt{C_b^2 r_o^2 P_{ey} P_{ez}} = C_b \frac{\pi}{L} \sqrt{\left(\frac{\pi E}{L} \right)^2 I_y C_w + EI_y GJ} \quad (5.6.3-7)$$

where C_b is the moment gradient modifier (see Section 5.3.5 of this module). Equation (4) is obtained by assuming $P_{ez} = 2.0P_{ny}$, which is a lower-bound value for all the ASTM A6 rolled

wide-flange section members with $KL_z \leq KL_y$, and by replacing $M_{e(Cb=1)}$ and P_{ey} by the design resistances $\phi_c P_{ny}$ and $\phi_b M_{nx(Cb=1)}$. The resulting equation provides a much improved assessment of the out-of-plane resistance of typical rolled column-type I-sections, particularly in cases where the design resistances are governed by inelastic buckling and/or yielding limit states.

Equation (4) is a simplified version of a comparable equation implemented in the Australian AS4100 Standard (SAA 1998) based on research conducted by Cuk and Trahair (1986) and Cuk et al. (1986). The simplifications relative to AS4100 are:

- The use of $P_{ez} = 2.0P_{ny}$ to remove the need for the calculation of P_{ez} , and
- The use of an appropriate C_b expression for flexure alone, whereas AS4100 provides a separate moment gradient modifier that captures enhanced moment gradient benefits for beam-columns subjected to moment and axial compression.

The AS4100 equations are reviewed and compared to other beam-column strength calculations by White and Clark (1997 a & b). It is emphasized that the flexural resistance anchor point $C_b \phi_b M_{nx(Cb=1)}$ is permitted to be greater than $\phi_b M_{px}$. The resulting out-of-plane resistance is “capped” by the in-plane resistance determined using Eqs. (5.6.2.1) but considering only the in-plane strength terms, i.e., neglecting the potentially smaller values of $\phi_c P_{ny}$ based on minor-axis flexural buckling and $C_b \phi_b M_{nx}$ based on lateral-torsional buckling. This “cap” is similar in concept to the way that the plateau strength M_{max} serves as a cap on the general LTB strength of I-section beams subjected to moment-gradient conditions ($C_b > 1$).

Figure 90 shows the shape of Eq. (5) for several values of P_{ez}/P_{ey} . For ASTM A6 wide-flange sections, P_{ez}/P_{ey} is generally greater than 2.0 when $KL_z \leq KL_y$. However, it is not uncommon for this parameter to be only slightly larger than 2.0. In this case, one can observe that Eqs. (5.6.2-1), with $\phi_c P_{ny}$ and $\phi_b M_{nx(Cb=1)}$ replaced by P_{ey} and $M_{e(Cb=1)}$, provide a slightly liberal characterization of the theoretical beam-column elastic buckling resistance for small values of P/P_{ey} . Interestingly, Eq. (5.6.2-1a) nearly matches Eq. (5) for $P/P_{ey} \leq 0.2$ when Eq. (5) is used with $P_{ez}/P_{ey} = \infty$. The base bilinear AISC (2010) beam-column strength curve defined by Eqs. (5.6.2-1) tends to be slightly conservative for large P/P_{ey} when P_{ez}/P_{ey} is close to 2.0, whereas it is significantly conservative relative to Eq. (5) for large P_{ez}/P_{ey} .

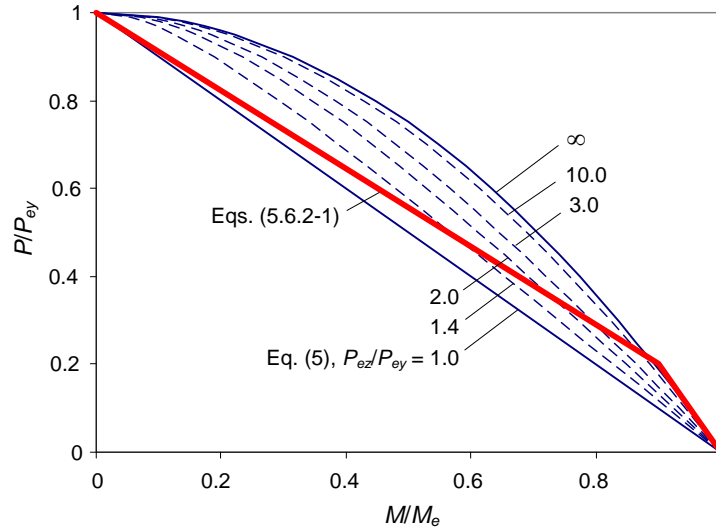


Figure 90 Theoretical elastic out-of-plane strength envelope for simply-supported doubly-symmetric I-section beam-columns versus the base AISC (2010) beam-column strength interaction curve.

It is useful to note that Eqs. (4) through (9) are usually considered in the context of assumed torsionally-simple end conditions, i.e., twisting of the member ends is prevented but the member ends are free to warp and bend laterally. In cases where I-section members are continuous with less critical adjacent unbraced segments, the adjacent segments may provide substantial warping and weak-axis bending restraint at the ends of the critical unbraced length. This restraint potentially can increase the true member capacity substantially, but it is typically neglected in design practice.

There is no implicit intent in the development of the AISC provisions to disallow the use of doubly-symmetric welded I-sections that have geometries comparable to rolled wide-flange sections. However, the ratio P_{ez}/P_{ny} can be smaller than 2.0 for some thin-web welded I-sections. However, there is no precedent for applying Eq. (4) to beam-columns having noncompact or slender cross-section elements, or to any type of tapered-web or generally nonprismatic beam-column members. It appears that there are no experimental or analytical solutions at the present time (2010) that substantiate the use of Eq. (4) for these cases. Some enhancement relative to Eqs. (5.6.2-1) is possible in certain situations. However, the precise shape of the beam-column strength envelope depends on the mode of failure (FLB, LTB or TFY in the limit of zero axial force, weak- or strong-axis flexural buckling, or torsional buckling about a centroidal axis or a constrained axis in the limit of zero moment, and variations between these limits for combined axial load and flexure). Stated alternately, the precise shape of the beam-column strength envelope depends on the specific member parameters that influence the resistance in the various axial and flexural modes of failure as well as the different interactions between these various failure modes. Further research is needed to determine how to best characterize these resistances. In the absence of further refinements, of the simple use of Eqs. (5.6.2-1) is recommended for general cases that go beyond the applicability of Eq. (4).

AISC (2010) Section H1 gives the following modification of the moment gradient modifier C_b for doubly-symmetric members subjected to axial tension:

$$C_b^* = C_b \sqrt{1 + P_u / P_{ey}} \quad (5.6.3-10)$$

This modified C_b factor, with the tension force P_u taken as a positive number, accounts for the beneficial influence of axial tension on the lateral-torsional buckling resistance and is to be applied with Eqs. (5.6.2-1). Equation (10) can be inferred from a version of Eq. (5) with the second term on the right-hand side taken equal to 1.0. Its application in the context of Eqs. (5.6.2-1) is ad hoc, but gives a reasonable estimate of the bulge within the lower quadrants of the strength envelope for these types of members.

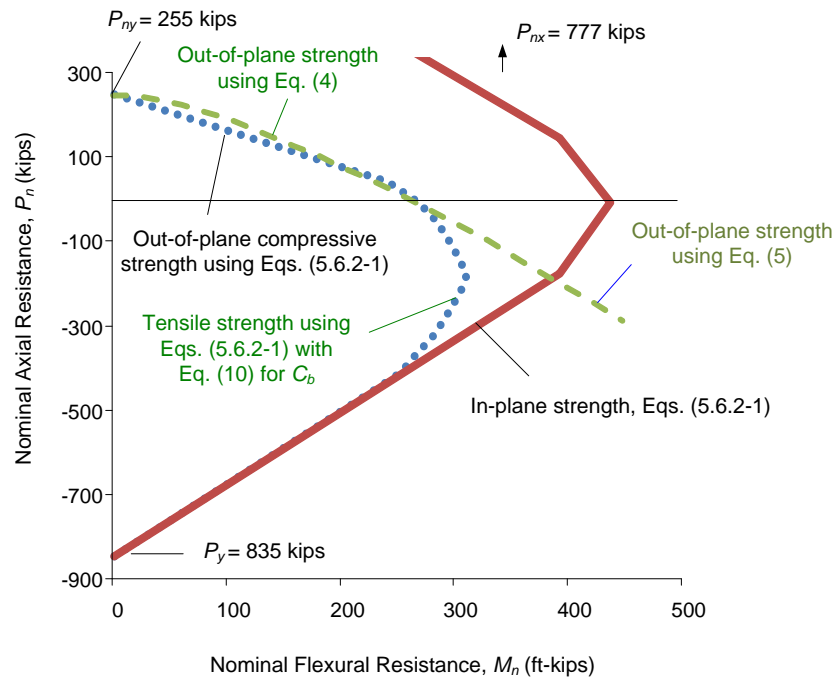


Figure 91 Beam-column resistances under tensile and compressive axial force (tension is shown as negative) and uniform primary bending (W16x57, $F_y = 50$ ksi, $L_b = 18.3$ ft, $C_b = 1.0$).

Figure 91 illustrates the combined influence of Eqs. (4) and (10) for a simply-supported wide-flange beam-column subjected to uniform bending. The example W16x57 member has an unbraced length $L_b = KL_x = KL_y = KL_z = 18.3$ ft, which is equal to L_r . Therefore, $M_n = M_{e(Cb=1)} = 269$ ft-kips is governed by elastic LTB at $F_{e,LTB} = F_{yr}$. (see Eqs. (5.3.5-24) and ((5.3.5-17))). Also, the out-of-plane compressive resistance P_n is governed by elastic flexural buckling at $P_{ny} = 0.877P_{ey} = 255$ kips, and $P_{ez} = 850$ kips = $3.33P_{ny}$ for this member. The resistance for pure axial tension with zero applied bending moment is taken as $P_y = 835$ kips, the in-plane axial compressive resistance is $P_{nx} = 777$ kips, and the in-plane flexural resistance is $M_p = 438$ ft-kips.

Three important sets of curves are shown in Figure 91:

The in-plane member strength determined using Eqs. (5.6.2-1) with the resistances P_{nx} , M_p and P_y , denoted by the outer-most bold strength curves,

The out-of-plane strength determined using Eqs. (5.6.2-1) with the resistances P_{ny} and $M_{n(Cb=1)}$ for the case of axial compression, and, for the case of axial tension, determined using Eqs. (5.6.2-1) with the resistances P_y and $M_{n(Cb=1)}$, but with $M_{n(Cb=1)}$ increased by C_b from Eq. (10) and capped by $C_b M_{n(Cb=1)} \leq M_p$. This strength is shown by the dotted curves.

The “enhanced” “rigorous” out-of-plane strength determined using Eq. (4) with the resistances P_{ny} and $M_{n(Cb=1)}$ for the case of axial compression (with ϕ_f and ϕ_c taken equal to 1.0), and, for the case of axial tension, determined using Eq. (5) with the resistance P_{ey} replaced P_{ny} in the terms on the right-hand side of the equation, and $M_e^2 = M_{e(Cb=1)}^2 = M_{nx(Cb=1)}^2$ in the denominator on the left-hand side of the equation. This strength is shown by the dashed curves.

For the third set of curves, Eq. (4) is only slightly more conservative compared to Eq. (5) for the case of axial compression, since $P_{ez}/P_{ny} = 3.33$ for the subject member whereas Eq. (4) uses the lower-bound value of $P_{ez}/P_{ny} = 2.0$. However, Eq. (5) is used for the axial tension case for this set of strength curves because Eq. (4) is slightly liberal relative to the exact analytical out-of-plane strength equation for tensile axial force.

One can observe that Eqs. (4) and (5) give a more liberal assessment of the out-of-plane strength, relative to the second set of curves, for the cases with high axial compression, although the increase in the strength for this uniform bending problem is relatively small for axial compression case. Conversely, for I-section members with column-type sections (i.e., $b_f \cong d$) subjected to moment-gradient loading, the benefits can be substantial. In fact, when these types of members are subjected to double-curvature, the out-of-plane resistance typically does not govern the strength. The most effective application of Eq. (4) is for this situation. In these cases, the most streamlined approach for member proportioning is to design the member assuming the out-of-plane strength does not govern, then check the resulting design using Eq. (4).

The C_b given by Eq. (10) captures some enhancement in the flexural resistance due to concurrent axial tension, as evidenced by the dotted curve, but not as substantial as the result from Eq. (5). However, the more liberal strength provided by Eq. (5) for the axial tension case is not specified in AISC (2010). One can observe that the dotted curve asymptotes to the in-plane axial tension strength in the first set of curves at approximately 400 kips axial tension. Equation (5) is more abruptly “capped” by the in-plane axial tension resistance at an axial tension slightly larger than $0.2P_y$, the axial tension force corresponding to the knee of the bilinear interaction curve.

5.6.3.3 Other types of beam-columns, general loading conditions

The above sections focus on the in-plane resistance of various types of beam-columns loaded about either their major or minor principal axis of bending, as well as the out-of-plane resistance of doubly- or singly-symmetric open-section members subjected to bending within their plane of symmetry. These applications constitute the vast majority of beam-column design situations in bridge construction.

The out-of-plane resistance of closed-section beam-columns bent about their strong-axis and subjected to axial compression, e.g., a beam-column with a box cross-section, is represented accurately to conservatively by Eqs. (5.6.2-1) with P_n taken as the smaller of the member axial resistances for flexural buckling about the strong- or weak-axis. Equations (5.6.2-1) may be applied to the design of arch ribs, which often are rectangular box sections (e.g., see Wright and Bunner (2006)). In cases where a refined buckling analysis is utilized to evaluate the stability of the arch, P_n may be calculated using Eqs. (5.2.1-1) with P_e taken as the axial force at the governing buckling condition. Also, AASHTO (2014) requires the use of a linear interaction equation rather than Eqs. (5.2.1-1) if the plate slenderness limits are relaxed by using applied stresses f_a , $f_a + f_b/3$ and $f_a + f_b$ instead of F_y in Eqs. (5.2.4-17) through (5.2.4-20).

In some cases, bridge members are subjected to biaxial bending in combination with axial tension or axial compression. In these cases, extensive research shows that Eqs. (5.6.2-1) generally provide an accurate to somewhat conservative representation of the true strength envelope for compact I- and box-section members (Galambos 1998). The true shape of the strength envelope between the major- and minor-axis bending moments can be highly convex. AISC (1999) Appendix H provides nonlinear interaction equations for compact I- and box-section members in braced frames that provide the best known estimate of the true resistances. These equations no longer appear in AISC (2010), apparently due to their infrequent usage in design practice. In addition, AISC (2010) Section H3 provides a strength interaction equation for combined torsion, shear, flexure and axial force in HSS members, including members in which the resistances can be influenced by local buckling. This equation indicates only a linear interaction between the flexural and axial capacity ratios. The author is not aware of any nonlinear beam-column interaction equations for axial loading and biaxial bending on open-section members with singly-symmetric cross-sections and/or noncompact or slender cross-section elements.

5.6.4 Composite Members

This section addresses the axial force-moment interaction for steel-concrete composite members. Two main types of members are considered: (A) I- and box-section members with a composite concrete deck, and (B) Concrete-encased sections and concrete-filled boxes and tubes.

5.6.4.1 I- and box-section members with a composite concrete deck

I-section members with a composite concrete deck behave in a fashion somewhat like the singly-symmetric steel I-sections with a large top flange discussed in Section 5.6.3 of this module. The flexural resistance in positive bending is based on the plastic section response or flange yielding depending on whether the section is classified as compact or noncompact (see Section 5.3.3 and 5.3.4). The member resistance in axial compression is based either on flexural buckling about the major axis of bending or on torsional buckling about an enforced axis of rotation located at the depth of the shear connectors (see Section 5.2.7). The member resistance in combined axial compression and positive bending may be obtained conservatively by applying Eqs. (5.6.2-1). However, a more liberal estimate may be obtained potentially by estimating the bulge in the strength envelope for loading within the upper-right quadrant. The appropriate calculations for this estimate are not readily apparent if the cross-section is noncompact in positive bending,

and/or if the I-section web is slender in uniform axial compression. The behavior of box-section members with a composite concrete deck is similar, except that, as noted previously in Section 5.6.3, torsional buckling of the steel section is not a consideration.

5.6.4.2 Concrete-encased sections and concrete-filled boxes and tubes

The AISC (2010) commentary provides guidelines for calculation of the resistance for encased composite columns and concrete infilled sections subjected to combined axial compression and bending moment. Three separate approaches may be utilized that vary in their level of conservatism and amount of calculation effort. All of the methods take advantage of the strength determination for a limited number of loading cases, and utilize interpolation or interaction equations to calculate the strengths for other cases.

The first approach is essentially the same as in AISC (1999). If the axial and flexural resistances are calculated using the AASHTO (2014) - AISC (1999) provisions, the beam-column strength assessment must be conducted using this method. In addition, the design of noncompact or slender concrete-filled sections is limited to this method (AISC 2010). This approach applies only to doubly-symmetric composite beam-columns. For these types of members, Eqs. (5.6.2-1) provide a conservative estimate of the member resistance for combined axial compression and flexure, given the axial resistance P_n calculated as discussed in Section 5.2.7 of this module and the flexural resistance calculated as outlined in Section 5.5.9(B). Also, this approach may be used for combined tension and flexure. The degree of conservatism depends on the extent of the concrete contribution to the strength, relative to that of the steel. Equations (5.6.2-1) are generally more conservative for members with a larger contribution from the concrete.

The second approach starts with a plastic analysis to determine the cross-section strength under combined bending and axial force. This approach is illustrated by considering the strength behavior for an encased I-section bent about its major axis and having only four bars as longitudinal reinforcement (see Figure 92). The “exact” cross-sectional strength interaction curve, shown by the bold solid curve in Figure 93, is obtained by a strain-compatibility analysis. The flexural strength, M , and axial load, P , may be estimated for various points along this curve by assuming a position of the plastic neutral axis, PNA, drawing the corresponding fully-plastic stress distributions, and summing their moments about the cross-section reference axis. The concrete under tension is neglected. Strain continuity is assumed between the steel and the concrete portions of the cross-section. This assumption, although not supported by much of the data from experimental tests where the interface was monitored, has a negligible influence on the ultimate strength and a minor influence on the stiffness of the cross-section (Galambos 1998).

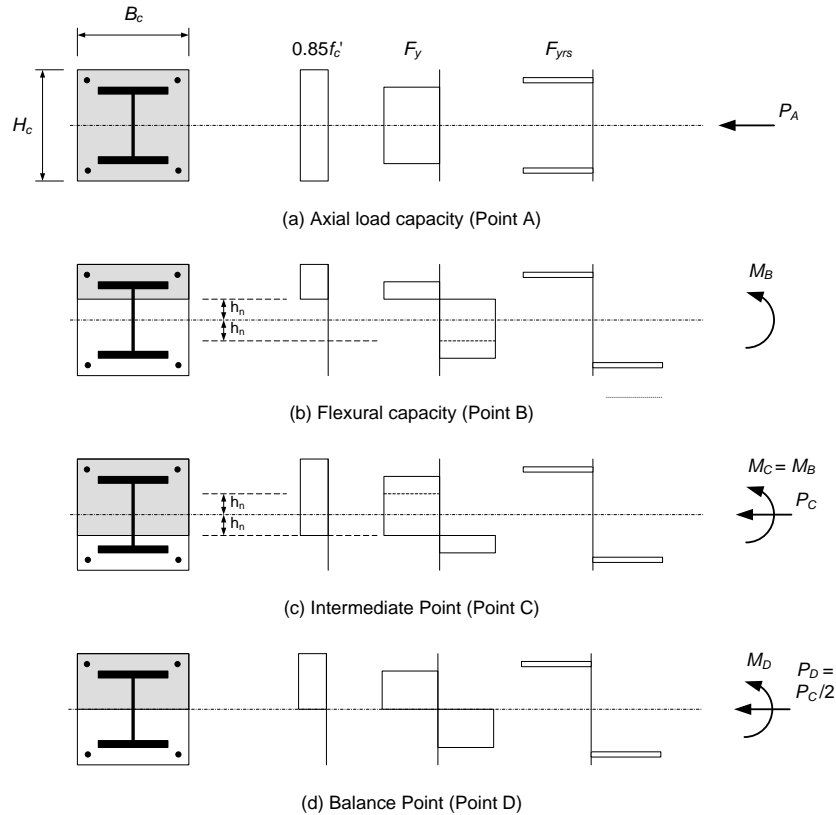


Figure 92 Stress distributions corresponding to key points on the beam-column strength envelope.

Rather than determine a continuous locus of points to define the cross-section plastic strength curve, it is sufficient to define the cross-section strength by locating the five points shown in Figure 93 (Roik and Bergmann 1992; Ziemian 2010; AISC 2010). The strengths are determined by linear interpolation for cases that fall between these points. Point A is the strength under concentric axial compression, determined as the value P_o in Section 5.2.7 of this module. Point B is the plastic cross-section flexural resistance for zero axial force. Point C corresponds to a PNA location that gives the same flexural capacity as point B but with a nonzero axial compression. Assuming that the PNA lies in the web of the steel I-section for Points B and C, and that it is located at a distance h_n above the mid-depth of the I-section for Point B, the corresponding PNA for Point C is located at the same distance h_n below the mid-depth of the I-section. In both of the stress distributions for Points B and C, the depth $2h_n$ is in the middle of the section and hence the stress block or blocks within this depth contribute no moment about the mid-depth reference axis of the cross-section. In addition, it should be recognized from Figure 92 that the axial forces from the reinforcement and the shaded portions of the stress blocks from the steel shape cancel out.

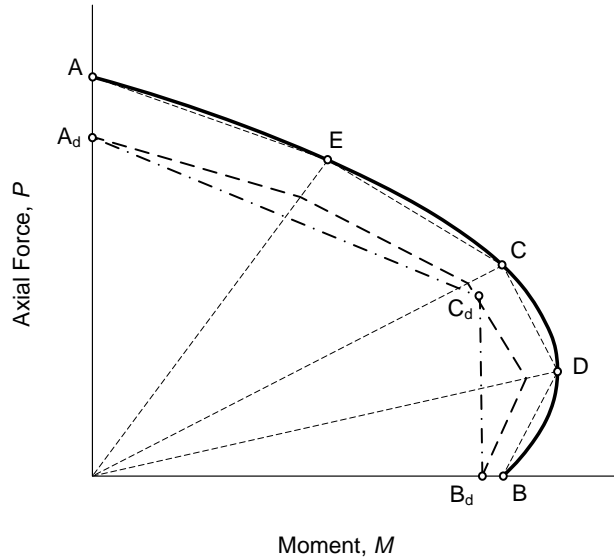


Figure 93 Strength envelope for encased or filled composite beam-column.

If one adds the stress distributions in Figure 92b and Figure 92c, the resulting axial force from the sum of these distributions is still the axial force P_C corresponding to the stress blocks in Figure 92c. This is because the total axial force in Figure 92b is zero. Furthermore, one can observe by summing the contributions from the distributions in Figure 92b and Figure 92c that the corresponding total axial force is equal to that given by the concrete section alone, i.e.

$$P_C = 0.85f'_c(B_c H_c - A_s - A_{sr}) \quad (5.6.4-1)$$

where B_c and H_c are the dimensions of the concrete section shown in Figure 92a, A_s is the area of the steel section, and A_{sr} is the area of reinforcing steel.

In a similar fashion, if the stress distribution in Figure 92b is subtracted from that of Figure 92c and the contribution of this sum to the axial force is considered, which is still equal to P_C , one obtains

$$P_C = (B_c - t_w)(2h_n)(0.85f'_c) + 2t_w(2h_n)F_y \quad (5.6.4-2)$$

This equation may be solved for h_n to obtain

$$h_n = \frac{P_C}{2(0.85B_c f'_c + t_w(2F_y - 0.85f'_c))} \quad (5.6.4-3)$$

Once h_n is determined, the moment capacity corresponding to points B and C is easily calculated.

The moment corresponding to the balance point (point D), where the moment capacity is largest, is obtained when the PNA is located at the mid-depth of the cross-section (since in this case, all the stress blocks contribute to the moment about the mid-depth reference axis). From Figure 92d,

one can observe that all the contributions to the axial load from the steel shape and the reinforcement cancel out, and that the axial load P_D corresponds to $0.85 f'_c$ acting over half of the cross-section, i.e., $P_D = P_C/2$.

Point E is an arbitrary point selected to improve the approximation of the “exact” cross-section strength curve between points A and C.

Given the above approximate cross-section plastic strength envelope and the column design axial strength $\phi_c P_n$, determined as discussed in Section 5.2.7 of this module (accounting for the column length effects), an appropriate design strength envelope may be determined by scaling the abscissa and ordinate of points A through E by the factor

$$s = \phi_f + \left(\frac{\phi_c P_n}{P_o} - \phi_f \right) \frac{2\theta}{\pi} \quad (5.6.4-4a)$$

where

$$\theta = \tan^{-1} \left(\frac{P_i}{M_i} \right) \quad (5.6.4-4b)$$

is the angle (in radians) that a radial line from the origin to the point (M_i, P_i) , $i = A, B, C, D$ or E . The commentary of AISC (2010) indicates that “...care should be taken in reducing Point D by a resistance factor or to account for member slenderness, as that may lead to an unsafe situation whereby additional flexural strength is permitted at a lower axial compressive strength than predicted by the cross-section strength of the member.” Equations (4) avoid this anomaly by shifting the cross-section strength along a radial line toward the origin by a factor that varies from ϕ_f for point B to $\phi_c P_n/P_o$ for point A.

The third approach is a simplification of the above procedure. In this approach, points A $(0, P_A)$, C (M_C, P_C) , A_d $(0, \phi_c P_n)$ and B_d $(\phi_f M_n, 0)$ are determined as described above. The axial force and moment coordinates of point C are then shifted by $\phi_c P_n/P_A$ and ϕ_f respectively to obtain point C_d. Finally, the strength envelope for the beam-column is expressed conservatively by linear interpolation between points A_d, C_d and B_d.

The first of the above approaches directly accommodates compression and biaxial bending, since Eqs. (5.6.2-1) accommodate bending about both the major and minor principal axes of the cross-section. Roik and Bergmann (1992) recommend the use of linear interpolation between the strength envelopes for axial compression and bending about each of the cross-section principal axes. This approximation may be applied in either of the above second or third methods. The axial compressive resistance $\phi_c P_n$ is taken as the smaller resistance for column flexural buckling about either of the cross-section principal axes in determining the point A_d for each of the uniaxial strength envelopes. The corresponding maximum second-order elastic moments along the member length are substituted into the strength interaction equation for bending about each of the principal axes (as discussed previously in the context of Eqs. (5.6.2-1), this is necessary because the interaction equations provide a simplified check of the combined influence of

strength and stability for the complete unbraced length of the member, not just a check of the resistance at a given cross-section).

5.6.5 Summary Assessment of Beam-Column Strength Calculations

It should be clear from the above discussions that the various design strength interaction equations are only coarse, albeit accurate to conservative, approximations of the true limit states response of general beam-column members. The nominal axial resistance P_n alone is governed in general by many different limit states. For axial compression, these limit states include flexural buckling about the x - or y -axis of the cross-section based on the effective lengths KL_x and KL_y , torsional buckling about the member centroidal axis (for doubly-symmetric open-section members) or about an axis at which the transverse displacements are constrained based on the effective length KL_z , or torsional-flexural buckling based on the effective lengths KL_y and KL_z , depending on the specifics of the member geometry and boundary conditions. For most practical member lengths, the member response involves significant inelasticity and corresponding reductions in stiffness prior to achieving these strength limit states. However, for longer members, the limit states response may be dominated by the elastic stability behavior. If the member cross-section contains slender elements under uniform axial compression, the column limit states response is influenced by the local buckling and post-buckling behavior of the component plates. For axial tension, the limit states include overall tension yielding, or tension fracture at a net section including shear lag effects associated with the connection geometry.

The nominal flexural resistance of noncomposite members and composite members with a composite concrete deck is governed by various idealizations of member elastic or inelastic lateral-torsional buckling, elastic or inelastic local buckling and postbuckling of the component plates, and potential extents of yielding through the cross-section depth, depending on the cross-section type. For encased composite members, the flexural resistance is based on different extents of yielding, depending on whether shear connectors are provided and whether the concrete meets limits on its maximum compressive strength in AISC (2010), and depending on the level of axial compression in AASHTO (2014) and AISC (1999).

The physical interaction between the various axial and flexural resistances, and the resulting shape of the physical strength envelopes, differs in general depending on the specific combinations of the above limit states. It can be argued explicit application of carefully validated numerical procedures that account for all the significant influences on the maximum strength provides the only practical means of gaining any substantial improvement in accuracy relative to the practical design interaction equations that have been discussed. Appendix 1 of the AISC (2010) Specification provides guidelines for the application of this type of approach. However, in many practical situations, the simple Specification strength interaction equations are sufficient to achieve an economical design.

6.0 CONCLUDING REMARKS

As stated in the introduction, this module aims to aid the Engineer in reviewing and understanding the essential principles of steel system and member strength behavior and design behind various Specification provisions for the design of steel bridge structures. That is, it is intended as a relatively comprehensive resource that engineers can consult to understand the background to the various Specification provisions so that the provisions can be properly applied for “standard” designs, and so the design considerations can be most appropriately be extended to the many “non-standard” situations that arise in bridge design practice. It should also be clear from the various discussions that there are always areas of potential further improvement. Nevertheless, the AASHTO (2014) and AISC (2010) Specifications represent a tremendous resource for the efficient, practical and economical design of steel bridge structures.

7.0 REFERENCES

1. AASHTO (2014). *AASHTO LRFD Bridge Design Specifications*, 7th Edition, , American Association of State and Highway Transportation Officials, Washington, D.C.
2. AASHTO (2004). *AASHTO LRFD Bridge Design Specifications*, 3rd Edition with 2006 Interim Provisions, American Association of State and Highway Transportation Officials, Washington, D.C.
3. AASHTO (2003). *Guide Specifications for Horizontally Curved Steel Girder Highway Bridges with Design Examples for I-Girder and Box-Girder Bridges*, American Association of State Highway and Transportation Officials, Inc., Washington, D.C.
4. AASHTO (2002). *Standard Specifications for Highway Bridges and Interim Specifications*, 17th Edition, HB-17, American Association of State and Highway Transportation Officials, Washington, D.C.
5. AASHTO (1998). *AASHTO LRFD Bridge Design Specifications*, 2nd Edition with 1999, 2000, 2001, 2002 and 2003 Interim Provisions, American Association of State and Highway Transportation Officials, Washington D.C.
6. AASHTO (1994). *AASHTO LRFD Bridge Design Specifications*, 1st Edition, American Association of State and Highway Transportation Officials, Washington D.C.
7. Abu-Hawash, A., Caparelli, L., Schwartz, P. and McDonald, N. (2005). “The Use of Straddle Bent Pier with a High Performance Steel Integral Cap, Innovative Design Solutions for Complex Geometry I-235 Braided Ramps,” *Time for Steel, Steel for Time*, Proceedings, 2005 World Steel Bridge Symposium, National Steel Bridge Alliance, 12 pp.
8. ACI (1977). *Building Code Requirements for Reinforced Concrete*, ACI 318/77, American Concrete Institute, Detroit, MI.
9. AISC (2005). *Specification for Structural Steel Buildings*, ANSI/AISC 360-05, American Institute of Steel Construction, Chicago, IL.
10. AISC (1999). *Load and Resistance Factor Design Specification for Structural Steel Buildings*, American Institute of Steel Construction, Chicago, IL.
11. AISC (1993). *Load and Resistance Factor Design Specification for Structural Steel Buildings*, American Institute of Steel Construction, Chicago, IL.
12. AISC (1989). *Specification for Structural Steel Buildings: Allowable Stress Design and Plastic Design*, 9th Ed., American Institute of Steel Construction, Chicago, IL.
13. AISC (1986). *Load and Resistance Factor Design Specification for Structural Steel Buildings*, American Institute of Steel Construction, Chicago, IL.

14. AISC (1969). *Specification for the Design, Fabrication and Erection of Structural Steel for Buildings*, American Institute of Steel Construction, New York, NY.
15. AISI (2001). *North American Specification for the Design of Cold-Formed Steel Structural Members with Commentary*, American Iron and Steel Institute, Washington, DC.
16. AISI (2000). *Short-Span Bridge Plans and Software*, Publication No. T-300, American Iron and Steel Institute, Washington, DC.
17. AISI (1986). *Specification for the Design of Cold-Formed Steel Structural Members*, with 1989 Addendum, American Iron and Steel Institute, Washington, D.C.
18. AISI (1968). *Specification for the Design of Cold-Formed Steel Structural Members*, American Iron and Steel Institute, New York, NY.
19. Anderson, J.M. and Trahair, N.S. (1972). "Stability of Monosymmetric Beams and Cantilevers," *Journal of the Structural Division*, ASCE, 98(ST1), 269-286.
20. ASCE (2000). *Design of Latticed Steel Transmission Structures*, ASCE 10-97, American Society of Civil Engineers, Reston, VA, 71 pp.
21. ASCE (1997), *Effective Length and Notional Load Approaches for Assessing Frame Stability: Implications for American Steel Design*, American Society of Civil Engineers Structural Engineering Institute's Task Committee on Effective Length under the Technical Committee on Load and Resistance Factor Design, 442 pp.
22. ASCE (1992). *Guidelines for Design of Cable-Stayed Bridges*, Committee on Cable-Suspended Bridges, American Society of Civil Engineers, Reston, VA.
23. ASCE (1968). "Design of Hybrid Steel Beams," Joint ASCE-AASHO Committee on Flexural Members, *Journal of the Structural Division*, ASCE, 94(ST6), 1397-1425.
24. ASTM (2004). *Standard Specification for Zinc-Coated Parallel and Helical Steel Wire Structural Strand*, American Society for Testing and Materials, Designation: A 586 – 04a, 6 pp.
25. ASTM (1998). *Standard Specification for Zinc-Coated Steel Structural Wire Rope*, American Society for Testing and Materials, Designation A 603 – 98 (Reapproved 2003), 6 pp.
26. Aslani, F. and Goel, S.C. (1991). "An Analytical Criteria for Buckling Strength of Built-Up Compression Members," *Engineering Journal*, AISC, 28(4), 159-168.
27. Aydemir, M., White, D.W. and Jung, S.K. (2004). "Shear Strength and Moment Shear Interaction in HPS Hybrid I-Girders," Structural Engineering, Mechanics and Materials Report No. 25, School of Civil and Environmental Engineering, Georgia Institute of Technology, Atlanta, GA.

28. Barker, M.G., Hartnagel, B.A., Schilling, C.G. and Dishongh, B.E. (1997). "Inelastic Design and Experimental Testing of Compact and Noncompact Steel Girder Bridges," Report 93-1, Missouri Cooperative Highway Research Program, 185 pp.
29. Barth, K.E., Hartnagel, B.A., White, D.W. and Barker, M.G. (2004). "Recommended Procedures for Simplified Inelastic Design of Steel I-Girder Bridges," *Journal of Bridge Engineering*, ASCE, 9(3), 230-242.
30. Barth, K.E., and White, D. W. (1997). "Finite Element Evaluation of Pier Moment-Rotation Characteristics in Continuous-Span Steel I-Girders." *Engineering Structures*, 20(8), 761-778.
31. Basler, K. (1963). "Discussion of K. Basler 'Strength of Plate Girders in Shear,'" *Transactions ASCE*, 128(II), 712-719.
32. Basler, K. (1961). "Strength of Plate Girders in Shear," *Journal of Structural Division*, ASCE, 87(ST7), 151-180.
33. Basler, K. and Thurlimann, B. (1961). "Strength of Plate Girders in Bending," *Journal of the Structural Division*, ASCE, 87(ST6), 153-181.
34. Basler, K., Yen, B.T., Mueller, J.A. and Thurlimann, B. (1960). "Web Buckling Tests on Welded Plate Girders," WRC Bulletin No. 64, Welding Research Council, New York, 1-63.
35. Beckmann, F. and Medlock, R.D. (2005). "Skewed Bridges and Girder Movements Due to Rotations and Differential Deflections," *Time for Steel, Steel for Time*, Proceedings, 2005 World Steel Bridge Symposium, National Steel Bridge Alliance, 11 pp.
36. Beshah, F. and Wright, W. (2010). "Testing of Composite Bridge," *Curved Steel Bridge Study*, Federal Highway Administration, April.
37. Bleich, F. (1952). *Buckling Strength of Metal Structures*, McGraw-Hill Book Company, INC., New York, NY, 508 pp.
38. Bradford, M.A. (1992). "Lateral-Distortional Buckling of Steel I-Section Members," *Journal of Constructional Steel Research*, 23, 97-116.
39. Brown, C.W. (1992). "Medium Span Bridges," Chapter 6.4, *Constructional Steel Design, An International Guide*, P.J. Dowling, J.E. Harding and R. Bjorhovde (ed.), Elsevier, Essex, England, 695-709.
40. BSI (1990). BS5950: Part 1: 1990, Structural Use of Steelwork in Building, Part 1, Code of Practice for Design in Simple and Continuous Construction: Hot Rolled Sections, British Standards Institution, London. Cassity, P., Serzan, K. and McDonald, N. (2003). "Fit to be Tied," *Roads and Bridges*, November, 28-31.

41. Burgan, B.A. and Dowling, P.J. (1985). "The Collapse Behavior of Box Girder Compression Flanges – Numerical Modeling of Experimental Results," CESLIC Report BG 83, Imperial College, University of London.
42. Carskaddan, P.S. and Schilling, C.G. (1974). "Lateral Buckling of Highway Bridge Girders." Research Laboratory Report 22-G-001 (109-3), United States Steel Corporation, Monroeville, PA.
43. CEN (1993). *Eurocode 3: Design of Steel Structures, Part 1.1 – General Rules and Rules for Buildings*, ENV 1992-1-1, European Committee for Standardization, Brussels, Belgium.
44. Chang, C.-J. and White, D.W. (2010). "Construction Simulation of Curved Steel I-Girder Bridges," Final Report to FHWA and Professional Services Industries, Inc., Curved Steel Bridge Research Project, Federal Highway Administration, November.
45. Chang, C.-J., White, D.W., Beshah, F. and Wright, W. (2005). "Design Analysis of Curved I-Girder Bridge Systems – An Assessment of Modeling Strategies," Annual Proceedings, Structural Stability Research Council, 349-369.
46. Chen, S.S., Aref, A.J., Ahn, I.-S., Chiewanichakorn, M., Carpenter, J.A., Nottis, A and Kalpakidis, I. (2005). "Effective Slab Width for Composite Steel Bridge Members," NCHRP Report 543, Transportation Research Board, 70 pp plus appendices.
47. Cheng, J.J.R. and Kulak, G.L. (2000). "Gusset Plate Connection to Round HSS Tension Members," *Engineering Journal*, AISC, 37(4), 133-139.
48. Clarke, M.J. and Bridge, R.Q. (1992). "The Inclusion of Imperfections in the Design of Beam-Columns," *Proceedings of the Annual Technical Session and Meeting*, Structural Stability Research Council, Univ. of Missouri - Rolla, Rolla, MO, 327-346.
49. Climenhaga, J.J. and Johnson, R.P. (1972). "Local buckling in continuous composite beams," *The Structural Engineer*, 50(9), 367-374.
50. Coletti, D., Fan, Z, Gatti, W., Holt, J. and Vogel, J. (2005). "Practical Steel Tub Girder Design," National Steel Bridge Alliance, Chicago, IL, April, 51 pp.
51. Coletti, D. and Yadlosky, J. (2005). "Behavior and Analysis of Curved and Skewed Girder Bridges," *Time for Steel, Steel for Time*, Proceedings, 2005 World Steel Bridge Symposium, National Steel Bridge Alliance, 13 pp.
52. Coletti, D., Fan, Z., Holt, J. and Vogel, J. (2006). "Practical Steel Tub Girder Design," Compendium of Papers CD-ROM, TRB 85th Annual Meeting, Transportation Research Board, Washington, DC, 15 pp.
53. Colville, J. (1972). "Shear Connector Studies on Curved Girders," Progress Report No. 45 for Maryland State Highway Administration and FHWA, The Design of Curved

Viaducts, Civil Engineering Department, University of Maryland, College Park, MD, 78 pp.

54. Cooper, P.B., Galambos, T.V. and Ravindra, M.K. (1978). "LRFD Criteria for Plate Girders," *Journal of the Structural Division*, ASCE, 104(ST9), 1389-1407.
55. Cooper, P.B. (1967). "Strength of Longitudinally Stiffened Plate Girders," *Journal of the Structural Division*, ASCE, 93(ST2), 419-451.
56. Cross, H. (1952). *Engineers and Ivory Towers*, R.C. Goodpasture (ed.), 1st ed., McGraw-Hill. 141 pp.
57. Cuk, P.E. and Trahair, N.S. (1986). "Inelastic Lateral Buckling of Steel Beam-Columns," *Journal of Constructional Steel Research*, 6(1), 21-52.
58. Cuk, P.E., Bradford, M.A. and Trahair, N.S. (1986). "Inelastic Lateral Buckling of Steel Beam-Columns," *Canadian Journal of Civil Engineering*, 13(6), 639-699.
59. Culver, C.G. (1972). "Design Recommendations for Curved Highway Bridges," Final Report for Research Project 68-32, PENDOT, Civil Engineering Department, Carnegie-Mellon University, June.
60. Dalal, S. T. (1969). "Some Non-Conventional Cases of Column Design." *Engineering Journal*, AISC, 6(1), January, Chicago, IL, 28-39.
61. Dexter, R. and Altstadt, S. (2004). "Ductile Fracture in Girders," *Steel Bridges: Emerging Technologies with Emphasis on High Performance Steel and Accelerated Bridge Construction*, Proceedings, 2004 FHWA Steel Bridge Conference, A. Azizinamini (ed.), 69-78.
62. Dowling, P.J. and Harding, J.E. (1992). "Box Girders," Chapter 2.7, *Constructional Steel Design, An International Guide*, P.J. Dowling, J.E. Harding and R. Bjorhovde (ed.), Elsevier, Essex, England, 175-196.
63. Dowling, P.J., Harding, J.E. and Frieze, P.A. (eds.) (1977). *Steel Plated Structures*, Proceedings, Imperial College, Crosby Lockwood, London.
64. Dowswell, B. (2002). "Lateral-Torsional Buckling of Wide-Flange Cantilever Beams," *Proceedings of the Annual Technical Session and Meeting*, Structural Stability Research Council, Univ. of Missouri - Rolla, Rolla, MO, 267-290.
65. Duan, L., Reno, M., and Uang, C.M. (2002). "Effect of Compound Buckling on Compression Strength of Built-up Members," *Engineering Journal*, 39(1), AISC, Chicago, IL, 30-37.
66. Dubas, C. (1948). "A Contribution to the Buckling of Stiffened Plates," IABSE 3rd Congress, Preliminary Publication, Liege, Belgium.

67. Dux, P.F., and Kitipornchai, S. (1983). "Inelastic Beam Buckling Experiments," *Journal of Constructional Steel Research*, 3(1), 3-9.
68. Dwight, J.G. and Little, G.H. (1974). "Stiffened Steel Compression Panels – A Design Approach," Technical Report CUED/C – Struct./TR 38, Cambridge University.
69. Easterling, W.S. and Gonzales, L. (1993). "Shear Lag Effects in Steel Tension Members," *Engineering Journal*, AISC, 30(3), 77-89.
70. Ellifritt, D.S., Wine, G., Sputo, T. and Samuel, S. (1992). "Flexural Strength of WT Sections," *Engineering Journal*, AISC, 29(2), 67-74.
71. El-Tayem, A. and Goel, S.C. (1986). "Effective Length Factor for the Design of X-Bracing Systems," *Engineering Journal*, AISC, 23(1), 41-45.
72. Falby, W.E. and Lee, G.C. (1976). "Tension-Field Design of Tapered Webs," *Engineering Journal*, AISC, 13(1), 11-17.
73. Fan, Z. and Helwig, T.A. (1999). "Behavior of Steel Box Girders with Top Flange Bracing," *Journal of Structural Engineering*, 125(8), 829-837.
74. Fisher, J.W., Pense, A.W., and Hausamman, H. (1988). "Analysis of Cracking of I-79 Bridge at Neville Island, Fracture Problems in the Transportation Industry," Fall Convention, ASCE, Detroit, 1-19.
75. Fisher, J.W., Pense, A.W. and Roberts R. (1977). "Evaluation of fracture of Lafayette Street Bridge," *Journal of Structural Engineering*, ASCE, 103(7), 1339-1357.
76. FHWA (1980). "Integral, No-Joint Structures and Required Provisions for Movement," FHWA Technical Advisory T 5140.13, Federal Highway Administration, January.
77. Frank, K.H. (2005). "Fabrication Tolerances for MAGLEV," presentation to HPS Design Advisory Group, AISI Bridge Task Force and AASHTO T-14, Baltimore, MD, August.
78. Frank, K.H. and Helwig, T.A. (1995). "Buckling of Webs in Unsymmetric Plate Girders," *Engineering Journal*, AISC, 32(2), 43-53.
79. Frost, R.W. and Schilling, C.G. (1964). "Behavior of Hybrid Beams Subjected to Static Loads," *Journal of the Structural Division*, ASCE, 90(ST3), 55-88.
80. Galambos, T.V. (2001a). "Strength of Singly Symmetric I-Shaped Beam-Columns," *Engineering Journal*, AISC, 38(2), 65-77.
81. Galambos, T.V. (2001b). Personal communication.

82. Galambos, T.V. (1998). *Guide to Stability Design Criteria for Metal Structures*, 5th ed., T.V. Galambos (ed.), Structural Stability Research Council, Wiley, New York, NY, 911 pp.
83. Galambos, T.V. (1991). "Design of Axially Loaded Compressed Angles," *Proceedings of the Annual Technical Session and Meeting*, Chicago, IL, Structural Stability Research Council, Univ. of Missouri - Rolla, Rolla, MO, 353-367.
84. Galambos, T.V. and Chapuis, J. (1980). "LRFD Criteria for Composite Columns and Beam-Columns," Revised Draft, Dept. of Civil Engineering, Washington University, St. Louis, MO, December.
85. Galambos, T.V. and Ravindra, M.K. (1976). "Load and Resistance Factor Design Criteria for Steel Beams," Research Report No. 27, Structural Division, Civil and Environmental Engineering Department, Washington Univ., St. Louis, MO, 67 pp.
86. Galambos, T.V. (1968). *Structural Members and Frames*, Prentice-Hall, Englewood Cliffs, NJ, 373 pp.
87. Galambos, T.V. and Ketter, R.L. (1959). "Columns under Combined Bending and Thrust," *Journal of the Engineering Mechanics Division*, ASCE, 85(2), 1-30.
88. Goldberg, J.E. and Leve, H.L. (1957). "Theory of Prismatic Folded Plate Structures," *IABSE*, Vol. 16, International Association for Bridge and Structural Engineers, Zurich, Switzerland, 59-86.
89. Grubb, M. A., and Carskaddan, P. S. (1981). *Autostress design of highway bridges, phase 3: Moment rotation requirements.*, Research Laboratory Rep., United States Steel Corporation, Monroeville, PA, 45 pp.
90. Grubb, M. A., and Carskaddan, P. S. (1979). *Autostress design of highway bridges, phase 3: Initial moment rotation tests.*, Research Laboratory Rep., United States Steel Corporation, Monroeville, PA, 36 pp.
91. Hall, D.H., M.A. Grubb and C.H. Yoo (1999). "Improved Design Specifications for Horizontally Curved Steel Girder Highway Bridges," Report 424, National Cooperative Highway Research Program, National Academy Press, Washington, D.C., 130 pp.
92. Hall, D.H. (1997). "Why Steel Box Girders?" *Bridge Crossings*, No. 6, Reprinted from *Modern Steel Construction*, National Steel Bridge Alliance, Chicago, IL, 4 pp.
93. Hall, D.H. (1992). "Short Span Bridges," Chapter 6.3, *Constructional Steel Design, An International Guide*, P.J. Dowling, J.E. Harding and R. Bjorhovde (ed.), Elsevier, Essex, England, 671-693.
94. Hanshin (1988). "Guidelines for the Design of Horizontally Curved Girder Bridges (Draft)," Hanshin Expressway Public Corporation and Steel Structure Study Subcommittee, October, 178 pp.

95. Hash, J.B. (2001). "Shear Capacity of Hybrid Steel Girders," M.S. Thesis, University of Nebraska, Lincoln, 407 pp.
96. Heins, C.P., Hou, C.K., and Kato, H. (1982). "Lateral wind bracing requirements for steel composite bridges," *Engineering Journal*, AISC, 19(3), 160-169.
97. Heins, C.P. and Hall, D.H. (1981). "Designer's Guide to Steel Box-Girder Bridges," *Booklet No. 3500*, Bethlehem Steel Corporation, Bethlehem, PA, 20-30.
98. Heins, C.P. and Firmage, D.A. (1979). *Design of Modern Highway Bridges*, Wiley, New York, NY, 463 pp.
99. Helwig, T., Yura, J., Herman, R., Williamson, E. and Li, D. (2007). "Design Guidelines for Steel Trapezoidal Box Girder Systems," Report No. FHWA/TX-07/0-4307-1, Center for Transportation Research, University of Texas at Austin, Austin, TX, 84 pp.
100. Helwig, T., Herman, R. and Zhou, C. (2005). "Lean-On Bracing for Steel Bridge Girders with Skewed Supports," *Proceedings of the Annual Technical Session and Meeting*, Montreal, Quebec, Structural Stability Research Council, Univ. of Missouri - Rolla, Rolla, MO, 295-306.
101. Helwig, T.A., Frank, K.H. and Yura, J.A. (1997). "Lateral-Torsional Buckling of Singly Symmetric I-Beams," *Journal of Structural Engineering*, ASCE, 123(9), 1172-1179.
102. Herman, R., Helwig, T., Holt, J., Medlock, R., Romage, M. and Zhou, C. (2005). "Lean-On Cross-Frame Bracing for Steel Girders with Skewed Supports," *Time for Steel, Steel for Time*, Proceedings, 2005 World Steel Bridge Symposium, National Steel Bridge Alliance, 10 pp.
103. Hindi, W.A. (1991). "Behavior and Design of Stiffened Compression Flanges of Steel Box Girder Bridges," Ph.D. Thesis, University of Surrey, January.
104. Horne, M.R. and Grayson, W.R. (1983). "Parametric Finite Element Study of Transverse Stiffeners for Webs in Shear," Instability and Plastic Collapse of Steel Structures, Proceedings of the Michael R. Horne Conference, L.J. Morris (ed.), Granada Publishing, London, 329-341.
105. HSBA (2005). Honshu-Shikoku Bridge Authority web page, www.hsba.go.jp/bridge/e-tatara.htm.
106. Ito, M., Hoshino, M.-A., Naga, M., Nakai, H. and Ohtsuki, S. (1992). "Long Span Bridges," Chapter 6.5, *Constructional Steel Design, An International Guide*, P.J. Dowling, J.E. Harding and R. Bjorhovde (ed.), Elsevier, Essex, England, 711-734.
107. Jetteur, P., Maquoi, R., Skaloud, M. and Zornerova, M. (1984). "Interaction of Shear Lag with Plate Buckling in Longitudinally Stiffened Compression Flanges," *Acta Technica CSAV*, 29(3), 376-397.

108. Johnston, B.G. (1976). *Guide to Stability Design Criteria for Metal Structures*, 3rd ed., B.G. Johnston (ed.), Structural Stability Research Council, Wiley, New York, NY, 616 pp.
109. Johnston, S.B. and Mattock, A.H. (1967). "Lateral Distribution of Load in Composite Box Girder Bridges," Highway Research Record No. 167, Bridges and Structures, Washington, DC.
110. Johnson, D.L. (1985). "An Investigation into the Interaction of Flanges and Webs in Wide-Flange Shapes," *Proceedings of the Annual Technical Session and Meeting*, Cleveland, OH, Structural Stability Research Council, Univ. of Missouri - Rolla, Rolla, MO, 397-405.
111. Jung, S.-K. and White, D.W. (2010). "Inelastic Behavior of Horizontally Curved Composite I-Girder Bridge Structural Systems," Final Report to FHWA and Professional Services Industries, Inc., Curved Steel Bridge Research Project, Federal Highway Administration, April.
112. Jung, S.K. and White, D.W. (2006). "Shear Strength of Horizontally Curved Steel I-Girders – Finite Element Studies," *Journal of Constructional Steel Research*, 62(4), 329-342.
113. Jung, S.K., White, D.W., Beshah, F. and Wright, W. (2005). "Ultimate Strength of Horizontally-Curved Composite I-Girder Bridge Structural Systems," Annual Proceedings, Structural Stability Research Council, 327-347.
114. Kaehler, R.C., White, D.W. and Kim, Y.D. (2011). *Frame Design Using Web-Tapered Members*, Design Guide 25, AISC, Chicago, IL.
115. Kase, R.A. (1997). "Twelve Commandments for Economic Steel Box Girders," *Bridge Crossings*, No. 9, reprinted from *Modern Steel Construction*, 4 pp.
116. Kavanagh, T.C. (1962). "Effective Length of Framed Columns," *Transactions of the American Society of Civil Engineers*, 127, 81-101.
117. Kemp, A.R. (1996). "Inelastic Local and Lateral Buckling in Design Codes," *Journal of Structural Engineering*, 122(4), 374-381.
118. Kim, Y.D., Jung, S.K. and White, D.W. (2007). "Transverse Stiffener Requirements in Straight and Horizontally Curved Steel I-Girders," *Journal of Bridge Engineering*, ASCE, 12(2), 174-183.
119. Kim, Y.D. and White, D.W. (2013). "Transverse Stiffener Requirements to Develop the Shear Buckling and Post-Buckling Resistance of Steel I-Girders," *Journal of Structural Engineering*, ASCE, 10.1061/(ASCE)ST.1943-541X.0000867, 04013098.

120. Kitipornchai, S., Wang, C.M. and Trahair, N.S. (1986). "Buckling of Monosymmetric I-Beams Under Moment Gradient," *Journal of Structural Engineering*, ASCE, 112(4), 781-799.
121. Kitipornchai, S. and Trahair, N.S. (1980). "Buckling Properties of Monosymmetric I-Beams," *Journal of the Structural Division*, ASCE, 109(ST5), 941-957.
122. Kulicki, J.M., Prickett, J.E., and LeRoy, D.H. (2006). "Truss Bridges," *Structural Steel Designer's Handbook*, Chapter 13, R.L. Brockenbrough and F.S. Merritt (ed.), McGraw-Hill, New York, NY, 50 pp.
123. Kulicki, J.M. (2000). "Highway Truss Bridges," *Bridge Engineering Handbook*, Chapter 16, W.-F. Chen and L. Duan (ed.), CRC Press, Boca Raton, FL, 34 pp.
124. Lamas, A.R.G. and Dowling, P.J. (1980). "Effect of Shear Lag on the Inelastic Buckling Behavior of Thin-Walled Structures," *Thin-Walled Structures*, J. Rhodes & A.C. Walker (eds.), Granada, London, p. 100.
125. Lee, S.C., Yoo, C.H., and Yoon, D.Y. (2003). "New Design Rule for Intermediate Transverse Stiffeners Attached on Web Panels," *Journal of Structural Engineering*, ASCE, 129(12), 1607-1614.
126. Lee, G.C., Ketter, R.L. and Hsu, T.L. (1981). *Design of Single Story Rigid Frames*, Metal Building Manufacturers Association, Cleveland, OH, 267 pp.
127. Lee, G.C. and Hsu, T.L. (1981). "Tapered Columns with Unequal Flanges," *Welding Research Council Bulletin*, No. 272, November.
128. LeMessurier, W.J. (1985). Personal communication.
129. Leon, R.T. and Aho, M. (2002). "Towards New Design Provisions for Composite Columns," *Composite Construction in Steel and Concrete IV*, Proceedings, J.F. Hajjar, M. Hosain, W.S. Easterling and B.M. Shahrooz (ed.), ASCE, Reston, VA, 518-527.
130. Liew, J.Y.R., White, D.W., and Chen, W.F. (1992). "Beam-Columns," Chapter 2.5, *Constructional Steel Design, An International Guide*, P.J. Dowling, J.E. Harding and R. Bjorhovde (ed.), Elsevier, Essex, England, 105-132.
131. Lukey, A.F., Smith, R.J., Hosain, M.U. and Adams, P.F. (1969). "Experiments on Wide-Flange Beams under Moment Gradient," *Welding Research Council Bulletin*, No. 142, July, 1-19.
132. Lutz, L.A. (2006). "Evaluating Single Angle Compression Struts Using an Effective Slenderness Approach," *Engineering Journal*, AISC, to appear.
133. Lutz, L.A. (1992). "Critical Slenderness of Compression Members with Effective Lengths about Non-principal Axes," *Proceedings of the Annual Technical Session and*

- Meeting*, Pittsburgh, PA, Structural Stability Research Council, Univ. of Missouri - Rolla, Rolla, MO, 107-125.
134. Maleck, Andrea E. (2001), "Second-Order Inelastic and Modified Elastic Analysis and Design Evaluation of Planar Steel Frames," Ph.D. Dissertation, Georgia Institute of Technology, 579 pp
 135. Maleck, A.E. and White, D.W. (2003). "Alternative Approaches for Elastic Analysis and Design of Steel Frames. I: Overview," *Journal of Structural Engineering*, ASCE, 130(8), 1186-1196.
 136. Massonnet, C. (1960). "Stability Considerations in the Design of Steel Plate Girders," *Journal of the Structural Division*, ASCE, 86(ST1), 71-98.
 137. Mattock, A.H. and Fountain, R.S. (1967). "Criteria for Design of Steel-Concrete Composite Box Girder Highway Bridges," U.S. Steel Corporation, August.
 138. McGuire, W. (1968). *Steel Structures*, Prentice-Hall, Englewood Cliffs, NJ, 1112 pp.
 139. Moffatt, K.R. and Dowling, P.J. (1976). "Shear Lag in Steel Box Girder Bridges," *The Structural Engineer*, Discussion, 54, August, 285-297.
 140. Moffatt, K.R. and Dowling, P.J. (1975). "Shear Lag in Steel Box Girder Bridges," *The Structural Engineer*, , 53, October, 439-447.
 141. Munse, W.H. and Chesson, Jr., E (1963). "Riveted and Bolted Joints: Net Section Design," *Journal of the Structural Division*, ASCE, 89(ST1), 49-106.
 142. Mozer, J., R. Ohlson and C. Culver (1971). "Stability of Curved Plate Girders – P2," Prepared for the Department of Transportation, Federal Highway Administration, and Participating States under Contract Number FH-11-7389, Department of Civil Engineering, Carnegie-Mellon University, Pittsburgh, PA, 121 pp.
 143. Nakai, H. and Yoo, C.H. (1988). *Analysis and Design of Curved Steel Bridges*, McGraw-Hill, New York, NY, 673 pp.
 144. Nethercot, D.A and Trahair, N.S. (1976). "Lateral Buckling Approximations for Elastic Beams," *The Structural Engineer*, 54(6), 197-204.
 145. NSBA (2006). "Guidelines for Design Details," AASHTO/NSBA Steel Bridge Collaboration, G1.4 – 2006, 21 pp.
 146. NSBA (2004). "Steel Bridge Bearing Design and Detailing Guidelines," AASHTO/NSBA Steel Bridge Collaboration, G 9.1 - 2004, AASHTO Document No. SBB-1, 42 pp.
 147. NSBA (1996). "V-Load Analysis – An Approximate Procedure, Simplified and Extended, for Determining Moments and Shears in Designing Horizontally-Curved

- Open-Framed Highway Bridges,” Vol. I, Chap. 12, *Highway Structures Design Handbook*, Reprint, National Steel Bridge Alliance, Chicago, IL, 53 pp.
148. Oehlers, D.J. and Bradford, M.A. (1999). *Elementary Behavior of Composite Steel and Concrete Structural Members*, Butterworth Heinemann, Oxford, 259 pp.
 149. Owen, D.R.J., Rockey, K.C. and Skaloud, M. (1970). “Ultimate Load Behavior of Longitudinally Reinforced Webplates Subjected to Pure Bending,” IABSE Publications, Vol. 30-1, 113-148.
 150. Peköz, T. (1987). Development of a Unified Approach to the Design of Cold-Formed Steel Members. Report CF87-1, American Iron and Steel Institute, Washington, D.C.
 151. Poellot, W.N. (1997). “Curved Steel Box Girder Bridges,” *Structural Engineering Handbook*, 4th ed., Section 21, E.H. Gaylord, Jr., C.N. Gaylord and J.E. Stallmeyer (eds.), McGraw-Hill.
 152. Petzold, E. (2005). “Design, Fabrication and Erection Issues for Long Span Steel Tied Arches: A Case Study,” *Time for Steel, Steel for Time*, Proceedings, 2005 World Steel Bridge Symposium, National Steel Bridge Alliance, 11 pp.
 153. Pfeifer, S. (2006). Personal communication.
 154. Podolny, W. and Goodyear, D. (2006). “Cable-Suspended Bridges,” *Structural Steel Designer’s Handbook*, Chapter 15, R.L. Brockenbrough and F.S. Merritt (ed.), McGraw-Hill, New York, NY, 91 pp.
 155. Podolny, W. and Scalzi, J.B. (1986). *Construction and Design of Cable-Stayed Bridges*, 2nd Ed., Wiley, New York, NY, 336 pp.
 156. Porter, D.M., Rockey, K.C. and Evans, H.R. (1975). “The Ultimate Load Behavior of Plate Girders Loaded in Shear,” *The Structural Engineer*, 53(8), 313-325.
 157. Rahal, K.N. and Harding, J.E. (1990). “Transversely Stiffened Girder Webs Subjected to Shear Loading – Part 1: Behaviour,” *Proceedings of the Institution of Civil Engineers*, Part 2, 89, March, 47-65.
 158. Richter, J.F. (1998). “Flexural Capacity of Slender Web Plate Girders,” M.S. Thesis, Univ. Texas, Austin, May, 133 pp.
 159. Roik, K. and Bergmann, R. (1992). “Composite Columns,” Chapter 4.2, *Constructional Steel Design, An International Guide*, P.J. Dowling, J.E. Harding and R. Bjorhovde (ed.), Elsevier, Essex, England, 443-470.
 160. SAA (1998). *Steel Structures*, AS4100-1998, Standards Association of Australia, Australian Institute of Steel Construction, Sydney, Australia.

161. Salmon, C.G. and Johnson, J.E. (1996). *Steel Structures – Design and Behavior*, 4th Ed., 1024 pp.
162. Salvadori, M. (1956). “Lateral Buckling of Eccentrically Loaded I-Columns,” *Transactions of the ASCE*, 122(1).
163. Sato, A. and Uang, C.-M. (2007). “Modified Slenderness Ratio for Built-up Members,” *Engineering Journal*, AISC, 44, 269-280.
164. Schilling, C.G., Barker, M.G., Dishongh, B.E. and Hartnagel, B.A. (1997). “Inelastic Design Procedures and Specifications,” Final report submitted to American Iron and Steel Institute, Washington, DC, 107 pp.
165. Schilling, C.G. (1996). “Yield-Interaction Relationships for Curved I-Girders,” *Journal of Bridge Engineering*, American Society of Civil Engineers, Reston, VA, 1(1), 26-33.
166. Schilling, C.G. (1968). “Bending Behavior of Composite Hybrid Beams,” *Journal of the Structural Division*, ASCE, 94(ST8), 1945-1964.
167. Sherman, D. (2005). Communication to AISC TC4, June.
168. Sherman, D.R. (1992). “Tubular Members,” Chapter 2.4, *Constructional Steel Design, An International Guide*, P.J. Dowling, J.E. Harding and R. Bjorhovde (ed.), Elsevier, Essex, England, 91-104.
169. Sherman, D.R. (1976). “Tentative Criteria for Structural Applications of Steel Tubing and Pipe,” American Iron and Steel Institute, Washington, DC.
170. SSRC (1979). “A Specification for the Design of Steel-Concrete Composite Columns,” *Engineering Journal*, AISC, 16(4), 101-115.
171. Stanway, G.S., Chapman, J.C. and Dowling, P.J. (1996). “A Design Model for Intermediate Web Stiffeners,” *Proceedings of the Institution of Civil Engineers, Structures and Buildings*, 116, February, 54-68.
172. Talbot, J. (2005) “Simple Made Continuous: Simplified Continuity Details Improve Economies for Short and Medium Span Rolled Steel Girder Bridges,” *Steel Bridge News*, 6(4), National Steel Bridge Alliance, 3 pp.
173. Tang, M.C. (2000). “Cable-Stayed Bridges,” *Bridge Engineering Handbook*, W.-F. Chen and L. Duan (ed.), CRC Press, Boca Raton, FL, 18 pp.
174. Tang, M.C. (1976). “Buckling of Cable-Stayed Girder Bridges,” *Journal of the Structural Division*, ASCE, 102(ST9), 1675-1684.
175. Timoshenko, S.P. and Gere, J.M. (1961). *Theory of Elastic Stability*, McGraw-Hill, New York, NY, 541 pp.

176. Troitsky, M.S. (1990). *Prestressed Steel Bridges: Theory and Design*, Van Nostrand Reinhold, New York, NY, 386 pp.
177. Troitsky, M.S. (1988). *Cable-Stayed Bridges*, Van Nostrand Reinhold, New York, NY.
178. Ugural, A. and Fenster, S.K. (2003). *Advanced Strength and Applied Elasticity*, Prentice Hall, Englewood Cliffs, NJ, 560 pp.
179. Viest, I.M., Fountain, R.S. and Singleton, R.C. (1958). *Composite Construction in Steel and Concrete for Bridges and Buildings*, McGraw-Hill, New York, NY, 174 pp.
180. Vincent, G.S. (1969). "Tentative Criteria for Load Factor Design of Steel Highway Bridges," *AISI Bulletin No. 15*, American Iron and Steel Institute, Washington, D.C., 65 pp.
181. von Kármán, T., Sechler, E.E., and Donnell, L.H. (1932). "The Strength of Thin Plates in Compression," *Transactions of the ASME*, 54
182. Wadell, J.A.L. (1916). *Bridge Engineering*, Wiley, New York, NY.
183. Walther, R., Houriet, B., Isler, W., Moia, P. and Klein, J.-F. (1999). *Cable-Stayed Bridges*, Thomas Telford, London, 225 pp.
184. Wasserman, E.P. and Walker, J.H. (1996). "Integral Abutments for Steel Bridges," *Highway Structures Design Handbook*, Vol. II, Chapter 5, AISI, 1996.
185. Wasserman, E.P. (1997). "Integral Post-Tensioned Concrete Bent Caps," *Bridge Crossings*, No. 8, July, 3 pp.
186. Weakley, K. (2005). "VDOT Integral Bridge Design Guidelines," *Integral Abutment and Jointless Bridges*, FHWA Conference, Baltimore, MD, organized by Constructed Facilities Center, College of Engineering and Mineral Resources, W. Virginia Univ., 61-70.
187. White, D.W. (2008). "Unified Flexural Resistance Equations for Stability Design of Steel I-Section Members – Overview," *Journal of Structural Engineering*, ASCE, 134(9), 1405-1424.
188. White, D.W., and Barker, M. (2008). "Shear Resistance of Transversely-Stiffened Steel I-Girders," *Journal of Structural Engineering*, ASCE, 134(9), 1425-1436.
189. White, D.W., and Jung, S.-K. (2008). "Unified Flexural Resistance Equations for Stability Design of Steel I-Section Members – Uniform Bending Tests," *Journal of Structural Engineering*, ASCE, 134(9), 1450-1470.
190. White, D.W., and Kim, Y.D. (2008). "Unified Flexural Resistance Equations for Stability Design of Steel I-Section Members – Moment Gradient Tests," *Journal of Structural Engineering*, ASCE, 134(9), 1471-1486.

191. White, D.W., Barker, M., and Azizinamini, A. (2008). "Shear Strength and Moment-Shear Interaction in Transversely-Stiffened Steel I-Girders," *Journal of Structural Engineering*, ASCE, 134(9), 1437-1449.
192. White, D.W., and Chang, C.-J. (2007). "Improved Flexural Stability Design of I-Section Members in AISC (2005) – A Case Study Comparison to AISC (1989) ASD," *Engineering Journal*, AISC, 44(4), 291-304.
193. White, D.W., and Jung, S.-K. (2007). "Effect of Web Distortion on the Buckling Strength of Noncomposite Discretely-Braced I-beams," *Engineering Structures*, 29(8), 1872-1888, [doi:10.1016/j.engstruct.2006.09.020](https://doi.org/10.1016/j.engstruct.2006.09.020).
194. White, D.W., Shafer, B.W. and Kim, S.-C. (2006). "Implications of the AISC (2005) Q-Factor Equations for Rectangular Box and I-Section Members," Structural Mechanics and Materials Report No. 34, School of Civil and Environmental Engineering, Georgia Institute of Technology, Atlanta, GA.
195. White, D.W. and Kim, Y.-D. (2006). "A Prototype Application of the AISC (2005) Stability Analysis and Design Provisions to Metal Building Structural Systems," Report to Metal Building Manufacturers Association, School of Civil and Environmental Engineering, Georgia Institute of Technology, Atlanta, GA, September, 157 pp.
196. White, D.W. and Grubb, M.A. (2005). "Unified Resistance Equations for Design of Curved and Tangent Steel Bridge I-Girders," *Proceedings of the 2005 TRB Bridge Engineering Conference*, Transportation Research Board, Washington, DC, July, 121-128.
197. White, D.W. and Grubb, M.A. (2003). "Lateral Torsional Buckling Resistance of Stepped Flanges," *Three-Span Continuous Straight Composite I Girder, Load and Resistance Factor Design, Third Edition (Customary Units)*, Appendix C, National Steel Bridge Alliance, pp. C-1 to C-4.
198. White, D.W. and Jung, S.-K (2003a). "Simplified Lateral-Torsional Buckling Equations for I-and Channel-Section Members," Structural Engineering, Mechanics and Materials Report No. 24a, School of Civil and Environmental Engineering, Georgia Institute of Technology, Atlanta, GA, 23 pp.
199. White, D.W. and Jung, S.-K (2003b). "Simplified Lateral-Torsional Buckling Equations for Singly-Symmetric I-Section Members," Structural Engineering, Mechanics and Materials Report No. 24b, School of Civil and Environmental Engineering, Georgia Institute of Technology, Atlanta, GA, 29 pp.
200. White, D.W. and Kim, S.-C. (2003). "Simplified Strength Calculations for Noncompact Web Beam-Columns," Structural Engineering, Mechanics and Materials Report No. 28, School of Civil and Environmental Engineering, Georgia Institute of Technology, Atlanta, GA, 41 pp.

201. White, D.W. (2002). "LRFD Article 6.10 Draft # 3, Sample Case Studies," Report to AISI-AASHTO Task Committee for Updating of AASHTO LRFD Article 6.10, October, 84 pp.
202. White, D.W., Zureick, A.H., Phoawanich, N. and Jung, S.-K. (2001). "Development of Unified Equations for Design of Curved and Straight Steel Bridge I-Girders," Final Report to American Iron and Steel Institute Transportation and Infrastructure Committee, Professional Services Industries, Inc. and Federal Highway Administration, October, 551 pp.
203. White, D.W. and Barth, K.E. (1998). "Strength and Ductility of Compact-Flange I Girders in Negative Bending," *Journal of Constructional Steel Research*, 45(3), 241-280.
204. White, D. W., Ramirez, J. A., and Barth, K. E. (1997). "Moment Rotation Relationships for Unified Autostress Designs of Continuous-Span Bridge Beams and Girders." *Final Report.*, Joint Transportation Research Program, West Lafayette, IN, 117 pp.
205. White, D.W. and Clarke, M.J. (1997a). "Design of Beam-Columns in Steel Frames. I: Philosophies and Procedures," *Journal of Structural Engineering*, ASCE, 123(12), 1556-1564.
206. White, D.W. and Clarke, M.J. (1997b). "Design of Beam-Columns in Steel Frames. II: Comparison of Standards," *Journal of Structural Engineering*, ASCE, 123(12), 1565-1575.
207. Winter, G. (1970). "Commentary on the 1968 Edition of the Specification for the Design of Cold-Formed Steel Structural Members," American Iron and Steel Institute, New York, NY.
208. Winter, G. (1947). "Strength of Thin Steel Compression Flanges," *Transactions of the ASCE*, 112, 547.
209. Wittry, D.M. (1993). "An Analytical Study of the Ductility of Steel Concrete Composite Sections," M.S. Thesis, Univ. of Texas, Austin, TX, December, 88 pp.
210. Wolchuk, R. (1997). "Steel-Plate-Deck Bridges and Steel Box Girder Bridges," *Structural Engineering Handbook*, 4th ed., Section 19, E.H. Gaylord, Jr., C.N. Gaylord and J.E. Stallmeyer (eds.), McGraw-Hill.
211. Wolchuk, R. and Mayrbaur, R.M. (1980). "Proposed Design Specifications for Steel Box Girder Bridges," Final Report, FHWA-TS-80-205, Washington, DC, 288 pp.
212. Wong-Chung, A.D. and Kitipornchai, S. (1987). "Partially Braced Inelastic Beam Buckling Experiments," *Journal of Constructional Steel Research*, 7, 189-211.
213. Woolcock, S.T. and Kitipornchai, S. (1986). "Design of Single Angle Web Struts in Trusses," *Journal of Structural Engineering*, 112(6), 1327-1345.

214. Wright, K.J. and Bunner, M.A. (2006). "Arch Bridges," *Structural Steel Designer's Handbook*, Chapter 14, R.L. Brockenbrough and F.S. Merritt (ed.), McGraw-Hill, New York, NY, 75 pp.
215. Xanthakos, P.P. (1994). *Theory and Design of Bridges*, Wiley, New York, NY, 1443 pp.
216. Xie, M. (2000). "Behavior and Design of Transversely Stiffened Plates Subject to Combined Shear and Direct In-Plane Loading," PhD Thesis, Department of Civil and Environmental Engineering, Imperial College, London.
217. Yannotti, A., Alampalli, S. and White, H. (2005). "New York State Department of Transportation's Experience with Integral Abutment Bridges," *Integral Abutment and Jointless Bridges*, FHWA Conference, Baltimore, MD, organized by Constructed Facilities Center, College of Engineering and Mineral Resources, W. Virginia Univ., 41-49.
218. Yoo, C.H. and Lee, S.C. (2006). "Mechanics of Web Panel Postbuckling Behavior in Shear," *Journal of Structural Engineering*, ASCE, to appear.
219. Yoo, C.H. and J.S. Davidson (1997). "Yield Interaction Equations for Nominal Bending Strength of Curved I-Girders," *Journal of Bridge Engineering*, ASCE, 2(2), 37-44.
220. Yu, D. and Sause, R. (2002). "Regression Study on the Inelastic Lateral Torsional Buckling Strength of I-Beams," ATLSS Center, Lehigh University, Bethlehem, PA, October, 38 pp.
221. Yura, J.A., Helwig, T., Herman, R. and Zhou, C. (2008). "Global Lateral Buckling of I-Shaped Girder Systems," *Journal of Structural Engineering*, ASCE, 134(9), 1487-1494.
222. Yura, J.A. and Widiyanto (2005). "Lateral Buckling and Bracing of Beams – A Re-evaluation After the Marcy Bridge Collapse," *Proceedings of the Annual Technical Session and Meeting*, Montreal, Quebec, Structural Stability Research Council, Univ. of Missouri - Rolla, Rolla, MO, 277-294.
223. Yura, J.A. and Helwig, T.A. (1996). "Bracing for Stability," Short Course Notes, Structural Stability Research Council.
224. Yura, J.A. (1992). Notes on development of k_c equation for AISC LRFD Specification.
225. Yura, J.A., Galambos, T.V. and Ravindra, M.K. (1978). "The Bending Resistance of Steel Beams," *Journal of the Structural Division*, ASCE, 104(9), 1355-1369.
226. Zandonini, R. (1985). "Stability of Compact Built-Up Struts: Experimental Investigation and Numerical Simulation," *Costruzioni Metalliche*, 4.

227. Zhou, C. (2006). "Utilizing Lean-On Cross-Frame Bracing for Steel Bridges," Ph.D. dissertation, University of Houston, Houston, TX, 382 pp.
228. Ziemian, R.D. (2010). *Guide to Stability Design Criteria for Metal Structures*, 6th ed., R.D. Ziemian (ed.), Structural Stability Research Council, Wiley, New York, NY.